Marius Widerøe

Magnetic Resonance Imaging of Hypoxic-Ischemic Brain Injury Development in the Newborn Rat

Manganese and diffusion contrasts

Thesis for the degree of Philosophiae Doctor

Trondheim, May 2012

Norwegian University of Science and Technology
Faculty of Medicine
Department of Laboratory Medicine, Children's and Women's Health

NTNU – Trondheim
Norwegian University of
Science and Technology

NTNU
Norwegian University of Science and Technology

Thesis for the degree of Philosophiae Doctor

Faculty of Medicine
Department of Laboratory Medicine, Children's and Women's Health

ISBN 978-82-471-3531-0 (printed ver.)
ISBN 978-82-471-3532-7 (electronic ver.)
ISSN 1503-8181

Doctoral theses at NTNU, 2012:125

Printed by NTNU-trykk

Magnetisk resonans avbildning av hypoksisk-iskemisk hjerneskade-utvikling hos nyfødte rotter

- bildekontrast med mangan og diffusjon

Hypoksi-iskemi er kombinasjonen av redusert oksygen og begrenset blodforsyning til hjernen. Dette er en av de vanligste årsakene til hjerneskade hos nyfødt barn og medfører økt dødelighet samt psykiske og fysiske problemer senere i livet. Behandlingsalternativene er begrenset og de langsiktige virkningene av behandlingsmetoder, slik som nedkjøling, som nylig er tatt i bruk er fortsatt ukjent. Hypoksi-iskemi setter i gang en skadeprosess som utvikler seg med vevsskade og død av hjerneceller i løpet av timer, dager og uker. Denne skadeprosessen ledsages av betennelsesreaksjoner som synes å spille en viktig rolle i skadeutviklingen gjennom aktivering av støtteceller (astroglia) og immunceller (microglia) i hjernen. Microglia har en viktig funksjon med å fjerne døde celler og vevs-rester etter skader, men microglia kan også bidra til økt skade gjennom utskillelse av stoffer som opprettholder betennelsen og forårsaker celledød. Midler som kan hemme betennelse i hjernen etter hypoksi-iskemi kan derfor være interessante som ny behandling.

Magnetisk resonans (MR) avbildning er et viktig verktøy for vurdering av hjerneskade hos nyfødte og har sammen med bruk av dyremodeller for hypoksisk-iskemisk hjerneskade hos nyfødte gitt verdifull kunnskap om mekanismene bak denne typen skade. En stor fordel med bruk av MR i dyrestudier er blant annet at man kan foreta gjentatte undersøkelser og målinger av strukturelle, cellulære og molekylære prosesser uten å ta ut vevsprøver. Dette gir muligheter til å studere utviklingen av skade og effekten av behandling over tid. Manganforsterket MR er en metode som kan være nyttig i en slik sammenheng. Mangan (Mn^{2+}) er et stoff som på grunn av sine magnetiske egenskaper kan fungere som kontrastmiddel ved MR avbildning. I kroppen oppfører mangan seg i mange sammenhenger som kalsium og kan blant annet gå inn i nerveceller og støtteceller (gliaceller) i hjernen gjennom kalsium-kanaler. Prosesser som fører til høyt kalsium i cellene, slik som celledød eller aktivitet i nerveceller, kan derfor potensielt avbildes med manganforsterket MR. Cellulære og molekylære prosesser som forårsaker endringer i bevegelse av vann i vevet, som for eksempel oppsvulming av celler eller økt vann i vevet (ødem), kan også visualiseres med MR. Ved å måle den retningsbestemte bevegelsen til vann med en teknikk kalt diffusjon tensor avbildning (DTI), kan nervebaner også avbildes i levende dyr. Forandringer i nervebanene som skyldes modning eller skade vil forårsake endringer i bevegelsen av vann som kan måles med DTI.

Målsetningen med denne avhandlingen var å etablere metoder for MR avbildning av hypoksisk-iskemisk hjerneskade i levende nyfødte rotter, med det mål å kunne studere

skadeutviklingen over tid samt å kunne vurdere hvordan tilførsel av ekstra oksygen og behandling med et betennelseshemmende stoff (doxycycline) påvirket skadeforløpet.

Arbeidet i denne avhandlingen demonstrerer hvordan manganforsterket MR kan være et nyttig verktøy for å følge skadeutviklingen med betennelsesreaksjoner, arr-utvikling samt medfølgende celledød etter hypoksisk-iskemisk skade i en nyføde rottehjerne. Økt mangankontrast var synlig sju dager etter påført hypoksisk-iskemisk skade og injeksjon av mangan. Reaktive microglia-celler og astroglia-celler ble funnet i hjerneområder med økt mangankontrast, og disse områdene gikk så i oppløsning i den etterfølgende perioden opp til seks uker etter påført skade. Disse studiene har vist at hypoksisk-iskemisk skade i den nyfødte hjerne er en langvarig prosess hvor betennelsesreaksjoner er et viktig element i skadeutviklingen. Diffusjons tensor avbildning ble brukt til å studere effekten av hypoksi-iskemi på nervebanene. Resultatene viste at hypoksi-iskemi gir skader på nervebanene samt synes å påvirke den naturlige utviklingen i form av redusert eller forsinket dannelse av myelin-skjeder rundt nervebanene. Tilførsel av rent oksygen (100 %) etter hypoksi viste seg å forverre slike skader i nervebanene i tillegg til å ha en generelt ugunstig effekt med økt tap av hjernevev og økt betennelsesreaksjon lenge etter at skaden ble påført. Doxycycline er et stoff som er kjent for å hemme microglia-celler. Som et behandlingsforsøk ble en enkelt dose med doxycycline gitt én time etter den hypoksisk-iskemisk skaden. Dette viste seg å beskytte hjernen, redusere tap av hjernevev samt redusere skadene på nervebanene. Doxycycline ser derfor ut til å ha et potensial som behandling for hypoksisk-iskemisk hjerneskade hos nyfødte.

Kandidat: Marius Widerøe
Institutt: Institutt for laboratoriemedisin, barne- og kvinnesykdommer
Veiledere: Ann-Mari Brubakk, Christian Brekken, Jon Skranes, Pål Erik Goa
Finansieringskilde: Medisinsk teknologi, Det medisinske fakultet, Norges Teknisk-Naturvitenskaplige Universitet

Ovennevnte avhandling er funnet verdig til å forsvares offentlig for graden
Philosophiae Doctor i klinisk medisin.
Disputasen finner sted i Auditoriet, Medisinsk teknisk forskningssenter, NTNU
tirsdag 29. mai 2012 kl 11.00

Acknowledgement

This research work presented in this thesis was carried out at the Department of Laboratory Medicine, Children's and Women's Health at the Norwegian University of Science and Technology. Funding was provided by the Strategic Area of Medical Technology at the Faculty of Medicine at Norwegian University of Science and Technology, and free use of the MR system was provided by FUGE Molecular Imaging Center at the MR Center in Trondheim.

First of all I would like to thank my main supervisor Professor Ann-Mari Brubakk who gave me the opportunity to start this research project. She has been present when needed, supportive and encouraging, and always dedicated to the project, with ever so inspiring enthusiasm and a constant flow of ideas. Thanks for challenging my thoughts and opinions and for battling my arguments.

I would also like to thank Professor Torstein Vik who got me interested in paediatric research during medical school. He inspired the researcher in me and gave me an excellent start in medical research which years later have led to this thesis.

I am very grateful for all the help and guidance provided by Dr. Christian Brekken and Dr. Pål Erik Goa. Christian aroused my interest in MRI with his inspiring enthusiasm. Thank you for all the valuable scientific discussions and for a great cruise into molecular imaging. Pål Erik made MR physics fun and our discussions have provided valuable lessons on all the aspects of MR imaging and image analysis. He has also been a great support in interpreting the results, writing of the manuscripts and this thesis.

Special thanks to Professor Jon Skranes for giving me valuable input in discussing the results, preparing the manuscripts and putting the animal experiments in a clinical perspective.

I am very grateful for all the help provided by my co-authors: Especially Tora Sund Morken for her close collaboration and for valuable discussions, Dr. Øystein Olsen for his countless efforts to quantify manganese-enhancement and automate tissue segmentation, Tina Bugge Pedersen for help with the animal experiments, Marianne B. Havnes and Dr. Annemieke Kaavelars for cutting and staining my histological sections, Paulo Girão for help with scanning them,

Professor Sverre Torp and Professor Cobi Heijnen for help with histological analyses, and Øyvind Salvesen for help with statistical analyses.

I would also like to thank my colleagues in the paediatric research group; Kari Anne Indredavik Evensen, Gro Løhaugen and Susanne Lindqvist and all the colleagues at the MR Center through the years. Tina Bugge Pedersen, Øystein Risa, Marte Thuen, Kristine Skårdal, Niels van Strien, Else Marie Huuse and Ioanna Sandvig, deserve special thanks for providing a great work environment, for all help, collaboration, inspiring discussions and for all the fun times. Olav Haraldseth also deserves special thanks for involving me in other types of MR research and for giving me the opportunity to pursuit new exciting MR projects in the future.

Finally I would like to thank friends and family for their support. Special thanks to my son Mathias for reminding me about the most important things in life and to my wonderful wife Marte who have endured cancelled weekends due to rat births and my long days and nights in the laboratory and in the office. Thank you for your love, support, encouragement and patience throughout this project and especially in the last months. It has been the best help I could ever dream of.

Marius Widerøe,

Trondheim, December 2011

Summary

Hypoxia-ischemia (HI) is the combination of reduced oxygen supply (hypoxia) and restricted blood supply (ischemia) to the brain. It is one of the most common causes of brain injury in newborn children and carries an increased risk for early death and mental, cognitive, motor and sensory problems in later life. The current therapeutic options for treating or preventing hypoxic-ischemic injuries are limited and the long-term effects of new treatments, like hypothermia, are still unknown. Hypoxic-ischemic injury starts with the energy failure of brain cells. This initiates cascades leading to delayed injury and cell death that evolves over hours, days and weeks. Hypoxia-ischemia triggers an inflammatory response that plays an important role in this delayed injury process through activation of microglial and astroglial cells. Microglia is the resident immune cell of the brain, and has important functions to clear dead cells and debris after injury. However, microglial cells also contribute to increased injury through release of mediators which sustain the inflammation and cause cell injury. Inhibition of brain inflammation is therefore an interesting option for new treatments.

Magnetic resonance imaging (MRI) has become an important clinical tool for assessment of neonatal hypoxic-ischemic brain injury. Together with a focus on mapping the cellular and molecular mechanisms of injury in animal models it has advanced the knowledge of the mechanism underlying hypoxic-ischemic injury. Use of MRI in animal studies has the great advantage of repeated non-invasive examinations and measurements that allow longitudinal studies of the structural, cellular and molecular injury processes and the possibility to evaluate the effect of interventions and treatments longitudinally. One such MRI method is manganese-enhanced MRI. Manganese (Mn^{2+}) acts as a MRI contrast agent due to its paramagnetic properties. In biological systems, Mn^{2+} acts an analogue for calcium and can enter neurons and glial cells through calcium channels. Processes leading to high intracellular calcium, such as cell death or neuronal cell activation, may therefore potentially be visualized with manganese-enhanced MRI. Cellular and molecular processes that cause changes in water diffusion in tissue, such as caused by cell swelling or oedema, can also be visualized by MRI. By measuring the directionality of diffusion with a technique called diffusion tensor imaging (DTI), neuronal white matter tracts can also be visualized *in vivo*. Injury or maturational changes to the white matter will cause changes in the water diffusion that can be measured using DTI.

The aims of this thesis were to establish methods for *in vivo* MR imaging of hypoxic-ischemic brain injury in a neonatal rat model to enable longitudinal evaluation of delayed tissue damage, injury progression and to test the effects of interventions on the injury process.

The work of this thesis demonstrates how manganese-enhanced MRI can be a useful tool to follow the injury process and detect the delayed inflammation and gliosis with concurring cell death following a hypoxic-ischemic insult to the neonatal rat brain. Manganese-enhancement was detectable on MRI seven days after the hypoxic-ischemic insult and manganese injection, and this enhancement was related to activated microglia and astrogliosis secondary to the HI injury. These manganese-enhanced areas liquefied during the period up to six weeks after the initial insult. These studies clearly show that hypoxic-ischemic injury in the neonatal brain is a prolonged process involving inflammation and gliosis. Injury to white matter microstructure and maturational development of white matter were studied using diffusion tensor imaging. The results showed that hypoxia-ischemia seems to affect the trajectory of white matter development with results indicating reduced or delayed myelination of major neuronal tracts. Exposure to 100% oxygen after hypoxia was shown to exacerbate such injuries, delayed maturational changes in white matter and to have a general detrimental effect with increased brain tissue loss and inflammation long after the insult. A single dose of doxycycline given one hour after the hypoxic-ischemic insult did, on the other hand, provide protection of the brain in the form of reduced tissue loss and less injury to white matter tracts and this effect of doxycycline increased with time after hypoxia-ischemia. This showed that doxycycline has potential as a treatment for hypoxic-ischemic brain injury in the neonate.

Symbols and abbreviation

2D	2-dimensional
3D	3-dimensional
α	Flip-angle
ADC	Apparent Diffusion Coefficient
ATP	Adenosine Tri-Phosphate
B_0	Static magnetic field
B_1^+	Excitation/transmit field
B_1^-	Receive field
BBB	Blood Brain Barrier
Ca	Calcium
CD68	Cluster of Differentiation 68
Cl	Chlorine
CNR	Contrast to Noise Ratio
CNS	Central Nervous System
COX	Cyclooxygenase
CSF	Cerebrospinal fluid
DNA	Deoxyribonucleic acid
DTI	Diffusion tensor Imaging
DWI	Diffusion weighted imaging
EPI	Echo Planar Imaging
FA	Fractional anisotropy
FID	Free Induction Decay
FLASH	Fast Low Angle Shot
FOV	Field-of-view
GFAP	Glial fibrillary acidic protein
GS	Glutamine Synthetase
γ	Gyromagnetic ratio
^1H	Proton
ħ	Planck's constant
HE	Hematoxylin-Eosin
HI	Hypoxia-ischemia / Hypoxic-ischemic
HIE	Hypoxic-ischemic encephalopathy
IL	Interleukin
iNOS	inducible nitric oxide synthase
ip	Intraperitoneal
IVH	Intraventricular haemorrhage
Kg	kilogram
l	litre

$\lambda_{\parallel}$	Axial diffusivity
$\lambda_{\perp}$	Radial diffusivity
M	Molar
m	metre
MAP-2	Microtubule-associated protein 2
MBP	Myelin Basic Protein
MD	Mean diffusivity
ME	Manganese enhanced / manganese enhancement
MEMRI	Manganese enhanced MRI
mg	milligram
min	minute(s)
µl	microlitre
ml	millilitre
mM	millimolar
MMP	Matrix metalloproteinases
Mn	Manganese
MnSOD	Manganese Superoxide Dismutase
MRI	Magnetic resonance imaging
MRS	Magnetic resonance spectroscopy
MSME	Multislice Multiecho
MTX	Acquisition matrix
Na	Natrium (Sodium)
NA	Number of averages
NF-κB	Nuclear Factor kappa Beta
nNOS	neuronal nitric oxide synthase
NO	Nitric oxide
P7	Postnatal day 7 (day 7 after birth)
PVL	Periventricular leucomalacia
RARE	Rapid Acquisition with relaxation enhancement
RF	Radio frequency
ROI	Region(s) of Interest
SAR	Specific Absorption Rate
SNR	Signal to Noise Ratio
T	Tesla
T_1	Longitudinal relaxation
T_2	Transverse relaxation
TE	Echo time
TR	Repetition time
ω_0	Larmor frequency

List of papers

Paper I

Manganese-Enhanced Magnetic Resonance Imaging of Hypoxic-Ischemic Brain Injury in the Neonatal Rat

Marius Widerøe, Øystein Olsen, Tina Bugge Pedersen, Pål Erik Goa, Annemieke Kavelaars, Cobi Heijnen, Jon Skranes, Ann-Mari Brubakk, Christian Brekken

Neuroimage (2009) 45: 880-890

Paper II

Longitudinal Manganese-Enhanced Magnetic Resonance Imaging of Delayed Brain Damage after Hypoxic-Ischemic Injury in the Neonatal Rat

Marius Widerøe, Christian Brekken, Annemieke Kavelaars, Tina Bugge Pedersen, Pål Erik Goa, Cobi Heijnen, Jon Skranes, Ann-Mari Brubakk

Neonatology (2011) 100(4): 363-372

Paper III

Effects of Doxycycline on the Longitudinal Development of Cerebral Grey and White Matter Injury in a Neonatal Rat Model of Hypoxia-Ischemia – a Magnetic Resonance Imaging study

Marius Widerøe, Marianne B. Havnes, Tora Sund Morken, Jon Skranes, Pål-Erik Goa, Ann-Mari Brubakk

Accepted for publication in European Journal of Neuroscience

Paper IV

Longitudinal Diffusion Tensor and Manganese–Enhanced MRI Detect Delayed Brain Injury after Hypoxia-Ischemia and Hyperoxia in the Immature Rat

Tora Sund Morken, Marius Widerøe, Christina Vogt, Stian Lydersen, Marianne Havnes, Jon Skranes, Pål-Erik Goa, Ann-Mari Brubakk

Submitted to Pediatric Research

Contents

Chapter 1 General introduction

1.1 Hypoxic-ischemic brain injury

Hypoxia-ischemia (HI) is one of the most common causes of brain injury in newborn children and it occurs, depending on the definition, in between 1-6 per 1000 live-born children in developed countries (Ferriero 2004; McGuire 2007). Early recognition and definition of the severity of hypoxic-ischemic injury is difficult, especially in the prematurely born infants, and this sometimes impedes the initiation of early treatment. In addition, the current therapeutic options for treating or preventing hypoxic-ischemic injuries are limited and the long-term effects are still unknown (Ferriero 2004; Gonzalez and Ferriero 2009). Hypoxic-ischemic insults may cause both acute brain injury and initiate cascades leading to delayed injury and cell death that affects both grey and white matter development with an increased risk for mental, cognitive, motor and sensory problems in childhood, adolescence and adulthood. These injuries have consequences for the individuals' daily living, school and work performance as well as for the public health system and society, and increased use of resources are needed to treat and assist these patients (Volpe 2009).

1.1.1 Aetiology of hypoxic-ischemic injury

Hypoxia-ischemia is the combination of reduced oxygen supply and restricted blood supply to an organ tissue. In the perinatal period, cerebral injury as a result of a hypoxia-ischemia may take place in pregnancy, during birth or in the neonatal period. In pregnancy. hypoxia-ischemia may occasionally be caused by maternal trauma, hypotension or uterine haemorrhage. However, factors such as preeclampsia, placenta infarctions, intrauterine growth retardation and infections are more likely to predispose for HI during labour and delivery by compromising the placental blood flow (Volpe 2008). The major cause of hypoxia-ischemia around birth is asphyxia with intrauterine disturbance of gas exchange across the placenta leading to cardiac insufficiency and loss of cerebrovascular autoregulation *in utero* and at time of birth. This may be caused by placental abruption, interruption of naval cord circulation (e.g. cord prolapse), prolonged labour or direct trauma to the foetal head, among others. In the period after birth a major cause is respiratory and cardiac insufficiency caused by for instance obstructed airways

(e.g. meconium aspiration), respiratory depression due to effects of drugs (e.g. opiates), respiratory distress, repetitive apnoea, patent ductus arteriosus or severe congenital heart failure. Furthermore, postnatal circulatory insufficiency secondary to persistent foetal circulation or vascular collapse, such as caused by severe infections, are major causes of HI (McGuire 2007; Volpe 2008). Although the brain is one of the most vulnerable organs due to its high energy and oxygen consumption, hypoxia-ischemia usually affects multiple organs of the body. The hypoxic-ischemic neonates are therefore often in need of advanced life support, and these critically ill children are more likely to have fluctuating blood pressures and blood oxygen levels due to impaired cerebrovascular autoregulation that increases the susceptibility of and can exacerbate hypoxic-ischemic injury (McLean and Ferriero 2004).

1.1.2 Neonatal encephalopathy

Neonatal hypoxic-ischemic brain injury is commonly recognized based on an encephalopathy that evolves over days after birth. The neonatal encephalopathy is a syndrome that is characterized by disturbed neurological function with altered levels of consciousness, reduced muscle tone, abnormal reflexes, respiratory problems, poor feeding and often seizures (Johnston *et al.* 2002; Ferriero 2004; Johnston *et al.* 2011). However, in some infants the presenting signs and symptoms are subtle and hard to recognize. Furthermore, in the prematurely born infants many of the same signs can be attributed to the immaturity of the nervous system. The difficulty in recognising hypoxia-ischemia may lead to delayed diagnosis with consequences for treatment and subsequent neurological sequela.

Although hypoxia-ischemia is a major cause of neonatal encephalopathy, several other pathological conditions may cause the same symptoms and signs, including arterial stroke or venous thrombosis, intraventricular haemorrhage (IVH), traumatic brain injury, infection, inborn metabolic disorders and intoxications, among others. It is important to differentiate between the different underlying conditions, since treatment, prognosis and follow-up are different. However, many of these underlying pathologies have overlapping aetiology and pathophysiology, and may also be complicated by concurring hypoxia-ischemia (Ferriero 2004).

1.1.3 Injury patterns are defined by the vulnerability of the neonatal brain

Different patterns of injury are observed after hypoxic-ischemic injury. They are linked to the nature of the insult and to selective vulnerability of different brain cells at different developmental stages. In addition, the regional vulnerability of the blood supply is a determining factor for the pattern of injury, as injury is usually more severe in the border zones between major cerebral arteries (Volpe 2009). The periventricular area has a particularly vulnerable blood supply in preterm children. Reflecting this, intraventricular haemorrhage

(IVH) and periventricular leucomalacia (PVL) are most frequently observed in these neonates born before gestational week 32 (Johnston *et al.* 2002; Ferriero 2004). PVL primarily leads to white matter injury that is caused by death of differentiating pre-oligodendrocytes and subplate neurons. The maturation-dependent characteristics of these cells make them particularly vulnerable to excitotoxicity and free radical attacks caused by hypoxia-ischemia and inflammation. Loss of these cells results in reduced myelination and axonal degeneration ultimately leading to impaired cortical and thalamic development (Volpe 2009). In term and near-term children, blood supply is particularly vulnerable in the parasagittal areas. Hence, injury of the parasaggital cortex and adjacent white matter is a frequent pattern in these neonates. Selective injury to neurons in deep grey matter structures like thalamus and basal ganglia as well as sensori-motor cortex dominates with more severe and prolonged hypoxic-ischemic insults (Johnston *et al.* 2002; Ferriero 2004; Volpe 2008). These patterns are also related to the increased susceptibility for glutamate excitotoxicity and oxidative stress at that time of brain development which affect neurons in particular (Johnston *et al.* 2002; Ferriero 2004). The reduced antioxidative defence and high iron content of the neonatal brain contribute to the susceptibility to free radical and oxidative stress. The vulnerability of the neonatal brain is further enhanced by its reduced capacity of cerebrovascular autoregulation. This increases the risk of cerebral hypo- and hypertension, both damaging for the brain (McLean and Ferriero 2004).

1.2 Pathophysiology of hypoxic-ischemic injury

In contrast to ischemic injury in adults, hypoxia-ischemia in the neonatal brain results in a injury with neuronal death that evolves over hours, days and weeks after the primary insult (Nakajima *et al.* 2000; Geddes *et al.* 2001; Ferriero 2004; Northington *et al.* 2005). During the insult, hypoxia-ischemia results in an energy-depletion in the brain. After resuscitation, the energy balance in the brain is at least partially restored, only to suffer a secondary energy failure about 24 hours after the hypoxic-ischemic insult (Volpe 2008; Johnston *et al.* 2011). This is noticeable in the clinical setting, where onset of seizures and other signs of encephalopathy are often delayed (Johnston *et al.* 2011). The series of events thought to evolve after a hypoxic-ischemic insult, starts with an excitotoxic cascade. The excitotoxicity is thought to exacerbate the initial energy failure and to initiate cellular events leading to the secondary energy failure and ultimately cell death (Johnston *et al.* 2002; McLean and Ferriero 2004). In addition, inflammation plays an important role in early and late events following hypoxia-ischemia (Volpe 2009; Johnston *et al.* 2011). The following paragraphs first discuss the early events leading to cellular injury and then focus on the delayed injury with inflammation that ensues.

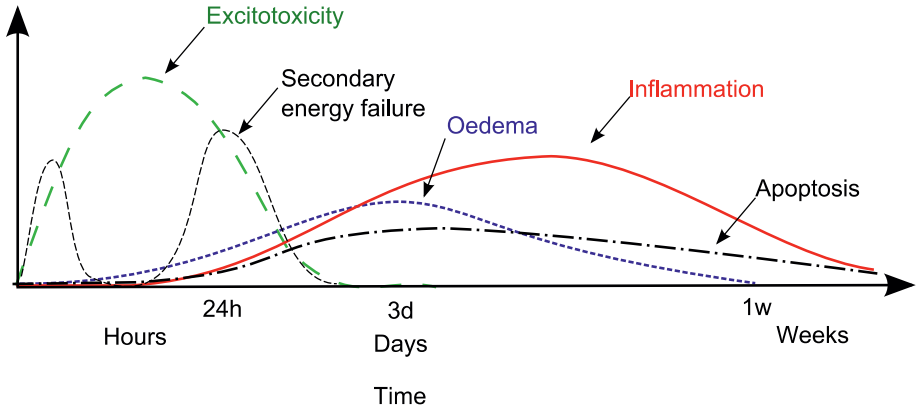

Figure 1.1: Putative evolution of brain injury after hypoxia-ischemia with timing of the different pathophysiological elements.

1.2.1 Early energy failure and cell death

Hypoxia-ischemia reduces the cell's ability to produce energy-rich phosphate compounds, such as ATP. These compounds are necessary for maintaining the cell membrane potential and vital cell functions. The depletion of energy-rich phosphate compounds results in a series of events, detrimental for cell survival. It starts with the failure of the ATP-dependent Na^+/K^+ pump in the outer cell membrane. With a severe insult, this leads to a rapid influx and accumulation of intracellular Na^+ with subsequent influx of Cl^-. This causes an osmotic gradient that brings increased water into the cell. The consequence is a rapid cell swelling and lysis with membrane disintegration – a necrotic cell death (Dirnagl *et al.* 1999; Volpe 2008). The cell swelling is also the pathophysiological process that lies behind the cytotoxic oedema that ensues only few hours after a hypoxic-ischemic insult, and can be detected by diffusion MRI (Volpe 2008).

With a less severe insult, the reduction in the cell membrane potential leads to a depolarization of the cell with subsequent high intracellular Ca^{2+}. In neurons, this initiates several cascades: High intracellular Ca^{2+} leads to the release of excitatory amino acids – among these, glutamate – from axon terminals into the synaptic cleft. Glutamate binds to receptors in the dendritic cell membrane of the neighbouring neurons causing influx of Ca^{2+} into the cell. This triggers a cascade of spreading depolarization and release of glutamate from neuron to neuron. Glutamate in the synaptic cleft is normally taken up into astrocytes, but this active uptake is drastically reduced since it dependents on energy-rich phosphate compounds. This contributes to an accumulation of glutamate in the synapses that further spills into the

surrounding extracellular space. The high extracellular glutamate sustains the continuous excitatory depolarization with influx of Ca^{2+} into the cells due to activation of NMDA-receptors and voltage-gated Ca^{2+}-channels. Due to the energy depletion of the cell, ATP-dependent Ca^{2+}-pumps fail and normal Ca^{2+}-balance with low Ca^{2+} concentration in cytosol cannot be re-established (Martin *et al.* 1998; McLean and Ferriero 2004; Volpe 2008). These events, termed excitotoxicity is generally thought to induce a series of events that lead to a secondary energy failure and delayed cell death.

1.2.2 Secondary energy failure and cell death

The excitotoxic process may lead to cell death by several routes that co-exist and are initiated by the high intracellular Ca^{2+} (Johnston *et al.* 2002). One is the activation of proteases, nucleases and lipases, which lead to disruption of cell cytoskeleton, damage to the nucleus, and injury to the cell membranes, respectively. All of these events ultimately lead to the disintegration of the cell (Volpe 2008).

The high intracellular Ca^{2+} also causes oxidative stress through activation of xanthine oxidase and neuronal nitric oxide synthase (nNOS) leading to production of free radicals like hydrogen perioxidase (H_2O_2), hydroxyl radicals (OH), nitric oxide (NO) and peroxynitrite causing damage to intracellular proteins and DNA (Johnston *et al.* 2011). NO also induces the production of radical oxygen species in the mitochondria, leading to impaired mitochondrial function (McLean and Ferriero 2004). The oxidative stress can be further increased in the reperfusion phase due to high blood oxygen concentrations boosting the production of free oxygen radicals. Nearby inflammatory cells, like microglia, can augment all these events by the release of free radicals, especially NO. Mitochondrial failure leads to further energy depletion and intracellular accumulation of lactic acid. Pro-apoptotic proteins are released from the mitochondria into cytoplasm and trigger cellular apoptosis (programmed cell death) through activation of caspase 3 and DNA-fragmentation (Johnston *et al.* 2011). Apoptosis can also be triggered directly by high intracellular Ca^{2+} through direct activation of caspase 3.

1.2.3 Delayed cell death

The mechanisms discussed above lead to either early or delayed cell death. In neonatal hypoxia-ischemia early neuronal death is mostly necrotic and confined to the ischemic core, while the prolonged and delayed neuronal death seen for days and weeks after the HI insult seems related to programmed cell death in surrounding areas that have only suffered a mild HI (Johnston *et al.* 2011). This temporal pattern of early and delayed cell death is different in different brain regions. In a rat animal model of hypoxia-ischemia, neuronal death in cerebral cortex, subcortical and periventricular white matter and striatum is largely necrotic with a rapid onset, whereas neuronal death in thalamus and hippocampus is delayed and largely

apoptotic (Nakajima *et al.* 2000; Northington *et al.* 2001a; Northington *et al.* 2001b; Northington *et al.* 2001c). It also seems clear that cellular death following HI is not either necrosis or apoptosis, but that a continuum from necrosis to apoptosis exists with hybrid forms of cell death, such as programmed necrosis (Martin *et al.* 1998). This continuum is especially present in neonates (Nakajima *et al.* 2000; Northington *et al.* 2007). The long and delayed injury process following hypoxia-ischemia has presented a possible window of opportunity for therapeutic intervention (Nakajima 2000, Vannucci 2004, Northington 2005), but it is still unclear how this process of delayed neuronal death is triggered and sustained. However, inflammation seems to play a role in this delayed cell death following hypoxia-ischemia.

1.2.4 Inflammation

Hypoxia-ischemia triggers a robust inflammatory response in the neonatal brain involving different cellular types, inflammatory mediators and intracellular signalling mechanisms. The inflammatory response is a complex balance between different elements. It is thought to be beneficial as a host defence against pathogens and to promote angiogenesis, tissue remodelling and regeneration after an injury. However, with insults of a certain magnitude, the response seems to get out of hand and become destructive.

The initiating factor of the inflammatory response after HI is the up-regulation of inflammatory mediators: Pro-inflammatory cytokines, such as Interleukin 1β (IL-1β) and tumour necrosis factor-α (TNF-α) have distinct increased expression early (<3 hours) and later (around 24 hours) after hypoxia-ischemia (Saito *et al.* 1996; Bona *et al.* 1999). They promote expression of other cytokines and activation of adhesion molecules leading to attraction and activation of immune cells (Vexler *et al.* 2006). Experimental induction of such cytokines has been shown to increase brain injury, while inhibition have reduced brain injury after HI (Vexler *et al.* 2006). Transcriptional factors, such as Nuclear Factor kappa Beta (NF-κB), are also induced after hypoxic ischemic insult and involved in regulating inflammation in a complex manner. For instance, NF-κB promote cell survival by up-regulation of anti-apoptotic factors in the early phase after HI, but promote expression of a number of pro-inflammatory cytokines and pro-apoptotic factors in the late phase leading to increased apoptosis and inflammation (Nijboer *et al.* 2008b, 2008a).

Chemo-attractant cytokines or chemokines are also expressed after HI and are thought to promote the activation and migration of macrophages, monocytes and neutrophilic leucocytes to the lesion site (Cowell *et al.* 2002; Vexler *et al.* 2006). The increased activation of adhesion molecules in vascular endothelium further promotes the migration of leucocytes from the blood stream and into the brain. Macrophage invasion usually occurs between three and six

days after ischemia and is more pronounced if there are large areas of necrosis and the blood brain barrier (BBB) is disrupted (Barron 1995). These cells contribute to the inflammation after HI by secretion of cytokines and free radicals, but also with phagocytosis of dead cells and debris (Vexler *et al.* 2006). In severe hypoxic-ischemic insults, the high inflammatory activity in combination with astrocyte death leads to disruption of the BBB. The ensuing oedema is vasogenic in nature and is caused by increased brain water content as a consequence of the increased leakage of proteins from blood plasma into the extracellular space (Hudome *et al.* 1997; Vannucci and Vannucci 2005). Animal studies have shown that brain oedema appear early in the first hours after HI. Depending on the severity of HI, brain oedema reaches a maximum between 36 and 72 hours, but may be present up to 6 days after HI (Vannucci and Vannucci 2005; Volpe 2008).

Microglia

More important than recruitment of circulating leucocytes is the activation the microglial cell – the resident macrophage of the CNS. This is the only glial cell of the brain that originates from a blood cell line. In neonatal HI injury it is one of the key elements of the inflammatory response. Shortly after hypoxia-ischemia resting, ramified microglia become activated and transform into round, amoebic shaped macrophages and start to proliferate and migrate towards the lesion sites (Bona *et al.* 1999; Chew *et al.* 2006). Microglia is activated through several mechanisms, including cytokines, release of intracellular contents after necrosis, disruption of tissue or invading microorganisms like bacteria (Chew *et al.* 2006). Activated microglia up-regulates and presents several surface molecules necessary for antigen presentation, molecules that facilitate migration and surface receptors. Stimulation of the latter enhances the production and secretion of chemokines and cytokines, which potentiates the inflammatory response and leads to more activation of microglial cells. Activated microglia also secretes matrix metalloproteinases (MMP), enzymes that participate in the disruption of the BBB, but primarily degrade the extracellular matrix and thereby allow phagocytosis of damaged tissue. The efficiency of phagocytosis is further increased by activation of the complement cascade (Cowell *et al.* 2003; Chew *et al.* 2006). Phagocytosis of debris and dead cells starts approximately 24 hours after the hypoxic-ischemic insult (Barron 1995). It is an important function of the microglia and is thought to limit the inflammatory reaction to the lesion site. However, in neonatal hypoxia-ischemia, the activated microglia seems also to have a more damaging role through production of free radicals and prostaglandins.

Activated microglia produce free radicals like superoxide ($O_2^{\cdot -}$) and nitric oxide (NO) that are neurotoxic (Li *et al.* 2005; Block *et al.* 2007). These free radicals also react to form the powerful oxidant peroxynitrite (ONO_2^-) which is an even more neurotoxic compound and has been

implicated as an important factor in neuronal and oligodendrocyte death, inducing both apoptotic and necrotic cascades (Li *et al.* 2005).

Prostaglandins are produced from arachidonic acid (AA) by cyclooxygenase (COX-1 or COX-2) in response to high intracellular calcium caused by the energy failure due to hypoxia-ischemia, mainly in microglia and astrocytes. Prostaglandin metabolites have a role in regulating blood flow and can cause vasodilatation and vasoconstriction, but are also potent inflammatory mediators and can be neurotoxic. This diversity may in part be related to the location and what type of prostaglandin metabolite that is produced. COX-1 is considered to provide a baseline level of prostaglandin and is located in most cell types, and the prostaglandin metabolites downstream of COX-1 seem to have beneficial effects in brain ischemia. COX-2 is induced by ischemia and inflammation and its downstream metabolites have more deleterious effects (Vexler *et al.* 2006). All these mechanisms contribute to the prolonged inflammation and microglia activation seen in brain injury in the neonatal period.

Astrogliosis

It is increasingly recognised that astrocytes play an important role in brain inflammation following hypoxia-ischemia. In response to CNS injury, astrocytes become reactive; a process named astrogliosis. It is characterized by the appearance of proliferating astrocytes that are gemistocytic in appearance: They have swollen cytoplasm, eccentric nucleus and show increased intracellular content of intermediate filament proteins, especially glial fibrillary acidic protein (GFAP). Increased GFAP is considered a hallmark of astrogliosis and found to be a sensitive biomarker for CNS injury (Zhang *et al.* 2010). Astrogliosis is seen somewhat later than the activation of microglia, but occurs within 24 hours after hypoxic-ischemic injury (Ohno *et al.* 1995; McRae *et al.* 1996). Microglia play an important role in triggering and modulating astrogliosis, and it has been shown that pro-inflammatory cytokines released from microglia induce astrogliosis (Bush *et al.* 1999; Zhang *et al.* 2010). Astrogliosis, with the formation of gliotic scars is thought to limit and define the lesion site. The reactive astrocytes contribute to maintaining and repairing the BBB after CNS injury, and they play a crucial role in regulating glutamate and restrict glutamate excitotoxicity to neurons and oligodendrocytes. Increased neuronal death and exacerbated tissue degeneration have been shown in the absence of reactive astrocytes (Bush *et al.* 1999; Zhang *et al.* 2010). Also, under normal conditions, astrocytes provide support and guide axonal growth after CNS injury. However, the glial scares formed by astrogliosis can inhibit axonal regeneration since they, instead of providing guidance, represent physical barriers to the growing axons (Privat 2003). Furthermore, astrogliosis can also be damaging to neurons and other cells and exacerbate CNS damage: Reactive astrocytes secrete inflammatory mediators, such as cytokines, chemokines and iNOS, which contribute to the inflammatory response and neuronal and oligodendrocyte

death by mechanisms described above (Vexler *et al.* 2006; Zhang *et al.* 2010). Inflammatory stimulation of TNF-α receptors on astrocytes can also inhibit glutamate transporters, leading to increased glutamate in the extracellular space and synapses, and increased excitotoxicity (Pickering *et al.* 2005).

1.3 Interventions and treatments for hypoxic-ischemic brain injury

1.3.1 Current treatment regimes

The aim of treatment is to minimize mortality and to reduce the short and long-term damage to the nervous system with minimal adverse effects. Apart from hypothermia, the treatment options for hypoxic-ischemic injury are limited, and current clinical practice is largely based on supportive therapy: inotropic support and fluids to maintain adequate blood pressure and circulation, correction of metabolic acidosis, correction of hypoglycemia, seizure control, and respiratory support with supplementary oxygen to maintain adequate oxygen saturation in tissue.

Hypothermia is increasingly being adopted into standard treatment regimes for hypoxic-ischemic encephalopathy. In several animal studies, hypothermia has been shown to be neuroprotective (Jacobs and Tarnow-Mordi 2010). The mechanisms are uncertain, but may include reduction of metabolic rate, reduced the level of secondary cellular energy failure (Thoresen *et al.* 1995), reduced excitotoxicity, reduced production of free radicals in brain (Globus *et al.* 1995) and reduced apoptosis (Edwards *et al.* 1995). Although, several early clinical studies failed to show any positive effects on outcome after treatment with hypothermia (McGuire 2007), recent clinical randomized control trials and meta-analyses show reduced mortality and a reduction in moderate to severe disabilities around 2 years after birth (Shankaran *et al.* 2005; Edwards *et al.* 2010; Jacobs *et al.* 2011). Although children treated with hypothermia have increased risk of bradycardia and coagulopathy and are in need of more inotropic support and blood transfusions (Eicher *et al.* 2005), the current view is that hypothermia, either by whole body cooling or selective head cooling, is safe in term or near-term neonates. In preterm born children, there is concern that hypothermia may be too dangerous due to complications like enhanced bleeding. It is therefore a great need for continued research into neuroprotective therapies, especially for preterm infants.

1.3.2 Oxygen supplementation during resuscitation – a detrimental intervention?

Although it is widely accepted that too much oxygen in the perinatal period can be damaging, there has been a longstanding controversy of whether to resuscitate asphyxiated children with oxygen or air. The rationale behind giving oxygen supplementation during resuscitation is to rapidly reverse the tissue hypoxia. However, high blood oxygen concentrations in the reperfusion phase have been shown to reduce cerebral blood flow (Davis *et al.* 2004), lead to

increased oxidative stress (Kutzsche *et al.* 2001; Davis *et al.* 2004), disrupt the BBB (Witt *et al.* 2008) and deplete pre-oligodendrocyte glial progenitors present in the cortex (Koch *et al.* 2008). Recently (2010), clinical guidelines have been changed and now recommend not more than 40% supplemental oxygen at the start of resuscitation, only to be increased if no adequate response is achieved. Evidence from both animal and clinical studies suggest that hyperoxia during resuscitation of neonates increases mortality and morbidity (Davis *et al.* 2004; Saugstad 2005; Saugstad *et al.* 2008), but literature on long term effects of oxygen treatment on brain injury development is sparse.

1.3.3 Treatments to reduce delayed cell death and inflammation

Due to the prolonged and delayed apoptotic cell death after hypoxic-ischemic injury, interventions aiming to ameliorate apoptosis by direct pharmacological inhibition have been sought. Several different drugs and targets have been investigated in animal models using inhibition of apoptotic pathways (Cheng *et al.* 1998; Han *et al.* 2002; Feng *et al.* 2003a, 2003b; Feng and LeBlanc 2003; Joly *et al.* 2004; Yin *et al.* 2006; Nijboer *et al.* 2007; Renolleau *et al.* 2007; Nijboer *et al.* 2010; Nijboer *et al.* 2011). Inhibition of apoptosis may provide neuroprotection after HI. However, apoptosis is a necessary mechanism for the natural growth, development and maturation of the neonatal brain, and the consequences for the subsequent brain development or risk for malignancies are still unclear (Northington *et al.* 2005).

As discussed above, the inflammatory response contributes to cell death after HI, and inhibition can therefore be beneficial. Corticosteroids have anti-inflammatory effects and may also reduce cerebral oedema, but the results from animal studies and clinical trials are conflicting. Antenatal steroids may reduce HI brain injury, but is also associated with reduced myelination and atrophy of brain regions (Whitelaw and Thoresen 2000). Current clinical data suggests that corticosteroids do not improve neurological outcomes (McGuire 2007). As discussed above, cytokines play an important role in initiating and sustaining the inflammatory response. Inhibition of cytokine production and their effects are therefore possible routes to neuroprotection. The IL-1 receptor antagonist IL-1ra has been shown to reduce HI brain injury in adult rodents (Martin *et al.* 1994; Loddick and Rothwell 1996; Mulcahy *et al.* 2003), the same has been shown for IL-6 (Loddick *et al.* 1998). In addition to the antioxidative effects of allopurinol, it has also been shown that allopurinol depletes neutrophilic leucocytes, which in itself is neuroprotective (Hudome *et al.* 1997; Palmer *et al.* 2004). Recently a multicenter randomized placebo controlled trial was initiated to look at the effect of antenatal allopurinol on brain damage after birth asphyxia (Kaandorp *et al.* 2010).

The second-generation tetracyclines; doxycycline and minocycline have been shown to exhibit anti-inflammatory effects in addition to their anti-bacterial properties (Buller *et al.* 2009) and have both been investigated for possible neuroprotection after brain hypoxic-ischemic injury. The neuroprotective effect of doxycycline was first shown by Clark *et al.* (1994) in ischemic brain injuries in adult rabbits, and a neuroprotective effect of minocycline in neonatal HI was demonstrated by Arvin *et al.* (2002). Several reports have then followed showing neuroprotective effects of minocycline and doxycycline in rat models of hypoxic-ischemic brain injury, mainly through inhibition of microglial activation and anti-apoptotic mechanisms (Jantzie *et al.* 2005; Cai *et al.* 2006; Fan *et al.* 2006; Jantzie *et al.* 2006; Carty *et al.* 2008; Jantzie and Todd 2010; Wixey *et al.* 2011). However, most studies have focused on short-term effects, up to seven days after HI. It is therefore uncertain how doxycycline affects the injury development in the long term and if the early neuroprotective effects can be extrapolated to a long term follow-up. No one has so far used non-invasive methods to follow and evaluate the long-term effect of anti-inflammatory treatments of hypoxic-ischemic brain injury. Such methods, like magnetic resonance imaging, may provide better insight to the effect of treatment on injury development, brain maturation and development and to the pathophysiological processes underlying the delayed dell death and injury after hypoxia-ischemia.

1.4 Magnetic resonance in neonatal hypoxic-ischemic brain injury

Magnetic resonance imaging (MRI) has become an important clinical tool and is the preferred imaging modality for assessment of neonatal hypoxic-ischemic brain injury (Volpe 2008). In this setting, the principal use of magnetic resonance (MR) is to provide early diagnosis so that appropriate treatment can be initiated and to detect lesions that allow prediction of long term prognosis and outcome (Robertson and Wyatt 2004). One primary use of MRI is to differentiate between hypoxic-ischemic injuries and those caused by for instance arterial stroke, venous thrombosis, intraventricular hemorrhage, traumatic brain injury or infection that may cause similar symptoms and signs. In the following paragraphs, MR in relation to hypoxic-ischemic brain injury in neonates will be discussed.

1.4.1 MR in term neonates

MRI in the acute phase of neonatal brain injury has mostly been restricted to the term or near-term neonates with signs suggestive of hypoxic-ischemic brain injury. In this setting, diffusion weighted imaging is the most sensitive imaging method, and restricted diffusion in affected areas may be seen as early as in the first hours after the insult. However, the signal on diffusion weighted images may normalize during the first 24-48 hours if the injury is mild, and usually normalizes in more severely injured areas during the first week. So far, early diffusion MR has not been shown to be as good a prognostic tool, as it has been in adult stroke

(Robertson and Wyatt 2004). Abnormalities on conventional MRI such as T_1- and T_2-weighted images are usually detectable 3 to 4 days after the hypoxic-ischemic insult. Conventional MRI in the first 48 hours may however be misleading as they mostly appear normal even in the presence of severe HI injury. The sensitivity of conventional MRI in detecting lesions that are correlated with adverse outcome increases with time after birth. Conventional MRI is therefore most appropriately performed towards the end of the first week after HI (Robertson and Wyatt 2004). The patterns of injury on both early diffusion MRI and later conventional MRI are closely correlated with the underlying pathologies and are good methods for differentiating between focal and global injuries (Volpe 2008). However, even though the sensitivity of MRI may be good, the specificity of MRI to predict adverse outcomes has been poor (Thayyil *et al.* 2010). The finding on MRI that is most predictive for poor outcome is signal change in the posterior limb of the internal capsule (Robertson and Wyatt 2004).

Magnetic resonance spectroscopy (MRS) with ^{31}P and ^{1}H have on the other hand proved to give valuable diagnostic and prognostic information in the very early phase (Robertson and Wyatt 2004). ^{31}P MRS can give valuable information about the energy failure following hypoxic-ischemic insults with reduced levels of phosphocreatine (PCr) after approximately 8 hours and can also be used to measure the increase in intracellular pH (Volpe 2008). Increased lactate on ^{1}H MRS is an abnormal finding in the first 24 hours after HI in near-term or term children and carries a bad prognosis together with reduced N-acetylaspartate (NAA). Increased α-glutamate /glutamine peaks in basal ganglia are also correlated with increased severity of the injury. Furthermore MRS have shown that abnormal brain metabolism can persist for months to years in infants with severe outcome after hypoxic-ischemic brain injury (Robertson and Wyatt 2004).

1.4.2 MR in preterm neonates

Also in preterm children, restricted diffusion in affected areas is an early finding, but usually normalizes within the first 10-12 days. Increased signal on T_1-weighted images, reflecting hemorrhagic necrosis may also be present (Osborn 2007). However, the clinical instability of preterm born children does not usually allow MRI to be performed early and is usually postponed until weeks after birth. A challenge with MRI in the preterms is that the signal on MRI and the configuration of the proton MR spectra are altered with gestational age as the brain matures. One of the underlying mechanisms for this signal change is the maturational development of white matter that occurs in the perinatal period (Volpe 2008). This makes the recognition of abnormal signal changes and distinction from normal maturational changes challenging. One approached has therefore been to image the prematurely born infants at term equivalent age. Ventricular dilation, periventricular volume loss, cystic changes, or more frequently diffuse white matter signal may be found in these premature infants (Osborn 2007).

Such white matter abnormalities as diffuse excessive high signal intensity (DEHSI) in cerebral white matter on T_2-weighted images have been correlated with altered diffusion properties, and is thought to reflect the pathological state of diffuse non-cystic PVL (Volpe 2008; Cheong *et al.* 2009). However, this view has been challenged, as these white matter signal abnormalities might also reflect a prematurity related developmental phenomenon (de Bruine *et al.* 2011).

1.4.3 MRI in rodent models of neonatal hypoxic-ischemic brain injury

Advantages of animal models are the possibilities to control experimental conditions (e.g. timing and magnitude of the insult), examine tissue and cellular reactions, measure biochemical substrates in the brain and test the effects of potential interventions and treatments. However, since the evaluation of tissue, cellular and biochemical processes mostly rely on *ex-vivo* methods, most studies in animal models of neonatal hypoxia-ischemia are limited to data on only one time-point per animal. One great advantage of using MRI in such studies is the possibility of repeated non-invasive examinations and measurements that allow longitudinal studies of the pathophysiological processes. By combining longitudinal MRI and *ex-vivo* techniques, such as immunohistochemistry, it is also possible to extract new knowledge of the tissue changes underlying the signal changes on MRI.

In recent years, MRI has been increasingly used in rodent models of neonatal hypoxic-ischemic brain injury to study the pathophysiology and injury development (see Table 1.1). The majority of the first of these MRI studies were focused on imaging during and very early after HI. Using primarily T_2-weighted and diffusion weighted imaging, they showed that HI induced restricted diffusion and increased tissue T_2 during hypoxia. This was followed by more or less normalization of tissue diffusion and increasing T_2 in the following days. These changes in diffusion and T_2 reflected the severity of the insult (Rumpel *et al.* 1995; Albensi *et al.* 1998; Tuor *et al.* 1998; Malisza *et al.* 1999; Tuor *et al.* 1999; Qiao *et al.* 2004; Meng *et al.* 2005; Meng *et al.* 2006). Some studies have also tried to correlate early changes on diffusion and T_2-weighted imaging and spectroscopy to later infarct volumes and shown that early decreased NAA and increased lactate, as well as restricted diffusion 24 hours after HI correlated with infarct volumes (Malisza *et al.* 1999; Wang *et al.* 2006; Wang *et al.* 2007; van de Looij *et al.* 2011). The temporal injury development after HI has also been examined. Studies have shown how the injury increases during the first days (Albensi *et al.* 1998; Tuor *et al.* 1998; Stone *et al.* 2008), and the evolving brain atrophy and development of porencephalic cyst that results in the following weeks are also evident in some studies (Ten *et al.* 2004; Mishima *et al.* 2005; Stone *et al.* 2008; Yang *et al.* 2008a; Yang and Wu 2008b). However, few of these studies have tried to quantify and evaluate this development from the first days to the final injury several weeks after. With the development and availability of diffusion tensor imaging, focus has

turned to white matter in the most recent years. Several studies have shown how white matter development is affected by hypoxia-ischemia in the weeks after the insult. (Stone *et al.* 2008; Wang *et al.* 2008; Chan *et al.* 2009; Wang *et al.* 2009b; Bockhorst *et al.* 2010).

MRI is increasingly being used in new ways as a non-invasive tool to study molecular events and cellular involvement in the disease process. One example is the use of DTI to study changes in tissue microstructure in cortex following HI (Sizonenko *et al.* 2007). Another example is the correlation between diffusion changes in white matter and glial activation 24 hours after HI (Lodygensky *et al.* 2011).

Use of new MRI methods to evaluate tissue microstructure in combination with longitudinal study design, can give new knowledge of the processes and cellular involvement in the delayed cell death and injury following HI. MRI can also be an excellent tool to evaluate the effect of interventions and treatments on this delayed injury process.

Table 1.1 Overview of MRI studies in rodent models of neonatal hypoxia-ischemia

Study	Animal model, time of HI	MRI methods	MRI time-points	Main findings
Rumpel et al 1995	P7 rats, uCCA ligation and 8% O_2 for 0, 15, 30 or 60 min.	DWI, T_2W	2 hours after HI and up to 7 days	Decreased ADC and T_2 with prolonged duration of hypoxia.
Albensi et al 1998	P7 rats, bilateral uCCA ligation and 30-45min 9% O_2.	T_1W, T_2W	1-6, 24, 48 and 72h after HI	Increased lesion size from 1.5h to 48 hours after HI.
Tuor et al 1998	P7 rats, uCCA ligation and 2h 8% O_2	DWI, T_2W	Before, during, 24, 48 and 72h after HI	Increased intensity on DWI and T_2W in the second hour of hypoxia, with decreased hyperintensity on DWI and increased hyperintensity on T_2W between 24 and 72 hours post HI.
Tuor et al 1999	P7 rats, uCCA ligation and 2h 8% O_2. Pre-treatment with dexamethasone	DWI, T_2W	During hypoxia and immediately after HI	Hyperintensity on DWI and T_2W during hypoxia with some recovery after in controls, but not in dexamethasone treated.
Malisza et al 1999	P6 and P7 rats, uCCA ligation and 2h 8% O_2	MRS, T_2W and DWI	0h, first hour after HI, 24 and 48h after HI	Early decreased NAA and elevated lactate correlated with increased infarction on T_2W and DWI.
Ten et al 2004	P7 mice, uCCA ligation and 20min 8% O_2	T_2W	10 weeks after HI	Large ipsilateral brain atrophy with porencephalic cyst formation and contralateral ventriculomegaly
Qiao et al 2004	P7 rats, uCCA ligation and 45-50 or 90 min of 8% O_2	T_1 and T_2 maps	24hours after HI	Increased T_1 and T_2 in white matter and less so in grey matter corresponding to the severity of the insult.
Mishima et al 2005	P7 rats, uCCA ligation hypoxia	T_1W	5, 9 and 57 weeks after HI	Slowly progressive evolution of brain damage.

Table 1.1 Continued

Study	Animal model, time of HI	MRI methods	MRI time-points	Main findings
Meng et al 2005	P7 rats, uCCA ligation and 1-2 hours of 8% O_2	T_2 and ADC maps	Before HI, last 5-10 min of HI and 1 or 24h after HI	Increased T_2 and decreased ADC at end of HI. Partial recovery of ADC but increasing T_2 to 24h after HI
Meng et al 2006	P7 rats, uCCA and 45-50min 8% O_2	Maps of T_1, T_2 and ADC, CBF	Before HI, 1, 24, 48 h and 7 days after HI	Increased T_1, T_2 and ADC and decreased CBF in white matter over time from HI, with maximum at 48 hours and normalization on day 7 after HI
Wang et al 2006	P7 rats, uCCA ligation and 2.5 hours of 8% O_2	DWI, T_2W	1-2 hours and 4 days after HI	Lesion volume on DWI 1-2h after HI correlated with, but underestimated histological infarct volume.
Wang et al 2007	P7 rats, uCCA ligation and 2.5 hours of 8%	DWI, T_2W	24h and 10 days after HI	Lesion volume on DWI 24h after HI is a good predictor of infarct volume 10d post HI
Sizonenko et al 2007	P3 rats, uCCA ligation and 30min 6% O_2	DTI	1 or 3 days after HI	Difference in ADC and FA between deep and external cortical layers with maturational reduction from P3 to P6. HI gave reduced ADC and FA which persisted to P6.
Yang et al 2008a	P7 rats, uCCA ligation and 3 hours of 8% O_2	MEMRI, T_2W, DWI	3h, 1, 2, 3, 7, 14, 21, 28 and 49 days after HI	Manganese-enhancement in cortex, basal ganglia and hippocampus from day 3 and became more localized pericystically in basal ganglia and cortex day 7 and diminished thereafter. ME found to correlate with GS and Mn-SOD expression.
Yang and Wu 2008b	P7 rats, uCCA ligation and 1 hour of 8% O_2	MEMRI, T_2W, DWI	3h, 1, 2, 3, 7, 8, 14 and 21 days after HI	Manganese-enhancement of lesion in grey matter detected from day 3 to day 21 after HI. Corresponded to GS and Mn-SOD on histology
Wang 2008	P7 rats, uCCA ligation and 50 or 90 min of 8% O_2	T_2W and DTI	1 and 7 days post HI	Changes in white matter diffusivity suggestive of reduced myelination in mild insult and axonal injury in severe insult.

Table 1.1 Continued

Study	Animal model, time of HI	MRI methods	MRI time-points	Main findings
Stone et al 2008	P7 rats, uCCA ligation and 45 min of 8% O_2	Ex-vivo DTI	1, 4, 6, 14, 21 or 35 days after HI	Severe and rapid volume loss, but regional differences. Axonal injury evident after 24h. HI interrupts normal developmental changes in white matter diffusivity
Chan et al 2009	P7 rats, uCCA ligation and 2h 8% O_2	T_2W, DTI	10 weeks after HI	Large porencephalic cyst. Changes in diffusivity and location of white matter tracts suggestive of white matter reorganization
Wang et al 2009	P7 rats, uCCA ligation and 50 min of 8% O_2	T_2W, DTI	1, 7, 14, 10 and 90 days after HI	Increasing FA, reducing radial diffusivity with time after HI. Lower FA and higher radial diffusivity in ipsilateral hemisphere white matter.
Bockhorst et al 2010	P7 rats, uCCA ligation and 90min 8% O_2, + 100% or 21% O_2	T_2W, DTI	1 day, 1 and 3 weeks after HI	Hyperoxia increased lesion volume and radial diffusivity, with most significant differences after 3 weeks.
van der Looij 2011	P3 rats, uCCA ligation and 30min 6% O_2	MRS, T_2W	5h, 1, 8 and 22 days after HI	Lesion size 6 hours after HI correlated with long-term cortical loss. Reduced metabolites and increased lactate after 24h, with minor metabolic changes after 22 days.
Lodygensky et al 2011	P7 rats, uCCA ligation and 45 min of 8% O_2	T_1W, T_2W, T_2 and ADC maps	24 hours after HI	Increased signal in hippocampus and adjacent white matter on T_2W. Reduced ADC in hippocampus, but was increased ADC in adjacent white matter and may be related to glial activation

uCCA: unilateral common carotid artery, T_2W: T_2-weighted image, T_1W: T_1-weighted image, DWI: Diffusion weighted images, DTI: Diffusion tensor imaging, ADC: Apparent diffusion coefficient, MEMRI: Manganese-enhanced MRI, FA: fractional anisotropy.

Chapter 2 Magnetic resonance imaging

Magnetic resonance imaging (MRI) is based on the principles of magnetic resonance first described in 1946 by Bloch *et al.* (Bloch *et al.* 1946) and Purcell *et al.* (Purcell *et al.* 1946). In the 1970'ies Lauterbur (Lauterbur 1973) and Mansfield (Mansfield and Grannell 1973) described the principles of how to create images from the magnetic resonance signal. These achievements subsequently led to the development of MRI as the valuable tool for medical imaging as we know it today. In the following chapter some of the principles of MRI will be outlined and a more detailed introduction to some of the MRI techniques used in the experiments of this thesis will be given.

2.1 Principles of magnetic resonance

Atoms with uneven mass numbers have nuclear spins with a proportional magnetic dipole moment. ^{1}H, ^{13}C, ^{19}F, ^{21}Na and ^{31}P are examples of such atoms, with the proton (^{1}H) being by far the most frequently used in MRI due to its abundance in biological tissue. Each nuclear spin acts as a small magnet (Haacke 1999). Under normal conditions such nuclear spins are randomly oriented (Figure 2.1A), but when placed in a static magnetic field (B_0), they align either parallel or anti-parallel to the direction of the field (Figure 2.1B) and precess around this axis with a frequency that is dependent on the nuclear properties and the strength of the magnetic field (Figure 2.1C).

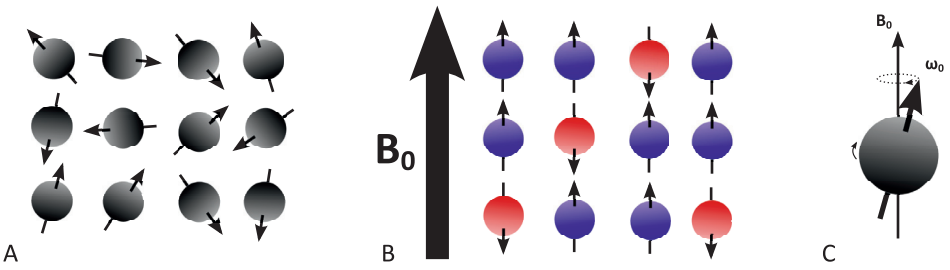

Figure 2.1: Nuclear spins outside (A) and inside (B) a magnetic field, where they precess (C).

This frequency is called the Larmor frequency, and is given by:

$$\omega_0 = \gamma B_0 \qquad \text{Eq. 2.1}$$

where γ is the gyromagnetic ratio and B_0 is the magnetic field strength. Spins that align parallel to the magnetic field have a low-energy state, whereas spins that align anti-parallel have a high-energy state. At thermal equilibrium more spins are in the low-energy state, and the small difference in energy between the parallel and the anti-parallel states increases with the strength of the magnetic field, and can be expressed as:

$$\Delta E = \hbar\omega_0 = \hbar\gamma B_0 \qquad \text{Eq. 2.2}$$

where ΔE is the energy difference and $\hbar$ is Planck's constant. The transition of a nuclear spin from a low energy state to a high energy state can be achieved by absorbing energy from a radio frequency pulse (RF-pulse). In order for the spins to absorb the energy, the pulse must be applied at the Larmor frequency (ω_0), also termed the resonance frequency. When the spin switches from a high energy state to a low energy state, energy is emitted at the same frequency.

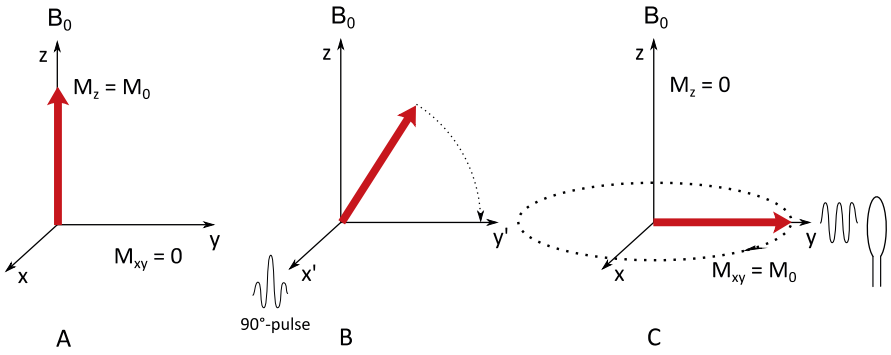

Figure 2.2: Visualisation of the behaviour of the magnetisation vector during RF-pulse excitation in a coordinate system rotating at the Larmor frequency.

At thermal equilibrium there are more spins parallel to the axis of the magnetic field, and since each spin acts as a magnet, this creates a net magnetization (M_0) which is parallel to the magnetic field B_0, along the z-axis (Figure 2.2A). In a classical description of MR, the orientation of this magnetic vector can be manipulated by an RF-pulse at the Larmor frequency – a process called excitation. In a coordinate system that rotates with the Larmor frequency (x',y',z), an on resonance RF-pulse that is applied in right angle to the magnetic field (B_0) creates a new magnetic field (B_1^+) along the x'-axis perpendicular to the B_0 field. Viewed in the rotating coordinate system, the spins will then start precessing around the x'-axis, which results in

tilting of this magnetic vector towards the y'-axis in the x'-y' plane (Figure 2.2B). The duration of the RF-pulse determines how far into the x'-y'-plane the magnetization vector is tilted. The magnetization vector M_0 can be decomposed into a net magnetization in the x'-y'-plane given by M_{xy}, and a magnetization along the z-axis referred to as M_z. If the magnetization vector is tilted all the way into the x'-y'-plane, this is referred to as a 90°-pulse. In this situation $M_{xy} = M_0$ and $M_z = 0$. In the laboratory coordinate system (x,y,z), this magnetic vector rotates around the z-axis, and will create an oscillating magnetic field that can induce a current in a coil placed in the x-y-plane (Figure 2.2C). This is how the MR signal is created.

2.1.1 Relaxation mechanisms

Immediately after a 90° pulse the net magnetization vector is in the x-y-plane (Figure 2.3A). Subsequently the system tends to return to thermal equilibrium by a process termed longitudinal relaxation or T_1-relaxation. Energy is released from the spins into the surrounding lattice. The ability of the lattice to absorb this energy determines the time it takes to return to equilibrium. During this process, the net magnetization vector returns to the z-axis at a rate determined by the T_1 of the spin population (Figure 2.3B). This gradually increases M_z. When thermal equilibrium has been re-established, all magnetization is along B_0 (Figure 2.3C).

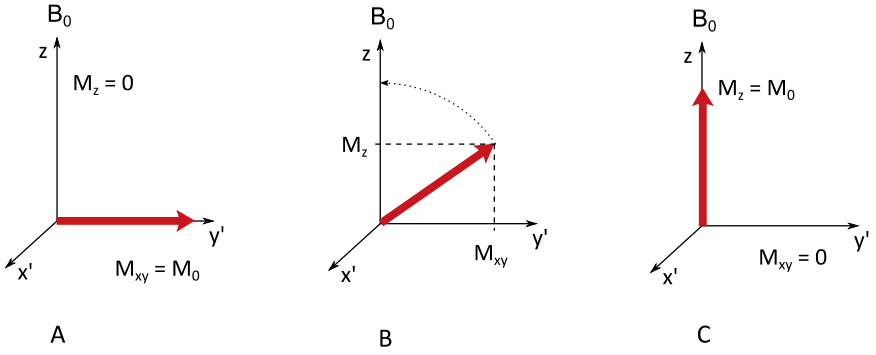

Figure 2.3: Longitudinal or T_1-relaxation.

Simultaneously, another process occurs that reduces the detectable signal in the x-y plane faster than that dictated by the T_1-relaxation. This is termed transverse relaxation, or T_2*-decay. Immediately after an RF-pulse, the rotation of the spin population around the z-axis is highly coordinated and reads as one magnetization vector in the x-y-plane (Figure 2.4A). However, due to small differences in precession frequency, spins rotate at slightly different speeds. Figuratively this can be described as many magnetization vectors that in the beginning are aligned, or in phase, and together act as one large vector. With time they get out phase with each other and instead oppose and null each other out (Figure 2.4B-C). The result is a

gradually decreasing current induced in the coil as the spins de-phase, and hence a decreasing signal is detected. This is called the free induction decay (FID) signal.

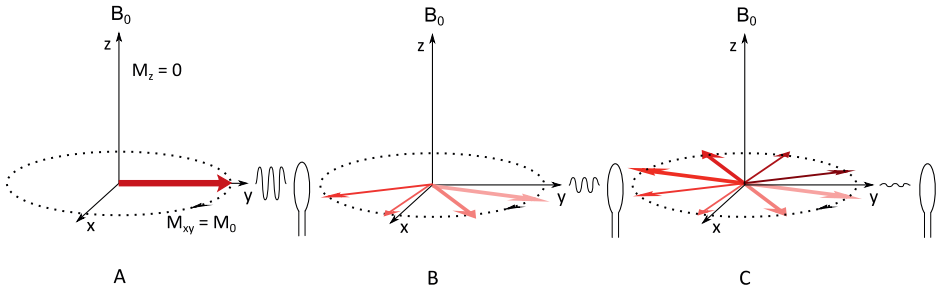

Figure 2.4: Transverse or T_2-relaxation.

The de-phasing of the spin populations causing this T_2*-decay has two origins. One is the local time-varying disturbances in the microscopic magnetic field associated with the magnetic properties of neighbouring atoms. This is termed spin-spin relaxation, or T_2-relaxation, and the de-phasing effect caused by this cannot be reversed. The other cause of de-phasing is the static inhomogeneities of the external magnetic field, which can be enhanced by magnetic material, like iron in the tissue. This type of de-phasing is fast and called T_2'-relaxation and can be reversed. By applying a 180°-pulse at time δ after a 90°-pulse, spins will be flipped 180° in the x-y-plane and start to re-phase at the same rate as they de-phased. At time 2δ they will be in phase and again act as one large magnetization vector and form what is called an echo. This pulse-sequence just described is called a spin-echo sequence, and the time between the excitation pulse and the echo is called the echo-time (TE). The magnitude of the signal created by the spin-echo will be given by the T_2-relaxtion time. In a gradient echo sequence, where the FID is de-phased and re-phased by the use of magnetic field gradients, the magnitude of the signal is dependent on the T_2*-decay. The relationship between T_2*-decay, T_2- and T_2'-relaxation is given by:

$$\frac{1}{T_2^*} = \frac{1}{T_2} + \frac{1}{T_2'} \qquad \text{Eq. 2.3}$$

A sequence can be repeated for more signal sampling (averaging) or for the purpose of creating images. The time between the first excitation pulse and the next is called the repetition time (TR).

2.1.2 MR imaging

The magnetic resonance signal can be spatially encoded by the use of magnetic gradients at different steps in the pulse-sequence (see Figure 2.5). When a gradient is applied to a static magnetic field, B_0, the location of the spin along the direction of the gradient field will determine its Larmor frequency. By applying a gradient (G_s) during excitation in the slice direction and tuning the excitation pulse to a specific range of frequencies, only spins that resonates within this frequency range will absorb the energy, resulting in a slice selective excitation. In a spin-echo sequence a gradient is then applied in another direction perpendicular to the G_s between the 90° and 180°-pulses. This introduces different phase to spins according to their position along the gradient and is thus called a phase-encoding gradient (G_p). By varying the gradient strength before each read-out of the signal (typically at each repetition in a spin-echo sequence) different phase encoding is achieved. Finally, a gradient is applied in the direction perpendicular to both G_s and G_p during readout of the echo. This read-out gradient (G_r) introduces frequency encoding of the detected signal, with a given frequency range corresponding to a given spatial location in that direction. The signal is sampled in a 2D k-space for each slice. Each horizontal line represents a different phase-encoding, while each point along the line represents the sampled signal at a given frequency range (see Figure 2.5A). In 3D imaging, the slice selective gradient is used to select a volume slab, and a phase gradient is also applied in the slice direction between the excitation pulse and the echo. The signal is thus phase encoded in two directions, and sampled in a 3D k-space. The encoded signal in k-space can be Fourier transformed into an image representing the spatially distributed amplitude of the MR signal.

There are different techniques of acquiring the signal and sampling k-space that can speed up image acquisition. One is to apply multiple 180°-pulses after the excitation pulse, resulting in multiple echos at different echo times. This can be used to estimate the T_2-decay, as the signal is slightly reduced with increasing echo-times. However, the multiple echos can also be given different phase-encoding and be used to sample different lines in k-space (see Figure 2.5B). Really fast acquisition can be achieved by sampling all k-space lines at once. One such technique is echo planar imaging (EPI), where a train of echos are created by rapid switching of the frequency-encoding gradient, while each echo is individually phase-encoded by rapidly turning the phase gradient on and off (see Figure 2.5C).

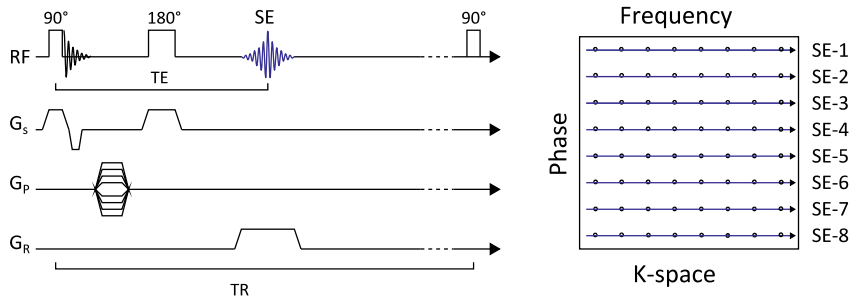

A: Spin echo

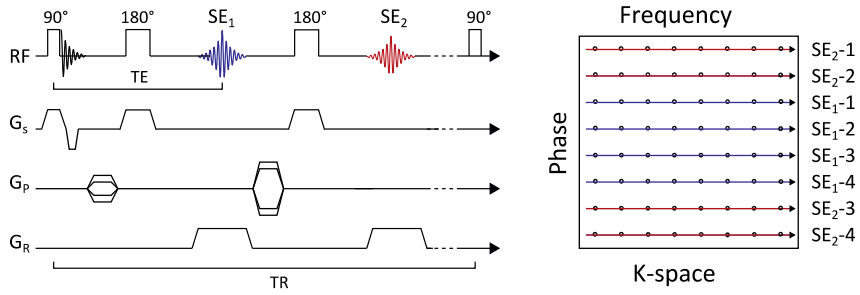

B: Fast spin echo or Rapid Acquisition with Relaxation Enhancement (RARE)

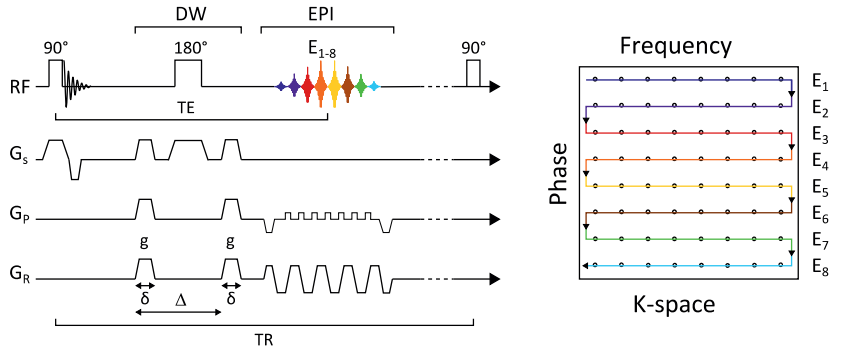

C: Echo planar imaging (EPI) sequence with Stejskal-Tanner diffusion weighting (DW)

Figure 2.5: Examples of pulse diagrams for different sequences with patterns of K-space sampling. A: Spin echo. B: Fast spin echo. C: Echo planar imaging with diffusion weighing. RF: radio frequency pulse. G_s: slice selective gradient. G_P: phase-encoding gradient. G_R: Frequency-encoding gradient. TE: echo time. TR: Repetition time. SE: Spin echo. DW: Diffusion weighting module: g: diffusion gradient slope. δ: diffusion gradient duration. Δ: time between the two diffusion gradients.

2.2 Tissue contrast and contrast agents in MRI

2.2.1 Intrinsic tissue contrasts in MRI

The proton (^{1}H) is by far the most abundant nucleus that can be used for MRI in biological tissue, and its tissue specific properties is the origin to the image contrasts in most MRI. For the sake of simplicity only proton MRI will therefore be discussed in the following sections.

There are primarily three basic tissue properties that are used to create contrast in MR images; the proton density (PD), the mean T_1 relaxation time and the mean T_2 relaxation time. Other intrinsic tissue properties that can be utilized for image contrast include flow and diffusion. PD, T_1 and T_2, will be discussed in this section and diffusion contrast later on in section 2.4.

The net magnetization, M_0, and signal intensity are directly proportional to the proton density in the tissue. Since most protons are found bound in water (H_2O), proton density largely depends on the tissue water content. For instance, cerebrospinal fluid (CSF) has high water content and a high PD, while bone has low water content and low PD. Proton weighting of an image can be achieved by using a sequence with a long repetition time (TR) between each relaxation pulse, allowing all protons to be relaxed back to the thermal equilibrium state before a new excitation, and a short echo time (TE) allowing little T_2 relaxation to occur before the signal is sampled.

T_1-relaxation originates as described above from energy transfer to the surrounding lattice of the proton and it is highly tissue dependent. For energy transfer to occur, the excited protons need to be exposed to a local magnetic field, for instance another nearby molecule, oscillating at the Larmor frequency. Most protons are bound in water molecules, which on a microscopic scale continuously changes orientation, or tumble. The tumbling rate of free water molecules is far more rapid than the Larmor frequency and makes energy transfer to neighbouring molecules inefficient. However, when water molecules are in the vicinity of large molecules like proteins they form temporary bonds that slow their tumbling rate. This makes energy transfer to the surroundings easier, hence reducing the average T_1 relaxation time of the water protons. Protons bound in other molecules, like hydrogen in fat, tumbles slowly and have more efficient energy exchange with the surrounding molecules. Fat has therefore a short T_1. T_1 weighting of an image can be achieved by using a short TR together with a short TE. The signal of the image will thus mainly

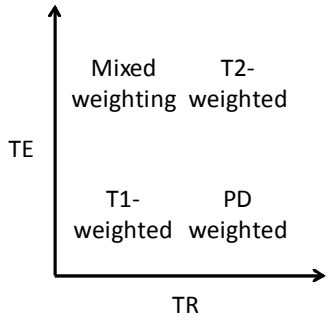

Figure 2.6 Relationship between sequence repetition time (TR) and echo time (TE) and image contrast.

come from the protons with short T_1 that have already relaxed before a new repetition of the excitation pulse. The short TE reduces the influence of T_2 relaxation on the signal.

Transverse relaxation times are also highly tissue dependent. As described above, transverse relaxation can be divided into spin-spin relaxation and T_2' relaxation mechanisms. The latter is caused by inhomogeneities in the static magnetic field and can be visualised by T_2*-weighting of the image. This is usually achieved by using a gradient echo MRI sequence. Spin-spin relaxation on the other hand is caused by interaction between neighbouring magnetic moments of nuclei and unpaired electrons. In slowly tumbling systems, like large molecules, high viscosity fluids and solids, T_2 becomes very short compared to T_1. In free fluids and fast tumbling systems, T_2 becomes long, but always shorter than T_1. T_2 weighting of images can be achieved by using long TR and relatively long TEs around the average T_2-time of the tissue.

2.2.2 Principles of contrast agents

The basic principle of a MRI contrast agents is to reduce relaxation times in specific tissue, hereby increasing tissue contrast. Today mainly two classes of contrast agents are in use; superparamagnetic and paramagnetic. Superparamagnetic substances such as iron oxides have large magnetic moments and create a large disruption in the local magnetic field. This causes primarily an extremely fast T_2 relaxation. The effect is far-reaching and the susceptibility effects reach into neighbouring tissue and is easily visualized in T_2*-weighted images. Paramagnetic substances such as Gd^{3+} and Mn^{2+}, have unpaired electrons in their outer shell, which in a magnetic field create magnetic moments larger than that of the nuclei spins. These substances create local fluctuating magnetic fields and have dipole-dipole interactions with surrounding protons. Both these mechanisms facilitate the relaxation of nearby protons. In pure water, the change in tissue relaxation is linear to the concentration of the contrast agent:

$$\Delta R_{1,2} = \Delta \frac{1}{T_{1,2}} = r_{1,2}[CA] \qquad \text{Eq. 2.4}$$

where $\Delta R_{1,2}$ is the change in either T_1- or T_2 relaxation caused by the contrast agent, $r_{1,2}$ describes the relaxation rate and [CA] is the concentration of contrast agent. In tissue, binding of the paramagnetic substance to larger molecules, like proteins, can increase the relaxation rates and further enhance tissue contrast. Paramagnetic substances reduce both T_1 and T_2 relaxation times in tissue, but due to their more pronounced T_1-effect, they are most often used as T_1-contrast agents.

2.3 Manganese-enhanced MRI

Manganese-enhanced MRI (MEMRI) is based on the paramagnetic properties of the divalent manganese ion (Mn^{2+}). It was one of the first substances suggested for use as a MRI contrast agent, and it was used by Lauterbur in 1973 to demonstrate the principle of MRI (Lauterbur 1973). In the recent years new attention has been given to manganese as a contrast agent for *in vivo* applications due to its biological properties (Koretsky and Silva 2004; Silva and Bock 2008).

2.3.1 Manganese and the brain

Mn^{2+} is an essential trace metal found in all tissues. It is involved in the metabolism of lipids, proteins and carbohydrates, and it is an important cofactor for a variety of enzymes in the brain including superoxide dismutase in mitochondria and glutamine synthetase that are primarily found in astrocytes (Takeda 2003; Erikson *et al.* 2005). In blood, Mn^{2+} binds to citrate, albumin and transferrin, but also exists in free ionic form, especially if the blood concentration is in excess of the binding capacity. Transferrin is the primary Mn^{2+} transport protein in blood. Transferrin-bound Mn^{2+} can enter the brain across the BBB through the transferrin-dependent transporter present on the surface of cerebral capillaries. After entering the endothelial cell, Mn^{2+} is released into the extracellular fluid and is available for neuronal and glial uptake. The transport into the brain using this mechanism is slow, but seems to be the most important under normal circumstances with low blood concentrations of Mn^{2+} (Aschner *et al.* 2007). After a bolus injection of Mn^{2+}, there are high concentrations of free Mn^{2+} ions in the blood (Takeda 2003), and a rapid entrance of Mn^{2+} into the brain through the choroid plexus dominates. This is thought to be mediated by the divalent metal transporter 1 (DMT-1) (Aschner *et al.* 2007). These transporters and mechanisms are present and active in the neonatal brain, but to what extent the neonatal BBB is permeable to Mn^{2+} is unknown (Erikson *et al.* 2007).

After entering the brain, Mn^{2+} in the extracellular fluid or CSF can enter neurons or glial cells. Transferrin-bound manganese enters cells through the transferrin transporter (Takeda 2003; Aschner *et al.* 2007). Free Mn^{2+} ion acts as a calcium analog, and enters cells through several transport systems including L-type voltage gates calcium channels (Narita *et al.* 1990), Na^{+}/Ca^{2+} exchanger, Na^{+}/Mg^{2+} antiporter and active Ca^{2+} uniporter (Takeda 2003). After entering the cell, Mn^{2+} is mainly stored in the endoplasmatic reticulum, but is also transported along microtubule and is released at the axonal terminal in the synaptic cleft and taken up into the dendrite of the next neuron (Takeda 2003).

Manganese in the brain is distributed in a certain pattern, with higher concentrations in the dentate gyrus and CA3 of the hippocampal formation, caudate putamen, globus pallidus

substansia nigra and subthalamic nuclei. The pattern of manganese distribution seems to follow that of iron (Fe) in these structures (Erikson *et al.* 2002; Aschner *et al.* 2007).

2.3.2 Imaging with manganese

The paramagnetic properties of Mn^{2+}, giving excellent T_1-contrast, in combination with the biological properties mentioned above can be utilized in several ways for brain studies in animals: First, systemic administration of Mn^{2+} gives specific enhancement of the cerebral architecture, by accumulation in structures with high cellular density or high affinity for Mn^{2+}. Among these are the olfactory bulbs, hippocampal formation, cerebellum, thalamus, lentiform and caudate nuclei (Aoki *et al.* 2004; Wadghiri *et al.* 2004; Watanabe *et al.* 2004b; Lee *et al.* 2005; Silva *et al.* 2008; Chuang *et al.* 2010). Using high doses of Mn^{2+}, the cellular layers of neocortex can also be visualized in vivo (Silva *et al.* 2008). Second, Mn^{2+} is transported antegrade and retrograde in axons as well as across synapses (Pautler *et al.* 1998; Pautler 2004) and can therefore be used for mapping of neuronal pathways *in vivo* (Van der Linden *et al.* 2002; Watanabe *et al.* 2004a; Thuen *et al.* 2005; Tucciarone *et al.* 2009; Sandvig *et al.* 2011). Third, activity induced MEMRI (AIM) has been used to map neuronal activity, based on the principle that Mn^{2+} enters excited neurons through voltage gated Ca^{2+}-channels during neuronal depolarisation (Lin and Koretsky 1997; Aoki *et al.* 2002). This technique has been used for functional MRI (Yu *et al.* 2005; Bissig and Berkowitz 2009; Chuang *et al.* 2009; Yang *et al.* 2011), but also for detecting cellular Ca^{2+} influx during acute ischemia (Aoki *et al.* 2003).

2.4 Diffusion weighted MRI

Diffusion Tensor Imaging (DTI) is a relatively new MRI technique introduced in the mid-1990'ies (Basser *et al.* 1994). Since then it has become a very useful tool for imaging white matter tracts in the brain.

2.4.1 Principles of diffusion weighted MRI

Water diffusion is a process where water molecules move randomly about driven by thermal energy. A MRI sequence can be sensitized to water diffusion by the use of linear magnetic gradients during the sequence (See Figure 2.5C). One of the most commonly used ways of achieving diffusion weighting was described by Stejskal and Tanner (1965). By applying a linear magnetic gradient before and after the 180°-pulse in a spin-echo sequence, the magnitude of the subsequent echo will be influenced by the degree of diffusion parallel to the diffusion gradient. The first gradient introduces a phase shift corresponding to the position of the proton along the direction of the gradient. The second gradient produces a phase shift equal to that produced by the first gradient. For stationary protons, the second gradient will (with the help of the 180°-pulse) undo the phase shift produced by the first gradient. However, protons moving parallel to the gradient direction will experience different phase shifts from the two

gradients, and the refocusing will be incomplete. This reduces the magnitude of the subsequent echo, and can be described by:

$$S = S_0 e^{-b \cdot D} \quad \text{Eq. 2.5}$$

were *S* is the attenuated signal caused by the diffusion weighting, S_0 is the signal without diffusion weighting, *b* is the degree of diffusion weighting in an image and *D* is the diffusion coefficient. This is, however, only valid if the diffusion is equal in all directions (isotropic) and in one compartment. In tissue, these conditions are not met, and *D* is instead referred to as the apparent diffusion coefficient (ADC). The b-value is determined by the amplitude (*g*) and duration (δ) of the gradients and the time between the two gradients (Δ):

$$b = \delta^2 \Delta g^2 \quad \text{Eq. 2.6}$$

Water diffusion can be free (Figure 2.7A) or restricted by boundaries like cell membranes or macromolecules (Figure 2.7B). In the intracellular compartment, water diffusion is largely restricted by the cell membrane, intracellular organelles, cytoskeleton and other proteins. This gives a low apparent diffusion coefficient (ADC). In the extracellular compartment diffusion is less restricted since there are fewer boundaries. One such example is water diffusion in cerebrospinal fluid of the ventricles of the brain that can be considered unrestricted and has a high ADC. By acquiring images with different diffusion weighing, maps of the apparent diffusion coefficient (ADC) can be calculated using equation 2.5.

ADC-maps or diffusion weighted images (DWI) can be used for early assessment of brain injury after ischemia. It is particularly the nature of the oedema secondary to the injury that causes changes in the diffusion. Cytotoxic oedema leads to reduced ADC: The associated cell swelling increases the intracellular water component and reduces the extracellular space. Since intracellular water has more restricted diffusion than extracellular water, the overall water diffusion is more restricted. Vasogenic oedema on the other hand, gives increased ADC. This is related to increased water content due to extravasation of water into the lesion causing increased water in the extracellular space, where water diffusion is little restricted. Although DWI is becoming more and more common in the early assessment of neonatal hypoxic-ischemic brain injury (Huppi *et al.* 1998; Inder *et al.* 1999; Huppi and Amato 2001; Counsell *et al.* 2003; Hunt *et al.* 2004; Rutherford *et al.* 2004; Krishnan *et al.* 2007), the pathologies underlying all the observed changes in diffusion are still not clear.

2.4.2 The diffusion tensor

In certain tissue types, the orientation of the boundaries that restrict diffusion is organized. An example of such tissues is white matter tracts. The cell membrane of the neuronal axon,

intracellular macromolecules that run along inside the axon (e.g. microtubuli) and oligodendrocytes that cover the axon with myelin sheets all constitute boundaries to diffusion perpendicular to the long axis of the axon. This leads to high water diffusion parallel to the axis of the axon with restricted diffusion perpendicular to the axon (Figure 2.7C). This highly directional diffusion is termed anisotropic diffusion, in contrast to the more isotropic diffusion experienced in grey matter of the brain, where diffusion boundaries are more randomly oriented and hence overall diffusion is less directional. ¨

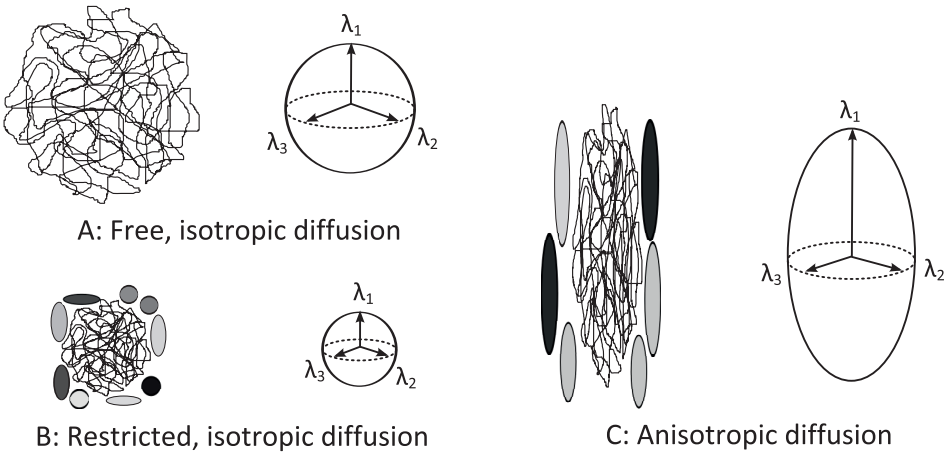

Figure 2.7: Illustrations of free isotropic (A), restricted isotropic (B), and anisotropic water diffusion (C) with the corresponding ellipsoids describing the three eigenvectors and the corresponding eigenvalues (λ_1, λ_2, λ_3) of the diffusion tensor.

In DWI, the degree of diffusion weighting in an image is dependent on the diffusion of water parallel to the direction of the diffusion gradient. By acquiring several diffusion weighted images with different directions of the diffusion gradients, the directionality of the diffusion in tissue can be calculated and diffusion tensor images (DTI) can made (Basser *et al.* 1994; Mori and Zhang 2006). At least six orthogonal directions are required in order to describe the full diffusion tensor $\underline{D}$, which can be written as the matrix:

$$\underline{D} = \begin{bmatrix} D_{xx} & D_{yx} & D_{zx} \\ D_{xy} & D_{yy} & D_{zy} \\ D_{xz} & D_{yz} & D_{zz} \end{bmatrix} \qquad \text{Eq. 2.7}$$

The diffusion tensor describes an ellipsoid with three eigenvectors with corresponding eigenvalues (λ_1, λ_2, λ_3) (See Figure 2.7). λ_1 is the diffusion along the longest axis of the ellipsoid. λ_2 and λ_3 are the diffusion along the two axis perpendicular to the longest axis. From these eigenvalues different measures of diffusivity and isotropy can be calculated.

The mean diffusivity (MD) is the average trace of diffusivity in the three perpendicular directions within a voxel. In the case of isotropic diffusion it is equivalent to the apparent diffusion coefficient (ADC). It describes the average water diffusion in tissue and is given by:

$$MD = \langle \lambda \rangle = \frac{\lambda_1 + \lambda_2 + \lambda_3}{3} \qquad \text{Eq. 2.8}$$

Axial diffusivity ($\lambda_{\parallel}$) is the magnitude of diffusion parallel to the primary diffusion direction (i.e. longest axis of the ellipsoid). This typically describes the diffusion within a voxel along the axis of a neuronal tract. Axial diffusivity is equivalent to the primary eigenvalue:

$$\lambda_{\parallel} = \lambda_1 \qquad \text{Eq. 2.9}$$

The radial diffusivity ($\lambda_{\perp}$) describes the average diffusivity perpendicular to the axis of the primary diffusion direction and is given by:

$$\lambda_{\perp} = \frac{\lambda_2 + \lambda_3}{2} \qquad \text{Eq. 2.10}$$

Fractional anisotropy (FA) is a measure of the degree of overall directionality of diffusion in tissue. It ranges from 0 when diffusion is equal in all direction (isotropic), to 1 when diffusion is only in one direction (total anisotropy). In tissue the FA value will lie between 0 and 1, depending on the tissue type. FA in white matter will be higher than in grey matter which will be higher than in the ventricles. FA is given by:

$$FA = \sqrt{\frac{3}{2}} \frac{\sqrt{(\lambda_1 - \langle \lambda \rangle)^2 + (\lambda_2 - \langle \lambda \rangle)^2 + (\lambda_3 - \langle \lambda \rangle)^2}}{\sqrt{\lambda_1 + \lambda_2 + \lambda_3}} \qquad \text{Eq. 2.11}$$

Since DTI can visualize and quantify the anisotropy of tissue within a voxel, it has become a valuable tool to assess the integrity of white matter. In the developing neonatal brain, changes in DTI parameter like FA, MD and radial diffusivity reflects the underlying maturation of white matter tracts (Huppi and Dubois 2006). During the course of white matter maturation FA steadily increases and radial diffusivity decreases, reflecting reduced diffusion perpendicular to the white matter fibre bundles. These changes coincide in time with the early pre-myelination and later myelination of the axons. Pre-myelination is characterized by increase in number of

microtubule-associated proteins in axons, change in axon calibre and maturation and organization of oligodendrocytes (Assaf *et al.* 2008). Myelination of axons is caused by formation of sheets of myelin inside oligodendrocytes surrounding the axons and increases as the oligodendrocytes mature in the newborn period. Axon packing, relative membrane permeability for water, internal axon structure and intra-axonal space also affects the anisotropy in brain areas. During the early development of white matter, the changes in FA and radial diffusivity are paralleled by a decrease in mean diffusivity/ADC (Huppi *et al.* 1998; Neil *et al.* 1998; Dudink *et al.* 2007). Damage to the brain in the perinatal period may result in injury to the developing oligodendrocytes, axonal injury or degeneration, with life-long consequences for white matter development and function. Several recent studies show how perinatal events are related to changes in white matter integrity on DTI in early life (Huppi *et al.* 2001; Counsell *et al.* 2006; Rutherford *et al.* 2006) and adolescents (Nagy *et al.* 2003; Vangberg *et al.* 2006; Skranes *et al.* 2007; Skranes *et al.* 2009).

Chapter 3 Objectives

The overall aim of this thesis was to establish methods for *in vivo* MR imaging of hypoxic-ischemic brain injury in a neonatal rat model to enable longitudinal evaluation of delayed tissue damage, injury progression and effects of interventions on the injury process.

More specific aims were:

- To depict delayed neuronal death after the initial hypoxic-ischemic insult using manganese-enhanced MRI (Paper I)
- To evaluate the specificity of manganese-enhanced MRI in detection of cells related to injury by comparison with histology and immunohistochemistry (Paper I and II)
- To examine the longitudinal evolution of brain injury up to six weeks following HI in the neonatal rat brain using manganese-enhanced MRI (Paper II and III)
- To examine the influence of hypoxia-ischemia on white matter development using diffusion tensor imaging (Paper III and IV)
- To examine the value of early detailed MRI in predicting the long-term extent of injury to cerebral grey and white matter (Paper III and IV).
- To evaluate the potential long-term neuroprotective effects of doxycycline and to examine the effect of doxycycline on the structural evolution of injury over weeks after the hypoxic-ischemic insult (Paper III).
- To evaluate how exposure to hyperoxia after a hypoxic-ischemic insult influences the prolonged injury process (Paper IV)

Chapter 4 Material and methods

4.1 Animal model

4.1.1 Animal handling

All animal experiments were conducted in accordance with European Communities Council Directive of 1986 (86/609/EEC) through guidelines set by the Norwegian Ethics Committee for Animal Research, and the experiments were approved by the responsible governmental authority (Forsøksdyrutvalget).

Wistar rats (Scanbur, Norway AS) were bred in the animal facility at the Norwegian University of Science and Technology in Trondheim (former Animal Facility at St. Olav University Hospital). Time-mated rats and their offspring were kept on a 12:12 hours light:dark cycle. Temperature in the animal room was kept at 22° and humidity at 55%. Offspring were weaned at the age of four weeks. Animals had food and water *ad libitum* at all times. All animal interventions, except the MRI, were conducted at the animal facility. MRI was performed at the MR Centre, located approximately 300m from the animal facility. Animals were transported through the underground passage to the MR Centre in a transport cage on the same morning or the day before the MRI. During the pilot period, the temperature within the transport cage were measured during transport and found to be stable and within the same levels as at the animal facility. During MR scanning, animals were kept in a designated animal room at the MR Centre with the same environmental conditions as at the animal facility.

4.1.2 Hypoxia-ischemia

A slightly modified version of the Vannucci procedure for hypoxic-ischemic brain damage was used (Rice *et al.* 1981; Vannucci and Vannucci 2005).

Seven days after birth, rat pups were anaesthetized with isoflurane (Baxter Medication Delivery, Oslo, Norway) (4% induction, 2% maintenance) in O_2. They lay supine on a heated surface with infrared heating above to avoid temperature loss during the procedure. A stereo microscope was used for optimal viewing during the operation. Through a mid-neck incision, the right common carotid artery was identified, thermo-cauterized and severed. Wounds were

sprayed with Xylocaine (2%) and closed with 5-0 Vicryl suture (Johnson& Johnson Intl c/o European Logistics Centre, St-Stevens-Woluwe, Belgium). Duration of operating procedure was 5-10min. After regaining consciousness from the anaesthesia, the pups were placed back with their dam for recovery and feeding for minimum 2 and maximum 4 hours, before exposure to hypoxia. In every litter two pups were sham-operated; the common carotid artery was identified under anaesthesia, but not damaged. Sham-operated animals were not subjected to hypoxia.

The set up for the hypoxia is shown in Figure 4.1. The hypoxia chamber consisted of a fibreglass box with a water-heated pad in the bottom connected to a water-heating circulation system. The hypoxia chamber was placed inside a neonatal incubator. The temperature inside the box was kept at 36±0.5 ºC throughout the hypoxia procedure. Three thermometers in different places inside the box were used to monitor the temperature. A whole litter, except the sham operated animals, was put inside the hypoxia chamber together. The box was flushed with pre-heated humidified air with 8% O_2 (in 92% N_2) (15 l/min) for approximately 3 minutes until the oxygen concentration in the box was 8%. Thereafter air flow was kept at 5 l/min and O_2 was measured to 8% throughout the procedure using an oxygen meter (OxyQuant S®, EnviteC GmbH, Wismar, Germany). After 60 or 75min of hypoxia, air flow of 8% oxygen was stopped, the lid taken off and room air filled the box, giving O_2-levels of 21% within approximately one minute. The pups were allowed to recover for 5 minutes before being placed back with their dam. This procedure resulted in a unilateral hypoxic-ischemic insult (HI) to the right cerebral hemisphere.

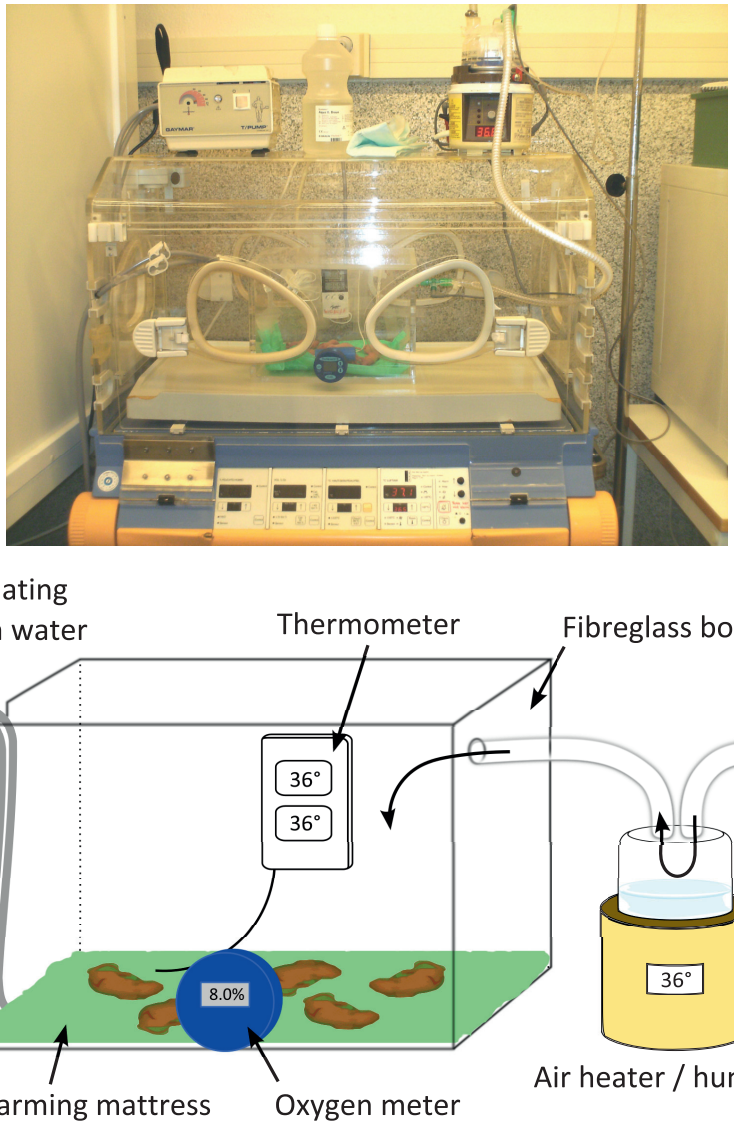

Figure 4.1: ***Top:*** **Image of the experimental set up for hypoxia showing the neonatal pups inside the fibreglass box inside the incubator.** ***Bottom:*** **Schematic drawing showing the fibreglass box with circulating warm water mattress, air heating and humidifying system for maintain the temperature inside the fibreglass box at 36°. An oxygen meter is mounted close to the mattress to control that the oxygen level inside the box is adequate.**

4.1.3 Hyperoxia

Exposure to hyperoxia was done in paper IV. Immediately after end of the hypoxic-ischemic procedure described above, the fibreglass box was flushed with pre-heated humidified 100% O_2 for 2 hours to obtain hyperoxia. The control group in this study was exposed to room air (21% O_2) in the same box for 2 hours. In both groups temperature inside the fibreglass box during the procedures was kept at 36±0.5ºC. Thereafter the pups were returned to their dams.

4.1.4 Manganese administration

Manganese was administered six hours after the hypoxia as a single dose of 40 mg $MnCl_2$ per kg bodyweight (~318µmol Mn^{2+}/kg). 1M $MnCl_2$ (# 7773-01-5, Sigma-Aldrich Inc., St. Louis, USA) was diluted to a concentration of 100mM using sterile water. The correct volume of $MnCl_2$ corresponding to the weight-dependent dose for each animal was drawn using a pipette and mixed with 0.9% NaCl to a total injection volume of 0.1ml (paper I and II) or 0.15ml (paper III and IV). Injections were given intraperitoneally. Control groups were injected with 0.1ml (paper I and II) or 0.15ml (paper III and IV) of 0.9% NaCl.

In the paper II, manganese was also administered 41 days after hypoxia-ischemia. Again a single dose of 40 mg $MnCl_2$ per kg bodyweight was given by intraperitoneal injection. $MnCl_2$ was prepared in the same way as described above, but not mixed with NaCl before injection. Total injection volume was on average 459 ± 25 µl.

In both study I and II, animals were randomly selected for manganese-injection, NaCl or sham operation at the time of CCA operation. All groups were represented in each litter.

4.1.5 Doxycycline treatment

In the paper III, pups were randomly selected for treatment with doxycycline or non-treatment at the start of the hypoxic-ischemic procedure. One hour after end of hypoxia, a single dose of 150µl doxycycline (Doxyferm, Nordic Drugs AB, Limhamn, Sweden) at a concentration of 1mg/ml (equivalent to 10mg/kg bodyweight for a 15g rat) was given by intraperitoneal injection to pups in the treatment group. Pups in the non-treated group received a single injection of 150µl 0.9% NaCl.

Table 4.1: Characteristics of the study designs with study and intervention groups in the different papers

	Paper I	Paper II	Paper III	Paper IV
Duration of HI	75 min	75 min	60 min	75 min
Manganese group	40mg/kg $MnCl_2$ 6 h after HI (n=16) or 6 days after HI (n=3)	40mg/kg $MnCl_2$ 6 h & 42 days after HI (n=7)	40mg/kg $MnCl_2$ 6 h after HI (n=16)	40mg/kg $MnCl_2$ 6 h after HI (n=16*)
Control group	100µl 0.9% NaCl 6 h after HI (n=10)	100µl 0.9% NaCl 6 h after HI (n=6)		150µl 0.9% NaCl 6 h after HI (n=31**)
Sham operated controls	40mg/kg $MnCl_2$ 6 h after HI (n=6)	40mg/kg $MnCl_2$ 6 h & 42 days after HI (n=4)	40mg/kg $MnCl_2$ 6 h after HI (n=4)	40mg/kg $MnCl_2$ 6 h after HI (n=4) 150µl 0.9% NaCl 6 h after HI (n=9)
Intervention group			Doxycycline 10mg/kg i.p. (n=8)	Hyperoxia: 100% O_2 for 2h (4 litters, n=28)
Control group			NaCl 0.9% 150µl i.p. (n=8)	Room-air: 21% O_2 for 2h (2 litters, n=19)
MRI time-points (days after HI)	1, 3 & 7; + 8, 10 & 14 for one group	1, 3, 7 & 42	1, 7, 21 & 42	1, 7, 21 & 42
Histology	Day 1, 3 and 7 HE, MAP2, CD68, GFAP, caspase 3 & Fluorojade B	Day 42 HE, MAP2, CD68, GFAP & caspase 3	Day 42 HE, MAP2, CD68 & MBP	Day 7 and 42 HE, CD68, GFAP & caspase 3

* One litter with hyperoxia exposure and one litter with room-air received $MnCl_2$

** Three litters with hyperoxia exposure and one litter with room-air received NaCl

4.2 Magnetic Resonance Imaging

MRI was performed using a 7T magnet (Biospec 70/20 AS, Bruker Biospin MRI, Ettlingen, Germany) with water-cooled (BGA-12, 400 mT/m) gradients. A 72mm volume resonator was used for RF transmission. An actively decoupled quadrature mouse head surface coil was used for RF reception on days 1, 3 and 7 after hypoxia ischemia, while an actively decoupled quadrature rat head surface coil was used for RF reception on days 21 and 42 after hypoxia-ischemia. The animals were anaesthetized with isoflurane (4% in 30% O_2, 70% N_2) before they were placed, prone, in a designated water heated animal bed (Bruker Biospin MRI), and their head was fixed with inbuilt tooth bar, nose mask and earplugs or polystyrene pieces (see Figure 4.2). This assured the same placement of the head of the animals within the magnet from scan to scan. The nose mask provided anaesthesia with isoflurane (approximately 2% in 30% O_2, 70% N_2) during scanning. The respiratory rate and body temperature was monitored with MR-compatible equipment (Small Animal Instruments Inc., Stony Brook, NY, USA), and anaesthesia and the animal bed heating were adjusted to keep respiratory rate and body temperature stable during scanning. To assure stable body temperature of the animals, a cotton wool cover was placed over their back and legs.

At all MRI time-points, a series of MRI sequences were used, starting with a gradient echo FLASH pilot scan (acquisition time approximately 1min) to do basic system adjustments and to acquire the initial images for correct placement of the slices in the subsequent MRI sequences. Table 4.2 provides an overview over the different MRI sequences used at the different time-points in the different papers.

Table 4.2: MRI sequences used at different time-points in the different papers.

	Day 1	**Day 3**	**Day 7**	**Day 21**	**Day 42**
Paper I & II	T_1-w FLASH MSME T_2-map	T_1-w FLASH MSME T_2-map	T_1-w FLASH MSME T_2-map		T_1-w FLASH
Paper III	ADC-map		T_1-w FLASH DTI-EPI	T_1-w FLASH DTI-EPI	T_1-w FLASH DTI-EPI
Paper IV	RARE T_2-map ADC-map		RARE T_2-map T_1-w FLASH	RARE T_2-map DTI-EPI	RARE T_2-map DTI-EPI

T_1-w: T_1-weighted

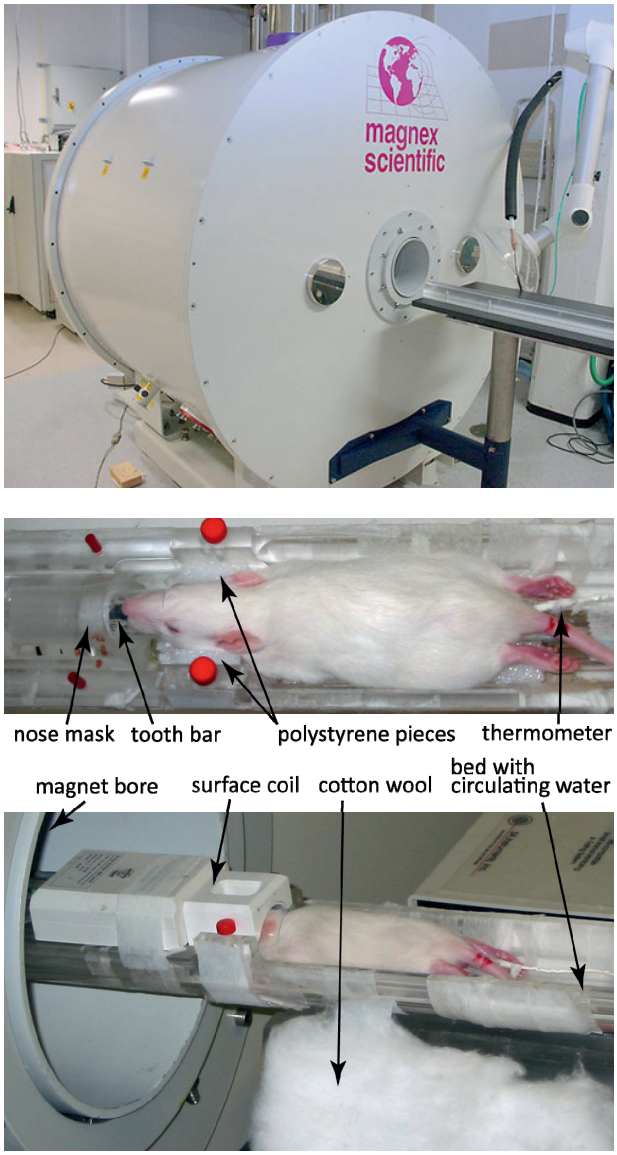

Figure 4.2: ***Top image:*** **The 7 Tesla Bruker Biospec 70/20 magnet used for MRI of the rats.** ***Lower images:*** **28 days old rat lying in the designated water heated bed. The head is fixed in a nose mask with tooth bar and polystyrene pieces. The nose mask also provides the anesthetic gas. The surface coil is placed on top of the head and fixed to the bed with tape. Cotton wool is used to cover the back and legs of the rat before the bed is pushed into the magnet bore.**

4.2.1 T_1-weighted MRI

To obtain high-resolution T_1-weighted images for detection of manganese-enhancement a 3D Fast Low Angle Shot (FLASH) sequence was used. The sequence was optimized using phantoms and animals *in vivo* to give high resolution images with high contrast-to-noise (CNR) within a given scan time. Echo time was set to almost the system minimum to reduce T_2*-effects, repetition time was reduced to almost minimum in combination with as many averages as possible within the given time frame. Flip angle was set to 30°, since that in practice gave the best contrast. Different field of view and matrix sizes were chosen at the different time-points to adjust for the growth of the animal head. These parameters were also changed from paper I and II to paper II and IV as the sequence was further optimized. Table 4.3 provides an overview over the different scan-parameters of the T_1-weighted FLASH sequence used at the different time-points in the different papers.

4.2.2 T_2-mapping

In paper I, images with different T_2-weighting were obtained with a 2D multi slice multi echo spin-echo sequence (MSME) with a repetition time (TR) of 2500ms, 40 echos with echo times (TE) of 7.6/ 15.2/…/304ms, slice thickness was 1mm. Field of view (FOV) was 18 × 18 mm and the acquisition matrix (MTX) 128 × 96 giving an in plane resolution of 140 µm × 187µm. The matrix was zero-filled during reconstruction to 128 ×128 giving an interpolated resolution of 140 µm isotropic. Acquisition time was 16min with 4 averages.

In paper IV, images with different T_2-weighting were obtained at all time-points with a Rapid Acquisition with Relaxation Enhancement (RARE) sequence with multiple echoes: Effective Echo Times (TE) = 25, 75, 125 ms; TR = 4000 ms; RARE- factor = 4; slice thickness was 1mm and 15 coronal slices were acquired with FOV = 25 × 20 mm (day 1 and day 7), 30 × 20 mm (day 21 and day 42); acquisition matrix 160 × 96 (day 1 and day 7) and 192 × 96 (day 21 and day 42) reconstructed to 160 × 128 and 192 × 128 respectively, giving an in-plane resolution of 156 × 156 µm. Acquisition time was 6.5min with 4 averages.

In both paper I and paper IV T_2-maps were calculated on a voxel-by-voxel basis by fitting a mono-exponential model to the signal intensity of the images with different TE-values using in-house developed software (MATLAB ver. R2010a, Math Works Inc, Natick MA, USA).

Table 4.3: Scan parameters of the T_1-weighted 3D FLASH sequence used for manganese-enhanced MRI at different time points in the different papers

		Day 1 & 3	Day 7	Day 21	Day 42
Paper I & II	α/TR/TE	30°/12ms/3ms	30°/12ms/3ms		30°/12ms/3ms
	FOV	20×20×17.5mm^3	20×20×17.5mm^3		30×35×25mm^3
	MTX	128×96×84	128×96×84		172×150×108
	(zero-filled)	(128×128×112)	(128×128×112)		(172×200×144)
	Resolution	156×156×156µm^3	156×156×156µm^3		174×175×174µm^3
	NA	16	16		16
	Scan time	25min	25min		52min
Paper III	α/TR/TE		30°/12ms/3ms	30°/12ms/3.25ms	30°/12ms/3.25ms
	FOV		25×25×17.5mm^3	30×25×20mm^3	30×30×20mm^3
	MTX		160×120×84	192×120×96	192×144×48
	(zero-filled)		(160×160×112)	(192×160×128)	(192×192×64)
	Resolution		156×156×156µm^3	156×156×156µm^3	156×156×312µm^3
	NA		16	16	8
	Scan time		32min	37min	11min
Paper IV	α/TR/TE		30°/12ms/3ms		
	FOV		25×25×17.5mm^3		
	MTX		160×120×84		
	(zero-filled)		(160×160×112)		
	Resolution		156×156×156µm^3		
	NA		16		
	Scan time		32min		

α: Flip-angle. TR: Repetition time. TE: Echo time. FOV: Field-of-view. MTX: Acquisition matrix. NA: Number of averages. (zero-filling): zero-filled matrix.

4.2.3 Apparent Diffusion Coefficient mapping

In paper III and IV, a series of diffusion weighted images were acquired using a spin echo sequence with Stjeskal-Tanner diffusion preparation and echo planar read-out of the signal (EPI). Duration of the diffusion gradients (δ) was 7ms and the two diffusion gradients was separated (Δ) by 14ms. Different diffusion weighting of the images was achieved by using 6 different b-values in addition to non-diffusion weighted image (b0). Multi shot EPI read-out in left-to-right direction was used, echo time was kept to a minimum, and receiver bandwidth was set to 250 000 Hz. Further sequence parameter details are shown in Table 4.4. Apparent diffusion coefficient (ADC) maps were calculated using in-house developed software (MATLAB ver. R2010a, Math Works Inc, Natick MA, USA) by fitting a mono exponential model to the signal intensity of the images with different diffusion weightings.

4.2.4 Diffusion Tensor Imaging

In paper III and IV, Diffusion tensor imaging (DTI) was performed using a spin echo sequence with Stjeskal-Tanner diffusion preparation and echo planar read-out of the signal (EPI). Duration of the diffusion gradients (δ) was 7ms and the two diffusion gradients was separated (Δ) by 14ms. 5 images were acquired without diffusion weighting (b0) and 30 images with diffusion weighting (b=1000ms) in different non-collinear directions. Multi shot EPI read-out in left-to-right direction was used, echo time was kept to a minimum, and receiver bandwidth was set to 250 000 Hz. Field of view was set to be far larger than the size of the animal head, and was adjusted to each MRI time-point together with matrix size according to the growth of the animal. Table 4.4 shows the scan parameters for the DTI sequences at the different time-points.

Table 4.4: Scan parameters of the diffusion imaging sequences used at different time points in paper III and IV

		Day 1	Day 7	Day 21	Day 42
Paper III		**ADC-map**	**DTI-EPI**	**DTI-EPI**	**DTI-EPI**
	TR	3000ms	2550ms	2550ms	3750ms
	TE	37.5ms	35	35	40
	b-values × directions	100/200/400/600/800/1000ms ×1	1000ms ×30	1000ms ×30	1000ms ×30
	FOV	30×20mm	30×40mm	30×40mm	40×49.6
	Slice thickness	1mm	0.5mm	0.5mm	0.5mm
	No. Slices	15 coronal	17 axial	17 axial	25 axial
	MTX	192×128	128×172	128×172	172×212
	Resolution	156×156μm^2	234×233μm^2	234×233μm^2	233×234μm^2
	NA	4	4	4	4
	Scan time	5.5min	24min	24min	35min
Paper IV		**ADC-map**		**DTI-EPI**	**DTI-EPI**
	TR	3000ms		3750ms	3750ms
	TE	40.6ms		40	40
	b-values × directions	100/200/400/600/800/1000ms ×3		1000ms ×30	1000ms ×30
	FOV	25×30mm		40×49.5mm	40×49.5mm
	Slice thickness	1mm		0.5mm	0.5mm
	No. Slices	15 coronal		25 axial	25 axial
	MTX	160×192		172×212	172×212
	Resolution	156×156μm^2		233×233μm^2	233×233μm^2
	NA	4		4	4
	Scan time	15min		35min	35min

TR: Repetition time. TE: Echo time. FOV: Field of view. MTX: Acquisition matrix. NA: Number of averages.

4.3 MRI data analysis

4.3.1 Signal correction of T_1-weighted MRI data

The spatially inhomogeneous sensitivity of the surface-coil used in the 3D T_1-weighted FLASH acquisition introduced spatially varying signal intensities in the image data set. To correct for this, two additional low-resolution FLASH scans were performed with the same sequence using the same sequence parameters as for the high-resolution 3D T_1-weighted FLASH scan, but with a acquisition matrix of only 32 × 32 × 32, 1 average and scan time of 2min each. The two scans were performed using the surface coil (coupled coil operation) and the volume coil (single coil operation) for reception, respectively. Since the B_1^+ transmit field and B_1^- receive field of the volume-coil could be considered homogeneous within the field of view, the signal intensity ratio in each voxel between the two low resolution scans could be used to normalize the signal intensity in the high-resolution data set. The correction-procedure was performed in Matlab (MATLAB ver 2007a, MathWorks Inc.). The MRI signal intensity in a voxel at location *(x,y,z)* was normalized using the following relation:

$$I_{SC}(x,y,z) = I_{CC}(x,y,z)\frac{C_{SC}(x,y,z)}{C_{CC}(x,y,z)} \qquad \text{Eq. 4.1}$$

where C_{CC} and C_{SC} is the coupled-coil and single-coil intensities in the correction scan datasets respectively, I_{CC} is the recorded couple-coil signal intensity in the main 3D data set, and I_{SC} is the resulting normalized signal intensity.

4.3.2 Signal intensity measurements in T_1-weighted images

The receiver gain was held constant for all scans and the signal scaling during reconstruction of the images was corrected for before quantitative analysis of the data.

Coronal image slices corresponding to approximately –3.25 mm from the bregma (Paxinos and Watson 1998) was used for regions of interest (ROI) analyses of signal intensity in paper I and II. ROI were manually placed in the cortex, hippocampus, external capsule and thalamus on day 1, 3 and 7 scans (paper I) and in areas of cortex, hippocampus, thalamus and amygdala on day 42 scans (paper II) in the right ipsilateral hemisphere and anatomically corresponding areas in the left contralateral hemisphere. Mean signal intensity (SI) was calculated for each ROI, and a measure of the normalized relative contrast was calculated for each ROI to compare the difference in signal intensity between the ipsilateral and contralateral hemispheres

between animals and groups of animals. Relative contrast (RC) was calculated using the following equation:

$$RC = \frac{SI_{ROI_{Ipsilateral}} - SI_{ROI_{Contralateral}}}{SI_{ROI_{Ipsilateral}} + SI_{ROI_{Contralateral}}} \quad \text{Eq. 4.2}$$

4.3.3 Defining manganese-enhancement

Manganese-enhancement was defined by higher signal intensity compared to a control in the T_1-weighted image. In paper I and II, pups injected with saline served as control to identify manganese-enhancement of cerebral tissue in general. For recognition of increased manganese-enhancement related to pathology, signal intensity in the injured, right brain hemisphere ipsilateral to the carotid artery ligation was compared to the contralateral, left brain hemisphere in each animal. In all papers, increased manganese-enhancement in brain areas in the ipsilateral cerebral hemisphere was defined by having higher signal intensity on T_1-weighted images than in anatomically corresponding areas in the contralateral hemisphere.

4.3.4 Volume measurements

The volumes of the right (ipsilateral) and left (contralateral) hemispheres as well as the cyst volume were measured by manually drawing the outlines of the remaining brain tissues and cyst in every image slice in the 3D T_1-weighted data set (paper II and III) and the T_2-maps (paper IV).

4.3.5 Apparent Diffusion Coefficient maps

ADC analyses were performed with the tools of the FMRIB software library (FSL ver. 4.1.4, Oxford Centre for Functional MRI of the Brain, UK; www.fmrib.ox.ac.uk/fsl) (Smith *et al.* 2004; Woolrich *et al.* 2009).

In paper III, a semi-automatic segmentation method was used to estimate the lesion volume on ADC-maps based on the assumption that changes in ADC in the right cerebral tissue were due to injury while ADC in the left hemisphere was preserved and normal. After initial manual masking of the brain hemispheres, automatic clustering was performed using FAST (part of FSL) (Zhang *et al.* 2001). The clustering was initialized with input on the initial tissue-type means based on average ADC values in different tissue (grey matter, white matter, thalamus, lesion with low ADC and lesion with high ADC). In this method all voxels in both hemispheres were assigned a class value from 1-5 reflecting their ADC-value, while taking into account the similarity of ADC-values of neighbouring voxels. For each class the volume of tissue in each hemisphere was calculated by counting the number of voxels. A volume difference between

the two hemispheres in each class was assumed to represent a lesion volume. The total lesion volume was then estimated from the sum of these volume differences across all classes.

In paper IV, regions of interest (ROI) were drawn in parietal cortex, thalamus, hippocampus and basal ganglia on coronal image slices corresponding to approximately –3.25 mm from the bregma (**Paxinos and Watson 1998**), and the mean ADC in each ROI calculated.

4.3.6 Diffusion tensor images

DTI analyses were performed with the tools of the FMRIB software library (FSL ver. 4.1.4, Oxford Centre for Functional MRI of the Brain, UK; www.fmrib.ox.ac.uk/fsl) (Smith *et al.* 2004; Woolrich *et al.* 2009).

Artefacts due to motion and eddy current distortions were minimized by affine transformation and co-registration of the diffusion encoded images to the b0 images. Data sets were inspected for ghosting artefacts and those with severe artefacts were excluded from the analysis. Masks for the brains were automatically created in each b0 image and the brains extracted using the Brain Extraction Tool (part of FSL). A voxelvise diffusion tensor model was then fitted to the diffusion image data using FDT ver2.0 (part of FSL), and maps for the mean diffusivity (MD), axial diffusivity ($\lambda_{\parallel}$), radial diffusivity ($\lambda_{\perp}$) and fractional anisotropy (FA) were created according to equations 2.6 to 2.9.

Regions of interest (ROI) were drawn in the centre of the genu, body and splenum of corpus callosum; internal capsule, external capsule, hippocampal fimbria and cingulum of the right and left cerebral hemisphere on the FA-maps and were double-checked to lie within the white matter structures on the b0 images and MD-maps. Since several of these ROI contained few voxels, especially in the ipsilateral hemisphere where the size of these structures were significantly reduced, several ROI were combined to three ROI (corpus callosum, right white matter, and left white matter) to get larger ROI and more robust measures. Mean FA, MD, $\lambda_{\perp}$ and $\lambda_{\parallel}$ was calculated in each of these three ROI in each animal.

4.4 Histology and immunohistochemistry

4.4.1 Tissue preparation and staining of sections

Animals were sacrificed after MRI acquisition at different time-points (see Table 4.1 for overview). They received an overdose of pentobarbital (300 mg/kg) and were perfused by intracardial injection of 4% paraformaldehyde (PAH) in phosphate-buffered saline (PBS). Brains were removed and embedded in paraffin.

Sections (8 µm), either coronal corresponding to –3.25 mm from the bregma (paper I, II and IV) or axial corresponding to –4.28 mm from the bregma (paper III) were cut and stained with either hematoxylin-eosin (H&E) (Klinipath, Duiven, the Netherlands), anti-MAP2 (Sigma-Aldrich, Steinheim, Germany) for neuronal integrity, anti-cleaved-caspase-3 (Cell Signaling) for apoptosis, anti-ED1-fitc (Serotec, Raleigh, NC) for CD68-positive activated microglia/macrophages, anti-MBP (Sternberger Monoclonals Inc., Lutherville, MD) for myelin, or anti-GFAP (Cymbus Biotechnology, Southampton, UK) as a marker for reactive astrocytes. After primary antibody incubation, sections were incubated with secondary antibodies; either rat-anti-FITC-biotin (Roche, Basel, Switzerland), goat-anti-rabbit-biotin (Vector Laboratories, Burlingame, CA) or horse-anti-mouse-biotin (Vector Laboratories, Burlingame, CA). Visualisation was performed using a Vectastain ABC kit (Vector Laboratories). In paper I, sections were also stained with Flourojade B (Chemicon International, Temecula, CA, USA) after incubation in 0.06% potassium-permanganate, embedded in DEPEX and visualized using a fluorescence-microscope in the FITC channel. Full section images were captured with a Nikon D1 digital camera (Nikon, Tokyo, Japan) in paper I, and with a MIRAX MIDI system (Carl Zeiss MicroImaging GmbH, Jena, Germany) in paper II, III and IV.

An overview of the different immunohistochemical stains that were used in the different papers can be found in Table 4.1.

4.4.2 Evaluation of immunohistochemistry

In paper I and II, immunohistochemical staining was qualitatively evaluated, and the areas with stained cells were compared to the areas with manganese-enhancement on the T_1-weighted images. A computer-based method was developed to evaluate the agreement between increased manganese-enhancement and different staining in paper I and is presented in that paper.

In paper II, III and IV, the number of cells with different immunohistochemical staining was semi-quantitatively evaluated by scoring the density of stained cells in different regions of the brain from 0 to 3. The criteria for the different scores, varied according to cell type and staining and are given in the respective papers.

In paper III, the tissue loss and neuronal loss were also evaluated semi-quantitatively in different regions of the right cerebral hemisphere and scored 0: no loss; 1: <33% tissue/neuronal loss; 2: 33-67% tissue/neuronal loss; 3: >67% tissue/neuronal loss and 4: Total tissue dissolution.

4.5 Statistical analyses

Different versions of Statistical Package for the Social Sciences (SPSS Inc., Chicago, IL, USA) and STATA ver. 10.1 (StataCorp LP, College Station, TX, USA) were used for statistical analysis and the level of significance was set to 0.05. T-tests were used to analyse mean differences in data with underlying normal distribution: Student's t-test to analyse mean differences between groups and paired t-test to analyse mean differences between time-points and between brain hemispheres. Mann-Whitney-U test was used to test differences between groups when the data was not considered to have an underlying normal distribution. In paper III and IV, linear mixed model was used to analyse the effect of experiment group, MRI time-point, and possible confounding factors. More details on the statistical methods are described in the respective papers.

Chapter 5 Synopsis of papers

Paper I

Manganese-Enhanced Magnetic Resonance Imaging of Hypoxic-Ischemic Brain Injury in the Neonatal Rat

Marius Widerøe, Øystein Olsen, Tina Bugge Pedersen, Pål Erik Goa, Annemieke Kavelaars, Cobi Heijnen, Jon Skranes, Ann-Mari Brubakk, Christian Brekken. *Neuroimage (2009)* ***45:*** *880-890*

The aim of this study was to depict delayed neuronal death after HI using Manganese-enhanced MRI (MEMRI) and to evaluate the specificity of MEMRI in detection of cells related to injury by comparison with histology and immunohistochemistry. To this end, seven-days-old rat pups were subjected to a one-sided hypoxic-ischemic brain injury (HI). $MnCl_2$ was injected intraperitoneally six hours afterwards in one group of HI animals (HI+Mn) and in one group of control animals (Sham+Mn), while another group of HI animals (HI+Vehicle) received NaCl. T_1-weighted images showed no increased manganese-enhancement (ME) in the injured hemisphere on day one or three after HI. Seven days after HI, increased ME was seen in parts of the injured cortex, hippocampus and thalamus among HI+Mn pups, but not among HI+Vehicle or Sham+Mn pups. Comparison with immunohistochemistry showed delayed neuronal death and inflammation in these areas with late ME corresponding best to areas with high concentrations of activated microglia.

This study demonstrated that increased manganese-enhancement seemed to be related to accumulation of manganese in activated microglia in areas of neuronal death rather than depicting neuronal death per se.

Paper II

Longitudinal Manganese-Enhanced Magnetic Resonance Imaging of Delayed Brain Damage after Hypoxic-Ischemic Injury in the Neonatal Rat

Marius Widerøe, Christian Brekken, Annemieke Kavelaars, Tina Bugge Pedersen, Pål Erik Goa, Cobi Heijnen, Jon Skranes, Ann-Mari Brubakk. *Neonatology (2011)* ***100(4):*** *363-372.*

The study aimed to follow brain injury after hypoxia-ischemia in rats longitudinally and compare manganese-enhancement of brain areas to the development of injury and presence

of reactive astrocytes and microglia. 7-days-old rat pups were subjected to one-sided hypoxic-ischemic (HI) brain injury. Pups were injected with either $MnCl_2$ or NaCl after 6 hours and again on day 41 after HI. Longitudinal T_1-weighted MRI demonstrated severe loss of cerebral tissue from day 7 to 42 days after HI. Most manganese-enhanced areas in the hippocampus, thalamus and basal ganglia on day 7 were liquefied after 42 days. Manganese-enhancement on day 42 corresponded to areas of activated microglia and reactive astrocytes in the remaining cortex, hippocampus and amygdala. However, the main area of enhancement was in the remaining thalamus in a calcified area surrounded by activated microglia and reactive astrocytes.

This study demonstrated that manganese-enhanced MRI can be a useful tool for *in vivo* identification of cerebral tissue undergoing delayed cell death and liquefaction after HI. Manganese-enhancement at a late stage seemed related to accumulation of manganese in calcifications and gliotic tissue.

Paper III

Effects of Doxycycline on the Longitudinal Development of Cerebral Grey and White Matter Injury in a Neonatal Rat Model of Hypoxia-Ischemia – a Magnetic Resonance Imaging Study

Marius Widerøe, Marianne B Havnes, Tora Sund Morken, Jon Skranes, Pål-Erik Goa, Ann-Mari Brubakk. *Accepted for publication in European Journal of Neuroscience*

The aim of this study was to examine potential long-term neuroprotection by doxycycline treatment on cerebral grey and white matter. Hypoxic-ischemic brain injury (HI) was induced in 7-days-old rats. Pups were treated with either doxycycline (HI+doxy) or saline (HI+vehicle) by intraperitoneal injection one hour after HI. Six hours after HI, $MnCl_2$ was injected intraperitoneally for later manganese-enhanced MRI. There was a tendency towards lower lesion volumes on diffusion maps among HI+doxy than HI+vehicle one day after HI. Volumetric MRI showed increasing differences between groups with time after HI with less cyst formation and less cerebral tissue loss among HI+doxy pups than HI+vehicle. HI+doxy pups had less manganese-enhancement on day seven after HI, indicating reduced inflammation. HI+doxy had higher fractional anisotropy on diffusion tensor imaging in major white matter tracts in the injured hemisphere than HI+vehicle, indicating less injury to white matter and better myelination. Histological examinations supported the MRI results. Lesion size on early MRI was highly correlated with final injury measures.

This study demonstrated that a single dose of doxycycline reduced long-term cerebral tissue loss and white matter injury after neonatal hypoxia-ischemia with increasing effect of treatment with time after injury.

Paper IV

Longitudinal Diffusion Tensor and Manganese–Enhanced MRI Detect Delayed Brain Injury After Hypoxia-Ischemia and Hyperoxia in the Immature Rat

Tora Sund Morken, Marius Widerøe, Christina Vogt, Stian Lydersen, Marianne Havnes, Pål-Erik Goa, Jon Skranes, Ann-Mari Brubakk. *Submitted to Pediatric Research*

We aimed to evaluate how exposure to hyperoxia after a hypoxic-ischemic insult influenced the prolonged injury process using a longitudinal study design using repeated MRI and DTI. Hypoxic-ischemic brain injury (HI) was induced in 7-days-old rats, and followed by exposure to either hyperoxia (100% O_2) or roomair (21% O_2) for two hours. Six hours after HI, $MnCl_2$ was injected intraperitoneally for later manganese-enhanced MRI. One day after HI, diffusion was more restricted in basal ganglia and hippocampus among hyperoxia animals, and the magnitude of restriction in diffusion correlated to the severity of long term tissue destruction. Seven days after HI more manganese-enhanced tissue and activated microglia were seen in the hyperoxia group. Brain tissue destruction was more severe in the hyperoxia than room-air group with increasing differences up to day 42. DTI showed reduced fractional anisotropy and increased radial diffusivity in corpus callosum among hyperoxia animals, indicating reduced myelination.

This study demonstrated that exposure to hyperoxia after hypoxia-ischemia in the newborn brain had severe long-term effects, worsening the trajectory of delayed grey and white matter injury.

Chapter 6 Discussion

6.1 Main findings

The main objective of this thesis was to establish methods for *in vivo* MR imaging of neonatal hypoxic-ischemic brain injury to enable longitudinal evaluation of delayed tissue damage, injury progression and effects of interventions on the injury process. This was achieved after first establishing a rat model for hypoxic-ischemic brain injury in the neonate.

In paper I and II, manganese-enhanced MRI in this model of neonatal hypoxic-ischemic injury was established. In paper I, we showed how manganese-enhancement was detectable seven days after the hypoxic-ischemic insult and manganese injection, and that the enhancement was related to microgliosis and astrogliosis secondary to the HI injury. In paper II, we examined the longitudinal development of these manganese-enhanced areas and showed how these areas liquefied up to six weeks after the initial HI insult. Activated microglia and reactive astrocytes were also present in some brain areas six weeks after hypoxic-ischemic injury, and manganese-enhancement was seen in these areas with gliosis and in areas with tissue calcifications. In paper III and IV, manganese-enhanced MRI was used as a tool to assess on-going tissue inflammation and gliosis seven days after the hypoxic-ischemic injury. In both studies, the volume of manganese-enhancement was influenced by intervention. The volume of manganese-enhanced tissue was also shown to correlate with the subsequent increase in cyst volume in paper III. These results demonstrated how manganese-enhanced MRI can be used to follow delayed tissue loss and accompanying gliotic and inflammatory processes.

In all papers, one of the main findings was that the brain injury following hypoxia-ischemia is a continuous process with tissue loss and reactive cells and cell death up to at least six weeks after the initial insult. Furthermore, using diffusion tensor imaging in paper III and IV, we also showed how the developmental maturation and injury to white matter tracts were affected over time by the hypoxia-ischemia and hyperoxia.

Although the cerebral injury was shown to evolve up to six weeks after the hypoxic-ischemic insult, lesion volume measurements (paper III) and restricted diffusion in thalamus (paper IV), both on diffusion (ADC) maps one day after hypoxia-ischemia, were found to predict the long-term cerebral lesion size and injury to white matter tracts.

In paper III, we examined the long term treatment effect of doxycycline, and found that a single dose provided neuroprotection in the form of reduced lesion size, reduced cyst formation and less injury to white matter tracts. The longitudinal design with repeated MRI measurements in this study demonstrated that the effect of doxycycline increased with time after hypoxia-ischemia. Another important finding in this study was that the injury size was correlated to the time between severing of the common carotid artery and hypoxia.

In paper IV, we explored the influence of exposure to hyperoxia after hypoxia on the brain injury development. The main finding of this study was that hyperoxia increased cerebral tissue loss, inflammatory response and white matter injury compared to room-air exposure. Again, longitudinal MRI demonstrated how the intervention affected the trajectory of injury development. In this study, structural and cellular changes were also seen in the contralateral hemisphere.

6.2 Methodological considerations

6.2.1 The animal model

The Vannucci model was chosen because it is a well established and well characterized model for hypoxic-ischemic brain injury in the neonate. Several studies have shown that the model gives reproducible insults that give injuries similar to what is seen in asphyxiated neonates (Rice *et al.* 1981; Vannucci and Vannucci 1997; Vannucci and Hagberg 2004; Vannucci and Vannucci 2005). Insults to the neonatal brain at different maturational stages can be modelled by giving the insult at different postnatal days. In this thesis seven days old rat pups were used since the maturation of the rat brain at that time has been shown to correlate to the brain maturation of a moderately premature human foetus around 32-34 weeks gestational age (Yager 2004).

Influence of recovery time between operation and hypoxia

One of the strengths of the model is that the magnitude of the insult can be adjusted by the duration of the hypoxia. However, other experimental factors like temperature, O_2-concentration, strain and laboratory environment also influence the lesion size. The duration of hypoxia and temperature during hypoxia were therefore optimized during a pilot phase. In our laboratory, 75 minutes with 8% O_2 at 36° gave consistent large injuries, with almost no mortality during hypoxia. This duration of hypoxia was used in paper I, II and IV. In paper III, the experimental conditions were the exact same, but the duration of hypoxia was reduced to 60 minutes to give smaller injuries. This resulted in a large variation in lesion size, ranging from no detectable injury to relatively large lesions with cyst formation. This was not likely due to genetic or environmental factors, as the pups were siblings of an inbred rat strain, making them genetically extremely similar and exposed to the same environment. We therefore

searched for factors in the experimental set up that could possibly explain this variation, like weight on postnatal day seven, operator, duration of operating procedure, incidents during operations (small bleeding, respiratory problems, anaesthesia problems, etc), litter effect, different exposure to hypoxia and injections of manganese, doxycycline and saline. However, the only parameter that correlated with lesion size on MRI was the recovery time from operation with severing of the right common carotid artery to the initiation of hypoxia; short recovery time gave larger lesions. Since pups in each litter are operated sequentially, but the entire litter is exposed to hypoxia simultaneously, the time to recover before hypoxia will vary between pups of the same litter. Short recovery time gives less time to recover from the anaesthesia and less time to feed. In the pilot phase, we noted that pups that died during hypoxia were often the ones which had not been fed properly before the hypoxia, i.e. not showing a white belly characteristic of a stomach filled with milk. Less feeding may give a subsequent risk of depletion of glucose reservoirs during hypoxia, and hypoglycaemia is known to increase the hypoxic-ischemic injury (Vannucci and Hagberg 2004; Vannucci and Vannucci 2005). Another explanation may be that the brain hemisphere ipsilateral to the severed common carotid artery is more susceptible to injury by hypoxia if the collateral circulation has had less time to adapt and ensure optimal redistribution of blood flow.

This correlation between recovery time and lesion size has to our knowledge not been reported before, but it is generally recommended that the time interval between severing of the carotid artery and hypoxia is kept between 2 and 4 hours. This condition was also met in our experiment with recovery time ranging from 2h 10min to 3h 47min, yet recovery time still influenced the severity of the injury. In paper I, II and IV, where the duration of hypoxia was 75 minutes and the lesions relatively large, we did not find such a correlation. Since most studies using the Vannucci model also have relatively large lesions, it seems that the influence of recovery time is only evident at shorter durations of hypoxia, and that there is a threshold for when hypoxic-ischemic injury ensues that is influenced by duration of hypoxia, but also by the recovery time.

Injury to the contralateral hemisphere

One advantage with the Vannucci model is the unilateral hypoxic-ischemic injury it creates. The cerebral hemisphere contralateral to the severed carotid artery is not usually damaged and can be used as a control (Rice *et al.* 1981; Towfighi *et al.* 1995; Vannucci and Vannucci 1997). In accordance with this, we found in paper I that the signal intensities on MRI in the contralateral hemisphere of hypoxic-ischemic pups after manganese-injection were similar to that of sham operated animals. Furthermore, there were no structural or cellular changes indicating injury in the contralateral hemisphere among the HI pups. We therefore took advantage of this and used the contralateral hemisphere as control in order to quantify

manganese-enhancement and injury size in paper I-IV. In paper II we further showed that the contralateral hemisphere was similar in size among HI pups to that of sham pups, and that no cellular changes or injuries were detectable on histology after six weeks. The same was shown in paper III, however in this paper the untreated animals had slightly lower volumes of the contralateral, left, hemisphere than sham, indicating some injury to that hemisphere. Furthermore, in paper IV we found reduced diffusion indicating injury in contralateral cortex one day after HI, and lower volumes of the contralateral hemisphere among HI animals than sham on days 7, 21 and 42 after HI. These findings may be explained by the overall more severe injury seen in this study. There was also a linear relationship between bodyweight and contralateral hemisphere volume on day 42, indicating that reduced brain volumes could be related to a general growth restriction. In paper III and IV, diffusion tensor imaging also indicated changes in the contralateral cerebral hemisphere among HI pups, with the most severe changes among animals with other signs of severe injury. In paper IV, where injuries were largest, these MR findings were accompanied by apoptotic cells in contralateral grey and white matter and activated microglial cells in contralateral white matter. Overall, the results from our studies suggest that large insults can induce damage to the contralateral hemisphere that can be quantified on MRI as reduced hemispheric volumes. Furthermore, even subtle injuries can be detected with techniques able to show changes in tissue microstructure, such as diffusion tensor imaging. Large insults may also give a general growth restriction that can influence the growth of both the ipsi- and contralateral hemisphere (Andiné *et al.* 1990). In consequence, caution must be advised when using the contralateral hemisphere as a control, and other controls, such as sham animals should be used in addition.

6.2.2 Possible effects on animal physiology during MRI acquisition

In the studies of this thesis, MRI has been used to follow the progression of hypoxic-ischemic injury over the course of time. The main advantages of MRI are that it is non-invasive and allows repeated measures of anatomical structures and functional correlates. However, factors related to the MRI acquisition could possibly influence the animal physiology that again could influence injury development.

Possible stressors related to MRI scanning

The animals were transported from the animal facility to the MR Centre. This transport and arrival in a new environment is likely to induce stress. The same may be true for the exposure to noise produced by the MR-machine. Animals were kept in an insulated room separate from the MR-machine, where the noise was barely audible to the human ear. Still, considering that rats have an extended range of hearing frequencies, stressful effects of the noise cannot be ruled out. When animals were in the MR-machine, they were anesthetized, so that noise

during scanning should not be perceived by the animal. However, if stressed, this may have contributed to worsening of the hypoxic-ischemic injury (Smith *et al.* 2011).

Possible effects of anaesthesia

For anaesthesia during MR-scanning, inhalation anaesthesia with Isoflurane was chosen, since it is the preferred method for anaesthesia in all rodents and is a safe and easy method that gives rapid induction of anaesthesia, provides good control over anaesthetic dept and rapid awakening after termination of anaesthesia (Flecknell 2009). However, isoflurane may, depending on the dose, give reduction in arterial blood pressure due to vasodilatation, and respiratory depression. Furthermore, there is evidence that isoflurane may be both neuroprotective and neurodegenerative in the developing brain (Zhao and Zuo 2004; Flecknell 2009; Istaphanous and Loepke 2009; Wang *et al.* 2009a; Chen *et al.* 2011). The neurodegenerative effect of isoflurane has primarily been linked to an increase in apoptosis (Xie *et al.* 2008; Istaphanous and Loepke 2009; Wang *et al.* 2009a). In our studies we did not see apoptotic cells in sham animals, and in paper I and II we did not see any apoptotic cells in the contralateral hemisphere, which could indicate pro-apoptotic effects of isoflurane administration in our experiments. The few numbers of apoptotic cells found six week after HI in ipsilateral hemisphere in paper II and IV, and in the contralateral hemisphere in paper IV may be related to repeated isoflurane exposure, but are more likely effects of a prolonged damage process caused by the severe hypoxic-ischemic insult.

Possible effects of magnetic fields and radiofrequency pulsing

Although MR imaging is generally considered safe, even at high magnetic fields like 7 Tesla, there are issues related to the static magnetic field, time-varying magnetic gradients and radiofrequency pulsing that may influence animal physiology and need to be discussed. A vast number of reports over several centuries have shown no evidence for biological effects caused by static magnetic fields, in humans, animals or cell cultures (Schenck 2000; Shellock and Crues 2004), but relatively few studies have examined the effects of high field MRI. In a study where human healthy volunteers were exposed to an 8 Tesla static magnetic field (for 5-25min at 8T and lower field strengths as the subject advanced into the magnet), a slight increase in systolic blood pressure was found (Chakeres *et al.* 2003). All other physiological vital signs, like heart rate, respiratory rate, diastolic blood pressure, blood oxygenation level, and core body temperature were unchanged. However, the exposure time was short compared to scan times in our experiments that ranged up to 1.5 hours.

More evidence exists to the biological effects of time-varying magnetic field gradients. These may induce electric currents that influence normal function of neurons and muscles, giving peripheral nerve discomfort or pain, muscle twitching, and may lead to cardiac and respiratory

stimulation at long ramp times and high slew rates of the magnetic field gradient (Schaefer *et al.* 2000; Shellock and Crues 2004). In our studies, animals were anesthetized during scanning and ramp times and slew rates were below estimated thresholds for cardiac and respiratory stimulations. All together, it is unlikely that effects of high field strength and time-varying magnetic field gradients should influence animal physiology in our experiments.

Radiofrequency pulsing on the other hand may have potential physiological effects in the animals, since the energy of the radiofrequency pulse is deposited in the tissue and may give rise to an increase in temperature. This deposition of energy, which measure is referred to as the specific absorption rate (SAR), depends on the amount of energy and the frequency with which the energy is deposited, the duration of exposure, in addition to the ability of the animal to redistribute and dispose of this heat (Shellock 2000; Shellock and Crues 2004). The energy needed to produce for instance a 90°-pulse increases with field strength and the problem is therefore highly relevant at 7 Tesla. Furthermore, neonates have poor temperature regulation, making them less able to adjust for such an increase in tissue temperature. A rise in cerebral temperature may have resulted from high SAR during MRI acquisition, and such hyperthermia, especially one day after hypoxia-ischemia, would potentially aggravate the hypoxic-ischemic injury (Corbett and Thornhill 2000; Yager *et al.* 2004). In our studies, we did not monitor SAR values. However, the low flip angle (30°) and gradient echo read-out of the signal in the sequence used for the manganese-enhanced imaging gives relatively low SAR values. The echo planar imaging sequence (EPI) with spin-echo diffusion preparation used for the DTI gives somewhat more SAR due to the 90°- and 180°-pulses in the diffusion preparation. In paper I and IV we also used a multi-spin-echo sequence (MSME) and a fast spin-echo sequence (RARE), respectively, to acquire T_2-maps. These sequences may potentially give high SAR values due to the use of multiple 180°-pulses after the excitation pulse for fast readout of multiple echoes and/or k-space lines (Shellock 2000). The duration of these two sequences was relatively short, and the total scan time on day one was below one hour in paper I and II and was further reduced in paper II and IV which gave a reduction in the total SAR (i.e. energy accumulation in tissue). The body temperature of the animals was measured during the experiment, and uncontrolled rise in temperature was not a problem, supporting that high SAR values was not a major problem in our studies.

Temperature control during MRI scanning

Due to the anaesthesia and relatively cold room-air surrounding the magnet, the challenge was rather to keep the animals warm during scanning. This was achieved using a designated bed with circulating warm water in addition to covering the rats with cotton wool. After a brief cooling (3-4 minutes), due to the induction of anaesthesia, the rat pups regained normal temperature within approximately 10 minutes. As hypothermia has neuroprotective effects

(Jacobs and Tarnow-Mordi 2010), this brief cooling may have reduced the hypoxic-ischemic injury.

In all of our studies, the influence of all these factors related to animal handling and MRI acquisition were controlled for by having control groups that had the same handling and MRI. Still, an interaction between severity of the insult and such environmental and physiological factors cannot be completely ruled out. Such an interaction may have influenced the results to give both larger and smaller differences; between treatment groups in paper III and between exposure groups in paper IV. One improvement to our study designs would have been to have control groups to examine the effects of repeated MRI and exposure to repeated anaesthesia on the development of hypoxic-ischemic injury. To our knowledge this has not been examined before, but one study has examined the effects of repeated MRI at 7 Tesla in both 15 days old rat embryos (E15) *in utero* and 14 days old neonatal rats (P14) using isoflurane anaesthesia (Zhu *et al.* 2011). After exposure to a similar MSME sequence as was used in this thesis for approximately 35 minutes four days in a row, no effects on cell proliferation, neurogenesis, astrogenesis, cell death or memory function were found. This supports a general conclusion that repeated MRI can be conducted safely in neonatal rat pups after hypoxic-ischemic injury.

6.2.3 Diffusion tensor imaging

Diffusion tensor imaging (DTI) is a good technique for imaging cerebral white matter, but is challenging to perform *in vivo* in the rodent brain due to the relatively small nerve fibre bundles compared to humans. Spin-echo DTI sequences using single line read-out of the signal have given good quality DTI of the rodent brains, but their disadvantage is the long scan times, up to several hours, to achieve sufficient resolution and number of diffusion directions. In our studies we therefore chose to use a diffusion sequence with Echo Planar Imaging (EPI) read-out technique that allows entire k-space to be acquired in one repetition, hence dramatically reducing scan time. This allows higher resolution and more diffusion directions *in vivo*, further improving the quality of the DTI maps. However, EPI is prone to eddy current and chemical shift artefacts and geometric distortions and ghosting effects in the image caused by magnetic field inhomogeneities and rapid gradient switching. For the studies in paper III and IV, we optimized a standard DTI-EPI sequence provided in the software on the magnet consol (Paravision 4.0; Bruker Biospin). Multi shot axial image slices in combination with a left-to-right read-out direction were chosen, since this in practice gave a combination of highest resolution for a given scan time with minimal ghosting effects and only minor geometric distortions. High receiver bandwidth was used to reduce chemical shift artefacts. Eddy currents that arise due to the fast switching of the gradients may modify the gradient pulse experienced by the spins, thus causing a phase shift. In the EPI sequence, after reconstruction, this translates into ghost images that appear half the field of view away from their origin (Le Bihan *et al.* 2006). To avoid

such ghosts to appear in the cerebral tissue of interest, field of view in the phase-encoding direction was large. After reconstruction, images were examined for ghosting that affected the signal of the brain, and some animals with severe ghosting, particularly in paper IV, where not included in the analyses. Furthermore, to reduce image artefacts due to motion and eddy current distortions, affine transformation and co-registration of the diffusion encoded images to the b0 images were performed, and the result of this procedure was visually inspected. Better shim of the magnetic field, better gradients and parallel imaging techniques could have further improved the image quality of the DTI-EPI sequence, but was not available at the time of the study.

The analyses of white matter diffusivity was challenging in the severely injured brain since much of the white matter tissue in the ipsilateral hemisphere had severely reduced thickness or was liquefied. In paper IV, injures were so severe that regions of interest analyses in the ipsilateral hemisphere were deemed meaningless, except for in the corpus callosum. In paper III, the white matter tracts were present, but sometimes with reduced size. Regions of interest were therefore placed in the centre of the structures to avoid partial volume effects, such as caused by including non-white matter tissue in the ROI. This however, resulted in ROI with few voxels in each white matter structure. To compensate for this and create a more robust measure, three large ROIs were created by combining genu, body and splenum of corpus callosum to one corpus callosum ROI; internal capsule, external capsule, hippocampal fimbria, and cingulum of the right and left cerebral hemisphere to right white matter ROI and left white matter ROI, respectively.

6.2.4 Toxic effects of manganese

Toxic effects of manganese are well known (Crossgrove and Zheng 2004; Silva *et al.* 2004; Wendland 2004; Aschner *et al.* 2005; Erikson *et al.* 2007; Rovetta *et al.* 2007) and are a major concern with regard to manganese-enhanced MRI (Silva and Bock 2008), and more so in a neonatal model (Erikson *et al.* 2007). Previous studies in humans and animal models have shown both acute liver toxicity (Crossgrove and Zheng 2004; Rovetta *et al.* 2007), cardiodepressive effects (Brurok *et al.* 1997; Crossgrove and Zheng 2004; Wendland 2004) and neurodepressive effects like somnolence, ataxia, convulsions and reduced seizure threshold (Silva *et al.* 2004) related to high loads of manganese. However, more common is the neurotoxic effects seen after chronic exposure to manganese, resulting in an irreversible syndrome called manganism. Manganism is thought to result from neuronal damage in the basal ganglia, and is characterized by neurological symptoms and sign similar to Parkinson's disease, including dystonia, bradykinesi and rigidity (Takeda 2003), but also by memory loss, head ache and insomnia (Crossgrove and Zheng 2004).

During the pilot period before the initial experiments published in paper I, different doses of $MnCl_2$ were tested. Based on previous studies in neonatal and adult rodents (Aoki *et al.* 2004; Wadghiri *et al.* 2004; Watanabe *et al.* 2004b; Lee *et al.* 2005), different doses of $MnCl_2$ ranging from 20 to 120 mg/kg were tested and evaluated with respect to contrast effect and tolerance in the neonatal pups. High mortality resulted from a dose of 120mg/kg, while doses of 20, 40 and 60mg/kg were well tolerated. Doses of both 40 and 60mg/kg gave good tissue contrast, but since the difference was small and sufficient contrast was obtained with 40mg/kg, this dose was chosen with respect to possible toxic effects. Different timing of the injections was also tested. In Initial tests, pups were injected immediately after severing of the carotid artery, but this resulted in high mortality during hypoxia. The cause was unclear, but can be related to both cardiodepressive effects and neurological effects like reduced seizure threshold caused by high manganese blood content (Crossgrove and Zheng 2004; Silva *et al.* 2004) in combination with the hypoxia. Injections six hours after the hypoxia were then tested, and were well tolerated and gave good general tissue contrast on MRI one day afterwards (Paper I).

When $MnCl_2$ was injected intraperitoneally at a concentration of 100mM in the initial tests, we sometimes saw local skin reactions. These skin reactions were avoided when the dose of $MnCl_2$ was diluted in 0.9% NaCl. This dilution also increased the accuracy for delivering the correct dose of $MnCl_2$, as the total injection volume increased from approximately 50µl to 100 or 150µl.

Apart from these acute effects, no toxic effects of manganese were seen in our studies. Although the studies were not specifically designed to examine the toxic effects of manganese, comparison of the hypoxic-ischemic injury and growth between manganese-exposed and controls was possible in paper I, II and IV. In these studies no additional effects of manganese were seen on body weight, weight gain, injury volumes, or histological and immune-histochemical evaluation of the brain tissue. However, subtle histological effects or effects on functional outcome were not tested for and may off course have been present.

There have also been reports that manganese induces microglial activation (Filipov *et al.* 2005). This may have influenced our results, but again since immunohistochemical findings were the same in HI animals with and without manganese, this is not likely. Furthermore, we did not see any microglial activation in sham animals that were given manganese in paper I, II and III.

6.2.5 Identification and quantification of manganese-enhancement

Manganese in tissue primarily reduces the tissue T_1, and is thus best visualized using T_1-weighted imaging. To quantify this effect, T_1-mapping can be used to give the actual reduction

in T_1 caused by manganese. In pure water, this reduction in T_1 is a function of the relaxivity and the concentration of manganese (see Eq. 2.4). Hence the manganese concentration can be estimated from the T_1-reduction. However, in tissue, with different compartments and binding of manganese, the relationship between tissue manganese concentration and change in T_1 is far more complex. Furthermore, T_1-mapping using spin-echo is time consuming due to long repetition times. Other time efficient methods with high spatial resolution, such as gradient echo sequences with variable flip-angles are widely used on clinical systems, but have shown to give unreliable measures of T_1 on our MR system (Huuse 2010).

In all papers of this thesis, a spoiled gradient echo (FLASH) sequence was used to acquire T_1-weighted images that were used to identify manganese-enhancement. The choice of a FLASH sequence for manganese-enhanced imaging was motivated by its properties that could give high resolution 3D T_1-weighted images in a short scan time. Furthermore, several previous studies had successfully used a FLASH sequence for MEMRI (Watanabe *et al.* 2004a; Alvestad *et al.* 2007; Thuen *et al.* 2008). In the pilot period this sequence was optimized using phantoms and animals. Since high spatial resolution was a high priority, repetition time and flip-angles were optimized to give best possible contrast-to-noise within a given scan time, at a given resolution. However, in retrospect, using this sequence, we experienced low contrast-to-noise in some of the manganese-enhanced areas with blurred boundaries between enhanced and non-enhanced tissue. This made it particularly difficult to design automated procedures for detection and segmentation of manganese-enhanced tissue. A better priority may therefore have been to reduce the resolution, increase repetition time and flip-angles to improve signal intensity and tissue contrast. Improved T_1 contrast may also have been obtained using saturation or inversion recovery preparations, or a T_1-weighted spin-echo sequence, but all at the cost of reduced resolution and / or increased scan time.

Since a T_1-weighted sequence was used for imaging, the identification of manganese-enhancement relied on differences in signal intensity between enhanced and non-enhanced tissue. Comparison of signal intensity is challenging as it is dependent on several factors: acquisition method, homogeneity of the excitation (B_1^+) and receive field (B_1^-), subject mass and placement in scanner, receiver gain and signal scaling. In our studies, the acquisition method was the same, signal intensity measures using only the volume-coil showed homogeneous signal intensity across the field-of-view in a phantom, receiver gain was held constant and signal scaling was corrected for during reconstruction. The spatial variation in the sensitivity of the receiver surface coils was a challenge that was overcome by performing a correction of the signal intensity based on the signal ratio between two low-resolution scans using the surface and volume coils for reception. Furthermore, other limitations of signal

intensity were compensated for by comparing the signal intensity in corresponding tissue areas in ipsilateral and contralateral hemispheres in the same brain.

There was a challenge to detect and quantify manganese-enhancement in pathological tissue, since normal tissue was also manganese-enhanced. In paper I and II we used regions of interest to test for differences in signal intensity between corresponding areas in the two hemispheres. The results from these two papers showed that manganese-enhancement could be defined by higher signal intensity in the ipsilateral hemisphere compared to the contralateral hemisphere and that this manganese-enhancement was related to pathological tissue. However, as demonstrated in paper I, at early time points pathological areas in the ipsilateral hemisphere showed increased signal related to manganese when compared to animals without manganese, but not when compared to the contralateral hemisphere or sham with normal manganese-enhancement. This demonstrated the disadvantage that MRI contrast agents are indirect methods for creating tissue contrast: Since contrast is created by reducing T_1 or T_2 of the tissue, hence altering the signal intensities in weighted images, other concurring tissue processes may also alter the signal in the same or opposite directions – increasing or reducing the effects of the contrast agent. In our animal model such concurring tissue processes on day one and day three could be tissue oedema or tissue liquefaction increasing tissue T_1 and T_2, and increased tissue iron that would result in T_2* effects with reduced signal. Such effects reduced the sensitivity of our method in detecting pathological manganese-enhancement and likely led to an underestimation of pathological manganese-enhancement also at later time-points.

In paper III and IV, manganese-enhancement was defined in the same way as in the first papers. We used this definition to manually trace the areas of manganese-enhancement in the ipsilateral hemisphere and calculated the volumes of manganese-enhanced tissue. We ideally wanted to develop a robust automated procedure to segment out these areas. However, comparison of signal in corresponding structures was difficult since the injury to the ipsilateral hemisphere led to a distorted anatomy in both the ipsi- and contralateral cerebral tissue. Such changes in anatomy were easily detected and compensated for by the human eye, but not by automated computer procedures. Hence a possible human bias was introduced in our analyses.

6.3 What does manganese-enhancement mean?

The purpose of using manganese as a MRI contrast agent in this thesis was initially to visualize the delayed neuronal death following hypoxia-ischemia. The hypothesis was that Mn^{2+} would act as a calcium analogue and therefore could be used as a proxy for high intracellular calcium associated with cell death. In paper I we explored this hypothesis and found no increased

manganese-enhancement at the time of maximum neuronal death one and three days after HI. The increased signal in sham animals and in the contralateral hemisphere of animals injected with manganese showed that manganese was present in the brain at these time-points, but not more so in areas with on-going neuronal death, as shown on histology. Therefore the original hypothesis, that manganese would accumulate in apoptotic and necrotic cells did not seem valid. The same conclusion was also drawn by two other studies that examined ischemic injury in neonatal and adult brain (Yang *et al.* 2008a; Kawai *et al.* 2010). Instead, increased manganese-enhancement was visible seven days after HI in areas which on histological examinations showed neuronal death, astrogliosis and activated microglia. We therefore concluded that with this method of MEMRI we did not visualize neuronal death per se, but that increased manganese-enhancement was related to delayed inflammatory reactions, such as astrogliosis and microgliosis secondary to the initial hypoxic-ischemic cell death.

Concurrent with our studies, Yang *et al*. (2008a; 2008b) conducted two studies, where they examined manganese-enhancement after severe and mild hypoxia-ischemia in the neonatal rat brain. In the first study with severe hypoxic-ischemic injury (Yang *et al.* 2008a), they saw the same pattern of manganese-enhancement as in our studies with a peak around day seven after HI, but with more enhancement on day three after hypoxia-ischemia than in our study. This earlier detection of significant enhancement can be related to an almost double dose of $MnCl_2$ (88mg/kg) than in our studies (Yang *et al.* 2008a). However, it may also be related to different imaging techniques. While we used a spoiled gradient-echo (FLASH) sequence, Yang et al used a T_1-weighted spin-echo sequence. The latter may have provided a better T_1-weighting giving better contrast to manganese in tissue, while the former may have been sensitive to signal reduction caused by T_2*-decay due to iron in the same area and thus reduced contrast. In the second study by Yang and Wu (2008b), they found the same temporal pattern of manganese-enhancement, this time with a mild hypoxic-ischemic insult giving a predominantly focal cortical lesion. In both studies, they compared manganese-enhancement with histology and found it to correlate spatially and temporally with Glutamine Synthetase (GS) and Manganese-Superoxide Dismutase (MnSOD). GS is found mainly in astrocytes and is up-regulated in response to glutamate excitotoxicity (Lehmann *et al.* 2009), while increased MnSOD is found primarily in mitochondria of neurons and microglia upon oxidative stress (Bidmon *et al.* 1998). However, Yang et al (2008a; 2008b) did not perform histological examinations to look for macrophages / activated microglia, reactive astrocytes or apoptosis. In our studies, we found a great overlap between reactive astrocytes, activated microglia and apoptosis in paper I and paper II, and the reactivity of these cells do usually concur (Zhang *et al.* 2010). In another study, Chan *et al.* (2008) demonstrated manganese-enhancement in striatum after unilateral middle cerebral artery occlusion, and concluded that manganese-

enhancement was related to increased GS, MnSOD and reactive astrocytes expressing GFAP in the lesion site 10 days after the ischemia. However, based on the images provided in the article, manganese-enhancement seemed far better co-localized with MnSOD expression than GFAP expression, which was predominantly localized in the periphery of the striatum and manganese-enhanced area. A similar pattern of increased GFAP expression in reactive astrocytes was also seen in another study using middle cerebral artery occlusion in the adult rat (Kawai *et al.* 2010), and was correlated to the manganese-enhancement seen 10 days after ischemia. In this study, immunohistochemical staining for activated microglia (Iba-1) and apoptosis (TUNEL) were performed and these cells were found mostly in the core of the lesion, where manganese-enhancement was less prominent. Although there was some overlap between the reactive astrocytes and activated microglial cells, Kawai *et al.* (2010) concluded that manganese-enhancement was related to astrogliosis and not to apoptosis or activated microglia / macrophages. They further speculated that increased manganese in astrocytes was related to increased GS expression and/or increased Mn^{2+} influx due to increased glutamate excitotoxicity, but that it also could be a result of increased density of Mn-containing astrocytes.

The conclusions to what lies behind the manganese-enhancement also differ in other manganese-enhanced MRI studies in other cerebral injury models. In a rat model of epileptogenesis induced by the neurotoxin kainic acid, one study concluded that increased manganese-enhancement in hippocampus was related to mossy fibre sprouting (Immonen *et al.* 2008). In a rat model of cathepsin D-deficiency, characterized by neuronal degeneration and gliosis, Haapanen *et al.* (2007) found a very good agreement between manganese-enhancement and areas of microglial activation, supporting the conclusion in paper I. However, also in that study there was some overlap between areas with reactive astrogliosis and activated microglia.

It therefore seems that more studies to reveal the exact mechanisms behind the manganese-uptake are warranted. However, in practice manganese-enhancement seems to be a good proxy for secondary inflammatory reactions after (hypoxic-)ischemic brain injury, and that MEMRI can be a useful tool to indirectly image the associated astrogliosis and microgliosis.

6.4 Brain injury development after HI

One of the main findings in all studies of this thesis is the progressive nature of the injury after hypoxia-ischemia. Previous studies have shown how MRI change over the course of the first days after injury, but few have examined the lesion volumes and volumes of cerebral tissue over an extended period of time after the hypoxic-ischemic insult. In papers II and IV we showed how there is a reduction in the relative volume of cerebral tissue from day seven to six

weeks after HI indicating atrophy of the ipsilateral cerebral hemisphere and increasing cystic volume, as demonstrated in paper IV. These findings are in accordance with a MRI study by Stone et al (Stone *et al.* 2008) who showed progressive cyst formation and reduced hippocampal volumes up to 21 days after HI. Furthermore, in another study using both MRI and histological methods, progressive brain damage has also been shown up to 54 weeks after HI (Mishima *et al.* 2005). However, in paper III, when the magnitude of the insult was reduced, no significant change in relative volume of the ipsilateral cerebral tissue was found from day seven to six weeks after HI. This may indicate that the progressiveness of the brain damage following HI can be related to the severity of the insult. However, such a conclusion is in contradiction with a study by Geddes et al (Geddes *et al.* 2001) where injury was evaluated by histological examinations on different time points following hypoxia-ischemia. They showed how cerebral atrophy of the ipsilateral hemisphere evolved up to 8 weeks after HI in animals with a short hypoxic exposure, whereas animals with a long hypoxic exposure had more severe infarctions at the early time points with no significant evolution of the injury. Their results were based on histological grading and measurements of hemispheric diameter on two coronal tissue sections, which is probably less accurate than volumetric measurements on 3D MRI. The repeated measurements with MRI in our studies also strengthen the accuracy in evaluating injury development. Furthermore, our results are supported by a study by van de Looij et al (van de Looij *et al.* 2011). They found higher cortical loss on day 22 than on day 8 after HI among pups with severe lesions on day one, whereas cortical loss was unchanged between day 8 and 22 after HI among pups with mild lesions on day one. However, in this study the difference in lesion was explained by gender, with male pups having significantly more severe lesions than females. In our studies, we did not see such gender effects.

In paper III and IV we also showed how the developmental maturation of white matter in the six weeks following hypoxia-ischemia also was influenced by the hypoxic-ischemic insults. In both studies, the maturational increase in fractional anisotropy was less in the most severely injured animals (non-treated in paper III and hyperoxia exposed in paper IV) compared to that of animals with less initial injury. These results can be viewed as a continuous effect of intervention over the course of injury development, but may also be related to different trajectories as a consequence of early interventional effects determining the initial severity of the insult. This supports a notion that development of brain injury following HI is affected by the severity of the insult, with more severe insults giving more progressive injury development.

Importantly, it seems possible to accurately estimate the trajectory of injury development based on early measures on MRI. In both paper III and IV we demonstrated that lesion volumes six weeks after HI insult were highly correlated with lesion volumes on ADC-maps and reduced

ADC-values measured in thalamus day one after HI. The same has also been shown in other animal studies (Wang *et al.* 2007; van de Looij *et al.* 2011). However, in clinical practice early conventional MRI or diffusion MRI has so far not been successful in predicting long-term outcome after hypoxic-ischemic injury. This may be related to the rapidly changing tissue contrast during the first hours and days after the insult, as demonstrated in paper I and by others (Rumpel *et al.* 1995; Albensi *et al.* 1998; Tuor *et al.* 1998; Malisza *et al.* 1999; Tuor *et al.* 1999; Qiao *et al.* 2004; Meng *et al.* 2005; Meng *et al.* 2006). The changing tissue contrasts make the determination of lesion size highly dependent on the timing of the MRI. Since accurately determining the timing of the insult in clinical practice can be difficult, as clinical signs and symptoms often are sparse in the first hours and days, especially in the prematurely born children, lesion size determination will often be inaccurate in a clinical setting. This can explain some of this discrepancy between animal and human studies.

6.5 The role of microgliosis and astrogliosis in delayed HI injury

It is increasingly acknowledged that inflammation plays an important role in the injury process following hypoxic-ischemic insults (Dirnagl *et al.* 1999; Khwaja and Volpe 2008). Studies using histological methods have shown that activated microglia and reactive astrogliosis are prominent tissue reactions accompanying neuronal death during the first week following a hypoxic-ischemic insult (Mcrae *et al.* 1995; Towfighi *et al.* 1995; Bona *et al.* 1999; Chew *et al.* 2006), and astroglial and microglial reactivity has also been shown for weeks thereafter suggesting a chronic inflammatory component in the delayed injury (Lin *et al.* 1998; Bona *et al.* 1999). However, the longitudinal involvement of inflammation in this injury process has not been studied before. As discussed above, manganese-enhanced MRI seems to be a method enabling such longitudinal studies of inflammation in the delayed injury process. The results from paper I and II clearly show that areas with astrogliosis and microgliosis dissolves and liquefy, suggesting that such inflammatory reactions is a major contributing factor to the delayed and sustained cell death seen after HI. This hypothesis is further supported by the results of paper III, where a correlation between the volume of manganese-enhanced tissue and increase in cystic volume was shown. Furthermore, in paper III we showed that animals treated with doxycycline, which is known to inhibit microglial activation, had reduced cyst formation and reduced loss of cerebral tissue compared to untreated animals. We also found that there was an interaction between doxycycline treatment and time after HI, indicating that the inhibition of inflammation influenced the trajectory of injury development.

It has been unclear whether the inflammatory reactions after HI is causal or if it is a modulatory response (Ferriero 2004). Inflammatory cytokines secreted by neurons, astrocytes and microglia as a response to tissue hypoxia and ischemia induce microglial activation with subsequent release of more inflammatory cytokines and mediators like prostaglandins and

free radicals This result in a perpetuating cycle of cell death and further inflammatory response (Vexler *et al.* 2006; Khwaja and Volpe 2008). On the other hand, activated microglia can act as phagocytes and clear dead cells and cell debris, and astrogliosis that border the lesion site is also thought to limit the spread of inflammation (Barron 1995; Zhang *et al.* 2010). From our studies it seems that both a causal and modulatory effect of gliosis may co-exist. The liquefaction of manganese-enhanced tissue speaks to the modulatory phagocytic actions of microglia, while the reduced injury seen after microglial inhibition with doxycycline clearly suggest that inflammation is a causal factor and that early inhibition of inflammation after hypoxia-ischemia is neuroprotective. The close overlap between astrogliosis and microgliosis seen in our studies can be taken as in indication of the close interaction between these two cell types, also shown by others (McRae *et al.* 1996; Zhang *et al.* 2010). As astrogliosis is known to inhibit neuronal plasticity and growth after neuronal damage (Privat 2003), treatments that reduced inflammation and astrogliosis may contribute to more neurogenesis and neuronal re-modelling after HI injury.

Chapter 7 Conclusions and future perspectives

Manganese-enhanced MRI has been shown to be feasible in a neonatal rat model of hypoxic-ischemic injury. It improves the tissue contrast in T_1-weighted images, thereby allowing high resolution images to be acquired in a short time. In addition manganese-enhanced MRI has been shown to be a useful tool to follow the injury process and detect the delayed gliosis with concurring cell death that follows the hypoxic-ischemic injury. However, the cellular specificity of manganese-enhancement remains unclear, as do the questions of whether uptake of manganese is dependent on Ca^{2+}-channels, other anion-channels or metal-transporters. Future research into these questions and optimization of MRI sequences and image post-processing to detect tissue manganese can further improve the usefulness of the method. Clinical use of manganese-enhanced MRI is still limited by safety issues concerning toxicity, and will for now remain an animal research tool. However, clinical manganese-enhanced MRI of the brain may be possible with the use of optimal doses or slow-release manganese from chelates, given that the safety of such applications can be established.

Hypoxic-ischemic injury to the neonatal brain is a prolonged injury process that lasts for several weeks after the insult in neonatal rats. This may translate into several years in humans, so there is clearly a need for long term follow-up in children exposed to hypoxia-ischemia in the perinatal period. Inflammation and gliosis seems to be one of the key elements of this delayed injury process. However, whether this is actually adds to the final injury, or if it can be considered part of a necessary re-modelling of brain tissue remains uncertain. Targeted contrast agents may in the future provide means of specific detection of cells and pathological processes *in vivo*. This may give more specific knowledge of the involvement of inflammation in brain development after hypoxia-ischemia in animals and human children.

The studies of this thesis have shown that maturational changes and injuries to white matter microstructure in the neonatal rat brain can be followed using diffusion tensor imaging. Furthermore, hypoxia-ischemia seems to affect the trajectory of white matter development with results on DTI indicating reduced or delayed myelination. Future improvements to the DTI acquisition, such as better field homogeneity, more powerful gradient systems, use of parallel imaging techniques and improved image reconstruction and post-processing algorithms, can provide better resolution and quality of the DTI data. Such improvements may give better

detection of subtle alterations in white matter integrity and can give new knowledge about how hypoxia-ischemia affects brain connectivity and neuronal networks in future studies. Changes in grey matter microstructure may also be visualized using DTI. In some of the animals in paper III, changes in fractional anisotropy and directionality of the axial diffusivity in the injured cortex were noted (data not shown in the paper). Further studies into such applications of DTI may carry interesting prospects.

Early MRI biomarkers for reliably detecting lesions and determining outcome are still needed. Estimated lesion volume and the apparent diffusion coefficient value in tissue on diffusion maps 24 hours after the hypoxic-ischemic insult, have both shown to be good predictors of long term lesion volume. However, the apparent diffusion coefficient can be an ambiguous measure. As demonstrated in paper III and IV, increased diffusion in certain brain areas was associated with mild injury, while the magnitude of the reduction of diffusion in other brain areas correlated with the severity of the injury at later time-points. Further research is needed to establish the cellular events underlying these changes in tissue diffusion.

Exposure to 100% oxygen after a hypoxic-ischemic insult increase brain injury and is detrimental to brain development. Supplemental oxygen during resuscitation and in the neonatal period should therefore be avoided when possible. Whether the fluctuating oxygen levels, which the unstable neonates often experiences, also cause or exacerbate brain injury after birth, is an interesting topic for future research.

Inhibition of brain inflammation by a single dose of doxycycline reduces long-term cerebral tissue loss and white matter injury after neonatal hypoxia-ischemia. More research is needed to establish the optimal dose and if repeated treatment can provide further neuroprotection. However, doxycycline has potential as a treatment for hypoxic-ischemic brain injury in the neonate, either alone, or in combination with for instance hypothermia. Other therapies that target the negative effects of brain inflammation and gliosis after hypoxic-ischemic injury should also be sought. Such therapies may involve treatment with for instance mesenchymal stem cells, which can provide a trophic environment that limit the inflammatory response, gliotic scar formation, in addition to stimulating neuronal growth and vascular formation. Labelling of such cells with magnetic particles can provide means to monitor the migration, viability and incorporation of these cells in cerebral tissue *in vivo* using MRI.

Chapter 8 Bibliography

Albensi, B. C., M. P. Schweizer, T. M. Rarick and F. Filloux (1998). *Magnetic resonance imaging of hypoxic-ischemic brain injury in the neonatal rat*. Invest Radiol **33**(7): 377-385.

Alvestad, S., P. E. Goa, H. Qu, O. Risa, C. Brekken, U. Sonnewald, O. Haraldseth, J. Hammer, O. P. Ottersen and A. Haberg (2007). *In vivo mapping of temporospatial changes in manganese enhancement in rat brain during epileptogenesis*. Neuroimage **38**(1): 57-66.

Andiné, P., M. Thordstein, I. Kjellmer, C. Nordborg, K. Thiringer, E. Wennberg and H. Hagberg (1990). *Evaluation of brain damage in a rat model of neonatal hypoxic-ischemia*. Journal of Neuroscience Methods **35**(3): 253-260.

Aoki, I., T. Ebisu, C. Tanaka, K. Katsuta, A. Fujikawa, M. Umeda, M. Fukunaga, T. Takegami, E. M. Shapiro and S. Naruse (2003). *Detection of the anoxic depolarization of focal ischemia using manganese-enhanced MRI*. Magn Reson Med **50**(1): 7-12.

Aoki, I., C. Tanaka, T. Takegami, T. Ebisu, M. Umeda, M. Fukunaga, K. Fukuda, A. C. Silva, A. P. Koretsky and S. Naruse (2002). *Dynamic activity-induced manganese-dependent contrast magnetic resonance imaging (DAIM MRI)*. Magn Reson Med **48**(6): 927-933.

Aoki, I., Y. J. Wu, A. C. Silva, R. M. Lynch and A. P. Koretsky (2004). *In vivo detection of neuroarchitecture in the rodent brain using manganese-enhanced MRI*. Neuroimage **22**(3): 1046-1059.

Arvin, K. L., B. H. Han, Y. Du, S. Z. Lin, S. M. Paul and D. M. Holtzman (2002). *Minocycline markedly protects the neonatal brain against hypoxic-ischemic injury*. Ann Neurol **52**(1): 54-61.

Aschner, M., K. M. Erikson and D. C. Dorman (2005). *Manganese dosimetry: species differences and implications for neurotoxicity*. Crit Rev Toxicol **35**(1): 1-32.

Aschner, M., T. R. Guilarte, J. S. Schneider and W. Zheng (2007). *Manganese: recent advances in understanding its transport and neurotoxicity*. Toxicol Appl Pharmacol **221**(2): 131-147.

Assaf, Y., T. Blumenfeld-Katzir, Y. Yovel and P. J. Basser (2008). *AxCaliber: a method for measuring axon diameter distribution from diffusion MRI*. Magn Reson Med **59**(6): 1347-1354.

Barron, K. D. (1995). *The microglial cell. A historical review*. J Neurol Sci **134 Suppl**: 57-68.

Basser, P. J., J. Mattiello and D. LeBihan (1994). *MR diffusion tensor spectroscopy and imaging*. Biophys J **66**(1): 259-267.

Bidmon, H. J., K. Kato, A. Schleicher, O. W. Witte and K. Zilles (1998). *Transient increase of manganese-superoxide dismutase in remote brain areas after focal photothrombotic cortical lesion*. Stroke **29**(1): 203-210; discussion 211.

Bissig, D. and B. A. Berkowitz (2009). *Manganese-enhanced MRI of layer-specific activity in the visual cortex from awake and free-moving rats*. Neuroimage **44**(3): 627-635.

Bloch, F., W. W. Hansen and M. Packard (1946). *Nuclear Induction*. Physical Review **69**(3-4): 127-127.

Block, M. L., L. Zecca and J. S. Hong (2007). *Microglia-mediated neurotoxicity: uncovering the molecular mechanisms*. Nat Rev Neurosci **8**(1): 57-69.

Bockhorst, K. H., P. A. Narayana, J. Dulin, R. Liu, H. C. Rea, K. Hahn, J. Wosik and J. R. Perez-Polo (2010). *Normobaric hyperoximia increases hypoxia-induced cerebral injury: DTI study in rats*. J Neurosci Res **88**(5): 1146-1156.

Bona, E., A. L. Andersson, K. Blomgren, E. Gilland, M. Puka-Sundvall, K. Gustafson and H. Hagberg (1999). *Chemokine and inflammatory cell response to hypoxia-ischemia in immature rats*. Pediatr Res **45**(4 Pt 1): 500-509.

Brurok, H., J. Schjott, K. Berg, J. O. Karlsson and P. Jynge (1997). *Manganese and the heart: acute cardiodepression and myocardial accumulation of manganese*. Acta Physiol Scand **159**(1): 33-40.

Buller, K. M., M. L. Carty, H. E. Reinebrant and J. A. Wixey (2009). *Minocycline: a neuroprotective agent for hypoxic-ischemic brain injury in the neonate?* J Neurosci Res **87**(3): 599-608.

Bush, T. G., N. Puvanachandra, C. H. Horner, A. Polito, T. Ostenfeld, C. N. Svendsen, L. Mucke, M. H. Johnson and M. V. Sofroniew (1999). *Leukocyte infiltration, neuronal degeneration, and neurite outgrowth after ablation of scar-forming, reactive astrocytes in adult transgenic mice*. Neuron **23**(2): 297-308.

Cai, Z., S. Lin, L. W. Fan, Y. Pang and P. G. Rhodes (2006). *Minocycline alleviates hypoxic-ischemic injury to developing oligodendrocytes in the neonatal rat brain*. Neuroscience **137**(2): 425-435.

Carty, M. L., J. A. Wixey, P. B. Colditz and K. M. Buller (2008). *Post-insult minocycline treatment attenuates hypoxia-ischemia-induced neuroinflammation and white matter injury in the neonatal rat: a comparison of two different dose regimens*. Int J Dev Neurosci **26**(5): 477-485.

Chakeres, D. W., A. Kangarlu, H. Boudoulas and D. C. Young (2003). *Effect of static magnetic field exposure of up to 8 Tesla on sequential human vital sign measurements*. J Magn Reson Imaging **18**(3): 346-352.

Chan, K. C., K. X. Cai, H. X. Su, V. K. Hung, M. M. Cheung, C. T. Chiu, H. Guo, Y. Jian, S. K. Chung, W. T. Wu and E. X. Wu (2008). *Early detection of neurodegeneration in brain ischemia by manganese-enhanced MRI*. Conf Proc IEEE Eng Med Biol Soc **2008**: 3884-3887.

Chan, K. C., P. L. Khong, H. F. Lau, P. T. Cheung and E. X. Wu (2009). *Late measures of microstructural alterations in severe neonatal hypoxic-ischemic encephalopathy by MR diffusion tensor imaging*. Int J Dev Neurosci **27**(6): 607-615.

Chen, H., M. Burris, A. Fajilan, F. Spagnoli, J. Tang and J. H. Zhang (2011). *Prolonged Exposure to Isoflurane Ameliorates Infarction Severity in the Rat Pup Model of Neonatal Hypoxia-Ischemia*. Transl Stroke Res **2**(3): 382-390.

Cheng, Y., M. Deshmukh, A. D'Costa, J. A. Demaro, J. M. Gidday, A. Shah, Y. Sun, M. F. Jacquin, E. M. Johnson and D. M. Holtzman (1998). *Caspase inhibitor affords neuroprotection with delayed administration in a rat model of neonatal hypoxic-ischemic brain injury*. J Clin Invest **101**(9): 1992-1999.

Cheong, J. L., D. K. Thompson, H. X. Wang, R. W. Hunt, P. J. Anderson, T. E. Inder and L. W. Doyle (2009). *Abnormal white matter signal on MR imaging is related to abnormal tissue microstructure*. AJNR Am J Neuroradiol **30**(3): 623-628.

Chew, L. J., A. Takanohashi and M. Bell (2006). *Microglia and inflammation: impact on developmental brain injuries*. Ment Retard Dev Disabil Res Rev **12**(2): 105-112.

Chuang, K. H., L. Belluscio and A. P. Koretsky (2010). *In vivo detection of individual glomeruli in the rodent olfactory bulb using manganese enhanced MRI*. Neuroimage **49**(2): 1350-1356.

Chuang, K. H., J. H. Lee, A. C. Silva, L. Belluscio and A. P. Koretsky (2009). *Manganese enhanced MRI reveals functional circuitry in response to odorant stimuli*. Neuroimage **44**(2): 363-372.

Clark, W. M., F. A. Calcagno, W. L. Gabler, J. R. Smith and B. M. Coull (1994). *Reduction of central nervous system reperfusion injury in rabbits using doxycycline treatment*. Stroke **25**(7): 1411-1415; discussion 1416.

Corbett, D. and J. Thornhill (2000). *Temperature modulation (hypothermic and hyperthermic conditions) and its influence on histological and behavioral outcomes following cerebral ischemia*. Brain Pathol **10**(1): 145-152.

Counsell, S. J., J. M. Allsop, M. C. Harrison, D. J. Larkman, N. L. Kennea, O. Kapellou, F. M. Cowan, J. V. Hajnal, A. D. Edwards and M. A. Rutherford (2003). *Diffusion-weighted imaging of the brain in preterm infants with focal and diffuse white matter abnormality*. Pediatrics **112**(1 Pt 1): 1-7.

Counsell, S. J., Y. Shen, J. P. Boardman, D. J. Larkman, O. Kapellou, P. Ward, J. M. Allsop, F. M. Cowan, J. V. Hajnal, A. D. Edwards and M. A. Rutherford (2006). *Axial and radial diffusivity in preterm infants who have diffuse white matter changes on magnetic resonance imaging at term-equivalent age*. Pediatrics **117**(2): 376-386.

Cowell, R. M., J. M. Plane and F. S. Silverstein (2003). *Complement activation contributes to hypoxic-ischemic brain injury in neonatal rats*. J Neurosci **23**(28): 9459-9468.

Cowell, R. M., H. Xu, J. M. Galasso and F. S. Silverstein (2002). *Hypoxic-ischemic injury induces macrophage inflammatory protein-1alpha expression in immature rat brain*. Stroke **33**(3): 795-801.

Crossgrove, J. and W. Zheng (2004). *Manganese toxicity upon overexposure*. NMR Biomed **17**(8): 544-553.

Davis, P. G., A. Tan, C. P. O'Donnell and A. Schulze (2004). *Resuscitation of newborn infants with 100% oxygen or air: a systematic review and meta-analysis*. Lancet **364**(9442): 1329-1333.

de Bruine, F. T., A. A. van den Berg-Huysmans, L. M. Leijser, M. Rijken, S. J. Steggerda, J. van der Grond and G. van Wezel-Meijler (2011). *Clinical Implications of MR Imaging Findings in the White Matter in Very Preterm Infants: A 2-year Follow-up Study*. Radiology **261**(3): 899-906.

Dirnagl, U., C. Iadecola and M. A. Moskowitz (1999). *Pathobiology of ischaemic stroke: an integrated view*. Trends Neurosci **22**(9): 391-397.

Dudink, J., M. Lequin, C. van Pul, J. Buijs, N. Conneman, J. van Goudoever and P. Govaert (2007). *Fractional anisotropy in white matter tracts of very-low-birth-weight infants*. Pediatr Radiol **37**(12): 1216-1223.

Edwards, A. D., P. Brocklehurst, A. J. Gunn, H. Halliday, E. Juszczak, M. Levene, B. Strohm, M. Thoresen, A. Whitelaw and D. Azzopardi (2010). *Neurological outcomes at 18 months of age after moderate hypothermia for perinatal hypoxic ischaemic encephalopathy: synthesis and meta-analysis of trial data*. BMJ **340**: c363.

Edwards, A. D., X. Yue, M. V. Squier, M. Thoresen, E. B. Cady, J. Penrice, C. E. Cooper, J. S. Wyatt, E. O. Reynolds and H. Mehmet (1995). *Specific inhibition of apoptosis after cerebral hypoxia-ischaemia by moderate post-insult hypothermia*. Biochem Biophys Res Commun **217**(3): 1193-1199.

Eicher, D. J., C. L. Wagner, L. P. Katikaneni, T. C. Hulsey, W. T. Bass, D. A. Kaufman, M. J. Horgan, S. Languani, J. J. Bhatia, L. M. Givelichian, K. Sankaran and J. Y. Yager (2005). *Moderate hypothermia in neonatal encephalopathy: efficacy outcomes*. Pediatr Neurol **32**(1): 11-17.

Erikson, K. M., Z. K. Shihabi, J. L. Aschner and M. Aschner (2002). *Manganese accumulates in iron-deficient rat brain regions in a heterogeneous fashion and is associated with neurochemical alterations*. Biol Trace Elem Res **87**(1-3): 143-156.

Erikson, K. M., T. Syversen, J. L. Aschner and M. Aschner (2005). *Interactions between excessive manganese exposures and dietary iron-deficiency in neurodegeneration*. Environ Toxicol Pharmacol **19**(3): 415-421.

Erikson, K. M., K. Thompson, J. Aschner and M. Aschner (2007). *Manganese neurotoxicity: a focus on the neonate*. Pharmacol Ther **113**(2): 369-377.

Fan, L. W., S. Lin, Y. Pang, P. G. Rhodes and Z. Cai (2006). *Minocycline attenuates hypoxia-ischemia-induced neurological dysfunction and brain injury in the juvenile rat*. Eur J Neurosci **24**(2): 341-350.

Feng, Y., J. D. Fratkin and M. H. LeBlanc (2003a). *Inhibiting caspase-8 after injury reduces hypoxic-ischemic brain injury in the newborn rat*. Eur J Pharmacol **481**(2-3): 169-173.

Feng, Y., J. D. Fratkin and M. H. LeBlanc (2003b). *Inhibiting caspase-9 after injury reduces hypoxic ischemic neuronal injury in the cortex in the newborn rat*. Neurosci Lett **344**(3): 201-204.

Feng, Y. and M. H. LeBlanc (2003). *Treatment of hypoxic-ischemic brain injury in newborn rats with TPCK 3 h after hypoxia decreases caspase-9 activation and improves neuropathologic outcome*. Dev Neurosci **25**(1): 34-40.

Ferriero, D. M. (2004). *Neonatal brain injury*. N Engl J Med **351**(19): 1985-1995.

Filipov, N. M., R. F. Seegal and D. A. Lawrence (2005). *Manganese potentiates in vitro production of proinflammatory cytokines and nitric oxide by microglia through a nuclear factor kappa B-dependent mechanism*. Toxicol Sci **84**(1): 139-148.

Flecknell, P. A. (2009). *Laboratory animal anaesthesia*. Amsterdam ; Boston ; London, Elsevier/Academic Press.

Geddes, R., R. C. Vannucci and S. J. Vannucci (2001). *Delayed cerebral atrophy following moderate hypoxia-ischemia in the immature rat*. Dev Neurosci **23**(3): 180-185.

Globus, M. Y., O. Alonso, W. D. Dietrich, R. Busto and M. D. Ginsberg (1995). *Glutamate release and free radical production following brain injury: effects of posttraumatic hypothermia*. J Neurochem **65**(4): 1704-1711.

Gonzalez, F. F. and D. M. Ferriero (2009). *Neuroprotection in the newborn infant*. Clin Perinatol **36**(4): 859-880, vii.

Haacke, E. M. (1999). *Magnetic resonance imaging : physical principles and sequence design*. New York, Wiley.

Haapanen, A., U. A. Ramadan, T. Autti, R. Joensuu and J. Tyynela (2007). *In vivo MRI reveals the dynamics of pathological changes in the brains of cathepsin D-deficient mice and correlates changes in manganese-enhanced MRI with microglial activation*. Magn Reson Imaging **25**(7): 1024-1031.

Han, B. H., D. Xu, J. Choi, Y. Han, S. Xanthoudakis, S. Roy, J. Tam, J. Vaillancourt, J. Colucci, R. Siman, A. Giroux, G. S. Robertson, R. Zamboni, D. W. Nicholson and D. M. Holtzman (2002). *Selective, reversible caspase-3 inhibitor is neuroprotective and reveals distinct pathways of cell death after neonatal hypoxic-ischemic brain injury*. J Biol Chem **277**(33): 30128-30136.

Hudome, S., C. Palmer, R. L. Roberts, D. Mauger, C. Housman and J. Towfighi (1997). *The role of neutrophils in the production of hypoxic-ischemic brain injury in the neonatal rat*. Pediatr Res **41**(5): 607-616.

Hunt, R. W., J. J. Neil, L. T. Coleman, M. J. Kean and T. E. Inder (2004). *Apparent diffusion coefficient in the posterior limb of the internal capsule predicts outcome after perinatal asphyxia*. Pediatrics **114**(4): 999-1003.

Huppi, P. S. and M. Amato (2001). *Advanced magnetic resonance imaging techniques in perinatal brain injury*. Biol Neonate **80**(1): 7-14.

Huppi, P. S. and J. Dubois (2006). *Diffusion tensor imaging of brain development*. Semin Fetal Neonatal Med **11**(6): 489-497.

Huppi, P. S., S. E. Maier, S. Peled, G. P. Zientara, P. D. Barnes, F. A. Jolesz and J. J. Volpe (1998). *Microstructural development of human newborn cerebral white matter assessed in vivo by diffusion tensor magnetic resonance imaging*. Pediatr Res **44**(4): 584-590.

Huppi, P. S., B. Murphy, S. E. Maier, G. P. Zientara, T. E. Inder, P. D. Barnes, R. Kikinis, F. A. Jolesz and J. J. Volpe (2001). *Microstructural brain development after perinatal cerebral white matter injury assessed by diffusion tensor magnetic resonance imaging*. Pediatrics **107**(3): 455-460.

Huuse, E. M. (2010). *Assessment of tumor microenvironment and treatment effects in human breast cancer xenografts using MR imaging and spectroscopy*. Faculty of Medicine, Department of Circulation and Medical Imaging. Trondheim, Norwegian University of Science and Technology. **Philosophiae Doctor:** 78.

Immonen, R. J., I. Kharatishvili, A. Sierra, C. Einula, A. Pitkanen and O. H. Grohn (2008). *Manganese enhanced MRI detects mossy fiber sprouting rather than neurodegeneration, gliosis or seizure-activity in the epileptic rat hippocampus*. Neuroimage **40**(4): 1718-1730.

Inder, T., P. S. Huppi, G. P. Zientara, S. E. Maier, F. A. Jolesz, D. di Salvo, R. Robertson, P. D. Barnes and J. J. Volpe (1999). *Early detection of periventricular leukomalacia by diffusion-weighted magnetic resonance imaging techniques*. J Pediatr **134**(5): 631-634.

Istaphanous, G. K. and A. W. Loepke (2009). *General anesthetics and the developing brain*. Curr Opin Anaesthesiol **22**(3): 368-373.

Jacobs, S. E., C. J. Morley, T. E. Inder, M. J. Stewart, K. R. Smith, P. J. McNamara, I. M. Wright, H. M. Kirpalani, B. A. Darlow and L. W. Doyle (2011). *Whole-Body Hypothermia for Term and Near-Term Newborns With Hypoxic-Ischemic Encephalopathy: A Randomized Controlled Trial*. Arch Pediatr Adolesc Med **165**(8): 692-700.

Jacobs, S. E. and W. O. Tarnow-Mordi (2010). *Therapeutic hypothermia for newborn infants with hypoxic-ischaemic encephalopathy*. J Paediatr Child Health **46**(10): 568-576.

Jantzie, L. L., P. Y. Cheung and K. G. Todd (2005). *Doxycycline reduces cleaved caspase-3 and microglial activation in an animal model of neonatal hypoxia-ischemia*. J Cereb Blood Flow Metab **25**(3): 314-324.

Jantzie, L. L., G. A. Rauw and K. G. Todd (2006). *The effects of doxycycline administration on amino acid neurotransmitters in an animal model of neonatal hypoxia-ischemia*. Neurochem Int **49**(8): 717-728.

Jantzie, L. L. and K. G. Todd (2010). *Doxycycline inhibits proinflammatory cytokines but not acute cerebral cytogenesis after hypoxia-ischemia in neonatal rats*. J Psychiatry Neurosci **35**(1): 20-32.

Johnston, M. V., A. Fatemi, M. A. Wilson and F. Northington (2011). *Treatment advances in neonatal neuroprotection and neurointensive care*. Lancet Neurol **10**(4): 372-382.

Johnston, M. V., W. Nakajima and H. Hagberg (2002). *Mechanisms of hypoxic neurodegeneration in the developing brain*. Neuroscientist **8**(3): 212-220.

Joly, L. M., V. Mucignat, J. Mariani, M. Plotkine and C. Charriaut-Marlangue (2004). *Caspase inhibition after neonatal ischemia in the rat brain*. J Cereb Blood Flow Metab **24**(1): 124-131.

Kaandorp, J. J., M. J. Benders, C. M. Rademaker, H. L. Torrance, M. A. Oudijk, T. R. de Haan, K. W. Bloemenkamp, M. Rijken, M. G. van Pampus, A. F. Bos, M. M. Porath, S. B. Oetomo, C. Willekes, A. W. Gavilanes, M. G. Wouters, R. M. van Elburg, A. J. Huisjes, S. C. Bakker, C. A. van Meir, J. von Lindern, J. Boon, I. P. de Boer, R. J. Rijnders, C. J. Jacobs, C. S. Uiterwaal, B. W. Mol, G. H. Visser, F. van Bel and J. B. Derks (2010). *Antenatal allopurinol for reduction of birth asphyxia induced brain damage (ALLO-Trial); a randomized double blind placebo controlled multicenter study*. BMC Pregnancy Childbirth **10**: 8.

Kawai, Y., I. Aoki, M. Umeda, T. Higuchi, J. Kershaw, M. Higuchi, A. C. Silva and C. Tanaka (2010). *In vivo visualization of reactive gliosis using manganese-enhanced magnetic resonance imaging*. Neuroimage **49**(4): 3122-3131.

Khwaja, O. and J. J. Volpe (2008). *Pathogenesis of cerebral white matter injury of prematurity*. Arch Dis Child Fetal Neonatal Ed **93**(2): F153-161.

Koch, J. D., D. K. Miles, J. A. Gilley, C. P. Yang and S. G. Kernie (2008). *Brief exposure to hyperoxia depletes the glial progenitor pool and impairs functional recovery after hypoxic-ischemic brain injury*. J Cereb Blood Flow Metab **28**(7): 1294-1306.

Koretsky, A. P. and A. C. Silva (2004). *Manganese-enhanced magnetic resonance imaging (MEMRI)*. NMR Biomed **17**(8): 527-531.

Krishnan, M. L., L. E. Dyet, J. P. Boardman, O. Kapellou, J. M. Allsop, F. Cowan, A. D. Edwards, M. A. Rutherford and S. J. Counsell (2007). *Relationship between white matter apparent diffusion coefficients in preterm infants at term-equivalent age and developmental outcome at 2 years*. Pediatrics **120**(3): e604-609.

Kutzsche, S., P. Ilves, O. J. Kirkeby and O. D. Saugstad (2001). *Hydrogen peroxide production in leukocytes during cerebral hypoxia and reoxygenation with 100% or 21% oxygen in newborn piglets*. Pediatr Res **49**(6): 834-842.

Lauterbur, P. C. (1973). *Image Formation by Induced Local Interactions - Examples Employing Nuclear Magnetic-Resonance*. Nature **242**(5394): 190-191.

Le Bihan, D., C. Poupon, A. Amadon and F. Lethimonnier (2006). *Artifacts and pitfalls in diffusion MRI*. J Magn Reson Imaging **24**(3): 478-488.

Lee, J. H., A. C. Silva, H. Merkle and A. P. Koretsky (2005). *Manganese-enhanced magnetic resonance imaging of mouse brain after systemic administration of MnCl2: dose-dependent and temporal evolution of T1 contrast*. Magn Reson Med **53**(3): 640-648.

Lehmann, C., S. Bette and J. Engele (2009). *High extracellular glutamate modulates expression of glutamate transporters and glutamine synthetase in cultured astrocytes*. Brain Res **1297**: 1-8.

Li, J., O. Baud, T. Vartanian, J. J. Volpe and P. A. Rosenberg (2005). *Peroxynitrite generated by inducible nitric oxide synthase and NADPH oxidase mediates microglial toxicity to oligodendrocytes*. Proc Natl Acad Sci U S A **102**(28): 9936-9941.

Lin, B., M. D. Ginsberg, R. Busto and W. D. Dietrich (1998). *Sequential analysis of subacute and chronic neuronal, astrocytic and microglial alterations after transient global ischemia in rats*. Acta Neuropathol **95**(5): 511-523.

Lin, Y. J. and A. P. Koretsky (1997). *Manganese ion enhances T1-weighted MRI during brain activation: an approach to direct imaging of brain function*. Magn Reson Med **38**(3): 378-388.

Loddick, S. A. and N. J. Rothwell (1996). *Neuroprotective effects of human recombinant interleukin-1 receptor antagonist in focal cerebral ischaemia in the rat*. J Cereb Blood Flow Metab **16**(5): 932-940.

Loddick, S. A., A. V. Turnbull and N. J. Rothwell (1998). *Cerebral interleukin-6 is neuroprotective during permanent focal cerebral ischemia in the rat*. J Cereb Blood Flow Metab **18**(2): 176-179.

Lodygensky, G. A., T. West, M. D. Moravec, S. A. Back, K. Dikranian, D. M. Holtzman and J. J. Neil (2011). *Diffusion characteristics associated with neuronal injury and glial activation following hypoxia-ischemia in the immature brain*. Magn Reson Med **66**(3): 839-845.

Malisza, K. L., P. Kozlowski, G. Ning, S. Bascaramurty and U. I. Tuor (1999). *Metabolite changes in neonatal rat brain during and after cerebral hypoxia-ischemia: a magnetic resonance spectroscopic imaging study*. NMR Biomed **12**(1): 31-38.

Mansfield, P. and P. K. Grannell (1973). *Nmr Diffraction in Solids*. Journal of Physics C-Solid State Physics **6**(22): L422-L426.

Martin, D., N. Chinookoswong and G. Miller (1994). *The interleukin-1 receptor antagonist (rhIL-1ra) protects against cerebral infarction in a rat model of hypoxia-ischemia*. Exp Neurol **130**(2): 362-367.

Martin, L. J., N. A. Al-Abdulla, A. M. Brambrink, J. R. Kirsch, F. E. Sieber and C. Portera-Cailliau (1998). *Neurodegeneration in excitotoxicity, global cerebral ischemia, and target deprivation: A perspective on the contributions of apoptosis and necrosis*. Brain Res Bull **46**(4): 281-309.

McGuire, W. (2007). *Perinatal asphyxia*. Clin Evid (Online) **2007**.

McLean, C. and D. Ferriero (2004). *Mechanisms of hypoxic-ischemic injury in the term infant*. Semin Perinatol **28**(6): 425-432.

McRae, A., E. Bona and H. Hagberg (1996). *Microglia-astrocyte interactions after cortisone treatment in a neonatal hypoxia-ischemia model*. Brain Res Dev Brain Res **94**(1): 44-51.

Mcrae, A., E. Gilland, E. Bona and H. Hagberg (1995). *Microglia Activation after Neonatal Hypoxic-Ischemia*. Developmental Brain Research **84**(2): 245-252.

Meng, S., M. Qiao, T. Foniok and U. I. Tuor (2005). *White matter damage precedes that in gray matter despite similar magnetic resonance imaging changes following cerebral hypoxia-ischemia in neonatal rats*. Exp Brain Res **166**(1): 56-60.

Meng, S., M. Qiao, K. Scobie, B. Tomanek and U. I. Tuor (2006). *Evolution of magnetic resonance imaging changes associated with cerebral hypoxia-ischemia and a relatively selective white matter injury in neonatal rats*. Pediatr Res **59**(4 Pt 1): 554-559.

Mishima, K., T. Ikeda, N. Aoo, N. Takai, S. Takahashi, N. Egashira, T. Ikenoue, K. Iwasaki and M. Fujiwara (2005). *Hypoxia-ischemic insult in neonatal rats induced slowly progressive brain damage related to memory impairment*. Neurosci Lett **376**(3): 194-199.

Mori, S. and J. Zhang (2006). *Principles of diffusion tensor imaging and its applications to basic neuroscience research*. Neuron **51**(5): 527-539.

Mulcahy, N. J., J. Ross, N. J. Rothwell and S. A. Loddick (2003). *Delayed administration of interleukin-1 receptor antagonist protects against transient cerebral ischaemia in the rat*. Br J Pharmacol **140**(3): 471-476.

Nagy, Z., H. Westerberg, S. Skare, J. L. Andersson, A. Lilja, O. Flodmark, E. Fernell, K. Holmberg, B. Bohm, H. Forssberg, H. Lagercrantz and T. Klingberg (2003). *Preterm children have*

disturbances of white matter at 11 years of age as shown by diffusion tensor imaging. Pediatr Res **54**(5): 672-679.

Nakajima, W., A. Ishida, M. S. Lange, K. L. Gabrielson, M. A. Wilson, L. J. Martin, M. E. Blue and M. V. Johnston (2000). *Apoptosis has a prolonged role in the neurodegeneration after hypoxic ischemia in the newborn rat*. J Neurosci **20**(21): 7994-8004.

Narita, K., F. Kawasaki and H. Kita (1990). *Mn and Mg influxes through Ca channels of motor nerve terminals are prevented by verapamil in frogs*. Brain Res **510**(2): 289-295.

Neil, J. J., S. I. Shiran, R. C. McKinstry, G. L. Schefft, A. Z. Snyder, C. R. Almli, E. Akbudak, J. A. Aronovitz, J. P. Miller, B. C. Lee and T. E. Conturo (1998). *Normal brain in human newborns: apparent diffusion coefficient and diffusion anisotropy measured by using diffusion tensor MR imaging*. Radiology **209**(1): 57-66.

Nijboer, C. H., F. Groenendaal, A. Kavelaars, H. H. Hagberg, F. van Bel and C. J. Heijnen (2007). *Gender-specific neuroprotection by 2-iminobiotin after hypoxia-ischemia in the neonatal rat via a nitric oxide independent pathway*. J Cereb Blood Flow Metab **27**(2): 282-292.

Nijboer, C. H., C. J. Heijnen, F. Groenendaal, M. J. May, F. van Bel and A. Kavelaars (2008a). *A dual role of the NF-kappaB pathway in neonatal hypoxic-ischemic brain damage*. Stroke **39**(9): 2578-2586.

Nijboer, C. H., C. J. Heijnen, F. Groenendaal, M. J. May, F. van Bel and A. Kavelaars (2008b). *Strong neuroprotection by inhibition of NF-kappaB after neonatal hypoxia-ischemia involves apoptotic mechanisms but is independent of cytokines*. Stroke **39**(7): 2129-2137.

Nijboer, C. H., C. J. Heijnen, M. A. van der Kooij, J. Zijlstra, C. T. van Velthoven, C. Culmsee, F. van Bel, H. Hagberg and A. Kavelaars (2011). *Targeting the p53 pathway to protect the neonatal ischemic brain*. Ann Neurol **70**(2): 255-264.

Nijboer, C. H., M. A. van der Kooij, F. van Bel, F. Ohl, C. J. Heijnen and A. Kavelaars (2010). *Inhibition of the JNK/AP-1 pathway reduces neuronal death and improves behavioral outcome after neonatal hypoxic-ischemic brain injury*. Brain Behav Immun **24**(5): 812-821.

Northington, F. J., D. M. Ferriero, D. L. Flock and L. J. Martin (2001a). *Delayed neurodegeneration in neonatal rat thalamus after hypoxia-ischemia is apoptosis*. J Neurosci **21**(6): 1931-1938.

Northington, F. J., D. M. Ferriero, E. M. Graham, R. J. Traystman and L. J. Martin (2001b). *Early Neurodegeneration after Hypoxia-Ischemia in Neonatal Rat Is Necrosis while Delayed Neuronal Death Is Apoptosis*. Neurobiol Dis **8**(2): 207-219.

Northington, F. J., D. M. Ferriero and L. J. Martin (2001c). *Neurodegeneration in the thalamus following neonatal hypoxia-ischemia is programmed cell death*. Dev Neurosci **23**(3): 186-191.

Northington, F. J., E. M. Graham and L. J. Martin (2005). *Apoptosis in perinatal hypoxic-ischemic brain injury: how important is it and should it be inhibited?* Brain Res Brain Res Rev **50**(2): 244-257.

Northington, F. J., M. E. Zelaya, D. P. O'Riordan, K. Blomgren, D. L. Flock, H. Hagberg, D. M. Ferriero and L. J. Martin (2007). *Failure to complete apoptosis following neonatal hypoxia-ischemia manifests as "continuum" phenotype of cell death and occurs with multiple manifestations of mitochondrial dysfunction in rodent forebrain*. Neuroscience **149**(4): 822-833.

Ohno, M., H. Aotani and M. Shimada (1995). *Glial responses to hypoxic/ischemic encephalopathy in neonatal rat cerebrum*. Brain Res Dev Brain Res **84**(2): 294-298.

Osborn, A. G. (2007). *Diagnostic imaging. Brain*. [Salt Lake City, Utah], Amirsys.

Palmer, C., R. L. Roberts and P. I. Young (2004). *Timing of neutrophil depletion influences long-term neuroprotection in neonatal rat hypoxic-ischemic brain injury*. Pediatr Res **55**(4): 549-556.

Pautler, R. G. (2004). *In vivo, trans-synaptic tract-tracing utilizing manganese-enhanced magnetic resonance imaging (MEMRI)*. NMR Biomed **17**(8): 595-601.

Pautler, R. G., A. C. Silva and A. P. Koretsky (1998). *In vivo neuronal tract tracing using manganese-enhanced magnetic resonance imaging*. Magn Reson Med **40**(5): 740-748.

Paxinos, G. and C. Watson (1998). *The rat brain in stereotaxic coordinates*. San Diego, Academic Press.

Pickering, M., D. Cumiskey and J. J. O'Connor (2005). *Actions of TNF-alpha on glutamatergic synaptic transmission in the central nervous system*. Exp Physiol **90**(5): 663-670.

Privat, A. (2003). *Astrocytes as support for axonal regeneration in the central nervous system of mammals*. Glia **43**(1): 91-93.

Purcell, E. M., H. C. Torrey and R. V. Pound (1946). *Resonance Absorption by Nuclear Magnetic Moments in a Solid*. Physical Review **69**(1-2): 37-38.

Qiao, M., S. Meng, K. Scobie, T. Foniok and U. I. Tuor (2004). *Magnetic resonance imaging of differential gray versus white matter injury following a mild or moderate hypoxic-ischemic insult in neonatal rats*. Neurosci Lett **368**(3): 332-336.

Renolleau, S., S. Fau, C. Goyenvalle, L. M. Joly, D. Chauvier, E. Jacotot, J. Mariani and C. Charriaut-Marlangue (2007). *Specific caspase inhibitor Q-VD-OPh prevents neonatal stroke in P7 rat: a role for gender*. J Neurochem **100**(4): 1062-1071.

Rice, J. E., 3rd, R. C. Vannucci and J. B. Brierley (1981). *The influence of immaturity on hypoxic-ischemic brain damage in the rat*. Ann Neurol **9**(2): 131-141.

Robertson, N. J. and J. S. Wyatt (2004). *The magnetic resonance revolution in brain imaging: impact on neonatal intensive care*. Arch Dis Child Fetal Neonatal Ed **89**(3): F193-197.

Rovetta, F., S. Catalani, N. Steimberg, J. Boniotti, M. E. Gilberti, M. A. Mariggio and G. Mazzoleni (2007). *Organ-specific manganese toxicity: a comparative in vitro study on five cellular models exposed to MnCl(2)*. Toxicol In Vitro **21**(2): 284-292.

Rumpel, H., R. Buchli, J. Gehrmann, A. Aguzzi, O. Illi and E. Martin (1995). *Magnetic resonance imaging of brain edema in the neonatal rat: a comparison of short and long term hypoxia-ischemia*. Pediatr Res **38**(1): 113-118.

Rutherford, M., S. Counsell, J. Allsop, J. Boardman, O. Kapellou, D. Larkman, J. Hajnal, D. Edwards and F. Cowan (2004). *Diffusion-weighted magnetic resonance imaging in term perinatal brain injury: a comparison with site of lesion and time from birth*. Pediatrics **114**(4): 1004-1014.

Rutherford, M., L. Srinivasan, L. Dyet, P. Ward, J. Allsop, S. Counsell and F. Cowan (2006). *Magnetic resonance imaging in perinatal brain injury: clinical presentation, lesions and outcome*. Pediatr Radiol **36**(7): 582-592.

Saito, K., K. Suyama, K. Nishida, Y. Sei and A. S. Basile (1996). *Early increases in TNF-alpha, IL-6 and IL-1 beta levels following transient cerebral ischemia in gerbil brain*. Neurosci Lett **206**(2-3): 149-152.

Sandvig, A., I. Sandvig, M. Berry, O. Olsen, T. B. Pedersen, C. Brekken and M. Thuen (2011). *Axonal tracing of the normal and regenerating visual pathway of mouse, rat, frog, and fish using manganese-enhanced MRI (MEMRI)*. J Magn Reson Imaging.

Saugstad, O. D. (2005). *Oxygen for newborns: how much is too much?* J Perinatol **25 Suppl 2**: S45-49; discussion S50.

Saugstad, O. D., S. Ramji, R. F. Soll and M. Vento (2008). *Resuscitation of newborn infants with 21% or 100% oxygen: an updated systematic review and meta-analysis*. Neonatology **94**(3): 176-182.

Schaefer, D. J., J. D. Bourland and J. A. Nyenhuis (2000). *Review of patient safety in time-varying gradient fields*. J Magn Reson Imaging **12**(1): 20-29.

Schenck, J. F. (2000). *Safety of strong, static magnetic fields*. J Magn Reson Imaging **12**(1): 2-19.

Shankaran, S., A. R. Laptook, R. A. Ehrenkranz, J. E. Tyson, S. A. McDonald, E. F. Donovan, A. A. Fanaroff, W. K. Poole, L. L. Wright, R. D. Higgins, N. N. Finer, W. A. Carlo, S. Duara, W. Oh, C. M. Cotten, D. K. Stevenson, B. J. Stoll, J. A. Lemons, R. Guillet and A. H. Jobe (2005). *Whole-body hypothermia for neonates with hypoxic-ischemic encephalopathy*. N Engl J Med **353**(15): 1574-1584.

Shellock, F. G. (2000). *Radiofrequency energy-induced heating during MR procedures: a review*. J Magn Reson Imaging **12**(1): 30-36.

Shellock, F. G. and J. V. Crues (2004). *MR procedures: biologic effects, safety, and patient care*. Radiology **232**(3): 635-652.

Silva, A. C. and N. A. Bock (2008). *Manganese-enhanced MRI: an exceptional tool in translational neuroimaging*. Schizophr Bull **34**(4): 595-604.

Silva, A. C., J. H. Lee, I. Aoki and A. P. Koretsky (2004). *Manganese-enhanced magnetic resonance imaging (MEMRI): methodological and practical considerations*. NMR Biomed **17**(8): 532-543.

Silva, A. C., J. H. Lee, C. W. Wu, J. Tucciarone, G. Pelled, I. Aoki and A. P. Koretsky (2008). *Detection of cortical laminar architecture using manganese-enhanced MRI*. J Neurosci Methods **167**(2): 246-257.

Sizonenko, S. V., E. J. Camm, J. R. Garbow, S. E. Maier, T. E. Inder, C. E. Williams, J. J. Neil and P. S. Huppi (2007). *Developmental changes and injury induced disruption of the radial organization of the cortex in the immature rat brain revealed by in vivo diffusion tensor MRI*. Cereb Cortex **17**(11): 2609-2617.

Skranes, J., G. C. Lohaugen, M. Martinussen, M. S. Indredavik, A. M. Dale, O. Haraldseth, T. R. Vangberg and A. M. Brubakk (2009). *White matter abnormalities and executive function in children with very low birth weight*. Neuroreport **20**(3): 263-266.

Skranes, J., T. R. Vangberg, S. Kulseng, M. S. Indredavik, K. A. Evensen, M. Martinussen, A. M. Dale, O. Haraldseth and A. M. Brubakk (2007). *Clinical findings and white matter abnormalities seen on diffusion tensor imaging in adolescents with very low birth weight*. Brain **130**(Pt 3): 654-666.

Smith, G. C., J. Gutovich, C. Smyser, R. Pineda, C. Newnham, T. H. Tjoeng, C. Vavasseur, M. Wallendorf, J. Neil and T. Inder (2011). *Neonatal intensive care unit stress is associated with brain development in preterm infants*. Ann Neurol **70**(4): 541-549.

Smith, S. M., M. Jenkinson, M. W. Woolrich, C. F. Beckmann, T. E. Behrens, H. Johansen-Berg, P. R. Bannister, M. De Luca, I. Drobnjak, D. E. Flitney, R. K. Niazy, J. Saunders, J. Vickers, Y. Zhang, N. De Stefano, J. M. Brady and P. M. Matthews (2004). *Advances in functional and structural MR image analysis and implementation as FSL*. Neuroimage **23 Suppl 1**: S208-219.

Stejskal, E. O. and J. E. Tanner (1965). *Spin Diffusion Measurements: Spin Echoes in the Presence of a Time-Dependent Field Gradient*. Journal of Chemical Physics **42**(1): 288-+.

Stone, B. S., J. Zhang, D. W. Mack, S. Mori, L. J. Martin and F. J. Northington (2008). *Delayed neural network degeneration after neonatal hypoxia-ischemia*. Ann Neurol **64**(5): 535-546.

Takeda, A. (2003). *Manganese action in brain function*. Brain Res Brain Res Rev **41**(1): 79-87.

Ten, V. S., E. X. Wu, H. Tang, M. Bradley-Moore, M. V. Fedarau, V. I. Ratner, R. I. Stark, J. A. Gingrich and D. J. Pinsky (2004). *Late measures of brain injury after neonatal hypoxia-ischemia in mice*. Stroke **35**(9): 2183-2188.

Thayyil, S., M. Chandrasekaran, A. Taylor, A. Bainbridge, E. B. Cady, W. K. Chong, S. Murad, R. Z. Omar and N. J. Robertson (2010). *Cerebral magnetic resonance biomarkers in neonatal encephalopathy: a meta-analysis*. Pediatrics **125**(2): e382-395.

Thoresen, M., J. Penrice, A. Lorek, E. B. Cady, M. Wylezinska, V. Kirkbride, C. E. Cooper, G. C. Brown, A. D. Edwards, J. S. Wyatt and et al. (1995). *Mild hypothermia after severe transient hypoxia-ischemia ameliorates delayed cerebral energy failure in the newborn piglet*. Pediatr Res **37**(5): 667-670.

Thuen, M., M. Berry, T. B. Pedersen, P. E. Goa, M. Summerfield, O. Haraldseth, A. Sandvig and C. Brekken (2008). *Manganese-enhanced MRI of the rat visual pathway: acute neural toxicity, contrast enhancement, axon resolution, axonal transport, and clearance of Mn(2+)*. J Magn Reson Imaging **28**(4): 855-865.

Thuen, M., T. E. Singstad, T. B. Pedersen, O. Haraldseth, M. Berry, A. Sandvig and C. Brekken (2005). *Manganese-enhanced MRI of the optic visual pathway and optic nerve injury in adult rats*. J Magn Reson Imaging **22**(4): 492-500.

Towfighi, J., N. Zec, J. Yager, C. Housman and R. C. Vannucci (1995). *Temporal evolution of neuropathologic changes in an immature rat model of cerebral hypoxia: a light microscopic study*. Acta Neuropathol **90**(4): 375-386.

Tucciarone, J., K. H. Chuang, S. J. Dodd, A. Silva, G. Pelled and A. P. Koretsky (2009). *Layer specific tracing of corticocortical and thalamocortical connectivity in the rodent using manganese enhanced MRI*. Neuroimage **44**(3): 923-931.

Tuor, U. I., P. Kozlowski, M. R. Del Bigio, B. Ramjiawan, S. Su, K. Malisza and J. K. Saunders (1998). *Diffusion- and T2-weighted increases in magnetic resonance images of immature brain during hypoxia-ischemia: transient reversal posthypoxia*. Exp Neurol **150**(2): 321-328.

Tuor, U. I., K. L. Malisza and P. Kozlowski (1999). *Prevention of both T2- and diffusion-weighted increases in image intensity during cerebral hypoxia-ischemia in infant rats pretreated with dexamethasone*. Exp Brain Res **125**(2): 217-220.

van de Looij, Y., A. Chatagner, P. S. Huppi, R. Gruetter and S. V. Sizonenko (2011). *Longitudinal MR assessment of hypoxic ischemic injury in the immature rat brain*. Magn Reson Med **65**(2): 305-312.

Van der Linden, A., M. Verhoye, V. Van Meir, I. Tindemans, M. Eens, P. Absil and J. Balthazart (2002). *In vivo manganese-enhanced magnetic resonance imaging reveals connections and functional properties of the songbird vocal control system*. Neuroscience **112**(2): 467-474.

Vangberg, T. R., J. Skranes, A. M. Dale, M. Martinussen, A. M. Brubakk and O. Haraldseth (2006). *Changes in white matter diffusion anisotropy in adolescents born prematurely*. Neuroimage **32**(4): 1538-1548.

Vannucci, R. C. and S. J. Vannucci (1997). *A model of perinatal hypoxic-ischemic brain damage*. Ann N Y Acad Sci **835**: 234-249.

Vannucci, R. C. and S. J. Vannucci (2005). *Perinatal hypoxic-ischemic brain damage: evolution of an animal model*. Dev Neurosci **27**(2-4): 81-86.

Vannucci, S. J. and H. Hagberg (2004). *Hypoxia-ischemia in the immature brain*. J Exp Biol **207**(Pt 18): 3149-3154.

Vexler, Z. S., X. N. Tang and M. A. Yenari (2006). *Inflammation in adult and neonatal stroke*. Clin Neurosci Res **6**(5): 293-313.

Volpe, J. J. (2008). *Neurology of the newborn*. Philadelphia, Saunders/Elsevier.

Volpe, J. J. (2009). *Brain injury in premature infants: a complex amalgam of destructive and developmental disturbances*. Lancet Neurol **8**(1): 110-124.

Wadghiri, Y. Z., J. A. Blind, X. Duan, C. Moreno, X. Yu, A. L. Joyner and D. H. Turnbull (2004). *Manganese-enhanced magnetic resonance imaging (MEMRI) of mouse brain development*. NMR Biomed **17**(8): 613-619.

Wang, S., K. Peretich, Y. Zhao, G. Liang, Q. Meng and H. Wei (2009a). *Anesthesia-induced neurodegeneration in fetal rat brains*. Pediatr Res **66**(4): 435-440.

Wang, S., E. X. Wu, K. Cai, H. F. Lau, P. T. Cheung and P. L. Khong (2009b). *Mild hypoxic-ischemic injury in the neonatal rat brain: longitudinal evaluation of white matter using diffusion tensor MR imaging*. AJNR Am J Neuroradiol **30**(10): 1907-1913.

Wang, S., E. X. Wu, C. N. Tam, H. F. Lau, P. T. Cheung and P. L. Khong (2008). *Characterization of white matter injury in a hypoxic-ischemic neonatal rat model by diffusion tensor MRI*. Stroke **39**(8): 2348-2353.

Wang, Y., P. T. Cheung, G. X. Shen, I. Bhatia, E. X. Wu, D. Qiu and P. L. Khong (2007). *Comparing diffusion-weighted and T2-weighted MR imaging for the quantification of infarct size in a neonatal rat hypoxic-ischemic model at 24h post-injury*. Int J Dev Neurosci **25**(1): 1-5.

Wang, Y., P. T. Cheung, G. X. Shen, E. X. Wu, G. Cao, I. Bart, W. H. Wong and P. L. Khong (2006). *Hypoxic-ischemic brain injury in the neonatal rat model: relationship between lesion size at early MR imaging and irreversible infarction*. AJNR Am J Neuroradiol **27**(1): 51-54.

Watanabe, T., J. Frahm and T. Michaelis (2004a). *Functional mapping of neural pathways in rodent brain in vivo using manganese-enhanced three-dimensional magnetic resonance imaging*. NMR Biomed **17**(8): 554-568.

Watanabe, T., J. Radulovic, J. Spiess, O. Natt, S. Boretius, J. Frahm and T. Michaelis (2004b). *In vivo 3D MRI staining of the mouse hippocampal system using intracerebral injection of MnCl2*. Neuroimage **22**(2): 860-867.

Wendland, M. F. (2004). *Applications of manganese-enhanced magnetic resonance imaging (MEMRI) to imaging of the heart*. NMR Biomed **17**(8): 581-594.

Whitelaw, A. and M. Thoresen (2000). *Antenatal steroids and the developing brain*. Arch Dis Child Fetal Neonatal Ed **83**(2): F154-157.

Witt, K. A., K. S. Mark, K. E. Sandoval and T. P. Davis (2008). *Reoxygenation stress on blood-brain barrier paracellular permeability and edema in the rat*. Microvasc Res **75**(1): 91-96.

Wixey, J. A., H. E. Reinebrant, S. J. Spencer and K. M. Buller (2011). *Efficacy of post-insult minocycline administration to alter long-term hypoxia-ischemia-induced damage to the serotonergic system in the immature rat brain*. Neuroscience **182**: 184-192.

Woolrich, M. W., S. Jbabdi, B. Patenaude, M. Chappell, S. Makni, T. Behrens, C. Beckmann, M. Jenkinson and S. M. Smith (2009). *Bayesian analysis of neuroimaging data in FSL*. Neuroimage **45**(1 Suppl): S173-186.

Xie, Z., D. J. Culley, Y. Dong, G. Zhang, B. Zhang, R. D. Moir, M. P. Frosch, G. Crosby and R. E. Tanzi (2008). *The common inhalation anesthetic isoflurane induces caspase activation and increases amyloid beta-protein level in vivo*. Ann Neurol **64**(6): 618-627.

Yager, J. Y. (2004). *Animal models of hypoxic-ischemic brain damage in the newborn*. Semin Pediatr Neurol **11**(1): 31-46.

Yager, J. Y., E. A. Armstrong, C. Jaharus, D. M. Saucier and E. C. Wirrell (2004). *Preventing hyperthermia decreases brain damage following neonatal hypoxic-ischemic seizures*. Brain Res **1011**(1): 48-57.

Yang, J., P. L. Khong, Y. Wang, A. C. Chu, S. L. Ho, P. T. Cheung and E. X. Wu (2008a). *Manganese-enhanced MRI detection of neurodegeneration in neonatal hypoxic-ischemic cerebral injury*. Magn Reson Med **59**(6): 1329-1339.

Yang, J. and E. X. Wu (2008b). *Detection of cortical gray matter lesion in the late phase of mild hypoxic-ischemic injury by manganese-enhanced MRI*. Neuroimage **39**(2): 669-679.

Yang, P. F., D. Y. Chen, J. W. Hu, J. H. Chen and C. T. Yen (2011). *Functional tracing of medial nociceptive pathways using activity-dependent manganese-enhanced MRI*. Pain **152**(1): 194-203.

Yin, W., G. Cao, M. J. Johnnides, A. P. Signore, Y. Luo, R. W. Hickey and J. Chen (2006). *TAT-mediated delivery of Bcl-xL protein is neuroprotective against neonatal hypoxic-ischemic brain injury via inhibition of caspases and AIF*. Neurobiol Dis **21**(2): 358-371.

Yu, X., Y. Z. Wadghiri, D. H. Sanes and D. H. Turnbull (2005). *In vivo auditory brain mapping in mice with Mn-enhanced MRI*. Nat Neurosci **8**(7): 961-968.

Zhang, D., X. Hu, L. Qian, J. P. O'Callaghan and J. S. Hong (2010). *Astrogliosis in CNS pathologies: is there a role for microglia?* Mol Neurobiol **41**(2-3): 232-241.

Zhang, Y., M. Brady and S. Smith (2001). *Segmentation of brain MR images through a hidden Markov random field model and the expectation-maximization algorithm*. IEEE Trans Med Imaging **20**(1): 45-57.

Zhao, P. and Z. Zuo (2004). *Isoflurane preconditioning induces neuroprotection that is inducible nitric oxide synthase-dependent in neonatal rats*. Anesthesiology **101**(3): 695-703.

Zhu, C., J. Gao, Q. Li, Z. Huang, Y. Zhang, H. Li, H. G. Kuhn and K. Blomgren (2011). *Repeated exposure of the developing rat brain to magnetic resonance imaging did not affect neurogenesis, cell death or memory function*. Biochem Biophys Res Commun **404**(1): 291-296.

Chapter 9 Contributions

Paper I

NeuroImage 45 (2009) 880–890

Contents lists available at ScienceDirect

NeuroImage

journal homepage: www.elsevier.com/locate/ynimg

Manganese-enhanced magnetic resonance imaging of hypoxic–ischemic brain injury in the neonatal rat

Marius Widerøe [a,*], Øystein Olsen [b], Tina Bugge Pedersen [c], Pål Erik Goa [c,d], Annemieke Kavelaars [e], Cobi Heijnen [e], Jon Skranes [a,f], Ann-Mari Brubakk [a,f], Christian Brekken [c]

[a] Department of Laboratory Medicine, Children's and Women's Health, Norwegian University of Science and Technology, Trondheim, Norway
[b] Department of Radiography, Sør-Trøndelag University College, Trondheim, Norway
[c] Department of Circulation and Medical Imaging, Norwegian University of Science and Technology, Trondheim, Norway
[d] Department of Radiology, St Olavs Hospital, Trondheim, Norway
[e] Department of Psychoneuroimmunology, University Medical Center Utrecht, Utrecht, The Netherlands
[f] Department of Pediatrics, St Olavs Hospital, Trondheim, Norway

ARTICLE INFO

Article history:
Received 24 June 2008
Revised 2 December 2008
Accepted 3 December 2008
Available online 24 December 2008

ABSTRACT

Hypoxic–ischemic injury (HI) to the neonatal brain results in delayed neuronal death with accompanying inflammation for days after the initial insult. The aim of this study was to depict delayed neuronal death after HI using Manganese-enhanced MRI (MEMRI) and to evaluate the specificity of MEMRI in detection of cells related to injury by comparison with histology and immunohistochemistry. 7-day-old Wistar rat pups were subjected to HI (occlusion of right carotid artery and 8% O_2 for 75 min). 16 HI (HI+Mn) and 6 sham operated (Sham+Mn) pups were injected with $MnCl_2$ (100 mM, 40 mg/kg) and 10 HI-pups (HI+Vehicle) received NaCl i.p. 6 h after HI. 3D T_1-weighted images (FLASH) and 2D T_2-maps (MSME) were acquired at 7 T 1, 3 and 7 days after HI. Pups were sacrificed after MR-scanning and brain slices were cut and stained for CD68, GFAP, MAP-2, Caspase-3 and Fluorojade B. No increased manganese-enhancement (ME) was detectable in the injured hemisphere on day 1 or 3 when immunohistochemistry showed massive ongoing neuronal death. 7 days after HI, increased ME was seen on T_1-w images in parts of the injured cortex, hippocampus and thalamus among HI+Mn pups, but not among HI+Vehicle or Sham+Mn pups. Comparison with immunohistochemistry showed delayed neuronal death and inflammation in these areas with late ME. Areas with increased ME corresponded best with areas with high concentrations of activated microglia. Thus, late manganese-enhancement seems to be related to accumulation of manganese in activated microglia in areas of neuronal death rather than depicting neuronal death per se.

Introduction

Hypoxic–ischemic brain injury in the perinatal period results in high mortality and morbidity among infants and children (Ferriero, 2004; Vannucci and Perlman, 1997; Vannucci and Hagberg, 2004). In contrast to adult stroke, hypoxia–ischemia in the neonatal brain results in a prolonged evolution of injury with neurons dying days and weeks after the primary insult. This has presented a possible window of opportunity for therapeutic intervention (Nakajima et al., 2000; Geddes et al., 2001; Vannucci and Hagberg, 2004; Northington et al., 2005), but in order to develop effective treatment strategies the complexity of the underlying injury mechanisms and evolution of injury has to be further investigated. One of the injury mechanisms that we are just beginning to elucidate the consequences and significance of is the inflammatory response after hypoxia–ischemia in the neonatal brain. Inflammatory cytokines have been shown to potentiate excitotoxic injury, and microglia, the resident macrophage of CNS, has been shown to be activated both acutely and delayed in the brain after hypoxia–ischemia. Although microglia by many means are considered a renovation cell through its phagocytosis of dead cells and debris, it is increasingly viewed as a possible cause of cell death through its release of glutamate, free radicals and nitric oxide (McRae et al., 1995; McLean and Ferriero, 2004; Ferriero, 2004).

The advances during the past decade in revealing the pathogenesis of neonatal hypoxic–ischemic brain injury are in part due to new neuroimaging techniques and a focus on mapping the cellular and molecular mechanisms of injury through animal models (Ferriero, 2004; Vannucci and Vannucci, 2005). Combining the strengths of MRI with neonatal animal models give the opportunity of longitudinal studies of brain injury *in vivo* where mechanisms of the evolution of injury can be investigated on a structural and cellular level. One novel versatile MRI technique is manganese-enhanced MRI (MEMRI). Manganese (Mn^{2+}) gives positive contrast on T_1-weighted images due to its paramagnetic properties that primarily shortens T_1 in solid

* Corresponding author. Medical Faculty, LBK, NTNU, MTFS, 7489 Trondheim, Norway. Fax: +47 73 55 13 50.
E-mail address: marius.wideroe@ntnu.no (M. Widerøe).

1053-8119/$ – see front matter © 2008 Elsevier Inc. All rights reserved.
doi:10.1016/j.neuroimage.2008.12.007

tissue (Koretsky and Silva, 2004; Silva et al., 2004). The divalent manganese ion (Mn^{2+}) functions as an analogue for Ca^{2+} in biological systems and is known to enter neurons and glial cells through voltage-gated Ca^{2+}-channels. During normal homeostasis systemic administration of Mn^{2+} gives signal enhancement on T_1-weighted images of brain areas with high neuronal activity (Watanabe et al., 2002; Wadghiri et al., 2004; Kuo et al., 2005). Under pathological conditions the properties of Mn^{2+} give MEMRI other potentials for use. Calcium plays an important role in neuronal death during brain ischemia either through rapid Ca^{2+}-influx as a result of depolarisation caused by energy failure or excitatory glutamate release or as a result of slow continued accumulation of intracellular Ca^{2+} associated with neuronal apoptosis (Ankarcrona et al., 1995; Kristián and Siesjö, 1998; Won et al., 2002; Aoki et al., 2003; Koretsky and Silva, 2004). Substituting Ca^{2+} with Mn^{2+} may lead to intracellular accumulation of Mn^{2+} in neurons undergoing cell death. Aoki et al. has demonstrated this during *early* neuronal death in the adult rat stroke model (Aoki et al., 2003, 2004). However, using the same principles we hypothesised that MEMRI may be utilised for imaging *delayed* neuronal death which would be particularly valuable for better understanding neonatal hypoxic–ischemic brain injury.

The main aim of the present study was to depict delayed neuronal death by MEMRI up to several days after the initial hypoxic–ischemic insult in the neonatal rat brain. In addition, we aimed to evaluate the specificity of MEMRI in detection of cells related to injury by comparison with histology and immunohistochemistry.

Materials and methods

Animals

Wistar rats (Scanbur, Norway AS) were bred in the animal facilities at the St. Olav University Hospital in Trondheim. Time-mated rats ($n=5$) and their offspring ($n=35$) were kept on a 12:12 h light:dark cycle. They had water and food ad libitum. Animal experiments where conducted in accordance with Guidelines set by the Norwegian Ethics Committee for Animal Research and the experiments were approved by the responsible governmental authority.

Hypoxia-ischemia (HI)

The Vannucci–Rice model for hypoxic–ischemic brain damage was used (Rice et al., 1981; Vannucci and Vannucci, 2005): P7 rats (mean weight: 15.1 ± 1.6 g) were anaesthetized with isoflurane (Baxter Medication Delivery, Oslo, Norway) (4% induction, 2% maintenance) in O_2. Through a mid-neck incision, the right common carotid artery was identified, thermo-cauterized and severed. Wounds were closed and sprayed with Xylocaine (2%). Duration of operating procedure was 5–10 min. The pups were then placed back with their dam for recovery and feeding for minimum 2 and maximum 4 h. Thereafter, pups were put in a fibreglass box inside an incubator. The temperature inside the box was kept at 36 ± 0.5 °C throughout the procedure. The box was flushed with pre-heated humified air with 8% O_2 (in 92% N_2) (15 l/min) for approximately 3 min until the oxygen concentration in the box was 8%. Thereafter air flow was kept at 5 l/min and O_2 was measured to 8% throughout the procedure using an OxyQuant S® (EnviteC GmbH, Wismar, Germany). After 75 min of hypoxia, the box was flushed with room air and the pups were allowed to recover for 5 min before being placed back with their dam. This procedure resulted in a unilateral hypoxic–ischemic insult (HI) to the right cerebral hemisphere. In every litter pups were sham-operated; carotid artery was identified under anaesthesia, but not damaged. Sham-operated animals were not subjected to hypoxia.

Study groups and manganese administration

Six hours after the hypoxia one group of HI pups (HI + Mn) ($n=16$) and the sham operated pups (Sham + Mn) ($n=6$) were given a single dose of $MnCl_2$ (# 7773-01-5, Sigma-Aldrich Inc., St. Louis, USA) intraperitoneally. A dose of 40 mg $MnCl_2$ per kg bodyweight (~318 μmol Mn^{2+}/kg) at a concentration of 100 mM was mixed with 0.9% NaCl to make an isotonic injection volume of 0.1 ml. Another group of pups (HI + Vehicle) ($n=10$) did not receive $MnCl_2$, but were instead injected with 0.1 ml of 0.9% NaCl to serve as controls (Fig. 1).

To evaluate whether there was active cellular uptake of manganese 7 days after hypoxia–ischemia (HI), one group of pups HI + Mn6 ($n=3$) followed the described protocol for hypoxia–ischemia on day 0, but received no injections until day 6 after HI. They were then injected with 40 mg $MnCl_2$ per kg at 100 mM mixed with 0.9% NaCl (total volume 0.1 ml).

Magnetic resonance imaging

MRI was performed on days 1, 3 and 7 after HI (day 0) using a 7 T magnet (Biospec 70/20 AS, Bruker Biospin MRI, Ettlingen, Germany) with water-cooled (BGA-12, 400 mT/m) gradients. A 72 mm volume resonator was used for RF transmission and an actively decoupled mouse head surface coil was used for RF reception. Pups injected with $MnCl_2$ on day 6 (HI + Mn6) were also imaged on days 8, 10 and 14 after HI. All animals were imaged longitudinally at all time-points until they were sacrificed for histology. During scanning the anaesthetized (2% isoflurane in 30% O_2, 70% N_2) pups lay prone in a dedicated water heated mouse bed (Bruker Biospin MRI) and the head of every animal was fixed in the same position with inbuilt earplugs, tooth bar and nose-mask. This assured the same placement of the head of the animals within the magnet from scan to scan.

After a gradient echo FLASH pilot scan (acquisition time 1 min), a 3D data set was obtained using a T_1-weighted gradient echo FLASH sequence with flip-angle = 30°, TR = 12 ms, TE = 3.0 ms. FOV = 20 × 20 × 17.5 mm and acquisition matrix was 128 × 96 × 84

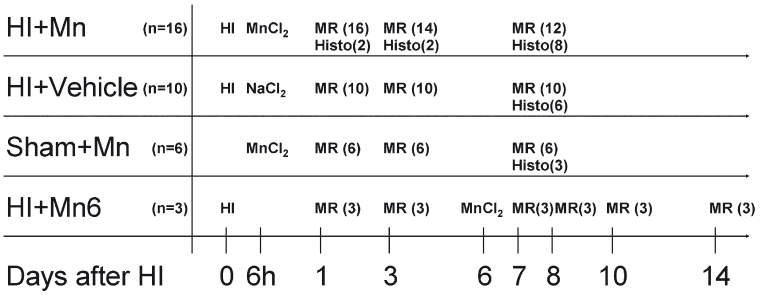

Fig. 1. Overview of the study design with study groups (HI + Mn, HI + Vehicle, Sham + Mn and HI + Mn6). Timing of hypoxia–ischemia (HI) and injection with $MnCl_2$ or Vehicle ($NaCl_2$), and timing of MR imaging (MR) and sacrificing for histological examinations (Histo).

giving an acquired resolution of 156 μm×208 μm×208 μm. With zero-filling of the matrix to 128×128×112, the interpolated resolution was 156 μm isotropic. Acquisition time was 25 min with 16 averages. 2D T_2-maps were obtained with a spin-echo sequence (MSME) with TR=2500 ms, TE=7.6 ms, 40 echoes, slice thickness 1 mm. FOV=18×18 mm and acquisition matrix 128×96 giving an in plane resolution of 140 μm×187 μm. With zero-filling of the matrix to 128×128 the interpolated resolution was 140 μm isotropic. Acquisition time was 16 min with 4 averages. The receiver gain was held constant for all scans and the signal scaling during reconstruction of the images was corrected for before quantitative analysis of the data.

The B1-field of the volume-coil was considered homogeneous within the field of view, while the spatially inhomogeneous sensitivity of the surface-coil used in the 3D T_1-weighted FLASH acquisition was corrected for using two additional scans in coupled and single coil operation: 3D T_1-weighted FLASH sequences: Flip-angle=30°, TR=12 ms, TE=3.0 ms, matrix size 32×32×32, acquisition-time was 2 min for each scan. FOVs were the same as those used to obtain 3D data set. The correction-procedure was performed in Matlab (MATLAB ver 2007a, MathWorks Inc.). The MRI signal intensity in a voxel at location *(x,y,z)* was normalized using the following relation:

$$I_{SC}(x,y,z) = I_{CC}(x,y,z)\frac{C_{SC}(x,y,z)}{C_{CC}(x,y,z)} \quad (1)$$

where C_{CC} and C_{SC} is the coupled-coil and single-coil intensities in the correction scan datasets respectively, I_{CC} is the recorded couple-coil signal intensity in the main 3D data set, and I_{SC} is the resulting normalized signal intensity.

Histology and immunohistochemistry

Animals were sacrificed after MRI acquisition on day 1 (HI+Mn, n=2), day 3 (HI+Mn, n=2) and day 7 (HI+Mn, n=8; HI+Vehicle, n=6; HI+Sham, n=3) following HI. They received an overdose pentobarbital (300 mg/kg) and were perfused intracardially with 4% paraformaldehyde (PAH) in phosphate-buffered saline (PBS). Brains were removed and embedded in paraffin. Coronal sections (8 μm) corresponding to −3.25 mm from the bregma (Paxinos and Watson, 1998) were cut and stained with either hematoxylin–eosin (Klinipath, Duiven, the Netherlands), anti-MAP2 (Sigma-Aldrich, Steinheim, Germany), anti-cleaved-caspase3 (Cell Signaling) or anti-ED1-fitc (Serotec, Raleigh, NC) and slices from HI+Mn pups on days 1 and 3 and 4 HI+Mn pups on day 7 were stained with anti-GFAP (Cymbus Biotechnology, Southampton, UK). Sections were then incubated with rat-anti-FITC-biotin (Roche, Basel, Switzerland), goat-anti-rabbit-biotin (Vector Laboratories, Burlingame, CA) or horse-anti-mouse-biotin (Vector Laboratories, Burlingame, CA). Visualization was performed using a Vectastain ABC kit (Vector Laboratories). Full section images were captured with a Nikon D1 digital camera (Nikon, Tokyo, Japan). Sections were also stained with Flourojade B (Chemicon International, Temecula, CA, USA) after incubation in 0.06% potassium-permanganate, embedded in DEPEX and visualized using a fluorescence-microscope in the FITC channel.

MR image analysis

In-house developed software was used for MR image analysis (MATLAB ver. R2007a, MathWorks Inc., Natick MA, USA). From the 3D T_1-weighted data set a coronal 2D image-slice (slice thickness 0.156 mm) approximately corresponding to the histological slice was extracted by tri-linear interpolation and used for image analysis. Using a rat brain atlas (Paxinos and Watson, 1998) for reference, regions of interest (ROI) were manually placed in the cortex, hippocampus, External capsule and thalamus in both hemispheres and mean signal intensity (SI) was calculated for each ROI.

To evaluate Manganese enhancement (ME), SI on T_1-weighted images in ROIs in the injured hemisphere (ipsilateral) was compared to the contralateral (unaffected) hemisphere. To allow comparison between animals and groups of animals, a measure of the relative contrast (RC) was calculated for each structure (cortex, hippocampus, external capsule and thalamus) in every animal using the 2D-image slices acquired on days 1, 3 and 7. RC was calculated using the following equation:

$$RC = \frac{SI_{\mathrm{ROI_{Ipsilateral}}} - SI_{\mathrm{ROI_{Contralateral}}}}{SI_{\mathrm{ROI_{Ipsilateral}}} + SI_{\mathrm{ROI_{Contralateral}}}}. \quad (2)$$

Comparison of histology and manganese enhancement

The histological slices with different staining were evaluated using standard and fluorescent microscopy. The extent and intensity of CD68 and GFAP staining and the number of stained cells in different areas of the injured hemisphere were compared to the extent and intensity of ME. The extent of MAP-2 loss was compared to the extent of ME. For this comparison 2D T_1-weighted images was viewed with a RGB lookup table where the threshold for the colour yellow was adjusted to right above the highest level of signal intensity recorded in the contralateral hemisphere for every animal. High signal areas in the injured hemisphere, indicating increased ME, would hence appear yellow.

The following computer-based method for evaluating agreement between increased ME on T_1-weighted images and histological staining was developed: manganese-enhancement in the injured hemisphere was defined by signal intensities above a threshold set by mean SI of a ROI placed in the thalamus of the contralateral hemisphere +1 SD of the image noise. A binary mask was created for the area of ME in the injured hemisphere. Images of whole histological slices stained for MAP-2, CD68 and GFAP were segmented in the RGB vector space using the Mahalanobis distance from an average colour calculated from a ROI manually placed in an area with uniform staining (Gonzalez et al., 2004). The segmented colours were defined to be in a distance equal or less than 1 SD from the average colour, where the SD was selected from the RGB component with the largest variance within the ROI. From this a binary mask for the area of staining was created. The T_1 weighted MR images and the histology images were then co-registered using landmark based image registration. After manually selecting approximately 15 pairs of anatomical points of reference in the two images, the transformation was calculated using a piecewise linear model. The transformation was applied to the segmented histology image which made us able to compare the manganese-enhanced areas and segmented histology staining on a pixel-to-pixel basis. The fit of the transformation was evaluated visually. The overlap between the area of histological staining ($Area_{Histology}$) and the segmented manganese-enhanced area ($Area_{ME}$) was evaluated using three different parameters, where the intersection of the areas of ME and histological staining was divided by either the union of the two areas, area of histological staining or the area of segmented ME:

$$Match = \frac{Area_{\mathrm{ME}} \cap Area_{\mathrm{Histology}}}{Area_{\mathrm{ME}} \cup Area_{\mathrm{Histology}}} \quad (3)$$

$$Sensitivity = \frac{Area_{\mathrm{ME}} \cap Area_{\mathrm{Histology}}}{Area_{\mathrm{Histology}}} \quad (4)$$

$$Prediction = \frac{Area_{\mathrm{ME}} \cap Area_{\mathrm{Histology}}}{Area_{\mathrm{ME}}}. \quad (5)$$

Statistics

SPSS version 14.0 (SPSS Inc., Chicago, IL, USA) was used for all statistical analysis and the level of significance was set to 0.05. Signal intensity data and relative contrast data are presented in figures as mean with error-bars representing±2 SEM. Mann–Whitney *U*-test was used to compare the mean signal intensities in ROIs and the mean relative contrast (RC) in different structures between groups. T_2-values are presented as mean±1 SD. Paired *t*-tests were used to analyze differences in T_2-values of the ROIs between the two hemispheres. Results from the pixel-wise comparison of T_1-weighted images with histology and T_2-maps are presented as mean±SEM.

Results

MR signal enhancement with manganese

T_1-weighted MR images of HI pups injected with $MnCl_2$ (HI+Mn) showed high signal intensities in large parts of the dorsolateral thalamus and in several animals also in parts of the hippocampus and remaining cortex on day 7 (Fig. 2). In a few HI+Mn pups some small spots were also seen in the thalamus on day 3, but no high signal intensities was seen in the injured hemisphere among HI+Mn pups prior to day 3. High signal changes were not seen in HI+Vehicle pups in the injured hemisphere on day 3 or day 7 (Fig. 2).

ROI analysis of the injured hemisphere showed higher signal intensities in cortex, hippocampus and external capsule among HI+Mn than HI+Vehicle pups on day 1. On days 3 and 7 signal intensities of ROIs in cortex, hippocampus and thalamus were higher among HI+Mn than HI+Vehicle pups (Fig. 3). Also, on day 7 signal intensity of ROIs in the injured hemisphere's cortex and thalamus of HI+Mn pups was significantly higher than among Sham+Mn pups (Fig. 3).

Signal intensities in ROI in the contralateral hemisphere of HI+Mn pups were similar to Sham+Mn at all times in all areas (data not shown).

Contrast enhancement on T_1-weighted MR images caused by manganese on day 7

In order to identify areas of high or low signal intensities in the injured hemisphere relative to the contralateral hemisphere and compare these between animals, a normalized relative contrast (RC) was calculated (see Materials and methods). In the dorsolateral thalamus of the HI+Mn pups there was a mean negative RC on day 1 that increased to a highly positive RC (SI injured hemisphere>SI contralateral hemisphere) on day 7. In cortex and hippocampus the same trend was seen with RC increasing from negative (injured<contralateral) on day 3 to around zero (injured=contralateral) on day 7. However, among HI+Vehicle pups the opposite trend was observed going from positive RC in all areas on day 1 to negative on day 3 and becoming more negative from day 3 till 7 (Fig. 4). This lead to a large difference between HI+Mn and HI+Vehicle pups with far more positive RC in cortex, hippocampus and thalamus among HI+Mn than HI+Vehicle pups on day 7 (Fig. 4).

Increased manganese-enhancement after injection on day 6

T_1-weighted MR images of animals injected with $MnCl_2$ on day 6 (HI+Mn6) were also obtained on days 7, 8, 10 and 14 after HI. On day 7, increased signal intensities were seen primarily in the borders surrounding the area of the dorsolateral thalamus of the injured hemisphere (Fig. 5). The area corresponded to that seen on day 7 in pups injected with $MnCl_2$ 6 h after HI. A ROI placed in this area showed significantly higher mean signal intensities on day 7 among HI+Mn6 pups than among HI+Vehicle pups. From day 7 till day 14 the contrast in this area increased with more uniformly high signal intensity in the centre of the area evolving during the week (Fig. 5). However, signal intensity of this ROI among HI+Mn6 pups never became as high as the equivalent ROI among HI+Mn pups on day 7 (i.e. one week after their $MnCl_2$ injection). Among HI+Mn6 pups RC was negative in thalamus and hippocampus on day 7, but steadily increased in both areas and became positive on day 14.

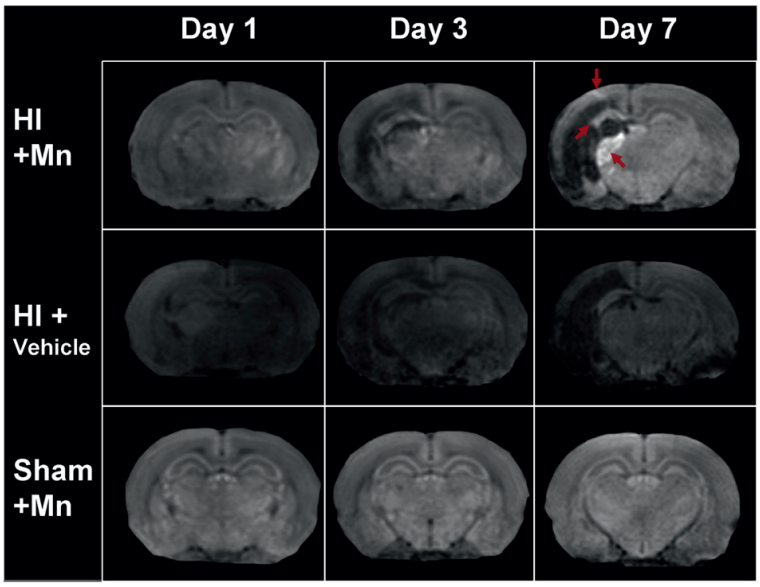

Fig. 2. T_1-weighted images of evolution of brain injury from day 1 till day 7 after hypoxia–ischemia in different groups. On day 7 high signal intensity is observed in the dorsolateral thalamus, and parts of the remaining cortex and hippocampus of the injured hemisphere of HI pups with injected $MnCl_2$ (arrows). These changes were not observed in HI+Vehicle or Sham+Mn pups.

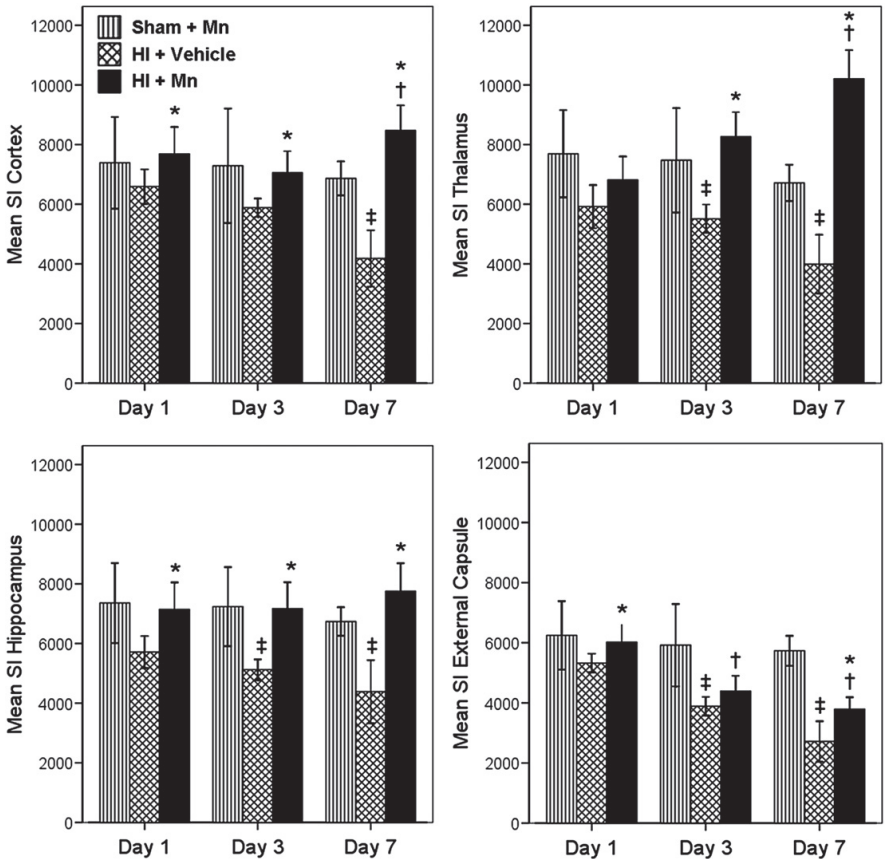

Fig. 3. Mean signal intensity (SI) in ROIs in cortex, thalamus, hippocampus and external capsule of the injured/ipsilateral hemisphere of Sham+Mn, HI+Vehicle and HI+Mn pups at different scan times. The graph shows how the mean SI of ROIs in cortex, hippocampus and thalamus increased over time among HI+Mn pups, with the most noticeable increase in thalamus, whereas among HI+Vehicle the SI steadily decreased in all areas. On day 1 SI among HI+Mn was on the same level as in Sham+Mn, but it was higher than among HI+Vehicles (thalamus $p=0.93$), indicating presence of manganese in these areas. SI in cortex and thalamus were significantly higher than both Sham+Mn and HI+Vehicle pups on day 7, indicating a pathological presence of manganese. SI in the external capsule ROI showed the same trend among HI+Mn and HI+Vehicle with decreasing values from day 1 till day 7. However, SI in this area was still higher among HI+Mn pups than HI+Vehicle on day 1 and 7. *$p<0.05$ HI+Mn vs. HI+Vehicle, †$p<0.05$ HI+Mn vs. Sham, ‡$p<0.05$ HI+Vehicle vs. Sham. (Error bars±2 SEM).

T_2-mapping

HI+Mn vs HI+Vehicles

At all scans times; the mean T_2 values measured in cortex, hippocampus and thalamus were significantly lower in HI+Mn than in HI+Vehicle pups. Among HI+Mn and HI+Vehicle pups mean T_2 values were elevated in cortex, hippocampus and thalamus in the injured hemisphere compared to the contralateral hemisphere on day 1. In HI+Vehicle, T_2 values in cortex and hippocampus of the injured hemisphere remained elevated, however slightly reduced from day 1 till day 3. T_2 in the same areas among HI+Mn pups were gradually reduced from day 1 till day 7 and was on the same level as in the contralateral hemisphere. In the dorsolateral thalamus, mean T_2 values were gradually reduced from day 1 till day 7 in both groups with the largest reduction among the HI+Mn pups. The mean T_2 value in dorsolateral thalamus of the injured hemisphere on day 7 was 24.5 ms±8.3 among HI+Mn pups vs. 54.3 ms±4.5 among HI+Vehicles ($p=0.001$) (Fig. 6). In the contralateral thalamus there were also a tendency to lower mean T_2 values among HI+Mn than HI+Vehicle pups (mean 48.6 ms±14.8 vs. mean 61.3 ms±6.9; $p=0.064$). The differences in T_2 values in thalamus between the injured and the contralateral hemisphere on day 7 were significant for both groups.

HI+Mn vs Sham+Mn

On day 1 there were increased mean T_2 values in cortex, hippocampus and thalamus of the injured hemisphere among HI+Mn pups compared to Sham+Mn. On days 3 and 7, mean T_2 values in these areas were reduced, resulting in significantly lower mean T_2 values in dorsolateral thalamus among HI+Mn pups than among Sham+Mn on day 7.

T2-mapping and manganese-enhancement

The area with reduced T_2 in dorsolateral thalamus of the injured hemisphere on day 7 in HI+Mn pups co-localized well with the manganese-enhanced areas on T_1-w images on visual analysis (Fig. 6). Software-based pixel-wise comparison of the overlap between the two segmented areas gave a mean match of 0.53±0.06, with a mean probability of 0.69±0.08 for a manganese-enhanced pixel to have a corresponding pixel with T_2-reduction.

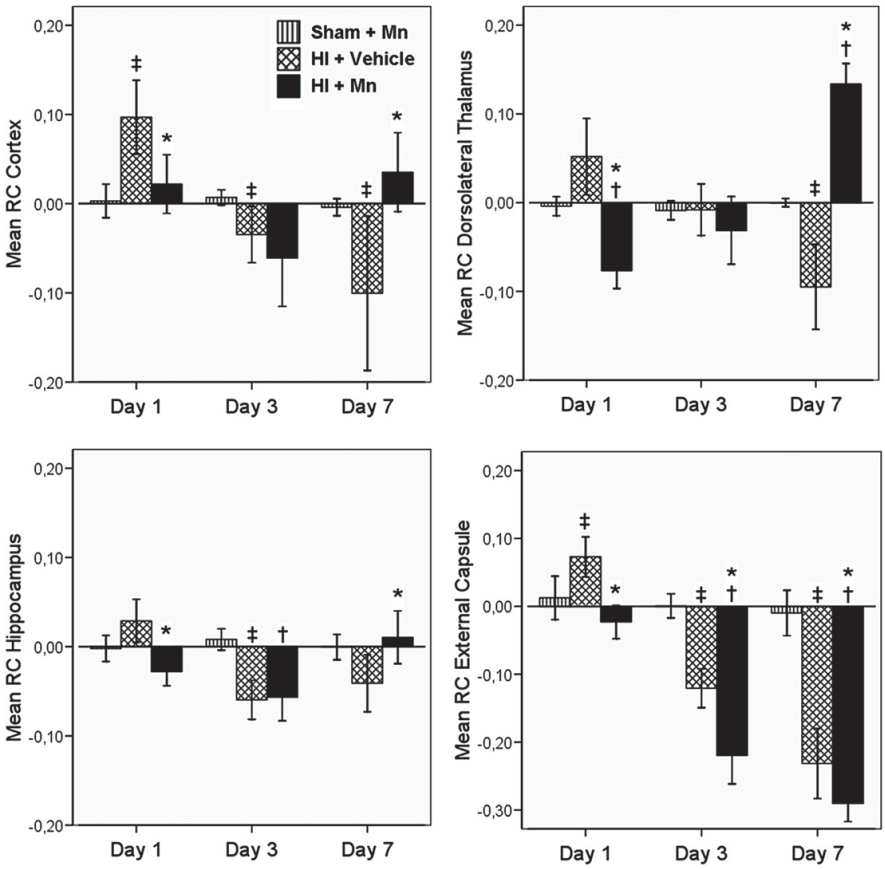

Fig. 4. Mean Relative Contrast (RC) in ROIs in cortex, thalamus, hippocampus and external capsule of Sham+Mn, HI+Vehicle and HI+Mn at different scan times. There was a highly positive relative contrast in thalamus among HI+Mn pups on day 7, meaning higher signal intensity in the injured- than the contralateral hemisphere. Notice the difference in development of RC between HI+Mn pups and HI+Vehicle in cortex, hippocampus and thalamus over time, with decreasing levels of RC among HI+Vehicle, whereas HI+Mn pups showed increasing RC from day 3 till 7. RC was significantly more positive in these areas on day 7 among HI+Mn than HI+Vehicle. External capsule showed the same development among both HI groups. $^{*}p<0.05$ HI+Mn vs. HI+Vehicle, $^{\dagger}p<0.05$ HI+Mn vs. Sham, $^{\ddagger}p<0.05$ HI+Vehicle vs. Sham. (Error bars±2SEM).

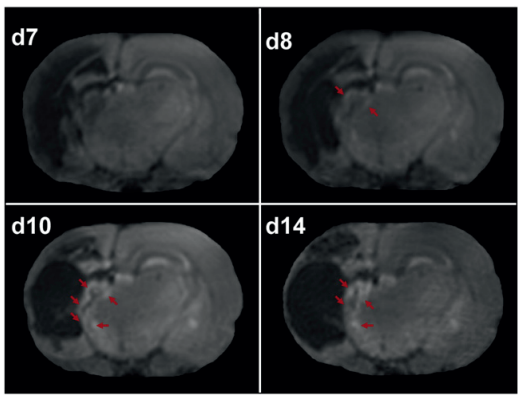

Fig. 5. T_1-weighted images 7, 8, 10 and 14 days after HI in rat pup injected with $MnCl_2$ day 6 after HI. Increasing signal intensity from day 7 till day 14 can be seen in an area of thalamus in the ipsilateral hemisphere (arrows).

Histology and immunohistochemistry

Day 1

On day 1 there was neuronal loss (areas not stained for MAP-2) in large parts of cortex, hippocampus and thalamus in the injured hemisphere with accompanying high number of cleaved caspase 3 positive cells in cortex and hippocampus and some in thalamus. Reactive astrocytes (staining positively for GFAP) and a few activated microglial cells (CD68 positive cells) were seen in widespread areas of the injured hemisphere.

Day 3

Histology on day 3 showed the same pattern of neuronal loss and cleaved caspase 3 positive cells as on day 1. Reactive astrocytes with intense GFAP staining were seen in all injured areas. Activated microglia/macrophages were evenly spread out in cortex, hippocampus and thalamus.

Day 7

Histological examination of brain sections showed no difference in lesion size, morphology, or immunohistochemical staining between HI+Mn and HI+Vehicle pups. The contralateral

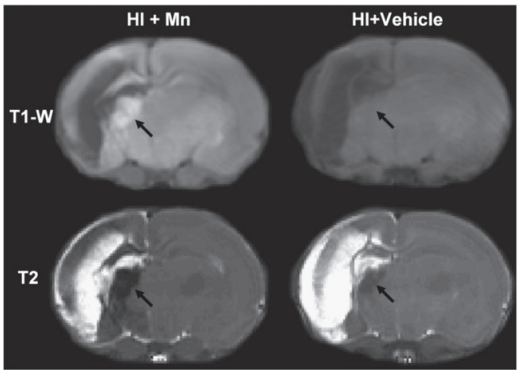

Fig. 6. T_1-weighted images and T_2-maps 7 days after HI of pups with and without injected $MnCl_2$. An area with highly reduced T_2 is seen in the dorsolateral thalamus of HI+Mn pups, corresponding to the manganese-enhancement on T_1-weighted image (arrows). In HI+Vehicle a smaller reduction in T_2 is observed in the same area, but with no corresponding increased signal intensity on T_1-weighted images (arrows).

hemisphere in these groups and among Sham+Mn pups showed no injury or abnormal pattern of staining. Immunohistochemical examination of the injured hemisphere in HI pups on day 7 showed widespread loss of tissue and cyst formation in the cortex and external capsule of the injured hemisphere. In the remaining tissue, neuronal loss was prominent and there were high numbers of Flourojade B positive dying neurons in cortex, hippocampus and dorsolateral thalamus in all HI animals (Fig. 7). Active caspase 3 positive cells were also present in all these areas, but in low numbers. Activated microglia/macrophages with intense CD68 staining were numerous in all these areas with the highest concentration in the dorsolateral thalamus. Numerous reactive astrocytes with intense GFAP staining were seen in large parts of the injured hemisphere with the highest concentration in hippocampus, cortex and dorsolateral thalamus.

Histology and manganese-enhancement on day 7

Areas with activated microglia (CD68 positive cells) had the best agreement with the areas of increased ME on T_1-weighted imaging. In 7 out of 8 HI+Mn pups increased ME was seen in the same areas that had high numbers of CD68 positive cells and vice versa. Also, the areas with activated microglia/macrophages and the areas of increased ME showed a similar morphological appearance, especially in the dorsolateral thalamus (Fig. 7). Furthermore, in two animals (HI+Mn) with very low density of activated microglia in the thalamus, there was almost no detectable ME on MRI. However, one animal had high density of CD68 positive cells, but little ME.

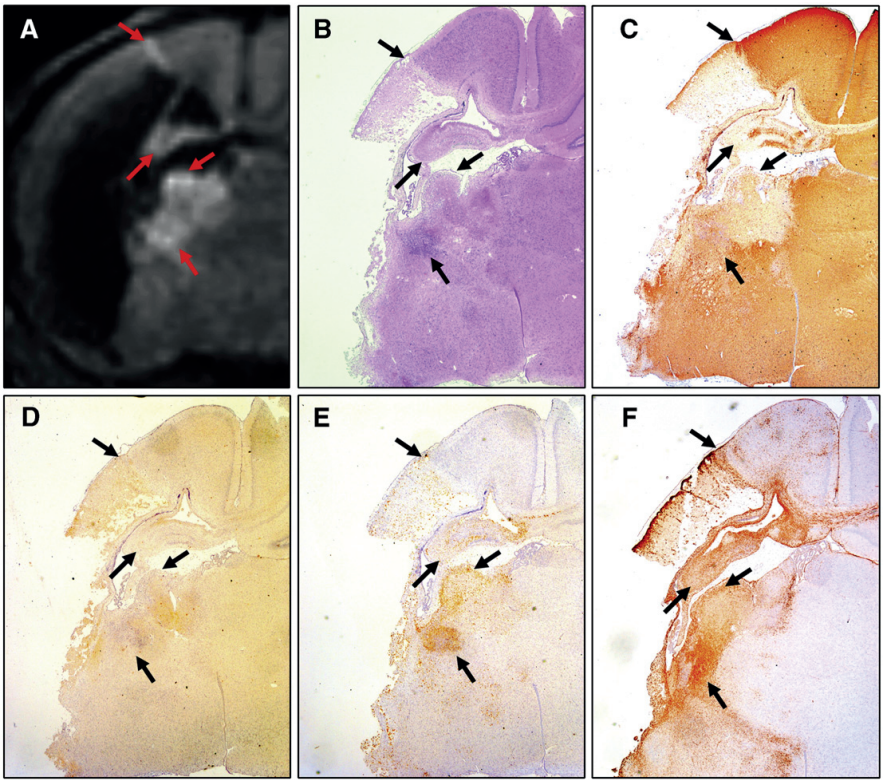

Fig. 7. T_1-weighted image (A) acquired day 7 after HI in pup injected with $MnCl_2$. Corresponding histological slices stained with HE (B) MAP-2 (C), Caspase-3 (D), CD68 (E) and GFAP (F) are shown. Arrows points to areas with increased manganese-enhancement in the T_1-weighted image and corresponding areas on histology. Comparison shows areas with dead neurons (not stained for MAP-2), activated microglia (CD68) and reactive astrocytes (GFAP) in areas with increased manganese-enhancement, but with best morphologic correlation between manganese-enhancement and staining for activated microglia.

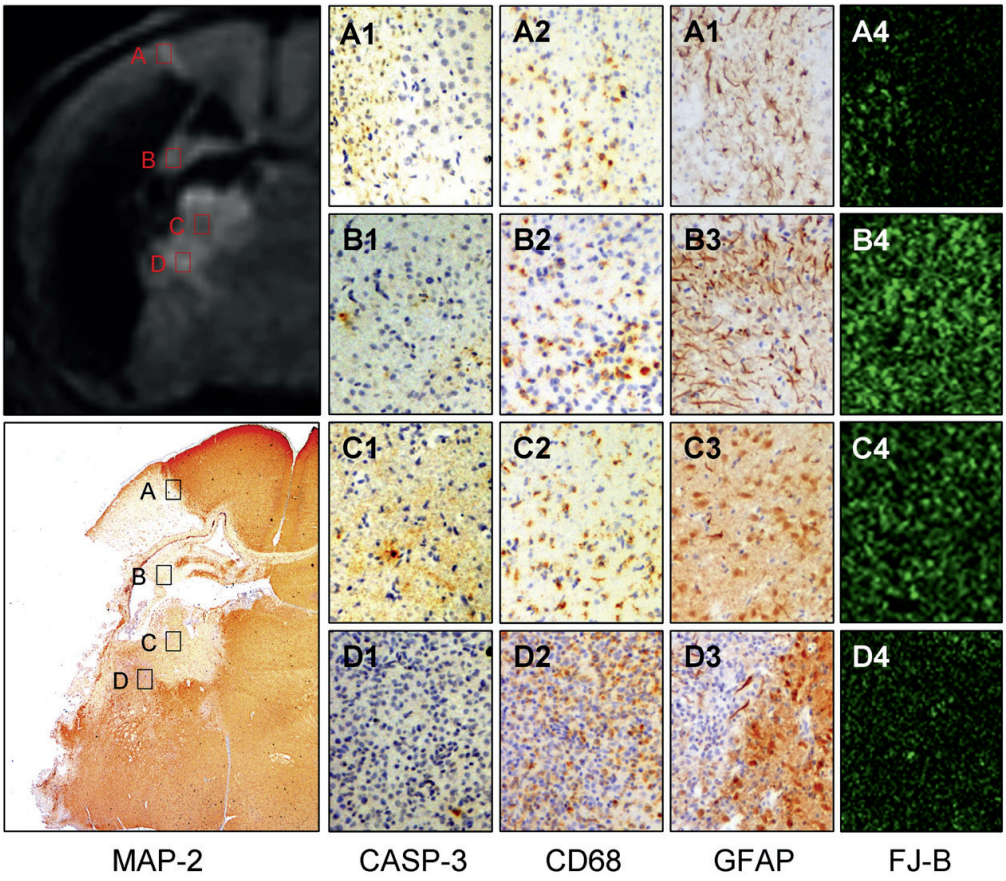

Fig. 8. Immunohistochemical staining with MAP-2, Caspase-3, CD68, GFAP and Flourojade B in different areas of varying intensity on T_1-weighted MR Image acquired day 7 after HI in pup injected with $MnCl_2$. Intensity of increased manganese-enhancement correlates well with staining for reactive astrocytes (GFAP) and activated microglia (CD68) and less with dying neurons (Flourojade B) and marker for apoptosis (Caspase-3).

Neuronal death (MAP-2 loss) and dying neurons (Fluorojade B positive cells) as well as reactive astrocytes (GFAP positive cells) were also found in the areas with increased ME on T_1-weighted images (Fig. 8). The morphological appearance of neuronal loss and the distribution of dying neurons (Fluorojade B positive cells) corresponded well with that of increased ME, but the degree of neuronal loss and density of dying neurons did not always agree well with the signal intensity of ME. The distribution of reactive astrocytes in the injured hemisphere was far more extensive than the detectable increased ME (Fig. 7). Also, the density of GFAP-staining in different areas did not always correspond with the degree of ME.

Areas with GFAP-staining, CD68 staining and MAP-2 loss were segmented and compared to areas of increased ME on a pixel-wise basis. The uncertainty in co-registration of images, made the comparison of ME and immunohistochemical staining in the small areas of cortex and hippocampus unreliable. Results of the comparison in the thalamus on day 7 are presented in Table 1 and suggest that the best match was found between increased ME and CD68 positive areas, in accordance with the results from the visual microscopic analysis.

Table 1
Overlap between manganese-enhancement and immunohistochemical staining

	n	Match	Sensitivity	Prediction
CD68	4	0.34 (±0.16)	0.44 (±0.23)	0.53 (±0.24)
GFAP	4	0.25 (±0.10)	0.27 (±0.12)	0.87 (±0.11)
MAP-2 loss	6	0.28 (±0.08)	0.31 (±0.09)	0.74 (±0.09)

Shows the results of a computer based comparison of immunohistochemical stainings and manganese-enhancement in the thalamus. Match gives the degree of overlap between the areas of manganese-enhancement and histological staining. Sensitivity gives the probability of manganese-enhancement of a pixel, given positive histological staining. Prediction gives the probability of positive staining on histology when a pixel is manganese-enhanced. The relative small area of CD68 positive staining made the predictive value very sensitive to errors in geometric overlap between MRI and histology. (Mean ± S.E.M).

Discussion

In the present study we have shown increased manganese-enhancement (ME) on T_1-weighted images in specific brain areas seven days after hypoxic–ischemic injury in the neonatal rat. High signal intensity on T_1-weighted images as well as reduced T_2-values were seen in the dorsolateral thalamus and parts of hippocampus and the remaining cortex of the injured hemisphere in pups that were injected with $MnCl_2$. Increased ME in these areas co-localized with reactive astrocytes, dying neurons and activated microglia/macrophages on immunohistochemical analysis, with the best spatial agreement with the activated microglia/macrophages.

Increased manganese-enhancement only detectable on day 7

In order to study pathological processes with MEMRI, the pathological ME always has to be compared to the normal physiological enhancement of the brain tissue architecture as shown by several studies (Wadghiri et al., 2004; Kuo et al., 2005; Watanabe et al., 2002; de Sousa et al., 2007). The strength of the current animal model is that only one hemisphere is injured, while the other is considered physiologically normal. In this study we have calculated a relative contrast parameter (RC) as a semi quantitative measure of the relative signal intensity and manganese enhancement in the two hemispheres. This also compensates for any variations in SI between days and animals. Considering the fact that RC was consistent with zero in Sham+Mn pups at all time points, any deviation of RC from zero in the injured animals was most likely due to different tissue characteristics and/or differences in manganese uptake in the two hemispheres and not to any acquisition artefacts or inhomogeneity of the B_1.

In the thalamus of the injured hemisphere, a specific increase in ME was observed on day 7 in the HI+Mn group (positive RC significantly different from shams). In hippocampus and cortex of the injured hemisphere, the positive and significantly higher RC among HI+Mn than among HI+Vehicle on day 7 indicates the presence of manganese in these structures, but is difficult to distinguish from the normal uptake in the uninjured hemisphere, as RC was not significantly different from shams.

The differences in RC between HI+Mn and HI+Vehicle pups on day 1 are interesting. The positive RC among HI+Vehicle pups indicates reduction of T_1 in the injured structures, compared to the uninjured hemisphere, which contradicts a study that showed increased T_1 (Qiao et al., 2004). The increase in T_2 in the same areas is more in accordance with the previous study, but the simultaneous high signal on T_1-weighted images is somewhat puzzling. Increased proton density in the injured hemisphere may be one explanation. Another may be that paramagnetic effects of degraded haemoglobin gives hyperintensity on T_1-weighting, while oedema of the tissue gives a predominantly T_2 increase. However, the exact cause of this finding remains unclear. Furthermore, assuming the same underlying tissue-changes in HI+Mn pups, the consistently lower RC among HI+Mn pups than among HI+Vehicle pups at day 1 can actually be interpreted as a lower Mn^{2+} uptake in the injured hemisphere compared to the uninjured hemisphere among HI+Mn pups at this time-point. Considering this, the temporal trends of RC in cortex, hippocampus and thalamus among HI+Mn pups suggest increasing Mn^{2+} concentrations from day 1 till day 7, which is also in accordance with the trends in signal intensity.

No increased manganese-enhancement at time of maximum neuronal death

Immunohistochemical analysis 1 and 3 days after HI showed widespread cell death and apoptosis in the affected hemisphere, in accordance with results from previous studies that cell death peaks 24–72 h after hypoxia–ischemia (Nakajima et al., 2000; Northington et al., 2001; Vannucci and Vannucci, 2005). The lack of increased ME at time of maximum neuronal death is in contrast with the results by Aoki et al, who found increased ME immediately after ischemia in the adult rat (Aoki et al., 2003, 2004). However, differences in animal model and MEMRI methodology make it difficult to compare the studies. Intra-arterial injection of $MnCl_2$ with disruption of the BBB with mannitol shortly after ischemia in the study by Aoki et al. (2003, 2004) may lead to a much higher availability of Mn^{2+} in the ischemic areas and less unspecific uptake in normal tissue compared to a slow diffusion of Mn^{2+} over the choroid plexus. The intentional distribution of Mn^{2+} to the brain tissue via choroid plexus in our model was confirmed on MRI on day 1 by better contrast of brain tissue architecture and generally higher signal on T_1-weighted images approximately 18 h after IP injection of $MnCl_2$. This is in accordance with previous studies (Wadghiri et al., 2004; Kuo et al., 2005; Watanabe et al., 2002; de Sousa et al., 2007). Some leakage of Mn^{2+} across the immature neonatal blood brain barrier (BBB) could also be expected, and this may have been further potentiated by the effect of hypoxia–ischemia (Takeda, 2003). Although caution must be exercised when comparing signal intensity between animals, even when the physical conditions during scanning are the same, the higher signal intensity on T_1-weighted images in the injured hemisphere on day 1 among HI+Mn pups than among HI+Vehicle pups indicates the presence of some Mn^{2+} in the injured brain tissue among HI+Mn pups. However, any specific Mn^{2+} uptake into dying neurons on day 1 or 3 seems to have been too small to give any significant T_1 contrast compared to normal tissue. One limitation of this study was that we were not able to quantify the concentration of Mn^{2+} in tissue. For future studies, quantification of T_1 could increase the sensitivity and give more clarity to the present concentration of Mn^{2+}in tissue.

Increased manganese-enhancement seven days after hypoxia–ischemia relates to inflammation

A process of delayed neuronal cell death in the dorsolateral thalamus several days after the initial injury has previously been reported by others (Northington et al., 2001, 2005; Vannucci and Hagberg, 2004; Ohno et al., 1994). Consistent with this, histology on day 7 in our study showed high degree of neuronal loss and high concentrations of dying neurons with some apoptotic cells especially in the dorsolateral thalamus, but also in areas of the remaining cortex and hippocampus. The increased ME found in the same areas suggested that increased ME visualized brain tissue with neuronal death. However, the increased ME was far better co-localized with areas with glial cell activation and inflammation than with apoptotic and dying neurons. The best co-localization was with activated microglia/macrophages, which were largely confined to the areas with ME, whereas the reactive astrocytes were found in a larger area than the increased ME. This co-localization and probable relation between activated microglia/macrophages and ME has also been reported in a MEMRI-study of cathepsin D-deficient mice (Haapanen et al., 2007). Moreover, the agreement between activated microglia and increased ME in our study was further supported by two animals that showed low density of activated microglia and almost no ME in the thalamus. However, one animal showed little ME with a high density of activated microglia, but this may be explained by reduced absorption or distribution of $MnCl_2$, for instance if the IP injection went into the gut or bladder or by differences in slice thickness and resolution between histology and MR-image slices or partial volume effects on MRI. Furthermore, the increase in ME from day 1 till day 7 was paralleled by the increase in activated microglia/macrophages, especially in the dorsolateral thalamus. This suggests that the appearance of increased ME in injured areas 7 days after HI and $MnCl_2$ injection could be explained by accumulation of Mn^{2+} in microglia/macrophages rather than specific uptake into dying neurons.

Increased manganese-enhancement may represent accumulation in phagocytes

Reactive astrocytes, activated microglia and macrophages all have the capability of phagocytosis in the aftermath of brain injury (Ito et al., 2007). A hypothesis that could explain our histological and MRI results is that during the first days after the hypoxic–ischemic insult these cells phagocytose dead cells and cell debris containing small amounts of Mn^{2+} in the large areas of early injury, resulting in an accumulation of Mn^{2+} in the phagocytes with time. When the phagocytosing cells are no longer needed in the areas with early injury that have been cleared of dead cells and debris, they may

migrate to areas with delayed cell death — among these the dorsolateral thalamus. Arrival of numerous manganese-laden phagocytes to the injury areas of the thalamus would give high concentrations of Mn^{2+} and a localized T_1-shortening effect on MRI and may hence explain the late increased ME and the high concentrations of activated microglia we observe on day 7.

Circulating macrophages that are also stained by anti-CD68 antibody have a peak infiltration of the injury site between 3 and 6 days after brain ischemia (Schilling et al., 2003; Tanaka et al., 2003; Ohno et al., 1994). These cells may have taken up Mn^{2+} while in the blood stream and contributed to the increased ME on day 7 that coincides well with their late infiltration. Since $MnCl_2$ is rapidly cleared from the circulating blood volume after a systemic injection, at least in the adult rat (Zheng et al., 2000), such an accumulation of Mn^{2+} in circulating macrophages must most likely have occurred during the first day after injection. Based on the estimates from Zheng et al. and assuming the approximately same kinetics for an IP injection of 40 mg/kg, the calculated time to return to baseline level of Mn^{2+} in our rat pups could be approximately 16 h. However, whether the pharmacokinetics of $MnCl_2$ after systemic injection is the same in the neonatal as the adult rat is unknown, and this needs further investigation.

Possible active uptake of Mn^{2+} one week after hypoxia–ischemia

Rapid clearance of Mn^{2+} from the blood makes any active uptake directly from the blood into the brain one week after the injection seem unlikely. However, to investigate whether the ME we observed on day 7 after HI and $MnCl_2$ injection could be due to active uptake at the time, we injected $MnCl_2$ IP in 3 animals on day 6 after HI (not previously injected with $MnCl_2$) and imaged them repeatedly during the following week. Increased signal around the edge of the injury area of the dorsolateral thalamus was seen on day 7, progressing towards a more uniformly increased signal in the whole injury area during the following days (Fig. 5). Since free Mn^{2+} or protein bound Mn^{2+} diffuses very rapidly across liquids, it is unlikely that the increasing ME from the edge to the centre of the area could be explained by passive diffusion of Mn^{2+}. These results therefore indicate that there may be a small active uptake in the area around day 7 and during the following week.

In a study by Fujioka et al., high signal was found on T_1-w-imaging in stroke areas after 1 week. They related this to increased induction of manganese superoxide dismutase (Mn-SOD) and glutamine synthetase (GS) in reactive astrocytes in the injured area (Fujioka et al., 2003). Increased induction of Mn-SOD occurring one week after a focal cortical lesion has been reported by another study (Bidmon et al., 1998). In our study, reactive astrocytes were found in the areas of ME alongside the activated microglia and could therefore be involved in an active Mn^{2+} uptake around one week after hypoxia–ischemia. Induction of GS and Mn-SOD in astrocytes and neurons seen after hypoxia–ischemia in the brain (Gunter et al., 2006; Takeda, 2003; Lindenau et al., 2000; Wedler and Denman, 1984) can be further potentiated by the release of free-oxygen radicals and glutamate from activated microglia in these areas and hence contribute to the late ME seen in this study. However, the increased signal intensity and the ME in animals on day 6 (HI+Mn6) never reached the level observed in animals injected 6 h after HI (HI+Mn). This suggests that the ME seen on day 7 in HI+Mn pups is mostly due to a steady accumulation of Mn^{2+} during the 7 days after injection, probably by activated microglia/macrophages, rather than an active uptake around day 7.

Reduction of T_2 is not only related to manganese

In both HI+Mn and HI+Vehicle pups there were reduced T_2-values in the thalamus of the injured hemisphere compared to the contralateral hemisphere. This reduction is contrary to previous studies which have found normal or increased T_2-levels in ischemic areas (Meng et al., 2006; Wegener et al., 2006). However, the results might be explained by the large injury that our pups suffered, as large injuries may lead to hemorrhagic infarctions and small bleeding in the tissue with subsequent iron deposits in phagocytes giving a T_2-reduction and T_2*-effect (Weber et al., 2005). Furthermore, the T_2 among HI+Mn pups was more reduced compared to the HI+Vehicle pups. Some of this reduction could be explained by a T_2-effect caused by the high concentration of Mn^{2+} in the area (Silva et al., 2004). There was a good co-localization of T_2-reduction and increased signal intensity on T_1-weighted images in the dorsolateral thalamus on visual examination (Fig. 6), where the pixel-wise comparison showed a quantified match of 53%. The lack of a complete match on pixel-wise analysis may in part be accounted for by differences in geometric distortions of the T_1- and T_2-sequences, partial volume effects and uncertainty in the geometric co-localization of images. The overlapping areas of ME and T_2-reduction are however interesting and although it is outside the scope of this study, a possible interpretation is that it may represent an interaction between iron and Mn^{2+}-uptake by astrocytes through up-regulation of divalent metal transporter (DMT-1) as previously reported in another setting (Erikson and Aschner, 2006).

Future and clinical implications

This study has shown that manganese-enhanced MRI (MEMRI) may be a useful tool in future studies to follow the cellular development of brain injury and detecting inflammatory processes related to delayed neuronal death over time in the newborn animal. Furthermore, MEMRI may also be utilised to evaluate the effect of anti-inflammatory treatments of hypoxic–ischemic injury in the neonatal brain *in vivo*. The results of this study suggest that late ME may be related specifically to inflammatory processes rather than cell death. Whether increased ME can be seen in relation to inflammation in other disease models without massive cell death remains to be investigated. However, MEMRI may prove to be a valuable tool to detect and follow brain inflammation in other disease models as well. It should be stressed that comparison of the MRI to histological examinations is mandatory to be able to interpret the specificity of ME in a given animal model.

Clinical use of MEMRI is still limited by safety issues concerning cardio- and neurotoxic effects of high dose manganese. Although our study was not designed for addressing this issue, no adverse effects of $MnCl_2$ were observed among the pups. In the future, use of low dose Mn^{2+} or Mn^{2+}-chelates as contrast agent for MEMRI of brain in human patients may become a reality when the safety of such applications has been established. *In vivo* high-resolution images of inflammation in human brains would be extremely valuable in investigating a number of different diseases including stroke and neurodegenerative diseases such as Alzheimer's.

Conclusions

During the first days after hypoxia–ischemia, there was no increased manganese-enhancement detected on MRI in areas of massive neuronal death in the injured hemisphere. Therefore, the method of MEMRI used in this study does not seem applicable for depiction of neuronal death per se. However, late increased manganese-enhancement was shown in brain areas with delayed neuronal death and inflammation seven days after hypoxia–ischemia. The areas with late manganese-enhancement corresponded best with areas with high concentrations of activated microglia on immunohistochemistry. The late manganese-enhancement may therefore be related to accumulation of manganese in activated microglia. However, other cell types may be involved and further studies are needed to reveal the specific mechanisms causing the late manganese-enhancement.

Acknowledgments

The authors would like to thank FUGE Molecular Imaging Center for technical support and use of imaging facilities. We would also thank Frank van Bel and Floris Groenendal at the University Medical Center Utrecht for help with the animal model, planning the study and valuable discussion of the results. This study was financially supported by a grant from the Medical Faculty at Norwegian University of Science and Technology.

References

Ankarcrona, M., Dypbukt, J.M., Bonfoco, E., Zhivotovsky, B., Orrenius, S., Lipton, S.A., Nicotera, P., 1995. Glutamate-induced neuronal death: a succession of necrosis or apoptosis depending on mitochondrial function. Neuron 15, 961–973.

Aoki, I., Ebisu, T., Tanaka, C., Katsuta, K., Fujikawa, A., Umeda, M., Fukunaga, M., Takegami, T., Shapiro, E.M., Naruse, S., 2003. Detection of the anoxic depolarization of focal ischemia using manganese enhanced MRI. Magn. Reson. Med. 50, 7–12.

Aoki, I., Naruse, S., Tanaka, C., 2004. Manganese-enhanced magnetic resonance imaging (MEMRI) of brain activity and applications to early detection of brain ischemia. NMR Biomed. 17, 569–580.

Bidmon, H.J., Kato, K., Schleicher, A., Witte, O.W., Zilles, K., Traystman, R.J., 1998. Transient increase of manganese–superoxide dismutase in remote brain areas after focal photothrombotic cortical lesion. Stroke 29, 203–211.

Erikson, K.M., Aschner, M., 2006. Increased manganese uptake by primary astrocyte cultures with altered iron status is mediated primarily by divalent metal transporter. Neurotoxicology 27, 125–130.

Ferriero, D.M., 2004. Neonatal brain injury. N. Engl. J. Med. 351, 1985–1995.

Fujioka, M., Taoka, T., Matsuo, Y., Mishima, K., Ogoshi, K., Kondo, Y., Tsuda, M., Fujiwara, M., Asano, T., Sakaki, T., Miyasaki, A., Park, D., Siesjo, B.K., 2003. Magnetic resonance imaging shows delayed ischemic striatal neurodegeneration. Ann. Neurol. 54, 732–747.

Geddes, R., Vannucci, R.C., Vannucci, S.J., 2001. Delayed cerebral atrophy following moderate hypoxia–ischemia in the immature rat. Dev. Neurosci., 23, 180–185.

Gonzalez, R.C., Woods, R.E., Eddins, S.L., 2004. Digital Image Processing Using Matlab. Pearson Education Inc., Pearson Prentice Hall, Upper Saddle River, New Jersey, USA.

Gunter, T.E., Gavin, C.E., Aschner, M., Gunter, K.K., 2006. Speciation of manganese in cells and mitochondria: a search for the proximal cause of manganese neurotoxicity. Neurotoxocology 27, 765–776.

Haapanen, A., Ramadan, U.A., Autti, T., Joensuu, R., Tyynelä, J., 2007. In vivo MRI reveals the dynamics of pathological changes in the brains of cathepsin D-deficient mice and correlates changes in manganese-enhanced MRI with microglial activation. Magn. Reson. Imag. 25, 1024–1031.

Ito, U., Nagasao, J., Kawakami, E., Oyanagi, K., 2007. Fate of disseminated dead neurons in the cortical ischemic penumbra. Ultrastructure indicating a novel scavenger mechanism of microglia and astrocytes. Stroke 38, 2577–2583.

Kristián, T., Siesjö, B.K., 1998. Calcium in ischemic cell death. Stroke 29, 705–718.

Koretsky, A.P., Silva, A.C., 2004. Manganese-enhanced magnetic resonance imaging (MEMRI). NMR Biomed. 17, 527–531.

Kuo, Y.T., Herlihy, A.H., So, P.W., Bhakoo, K.K., Bell, J.D., 2005. In vivo measurement of T1 relaxation times in mouse brain associated with different modes of systemic administration of manganese chloride. J. Magn. Reson. Imag. 21, 334–339.

Lindenau, J., Noack, H., Possel, H., Asayama, K., Wolf, G., 2000. Cellular distribution of superoxide dismutases in the rat CNS. Glia 29, 25–34.

McLean, C., Ferriero, D., 2004. Mechanisms of hypoxic–ischemic injury in the term infant. Semin. Perinatol. 28, 425–432.

McRae, A., Gilland, E., Bona, E., Hagberg, H., 1995. Microglia activation after neonatal hypoxic–ischemia. Dev. Brain Res. 84, 245–252.

Meng, S., Qiao, M., Scobie, K., Tomanek, B., Tuor, U.I., 2006. Evolution of magnetic resonance imaging changes associated with cerebral hypoxia–ischemia and a relatively selective white matter injury in neonatal rats. Pediatr. Res. 59, 554–559.

Nakajima, W., Ishida, A., Lange, M.S., Gabrielson, K.L., Wilson, M.A., Martin, L.J., Blue, M. E., Johnston, M.V., 2000. Apoptosis has a prolonged role in the neurodegeneration after hypoxic ischemia in the newborn rat. J. Neurosci. 20, 7994–8004.

Northington, F.J., Ferriero, D.M., Graham, E.M., Traystman, R.J., Martin, L.J., 2001. Early neurodegeneration after hypoxia–ischemia in neonatal rat is necrosis while delayed neuronal death is apoptosis. Neurobiol. Dis. 8, 207–219.

Northington, F.J., Graham, E.M., Martin, L.J., 2005. Apoptosis in perinatal hypoxic–ischemic brain injury: how important is it and should it be inhibited? Brain. Res. Brain. Res. Rev. 50, 244–257.

Ohno, M., Aotani, H., Shimada, M., 1994. Glial responses to hypoxic/ischemic encephalopathy in neonatal rat cerebrum. Dev. Brain. Res. 84, 294–298.

Paxinos, G., Watson, C., 1998. The Rat Brain in Stereotaxic Coordinates, 4th ed. Academic Press, San Diego, CA.

Qiao, M., Latta, P., Meng, S., Tomanek, B., Tuor, U.I., 2004. Development of acute edema following cerebral hypoxia–ischemia in neonatal compared with juvenile rats using magnetic resonance imaging. Pediatr Res. 55, 101–106.

Rice, J.E., Vannucci, R.C., Brierley, J.B., 1981. The influence of immaturity on hypoxic–ischemic brain damage in the rat. Ann. Neurol. 9, 131–141.

Schilling, M., Besselmann, M., Leonhard, C., Mueller, M., Ringelstein, E.B., Kiefer, R., 2003. Microglial activation precedes and predominates over macrophage infiltration in transient focal cerebral ischemia: a study in green fluorescent protein transgenic bone marrow chimeric mice. Exp. Neurol. 183, 25–33.

Silva, A.C., Lee, J.H., Aoki, I., Koretsky, A.P., 2004. Manganese-enhanced magnetic resonance imaging (MEMRI): methodological and practical considerations. NMR Biomed. 17, 532–543.

de Sousa, P.L., de Souza, S.L., Silva, A.C., de Souza, R.E., de Castro, R.M., 2007. Manganese-enhanced magnetic resonance imaging (MEMRI) of rat brain after systemic administration of MnCl2: changes in T1 relaxation times during postnatal development. J. Magn. Reson. Imag. 25, 32–38.

Takeda, A., 2003. Manganese action in brain function. Brain. Res. Brain. Res. Rev. 41, 79–87.

Tanaka, R., Komine-Kobayashi, M., Mochizuki, H., et al., 2003. Migration of enhanced green fluorescent protein expressing bone marrow-derived microglia/macrophage into the mouse brain following permanent focal ischemia. Neuroscience 117, 531–539.

Vannucci, S.J., Hagberg, H., 2004. Hypoxia–ischemia in the immature brain. J. Experim. Biol. 207, 3149–3154.

Vannucci, R.C., Perlman, J.M., 1997. Interventions for perinatal hypoxic–ischemic encephalopathy. Pediatrics 100, 1004–1014.

Vannucci, R.C., Vannucci, S.J., 2005. Perinatal hypoxic–ischemic brain damage: evolution of an animal model. Dev. Neurosci. 27, 81–86.

Wadghiri, Y.Z., Blind, J.A., Duan, X., Moreno, C., Yu, X., Joyner, A.L., Turnbull, D.H., 2004. Manganese-enhanced magnetic resonance imaging (MEMRI) of mouse brain development. NMR Biomed. 17, 613–619.

Watanabe, T., Natt, O., Boretius, S., Frahm, J., Michaelis, T., 2002. In vivo 3D MRI staining of mouse brain after subcutaneous application of $MnCl_2$. Magn. Reson. Med. 48, 852–859.

Wedler, F., Denman, R., 1984. Glutamine synthetase: the major Mn(II) enzyme in mammalian brain. Curr. Top. Cell. Regul. 24, 153–169.

Weber, R., Wegener, S., Ramos-Cabrer, P., Wiedermann, D., Hoehn, M., 2005. MRI detection of macrophage activity after experimental stroke in rats: new indicators for late appearance of vascular degradation? Magn. Reson. Med. 54, 59–66.

Wegener, S., Weber, R., Ramos-Cabrer, P., Uhlenkueken, U., Sprenger, C., Wiedermann, D., Villringer, A., Hoehn, M., 2006. Temporal profile of T2-weighted MRI distinguishes between pannecrosis and selective neuronal death after transient focal cerebral ischemia in the rat. J. Cereb. Blood Flow Metab. 26, 38–47.

Won, S.J., Kim, D.Y., Gwag, B.J., 2002. Cellular and molecular pathways of ischemic neuronal death. J. Biochem. Mol. Biol. 35, 67–86.

Zheng, W., Kim, H., Zhao, Q., 2000. Comparative toxicokinetics of manganese chloride and methylcyclopentadienyl manganese tricarbonyl (MMT) in Sprague–Dawley rats. Toxicol. Sci. 54, 295–301.

Paper II

Original Paper

Neonatology

Neonatology 2011;100:363–372
DOI: 10.1159/000328705

Received: December 7, 2010
Accepted after revision: April 20, 2011
Published online: July 27, 2011

Longitudinal Manganese-Enhanced Magnetic Resonance Imaging of Delayed Brain Damage after Hypoxic-Ischemic Injury in the Neonatal Rat

Marius Widerøe[a] Christian Brekken[b] Annemieke Kavelaars[e]
Tina Bugge Pedersen[b] Pål Erik Goa[b, c] Cobi Heijnen[e] Jon Skranes[a]
Ann-Mari Brubakk[a, d]

Departments of [a]Laboratory Medicine, Children's and Women's Health and [b]Circulation and Medical Imaging, Norwegian University of Science and Technology, and Departments of [c]Medical Imaging and [d]Pediatrics, St. Olavs Hospital, Trondheim, Norway; [e]Department of Psychoneuroimmunology, University Medical Center Utrecht, Utrecht, The Netherlands

Key Words
Manganese-enhanced MRI · Neonatal brain · Hypoxia-ischemia · Brain injury · Inflammation · Microglia

Abstract
Background: Hypoxia-ischemia (HI) in the neonatal brain results in a prolonged injury process. Longitudinal studies using noninvasive methods can help elucidate the mechanisms behind this process. We have recently demonstrated that manganese-enhanced magnetic resonance imaging (MRI) can depict areas with activated microglia and astrogliosis 7 days after hypoxic-ischemic brain injury. ***Objective:*** The current study aimed to follow brain injury after HI in rats longitudinally and compare manganese enhancement of brain areas to the development of injury and presence of reactive astrocytes and microglia. ***Methods:*** The Vannucci model for hypoxic-ischemic injury in the neonatal rat was used. Pups were injected with either $MnCl_2$ or saline after 6 h and again on day 41 after HI. Longitudinal MRI (T_1 weighted) was performed 1, 3, 7 and 42 days after HI. The brains were prepared for immunohistochemistry after the final MRI. ***Results:*** There was severe loss of cerebral tissue from day 7 to day 42 after HI. Most manganese-enhanced areas in the hippocampus, thalamus and basal ganglia at day 7 were liquefied after 42 days. Manganese-enhancement on day 42 corresponded to areas of activated microglia and reactive astrocytes in the remaining cortex, hippocampus and amygdala. However, the main area of enhancement was in the remaining thalamus in a calcified area surrounded by activated microglia and reactive astrocytes. ***Conclusion:*** Manganese-enhanced MRI can be a useful tool for in vivo identification of cerebral tissue undergoing delayed cell death and liquefaction after HI. Manganese enhancement at a late stage seems to be related to the accumulation of manganese in calcifications and gliotic tissue.

Introduction

Perinatal asphyxia causing hypoxic-ischemic brain injury is a major cause of mortality and neurologic deficits among infants and children [1–4]. Although many questions still remain unanswered, previous research in humans and animal models has given important insight

KARGER

Fax +41 61 306 12 34
E-Mail karger@karger.ch
www.karger.com

1661–7800/11/1004–0363$38.00/0

Accessible online at:
www.karger.com/neo

Marius Widerøe, MD
LBK, Medical Faculty, NTNU
MTFS
NO–7489 Trondheim (Norway)
Tel. +47 7359 8830, E-Mail marius.wideroe@ntnu.no

into the pathophysiological mechanisms underlying the brain injury after a hypoxic-ischemic insult. Animal models have shown that hypoxia-ischemia (HI) in the neonatal brain primarily affects the cerebral cortex, subcortical and periventricular white matter, striatum (basal ganglia), and hippocampus [5, 6]. Moreover, an important finding is that HI in the neonatal brain results in a prolonged evolution of injury with neurons dying days and weeks after the primary insult [5–8]. However, how this delayed injury process is triggered and sustained remains unclear, and needs further investigation.

Magnetic resonance imaging (MRI) is a superior tool for investigating delayed injury, allowing high-resolution images and repeated examinations of the same subject. Manganese-enhanced MRI (MEMRI) is a technique, where the dual properties of manganese as an MR contrast agent and biological substance are utilized. Due to its paramagnetic properties, divalent manganese (Mn^{2+}) shortens the T_1 of biological tissue giving increased signal and positive contrast at short repetition times, allowing for faster acquisition and thereby high-resolution images [9]. Mn^{2+} is naturally found in glial cells as an important factor of manganese superoxide dismutase and glutamine synthetase [10, 11]. It can enter cells through voltage-gated Ca^{2+} channels, and this property has been used in imaging of neuronal activity and acute necrosis [12]. In addition to enhancing anatomical structures of the brain on T_1-weighted images, manganese can be used as a contrast agent for detecting pathology [13–15].

In a previous study of an animal model of neonatal HI using MEMRI, we were unable to detect any manganese enhancement 1 or 3 days after the hypoxic-ischemic insult and manganese injection. However, 7 days after HI manganese enhancement was observed in the remaining cortex, hippocampus and thalamus and found to correlate with activated microglia and reactive astrocytes on immunohistochemistry [16]. The primary objective of the current study was to follow up on the results from our previous study and to examine the longitudinal evolution of brain injury up to 6 weeks following HI in the neonatal rat brain, focusing on further tissue loss, manganese-enhanced tissue and related cell responses beyond 7 days after HI.

Animals and Methods

Animals

Wistar rats (Scanbur, Norway AS) were bred in the animal facilities at the St. Olav University Hospital in Trondheim, Norway. Time-mated rats and their offspring (n = 16) were kept on a 12:12-hour light:dark cycle with water and food ad libitum. Animal experiments were conducted in accordance with Guidelines set by the Norwegian Ethics Committee for Animal Research, and the experiments were approved by the responsible governmental authority.

Hypoxia-Ischemia

The Vannucci model for hypoxic-ischemic brain injury was used [3, 17]. In short, the right common carotid artery of postnatal day 7 rats was identified, thermocauterized and severed under isoflurane anesthesia. After recovering from the operation, pups were put in a fiberglass box inside an incubator holding 36 ± 0.5°C. The box was flushed with preheated humidified air with 8% O_2 (in 92% N_2) for 75 min. Pups were allowed to recover for 5 min before being returned to their dam. This procedure resulted in a unilateral hypoxic-ischemic insult (HI) to the right cerebral hemisphere. One group of pups was sham operated; the carotid artery was identified, but not damaged. Sham-operated animals were not subjected to hypoxia.

Study Groups and Manganese Administration

$MnCl_2$ (No. 7773-01-5, Sigma-Aldrich Inc., St. Louis, Mo., USA) was given as a dose of 40 mg/kg bodyweight (~318 μmol Mn^{2+}/kg) at a concentration of 100 mM by intraperitoneal injection to one group of HI pups (HI + Mn; n = 7) and the sham-operated pups (sham + Mn; n = 3) 6 h after the hypoxia, and again 1 day prior to MRI 42 days after hypoxia. Another group of pups (HI + vehicle; n = 6) did not receive $MnCl_2$, but were instead injected with 0.9% NaCl to serve as controls.

Magnetic Resonance Imaging

MRI was performed on days 1, 3, 7 and 42 after HI (day 0), and all animals were imaged longitudinally at all time points using a 7-tesla magnet (Biospec 70/20 AS, Bruker Biospin MRI, Ettlingen, Germany) with water-cooled gradients (BGA-12, 400 mT/m). A 72-mm volume resonator was used for radiofrequency (RF) transmission and an actively decoupled mouse head surface coil was used for RF reception (Bruker Biospin MRI). During scanning, the anaesthetized (2% isoflurane in 30/70 O_2/N_2) pups lay prone in the dedicated water-heated mouse bed, and the head of every animal was fixed in the same position with inbuilt earplugs, tooth bar and nose mask.

After a gradient echo FLASH pilot scan (1 min), a T_1-weighted 3-D data set was obtained with a gradient echo FLASH sequence (FA = 30°, TR = 12 ms, TE = 3.0 ms). Field of view (FOV) was 20 × 20 × 17.5 mm^3 and acquisition matrix 128 × 96 × 84, zero-filled to 128 × 128 × 112. The interpolated resolution was 156 μm isotropic. Acquisition time was 25 min with 16 averages. Due to the growth of the animals, MRI on day 42 was performed with a larger water-heated rat bed with a rat head surface coil for RF reception, and the geometry of the scan was altered: FOV = 30 × 35 × 25 mm^3, acquisition matrix 172 × 150 × 108, zero-filled to 172 × 200 × 144 giving a interpolated resolution of 174 × 175 × 174 μm^3. Acquisition time was 52 min. All other scan parameters were kept unchanged.

Two additional low-resolution scans in coupled and single coil operation using the 3-D FLASH sequences with the same contrast parameters described above (2 min each) were acquired and used to correct the signal intensity of the T_1-weighted 3-D data set for the effect of the spatially inhomogeneous sensitivity of the surface

coils. The correction procedure was performed in MATLAB (version 2007a, MathWorks Inc.), and is described in more detail elsewhere [16].

Histology and Immunohistochemistry

Animals were sacrificed after MRI acquisition on day 42 following HI. They received an overdose of pentobarbital (300 mg/kg) and were perfused intracardially with 4% paraformaldehyde in phosphate-buffered saline. Brains were removed and embedded in paraffin. Coronal sections (8 μm) corresponding to –3.25 mm from the bregma [18] were cut and stained with either hematoxylin-eosin (HE; Klinipath, Duiven, The Netherlands), anti-microtubule-associated protein 2 (anti-MAP2; Sigma-Aldrich, Steinheim, Germany) for neuronal integrity, anti-cleaved caspase-3 (Cell Signaling) for apoptosis, anti-ED1-fitc (Serotec, Raleigh, N.C., USA) for cluster of differentiation 68 (CD68)-positive activated microglia/macrophages or anti-glial fibrillary acidic protein (anti-GFAP; Cymbus Biotechnology, Southampton, UK) as a marker for reactive astrocytes. Sections were then incubated with rat anti-FITC-biotin (Roche, Basel, Switzerland), goat anti-rabbit-biotin (Vector Laboratories, Burlingame, Calif., USA) or horse anti-mouse biotin (Vector Laboratories). Visualization was performed using a Vectastain ABC kit (Vector Laboratories). Full-section images were captured with a MIRAX MIDI system (Carl Zeiss Microimaging GmbH, Jena, Germany). The number of cells stained positively for GFAP, CD68 and caspase-3 were evaluated semiquantitatively at ×20 in both hemispheres in four brain regions; cortex, hippocampus, thalamus and amygdala. Scores were given based on the most densely stained area within the region, ranging from 0: no stained cells, 1: <33% of cells in area stained, 2: 33–67% stained to 3: >67% stained.

MR Image Analysis

ImageJ (v1.40 g, National Institutes of Health, USA) was used for MR image analysis [19]. Outlines of the brain hemispheres were manually drawn on every slice in the 3-D T_1-weighted data set, and the volumes of the two hemispheres were measured. The ratio of the right-to-left hemisphere volume was calculated and compared between groups and time points. For recognition of manganese enhancement, T_1-weighted images were viewed with a Lookup table, where pixels with low signal intensity were grayscale, and pixels with signal intensities above a given threshold were colored red. This threshold was adjusted for each 3-D data set to be equal to the highest level of signal intensity in the hemisphere contralateral to the injury for every animal. Hence, high signal areas in the injured hemisphere, indicating increased manganese enhancement, would appear red. On images from day 42, regions of interest were placed in areas of the cortex, hippocampus, thalamus and amygdala in the right hemisphere, and in anatomically corresponding areas in the left hemisphere. The normalized relative contrast in each region of interest was calculated for each animal as previously described [16]. Areas with tissue loss, injury and manganese-enhanced structures were anatomically identified by comparing reconstructed coronal slices of the 3-D T_1-weighted data set with drawings in a rat brain atlas [18].

Comparison of Histology and Manganese Enhancement

The slices stained for immunohistochemistry were evaluated using standard microscopy. The extent and density of caspase-3-, CD68- and GFAP-stained cells in different areas of the injured hemisphere were compared to the extent and intensity of manganese enhancement on reconstructed coronal 2-D T_1-weighted images, viewed with the lookup table described above. The MAP-2 loss was also compared to the extent of manganese enhancement.

Statistics

SPSS (v16.0, SPSS Inc., Chicago, Ill., USA) was used for all statistical analysis, and the level of significance was set to 0.05. For the normally distributed data, Student's t tests were used to compare mean brain hemisphere volumes and cell density scores between groups. Paired t tests were used to analyze differences in volumes between the two hemispheres and hemisphere volumes at different time points.

Results

Manganese Enhancement on MRI

In HI + Mn pups, high signal indicating manganese enhancement was clearly visible in areas of the injured right cerebral hemisphere 7 days after HI and injection with $MnCl_2$ (fig. 1). The main areas were in the most dorsal and lateral parts of the remaining thalamus, close to the dilated ventricle/cyst, and in the anterior part of caudate putamen and in the external globus pallidus. Anterior parts of the piriform cortex and the endopiriform nuclei were also manganese enhanced. Although most of the cortex and hippocampus in the right hemisphere was liquefied 7 days after HI, appearing as low signal areas on T_1-weighted images, some manganese enhancement was also seen on the edge of the remaining cortex and in the remaining CA1 of the hippocampus. HI + vehicle pups showed the same morphological changes as HI + Mn pups, but there were no areas with high signal like the ones in HI + Mn pups (fig. 1C).

More extensive tissue loss with a large cystic lesion was seen on MRI on day 42 in both HI groups. Large areas of the septal region, striatum, hippocampus, cortex and lateral and posterior thalamic nuclei that were intact on MRI on day 7 had a very low signal intensity equal to CSF on the T_1-weighted images on day 42, indicating liquefaction. Among HI + Mn pups, most areas with manganese enhancement on day 7 had low signal equal to CSF on day 42 (fig. 1B). Moreover, high signal and increased relative contrast indicating manganese enhancement could be seen in the remaining thalamus, close to the cystic area and also some spots in the remaining cortex, hippocampus and amygdala in the majority of HI + Mn pups (fig. 1B, 2A). These signal changes were not detected in HI + vehicle pups (fig. 1C, 2A).

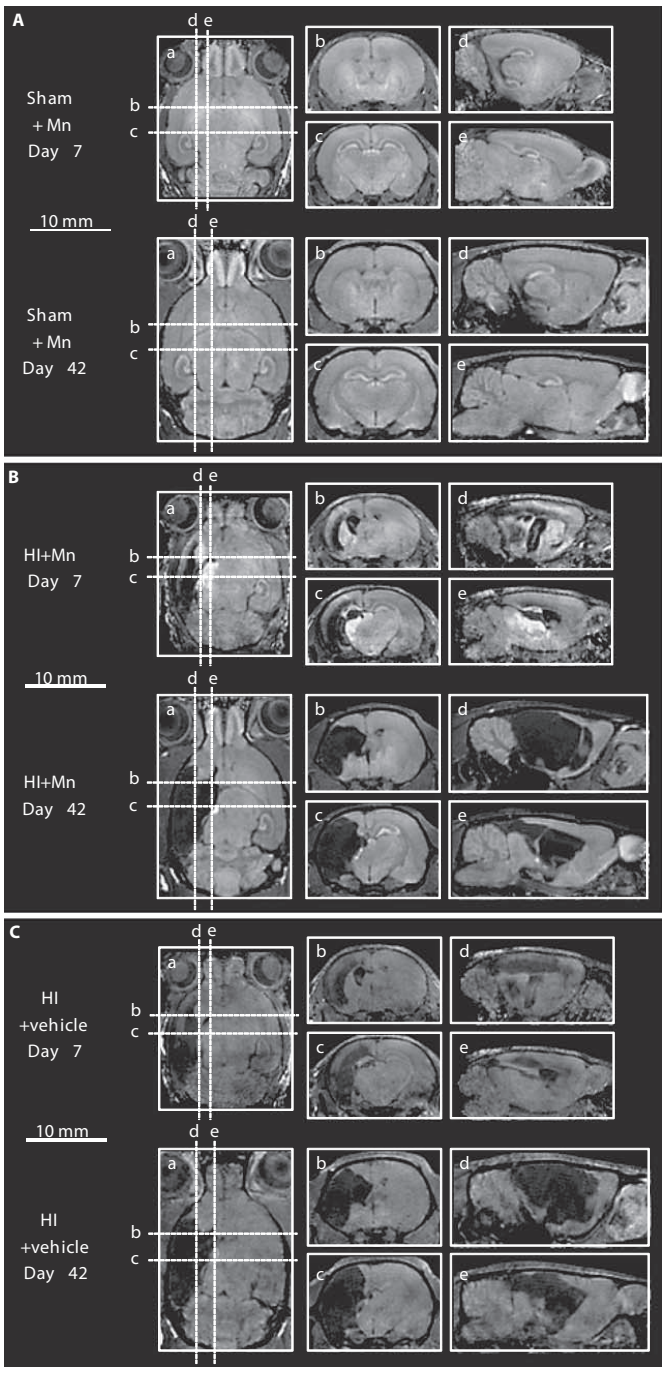

Fig. 1. Reconstructed T_1-weighted MR images in axial (a), coronal (b, c) and sagittal (d, e) view on days 7 and 42 after HI. **A** Sham-operated control animals injected with $MnCl_2$ (Sham + Mu) showed general signal enhancement in non-white matter structures, especially the olfactory bulbs and the hippocampus. **B** Evolution of brain injury in HI animals injected with $MnCl_2$ (HI + Mn). Notice the high signal areas in the remaining thalamus, in the anterior part of caudate putamen and in the external globus pallidus and in parts of the remaining cortex on day 7, and how these areas have been liquefied, replaced by a cyst and appear with low signal (dark) on day 42. High signal intensity in the remaining thalamus and also some spots in the remaining cortex, hippocampus and amygdala can be seen on day 42-images of HI + Mn. **C** HI + vehicle pup with generally lower signal, and with no high signal areas either at day 7 or 42. Notice the same increase in cyst size and loss of cerebral tissue from day 7 to day 42 in HI + Mn and HI + vehicle pups, and also the growth of cerebrum from day 7 to 42, particularly in the caudal-rostral direction.

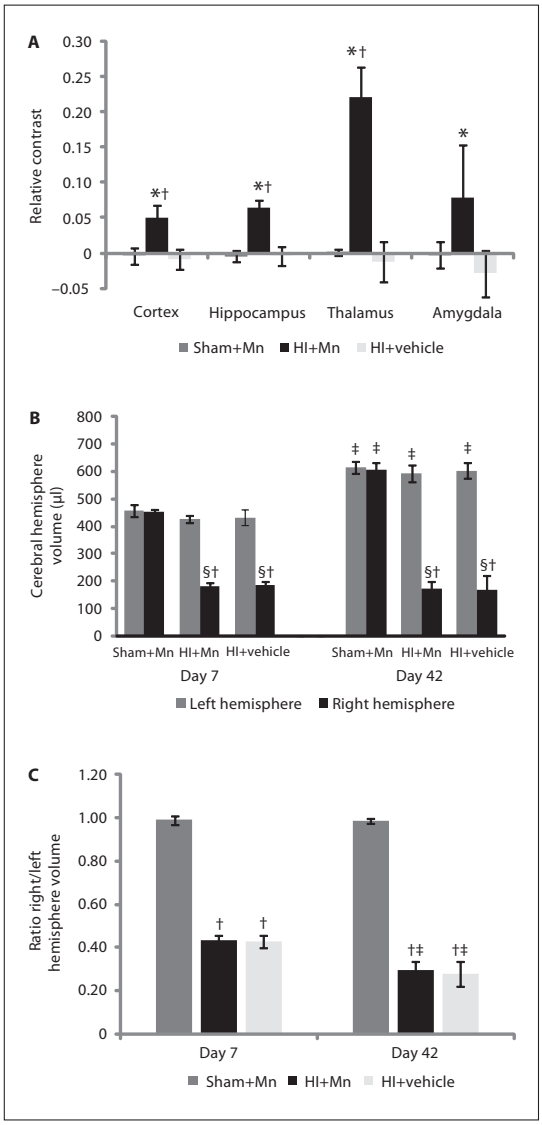

Fig. 2. A Mean relative contrast (normalized signal difference between the two hemispheres) in four brain regions in the right hemisphere at day 42 as measured on T_1-weighted images. A small increase in the relative contrast was seen in the cortex, hippocampus and amygdala with a large increase in the remaining thalamus among HI + Mn pups; thus, the signal intensity of these regions in the right hemisphere was increased compared to the left. **B** Graph shows how the volumes of the right cerebral hemisphere among HI + Mn and HI + vehicle were reduced compared to the left and to sham + Mn on days 7 and 42, but with no difference between the two time points and the two HI groups. Notice how the volume of the left cerebral hemisphere increased from day 7 to day 42 in all groups indicating natural growth of the brain. **C** Graph shows how the ratios of the right-to-left hemisphere volumes in the HI + Mn and the HI + vehicle group were reduced from day 7 to day 42, showing a relative reduction in the right hemisphere. * $p < 0.05$, HI + Mn versus HI + vehicle. † $p < 0.05$, HI + Mn or HI + vehicle versus sham + Mn. ‡ $p < 0.05$, day 7 versus day 42. § $p < 0.05$, right versus left hemisphere. Error bars: 2 × SEM.

Brain Injury Volume Development on MRI

Among both groups of hypoxic-ischemic pups, the right cerebral hemisphere volume was significantly smaller than the contralateral hemisphere volume, both at 7 and 42 days after HI (fig. 2B). Even though there was no difference in the absolute volume of the right hemisphere between day 7 and 42 among either group of HI pups, there was a significant relative reduction in right hemisphere volumes shown by a reduction in the ratios of the right-to-left hemisphere volume (fig. 2C). The left hemispheres were significantly larger after 42 days compared to 7 days in both HI groups, and the same increase was also seen in both hemispheres of sham + Mn pups (fig. 2B).

Histology 42 Days after HI

The same histological picture was seen in HI + Mn pups and HI + vehicle pups, and the morphology of the stained cells was the same. A cystic lesion dominated the right hemisphere. A typical picture of chronic infarction with reactive astrogliosis and activated microglia was seen in small areas of the remaining tissue of the cortex, hippocampus, thalamus and amygdala in the right hemisphere close to the cystic lesion (fig. 3). Loss of MAP-2 staining was seen in the same areas (fig. 3). The reactive astrocytes were mostly gemistocytic with strong GFAP staining, but in some areas they were more fibrillary in appearance (fig. 3). Apoptotic cells were seen in low numbers in the same areas, but not in all gliotic areas. All HI + vehicle pups had lesions with some apoptotic cells, whereas 2 out of 7 HI + Mn pups and all sham + Mn had no visible caspase-3-positive cells. In 8 out of 13 hypoxic-ischemic pups, there was a focal lesion in the remaining thalamus with the typical morphological appearance of a dystrophic calcification, with central necrosis and surrounding astrogliosis with activated microglia (fig. 4). The size of this calcification varied between animals, but it was located in approximately the

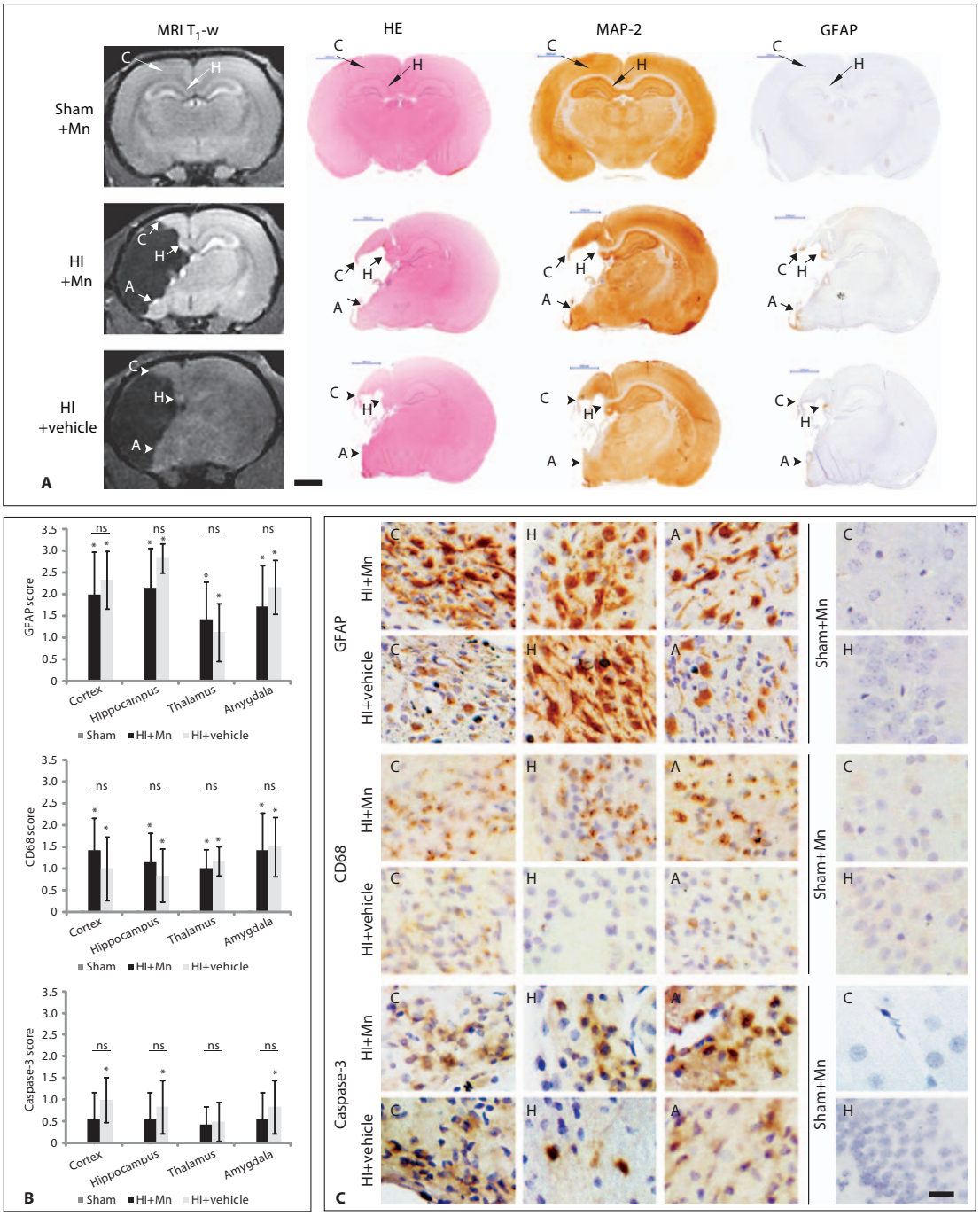
MRI T1-w
HE
MAP-2
GFAP
Sham +Mn
HI +Mn
HI +vehicle
A
B
C
GFAP score
CD68 score
Caspase-3 score
Cortex
Hippocampus
Thalamus
Amygdala
Sham
HI+Mn
HI+vehicle
ns
GFAP
CD68
Caspase-3
HI+Mn
HI+vehicle
Sham+Mn

3

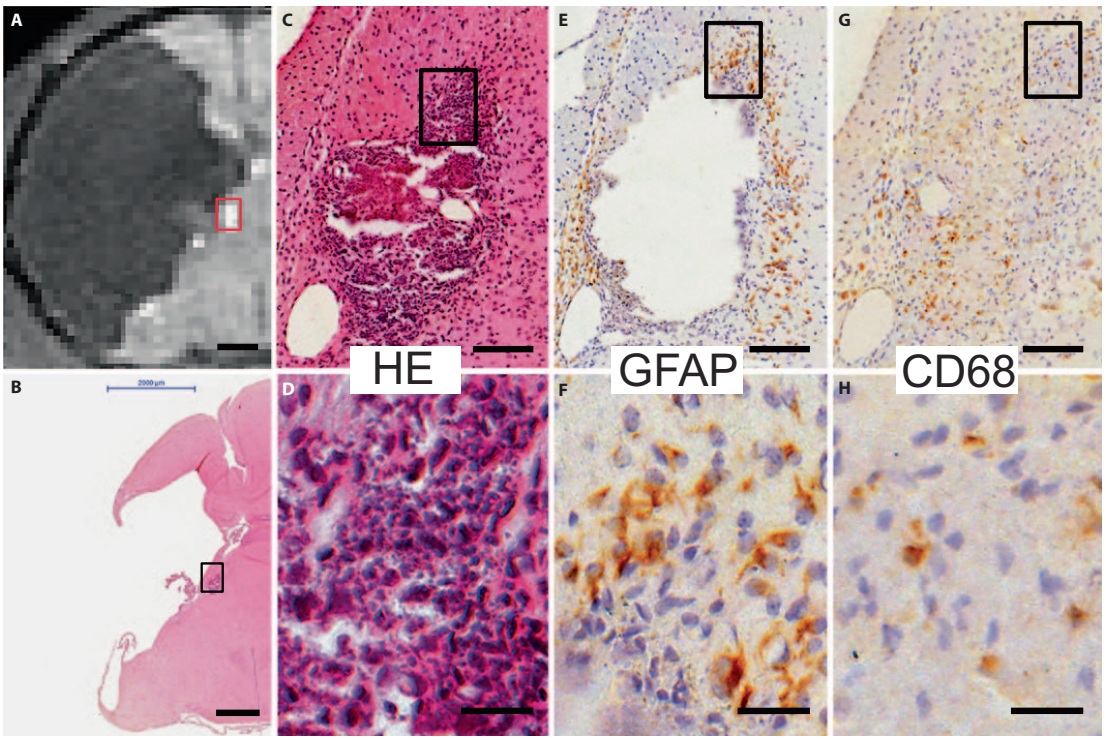

Fig. 4. Main manganese enhancement on day 42 was seen in the remaining thalamus (**A**, boxed). The corresponding area on HE stains (**B–D**) showed the classic morphology of a dystrophic calcification with necrotic cells in which calcium deposits appear as basophilic, amorphous granules (**D**). There was also surrounding reactive astrogliosis with increased GFAP staining (**E** and **F**) and activated microglia stained with CD68 (**G** and **H**). Scale bars = 1 mm (**A** and **B**), 100 μm (**C**, **E** and **G**) and 20 μm (**D**, **F** and **H**).

Fig. 3. A Comparison of manganese enhancement on T_1-weighted MR images and corresponding histological slices stained with HE and for MAP-2 and GFAP at day 42 after HI for three representative animals in the three groups (sham + Mn, HI + Mn and HI + vehicle). In sham + Mn, normal manganese enhancement can be seen corresponding to non-white matter structures and especially the neuronal layers of the hippocampus (long arrow H). In HI + Mn pups, the small spots of increased signal intensity on T_1 found in the cortex (C), hippocampus (H) and amygdala (A; short arrows) correlated with the increased GFAP staining, and to some extent to loss of MAP-2 staining (cortex and hippocampus). In HI + vehicle pups, there was no increased signal in those areas, while histology showed the same increased GFAP staining and MAP-2 loss (arrowheads) as in HI + Mn pups. Scale bar = 2 mm. **B** Mean scores (error bars: 2 × SEM) for density of GFAP-, CD68- and caspase-3-positive cells in the right cortex, hippocampus, thalamus and amygdala for the three groups. In sham + Mn, all scores were 0, thus the columns are not visible in the graphs. There were no significant (ns) differences between the HI + Mn and HI + vehicle groups. GFAP and CD68 scores were higher among HI + Mn and HI + vehicle than sham + Mn (* $p < 0.05$), while the caspase-3 score was only significantly increased among HI + vehicle pups compared to shams in the cortex, hippocampus and amygdala. **C** Examples of the stained cells at high magnification taken from the individuals in the upper panel. Magnified areas correspond to the areas marked with arrows in **A**. Scale bar = 20 μm.

same area in all animals. The left hemisphere of both HI groups and both hemispheres of the sham + Mn pups showed the same staining pattern for MAP-2, and just occasional reactive astrocytes, activated microglia or apoptotic cells.

Correlation of Histology and Manganese Enhancement on MRI

The main manganese enhancement after 42 days was seen in the thalamus and corresponded to the dystrophic calcification observed on histological slices (fig. 4). All HI + Mn pups with calcification on histology showed manganese enhancement in this area. In addition, there was manganese enhancement in thalamus in one of the HI + Mn animals that had no visible necrotic/calcified area. However, this animal had significant amounts of reactive astrocytes and activated microglia in the same area as the manganese enhancement. None of the HI + vehicle animals with calcification showed signal increase on MRI. The small areas with manganese enhancement in the remaining cortex, hippocampus and amygdala corresponded to a large extent to the MAP-2 loss and astrogliosis with activated microglia observed in these areas with immunohistochemistry (fig. 3).

Discussion

In this study, we have shown that longitudinal MEMRI can depict the process of cerebral tissue loss after HI and the remnants of the disease process in the neonatal rat brain up to 6 weeks after the initial insult. Significant amounts of cerebral tissue became liquefied in the period from 7 to 42 days after the hypoxic-ischemic insult, and several of these areas could be identified by manganese enhancement on day 7. Areas of manganese enhancement were also visible after 42 days, and were related to calcifications and astrogliosis with activated microglia, representing remnants of the infarction and the injury processes 6 weeks after the initial insult.

Manganese Enhancement

Increased manganese enhancement in the injured hemisphere was defined by higher signal intensity on T_1-weighted images than on the contralateral side, where normal uptake and manganese enhancement [13] were assumed. The signal increase and contrast on the contralateral side were similar to those observed in the shams injected with manganese, supporting the assumption above. Reducing the threshold would have given higher sensitivity for detecting manganese enhancement, but would also reduce the specificity of the detection, and the threshold was chosen to avoid false positives. However, it is likely that the reduced sensitivity may have led to an underestimation of the manganese-enhanced areas in the injured hemisphere. Although the MR protocol was optimized for high contrast to noise, calculations of T_1 and relaxivity maps might have improved the sensitivity for detecting manganese and making quantification of the manganese enhancement easier. However, this would also limit the spatial resolution of the imaging within the same time frame, and the latter was prioritized in this study.

Manganese Enhancement Related to Dystrophic Calcifications on Day 42

In a previous study in the same animal model, we have shown that high signal intensity areas due to manganese enhancement on day 7 corresponded to areas with activated microglia and reactive astrocytes on immunohistochemistry [16]. On day 42 after HI, activated microglia, reactive astrocytes and MAP-2 loss, indicating neuronal loss, were also found in the small areas with high signal intensity on T_1-weighted images in remaining cerebral structures. However, the main areas with high signal intensity were related to dystrophic calcified areas in the thalamus with surrounding gliosis and activated microglia. Although intracranial calcifications can occasionally give high signal intensity on T_1-weighted MRI [20], the signal increase is more likely due to manganese enhancement since high signal intensity in these calcified areas was only detected in animals injected with $MnCl_2$. Manganese enhancement of normal brain tissue peaks about 24 h after administration [15], and the manganese enhancement seen at day 42 may therefore be related to new manganese uptake in the surrounding astrogliosis [21]. However, our previous results [16] also indicate that it may take more time for manganese to accumulate in pathological tissue. It is possible that longer time between administration and image acquisition could improve new manganese enhancement related to the pathological processes. The manganese enhancement seen after 42 days may also represent Mn^{2+} deposits within the calcifications and gliotic areas originating from the early $MnCl_2$ injection. Although manganese is normally not detectable on MRI in the brain 3 weeks after administration [15], pathological processes following hypoxia and ischemia like calcifications, gliosis and chronic inflammation may lead to more accumulation and stronger and longer-lasting binding of manganese. In a study by Fu-

jioka et al. [22], high signal intensity areas on T_1-weighted images related to increased concentrations of native manganese were found from 1 to 16 weeks after ischemia in the rat brain. It is therefore possible that the manganese enhancement found after 6 weeks in our study can be related to manganese deposits originating from the $MnCl_2$ injected 6 h after the hypoxia, rather than new uptake of manganese into cells after injection 24 h prior to imaging on day 42.

Longitudinal Brain Injury Development and Tissue Loss

As this study demonstrates, delayed injury and destruction of cerebral tissue after HI is a prolonged process lasting several weeks. Although there was no change in the absolute volume of the right cerebral hemisphere from 7 to 42 days after HI, there was a significant reduction in the relative volume shown by a reduction in the right-to-left hemisphere volume ratios. This result can be explained by normal growth of the cerebral tissue in the left hemisphere and two simultaneous processes in the right hemisphere – growth of cerebral tissue in combination with simultaneous tissue loss due to clearance of cell debris and delayed cell death in injured areas. Tissue loss was clearly visible on the MR images as cerebral areas that appeared normal or with manganese enhancement on day 7 were replaced by low signal equivalent to CSF on day 42 (fig. 1B, C). This indicates that liquefaction and cyst formation was the major response to injury, and is further supported by histology that showed few and small areas with gliosis. This is in accordance with previous studies showing that injury to the neonatal brain causes primarily dilation of ventricles and cyst formation, rather than gliosis and scar formation as replacement for the loss of neurons [4]. The pattern we found in our study of delayed tissue loss in thalamus and basal ganglia has also been described by others in both animal and clinical studies [4, 7, 23–27]. Interestingly, the thalamus and basal ganglia are extensively connected with the cortical areas that liquefy during the first week. It has been proposed earlier that loss of connections may lead to a target deprivation and induce neuronal death in connected areas [27, 28]. More important, the results of the longitudinal manganese-enhanced MR imaging in this study, showing manganese enhancement on day 7 after HI in large parts of these brain structures that later liquefy, indicate that a continuing inflammatory process is an important factor in the process of delayed cell death and development of cysts, since the manganese enhancement on day 7 was correlated with activated microglia and reactive astrocytes in our previous study [16]. Furthermore, as shown by the images in figure 1B, the manganese-enhanced areas with astrogliosis and activated microglia on day 42 are adjacent to the manganese-enhanced areas on day 7, which may indicate that more brain areas are affected by the injury over time. The finding of apoptotic cells and activated microglia in cerebral areas with reactive astrogliosis indicates that elements of the injury process are still active 42 days after the brain infarction. Although microglial cells have an important role in phagocytosing and cleaning up dead cells, these cells can also contribute to cell injury and death by generation of free radicals, secretion of cytokines and increased excitotoxicity [1, 4], and there is also evidence to suggest that microglia can influence the development of astrogliosis [29].

Conclusion

This study shows that hypoxic-ischemic injury to the neonatal brain is a prolonged pathological process lasting several weeks. MEMRI has been shown to be a useful tool to follow this process in vivo by depicting pathological tissue that later undergoes liquefaction and disappears. Manganese also seems to accumulate in calcified and gliotic tissue over time. In future studies of novel neuroprotective strategies, MEMRI should be considered as a useful tool to evaluate the efficacy of the treatment by visualizing its effect on the ongoing processes following CNS injury.

Acknowledgements

The authors would like to thank FUGE Molecular Imaging Center (Trondheim, Norway) for technical support and use of imaging facilities, Dr. Frank van Bel and Dr. Floris Groenendaal at the University Medical Center Utrecht for help with the animal model, planning the study and valuable discussion of the results, Mrs. Jitske Zijlstra, to whom the authors are greatly indebted for expert technical assistance, Prof. Menno Witter and Paulo Girão at the Kavli Institute for Systems Neuroscience and Centre for the Biology of Memory for imaging the histological sections, and Prof. Sverre Torp at the Department of Morphology at NTNU for assistance with the histological analysis. This study was financially supported by a grant from the Medical Faculty at Norwegian University of Science and Technology.

References

1 Ferriero DM: Neonatal brain injury. N Engl J Med 2004;351:1985–1995.
2 Vannucci RC, Perlman JM: Interventions for perinatal hypoxic-ischemic encephalopathy. Pediatrics 1997;100:1004–1014.
3 Vannucci RC, Vannucci SJ: Perinatal hypoxic-ischemic brain damage: evolution of an animal model. Dev Neurosci 2005;27:81–86.
4 Volpe JJ: Brain injury in premature infants: a complex amalgam of destructive and developmental disturbances. Lancet Neurol 2009;8:110–124.
5 Northington FJ, Graham EM, Martin LJ: Apoptosis in perinatal hypoxic-ischemic brain injury: how important is it and should it be inhibited? Brain Res Rev 2005;50:244–257.
6 Vannucci SJ, Hagberg H: Hypoxia-ischemia in the immature brain. J Exp Biol 2004;207:3149–3154.
7 Nakajima W, Ishida A, Lange MS, Gabrielson KL, Wilson MA, Martin LJ, Blue ME, Johnston MV: Apoptosis has a prolonged role in the neurodegeneration after hypoxic ischemia in the newborn rat. J Neurosci 2000;20:7994–8004.
8 Geddes R, Vannucci RC, Vannucci SJ: Delayed cerebral atrophy following moderate hypoxia-ischemia in the immature rat. Dev Neurosci 2001;23:180–185.
9 Mendonca DM, Gaggelli E, Lauterbur PC: Paramagnetic contrast agents in nuclear magnetic resonance medical imaging. Semin Nucl Med 1983;13:364–376.
10 Narita K, Kawasaki F, Kita H: Mn and Mg influxes through Ca channels of motor nerve terminals are prevented by verapamil in frogs. Brain Res 1990;510:289–295.
11 Takeda A: Manganese action in brain function. Brain Res Brain Res Rev 2003;41:79–87.
12 Aoki I, Naruse S, Tanaka C: Manganese-enhanced magnetic resonance imaging (MEMRI) of brain activity and applications to early detection of brain ischemia. NMR Biomed 2004;17:569–580.
13 Aoki I, Wu YJ, Silva AC, Lynch RM, Koretsky AP: In vivo detection of neuroarchitecture in the rodent brain using manganese-enhanced MRI. Neuroimage 2004;22:1046–1059.
14 Koretsky AP, Silva AC: Manganese-enhanced magnetic resonance imaging (MEMRI). NMR Biomed 2004;17:527–531.
15 Silva AC, Lee JH, Aoki I, Koretsky AP: Manganese-enhanced magnetic resonance imaging (MEMRI): methodological and practical considerations. NMR Biomed 2004;17:532–543.
16 Widerøe M, Olsen Ø, Pedersen TB, Goa PE, Kavelaars A, Heijnen C, Skranes J, Brubakk AM, Brekken C: Manganese-enhanced magnetic resonance imaging of hypoxic-ischemic brain injury in the neonatal rat. Neuroimage 2009;45:880–890.
17 Rice JE, Vannucci RC, Brierley JB: The influence of immaturity on hypoxic-ischemic brain damage in the rat. Ann Neurol 1981;9:131–141.
18 Paxinos G, Watson C: The Rat Brain in Stereotaxic Coordinates, ed 4. San Diego, Academic Press, 1998.
19 Rasband WS: ImageJ. US National Institutes of Health, Bethesda, 1997–2009; http://rsb.info.nih.gov/ij/.
20 Henkelman RM, Watts JF, Kucharczyk W: High signal intensity in MR images of calcified brain tissue. Radiology 1991;179:199–206.
21 Kawai Y, Aoki I, Umeda M, Higuchi T, Kershaw J, Higuchi M, Silva AC, Tanaka C: In vivo visualization of reactive gliosis using manganese-enhanced magnetic resonance imaging. Neuroimage 2010;49:3122–3131.
22 Fujioka M, Taoka T, Matsuo Y, Mishima K, Ogoshi K, Kondo Y, Tsuda M, Fujiwara M, Asano T, Sakaki T, Miyasaki A, Park D, Siesjo BK: Magnetic resonance imaging shows delayed ischemic striatal neurodegeneration. Ann Neurol 2003;54:732–747.
23 Martin LJ, Brambrink A, Koehler RC, Traystman RJ: Primary sensory and forebrain motor systems in the newborn brain are preferentially damaged by hypoxia-ischemia. J Comp Neurol 1997;377:262–285.
24 Vannucci RC, Connor JR, Mauger DT, Palmer C, Smith MB, Towfighi J, Vannucci SJ: Rat model of perinatal hypoxic-ischemic brain damage. J Neurosci Res 1999;55:158–163.
25 Barkovich AJ, Sargent SK: Profound asphyxia in the premature infant: imaging findings. Am J Neuroradiol 1995;16:1837–1846.
26 Roland EH, Poskitt K, Rodriguez E, Lupton BA, Hill A: Perinatal hypoxic-ischemic thalamic injury: clinical features and neuroimaging. Ann Neurol 1998;44:161–166.
27 Northington FJ, Ferriero DM, Graham EM, Traystman RJ, Martin LJ: Early neurodegeneration after hypoxia-ischemia in neonatal rat is necrosis while delayed neuronal death is apoptosis. Neurobiol Dis 2001;8:207–219.
28 Martin LJ, Al-Abdulla NA, Brambrink AM, Kirsch JR, Sieber FE, Portera-Cailliau C: Neurodegeneration in excitotoxicity, global cerebral ischemia, and target deprivation: a perspective on the contributions of apoptosis and necrosis. Brain Res Bull 1998;46:281–309.
29 Zhang D, Xiaoming H, Qian L, O'Callaghan JP, Hong J-S: Astrogliosis in CNS pathologies: is there a role for microglia? Mol Neurobiol 2010;41:232–241.

Paper III

Effects of doxycycline on the longitudinal development of cerebral grey and white matter injury in a neonatal rat model of hypoxia-ischemia – a magnetic resonance imaging study.

Marius Widerøe[1], Marianne B Havnes[2], Tora Sund Morken[1], Jon Skranes[1], Pål-Erik Goa[3], and Ann-Mari Brubakk[1,4].

[1]Department of Laboratory Medicine, Children's and Women's Health and [2]Department of Circulation and Medical Imaging, Norwegian University of Science and Technology, Trondheim, N-7491, Norway.
[3]Department of Medical Imaging and [4]Department of Pediatrics, St. Olav University Hospital, Trondheim, N-7006, Norway

Submitted to European Journal of Neuroscience

Abstract

Doxycycline may potentially be a neuroprotective treatment for neonatal hypoxic-ischemic brain injury through its anti-inflammatory effects. The aim of this study was to examine any long-term neuroprotection by doxycycline treatment on cerebral grey and white matter. Hypoxic-ischemic brain injury (HI) was induced in seven days old rats. Pups were treated with either doxycycline (HI+doxy) or saline (HI+vehicle) by intraperitoneal injection one hour after HI. Six hours after HI, $MnCl_2$ was injected intraperitoneally for later manganese-enhanced MRI. MRI was performed with diffusion weighted imaging day one and T_1-weighted imaging and diffusion tensor imaging (DTI) 7, 21 and 42 days after HI. Animals were sacrificed after MRI on day 42 and histological examinations of the brains were performed. There was a tendency towards lower lesion volumes on diffusion maps among HI+doxy than HI+vehicle one day after HI. Volumetric MRI showed increasing differences between groups with time after HI, with less cyst formation and less cerebral tissue loss among HI+doxy pups than HI+vehicle. HI+doxy pups had less manganese-enhancement on day seven after HI, indicating reduced inflammation. HI+doxy had higher fractional anisotropy on DTI in major white matter tracts in the injured hemisphere than HI+vehicle, indicating less injury to white matter and better myelination. Histological examinations supported the MRI results. Lesion size on early MRI was highly correlated with final injury measures. In conclusion, a single dose of doxycycline reduced long-term cerebral tissue loss and white matter injury after neonatal hypoxia-ischemia, with increasing effect of treatment with time after injury.

Key words: Manganese-enhanced MRI, DTI, brain injury, inflammation, microglia.

Abbreviations: ADC - Apparent Diffusion Coefficient; **CCA** - Common Carotid Artery; **DTI** - Diffusion Tensor Imaging; **FA** - Fractional Anisotropy; HI - Hypoxia-Ischemia; **MRI** - Magnetic Resonance Imaging.

Introduction

Hypoxic-ischemic insults to the neonatal brain are a major cause of death and neurological deficits among children (Ferriero, 2004; Volpe, 2009). The current therapeutic options for treating or preventing hypoxic-ischemic injuries are limited and the long-term effects are still unknown (Ferriero, 2004; Gonzalez & Ferriero, 2009). Inflammation is a key element in the response to hypoxic-ischemic insults, and the release of cytokines, free radicals and nitric oxides from activated microglia is one of the contributing injury mechanisms (Mcrae *et al.*, 1995; Ferriero, 2004; Khwaja & Volpe, 2008; Volpe, 2009). Activated microglia and macrophages also seem important in the delayed injury response (Mcrae *et al.*, 1995; Khwaja & Volpe, 2008). Inhibition of brain inflammation is therefore an interesting target for new treatments (Gonzalez & Ferriero, 2009).

Doxycycline and minocycline are second-generation tetracyclines that have been used for treatment of infectious diseases for decades. In addition to the antibacterial properties, they exhibit anti-inflammatory effects (Buller *et al.*, 2009). The neuroprotective abilities of doxycycline were first shown in ischemic brain injuries in adult rabbits (Clark *et al.*, 1994). Since then, neuroprotection after neonatal hypoxic-ischemic brain injury has been shown with both minocycline and doxycycline in rat models, mainly through inhibition of microglial activation and anti-apoptotic mechanisms (Arvin *et al.*, 2002; Jantzie *et al.*, 2005; Cai *et al.*, 2006; Fan *et al.*, 2006; Jantzie *et al.*, 2006; Carty *et al.*, 2008; Jantzie & Todd, 2010; Wixey *et al.*, 2011). However, most studies have focused on short-term effects, up to seven days after HI. Considering that hypoxic-ischemic injury to the neonatal brain is a prolonged pathological process that lasts for several weeks in the neonatal rat (Geddes *et al.*, 2001; Wideroe *et al.*, 2011), it is important to examine whether doxycycline has additional long-term effects on delayed brain injury, via inhibition of the prolonged inflammatory response.

Longitudinal studies using magnetic resonance imaging (MRI) are especially suited to answer these questions. We have previously used manganese-enhanced MRI to visualize the delayed injury process with astrogliosis and inflammation after neonatal hypoxic-ischemic brain injury (Wideroe *et al.*, 2009; Wideroe *et al.*, 2011). Diffusion tensor imaging (DTI) is another MRI method that allows visualization of injury and developmental maturation of white matter tracts *in vivo* (Mori & Zhang, 2006). In this study we have used DTI in addition to manganese-enhanced MRI to assess the effects of doxycycline on the longitudinal development of cerebral grey and white matter injury in a neonatal rat model of hypoxia-ischemia.

The main aim was to evaluate the potential long-term neuroprotective effects of doxycycline and to examine the effect of doxycycline on the structural evolution of injury over weeks after the hypoxic-ischemic insult. We also wanted to examine the value of early detailed MRI in predicting the long-term extent of injury to cerebral grey and white matter.

Material and methods

Animals

Wistar rats (Scanbur, Norway AS) were bred in the Animal Facility at the Norwegian University of Science and Technology in Trondheim. Time-mated rats and their offspring (n=20) of both genders were kept on a 12:12 hours light:dark cycle. They were weaned at the age of four weeks and had food and water ad libitum. Animal experiments were conducted in accordance with European Communities Council Directive of 1986 (86/609/EEC) through guidelines set by the Norwegian Ethics Committee for Animal Research, and the experiments were approved by the responsible governmental authority (Forsøksdyrutvalget).

Hypoxia-Ischemia (HI)

The Vannucci model for hypoxic-ischemic brain injury was used (Rice *et al.*, 1981; Vannucci & Vannucci, 2005). In short, the right common carotid artery (CCA) of seven days old rats was identified, thermo-cauterized and severed under isoflurane anaesthesia. After recovering from this operation for between 2 and 4 hours, pups were put in a fibreglass box inside an incubator holding 36±0.5 ºC. The box was flushed with pre-heated humidified air with 8% O_2 (in 92% N_2) for 60 min. Pups were allowed to recover for 5 minutes before they were returned to their dam. In each litter two pups were sham-operated; the right CCA was identified, but not severed. Sham-operated animals were not subjected to hypoxia.

Study groups and drug administration

Pups were randomised to HI with treatment (HI+doxy; n=8), HI without treatment (HI+vehicle; n=8) and sham-operation (sham; n=4) at time of surgical procedure on day seven after birth. One hour after end of hypoxia, a single dose of 150µl doxycycline (Doxyferm®, Nordic Drugs AB, Limhamn, Sweden) at a concentration of 1mg/ml (equivalent to 10mg/kg bodyweight for a 15g rat) was given by intraperitoneal injection to pups in the treatment group (HI+doxy), while non-treated pups (HI+vehicle) received a single injection of 150µl 0.9% NaCl. For the manganese-enhanced MRI, $MnCl_2$ (# 7773-01-5, Sigma-Aldrich Inc., St. Louis, USA) was given as a dose of 40 mg/kg bodyweight (~318µmol Mn^{2+}/kg) at a concentration of 100mM (diluted with 0.9% NaCl to a volume of 150µl) by intraperitoneal injection to all pups six hours after the end of hypoxia. One animal (HI+vehicle) died 4 weeks after HI for unknown reasons.

Magnetic Resonance Imaging

MRI was performed on days 1, 7, 21 and 42 after HI using a 7T magnet (Biospec 70/20 AS, Bruker Biospin MRI, Ettlingen, Germany) with water-cooled gradients (BGA-12, 400 mT/m). A volume resonator was used for RF transmission and actively decoupled head surface coils (Bruker Biospin) were used for RF reception. Animals were imaged longitudinally at all time-points. During scanning the anaesthetized (2% isoflurane in 30% O_2, 70% N_2) pups lay prone in a dedicated water heated bed and the head of every animal was fixed in the same position

with tooth bar, nose-mask and polystyrene. Temperature and respiration were monitored during the scanning procedure.

On day one, diffusion weighted images were obtained using a Echo Planar Imaging (EPI) sequence with 6 b-values (100/200/400/600/800/1000ms); TE = 37.50 ms; TR = 3000ms; field of view (FOV) 30 × 20 mm^2; acquisition matrix (MTX) 192 × 128; 15 coronal slices á 1 mm; 4 averages; 5min 36sec acquisition time.

On days 7, 21 and 42 T_1-weighted 3D data sets were obtained with a gradient echo FLASH sequence (FA = 30º, TR = 12ms, TE = 3.25ms). While all other scan parameters were kept unchanged, the geometry and scan time differed for each time-point: On day 7: FOV = 25 × 25 × 17 mm^3; MTX = 160 × 120 × 84; 16 averages; 32min acquisition time. On day 21: FOV = 30 × 25 × 20 mm^3; MTX = 192 × 120 × 96; 16 averages; 37min acquisition time. On day 42: FOV = 30 × 30 × 20 mm^3; MTX = 192 × 144 × 48; 8 averages; 11min acquisition time. At each time-point, two additional low-resolution FLASH sequences in coupled and single coil operation were acquired with the same contrast parameters and FOV as described above (2 min each) and used to correct the signal intensity of the T_1-weighted 3D data set for the effect of the spatially inhomogeneous sensitivity of the surface coils. The correction procedure was performed in MATLAB (ver. R2010a, MathWorks Inc, Natick MA, USA), and is described in more detail elsewhere (Wideroe *et al.*, 2009).

On days 7, 21 and 42 diffusion tensor imaging (DTI) was performed with an EPI sequence using 30 directions and b = 1000ms; 5 b0 images and the following scan parameters: On days 7 and 21: TE = 35; TR = 2550 ms; FOV = 30 × 40 mm^2; MTX = 128 × 172; 4 averages; 17 axial slices á 0.5 mm; 24min acquisition time. On day 42: TE = 40; TR = 3750 ms; FOV = 40 × 49.6 mm^2; MTX = 172 × 212; 4 averages; 25 axial slices á 0.5 mm; 35min acquisition time.

Histology and immunohistochemistry

Animals were sacrificed after MRI acquisition on day 42 after HI. They received an overdose of pentobarbital (300 mg/kg) and were perfused intracardially with 4% paraformaldehyde (PAH) in phosphate-buffered saline (PBS). Brains were removed and embedded in paraffin. Axial sections (8 µm) corresponding to –4.28 mm from the bregma (Paxinos & Watson, 1998) were cut and stained with either hematoxylin-eosin (HE) (Klinipath, Duiven, the Netherlands), anti-MAP2 (Sigma-Aldrich, Steinheim, Germany) for neuronal integrity, anti-ED1-fitc (Serotec, Raleigh, NC) for CD68-positive activated microglia/macrophages, or anti-MBP (Sternberger Monoclonals Inc., Lutherville, MD) for myelin. Sections were then incubated with rat-anti-FITC-biotin (Roche, Basel, Switzerland), goat-anti-rabbit-biotin (Vector Laboratories, Burlingame, CA) or horse-anti-mouse-biotin (Vector Laboratories, Burlingame, CA). Visualization was performed using a Vectastain ABC kit (Vector Laboratories). Full section images were captured with a MIRAX MIDI system (Carl Zeiss MicroImaging GmbH, Jena, Germany). Tissue loss and neuronal loss was evaluated semi-quantitatively at x20 in 12 regions of the right cerebral hemisphere. Putamen, thalamus and five subregions of the hippocampal structure (Subiculum, dentate gyrus, CA1, CA2 and CA3) were scored: 0: no loss; 1: <33% tissue/neuronal

loss; 2: 33-67% tissue/neuronal loss; 3: >67% tissue/neuronal loss and 4: Total dissolution. The five cortical regions (see figure 6) were scored: 0: no loss; 1: neuronal loss in small areas limited to layer III; 2: Patchy neuronal loss involving more layers; 3: reduced cortical thickness and 4: Total dissolution. Histological injury score was defined as the average score of all regions. The presence of CD68 positive microglial cells was also evaluated semi-quantitatively in the same regions and scored from 0: no CD68 positive cells; 1: patchy few cells in one area; 2: patchy groups of cells in several areas; to 3: large areas with many cells. For regions that were in total dissolution, no score was given and the average of the scored regions were defined as the CD68 score.

MR Image analysis

Apparent diffusion coefficient (ADC) maps were calculated using in-house developed software (MATLAB ver. R2010a) by fitting a mono exponential model to the signal intensity of the images with different b-values. Further analyses of ADC-maps, T_1-weighted images and DTI were performed with the tools of the FMRIB software library (FSL ver. 4.1.4, Oxford Centre for Functional MRI of the Brain, UK; www.fmrib.ox.ac.uk/fsl) (Smith *et al.*, 2004; Woolrich *et al.*, 2009).

A semi-automatic segmentation method was used to estimate the lesion volume on ADC-maps based on the assumption that changes in ADC in the right cerebral tissue were due to injury while ADC in the left hemisphere was preserved and normal. After initial manual masking of the brain hemispheres, automatic clustering was performed using FAST (part of FSL) (Zhang *et al.*, 2001). In this method all voxels in both hemispheres were assigned a class value from 1-5 reflecting their ADC-value, while taking into account the similarity of ADC-values of neighboring voxels. For each class the volume of tissue in each hemisphere was calculated by counting the number of voxels. A volume difference between the two hemispheres in each class was assumed to represent a lesion volume. The total lesion volume was then estimated from the sum of these volume differences across all classes.

T_1-weighted MR images were used to measure volumes of the cerebral tissue and manganese-enhancement. Masks for the cerebral tissue in the right and the left hemispheres as well as cyst in the right cerebral hemisphere were manually drawn on the T_1-weighted 3D data sets in Fslview (part of FSL), and the volumes were measured. Total brain volume was calculated as the sum of cyst, right and left cerebral tissue. The relative volume of right cerebral tissue was calculated by dividing the volume of right cerebral tissue by the total brain volume. Manganese-enhanced areas in the right cerebral hemisphere were defined by having higher signal intensity on T_1-weighted images day seven than on the contralateral side (see Wideroe *et al.* (2011) for more details). Masks for the manganese-enhanced tissue were manually drawn and the volumes calculated.

To examine cerebral white matter maturation and injury, the DTI images were analyzed. Images were preprocessed to reduce image artifacts due to motion and eddy current distortions by affine transformation and co-registration of the diffusion encoded images to the

b0 images. Brains were segmented using the Brain Extraction Tool (part of FSL). FDT ver2.0 (part of FSL) was used to fit a voxelvise diffusion tensor model to the DTI data (Behrens *et al.*, 2003). Maps for fractional anisotropy (FA), mean diffusivity (MD), radial diffusivity ($\lambda_{\perp}$) and axial diffusivity ($\lambda_{\parallel}$) were created. Regions of interest (ROIs) were manually drawn in centre of the corpus callosum (genu, body and splenium), right and left major white matter areas (internal capsule, external capsule, hippocampal fimbria and cingulum) on the FA-maps. Mean FA, MD, $\lambda_{\perp}$ and $\lambda_{\parallel}$ were calculated in each of the three ROIs in each animal.

Statistics

PASW Statistics 18 (release 18.0.2, SPSS Inc., Chicago, IL, USA) was used for all statistical analysis and the level of significance was set to 0.05. Linear regression was used to test for correlations between early measures of injury and later outcome measures. Paired t-tests were used to analyze differences in volumes and DTI data between the two hemispheres. Linear mixed models were used to analyse lesion volume on ADC-maps, volume of manganese-enhanced tissue, brain volume data, and the DTI data using experiment group and time-point as fixed factors. We fitted models of restricted maximum likelihood ratio to test for effects of experiment group, time, and interaction between time and group, with post hoc Least Significant Difference tests. Models were also tested with recovery time from CCA operation to start of hypoxia as fixed factor to control for possible confounding effects. These data are presented as estimated marginal means with 95% confidence intervals, unless stated otherwise. Differences in histological injury score and CD68 score between the treatment groups were analysed with Mann-Whitney-U test.

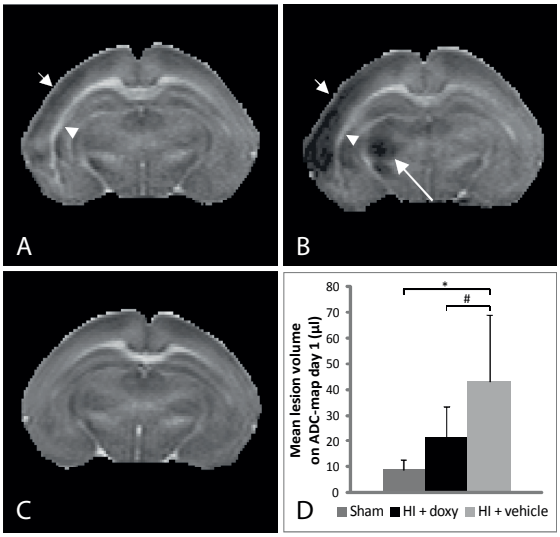

Figure 1 Lesions on ADC-maps day one after HI.
Images A-C show examples of ADC-maps. ***A:*** HI+doxy pup with mild injury. Notice reduced ADC in cortex (short arrow) and increased ADC in external capsule (arrow head). ***B:*** HI+vehicle pup with severe injury. Notice the large reduction of ADC in cortex (short arrow) and thalamus (long arrow) with increased ADC in external capsule (arrow head). ***C:*** Sham; no difference between hemispheres. ***D:*** Bar chart shows mean lesion volumes on ADC-maps day one with 95% confidence intervals in Sham, HI+doxy and HI+vehicle groups. HI+vehicle had higher lesion volumes than that measured in Sham (* $p < 0.05$). The tendency of higher lesion volumes in HI+vehicle versus HI+doxy ($p = 0.075$), became significant after including recovery time from carotid artery operation to hypoxia as a covariate in the analyses (# $p < 0.05$).

Results

Lesions on ADC-maps one day after HI

One day after HI, lesions were seen on the ADC-maps as reduced ADC in the right cortex, hippocampus, thalamus and putamen, and increased ADC in the right external capsule close to the hippocampus (Figure 1). There was a large variation in lesion size on ADC-maps among both HI+doxy and HI+vehicle, but with a tendency towards larger lesion volumes among HI+vehicle pups than HI+doxy pups (p=0.075) (Figure 1). This variation in lesion volume could to some extent be explained by the recovery time from CCA operation to hypoxia. Shorter recovery time resulted in larger lesion volumes on ADC day one, and reduced volumes of right cerebral tissue on later time points (Figure 2). Litter, gender, body weight or duration of operating procedure did not affect the outcome measures. When recovery time was included as a covariate in the analysis, the difference in lesion volume between HI+doxy and HI+vehicle on ADC-maps on day one became statistically significant (p=0.026).

The lesion volumes on ADC-maps on day one were positively correlated with cyst volumes and negatively correlated with absolute and relative volumes of right cerebral tissue on days 7, 21

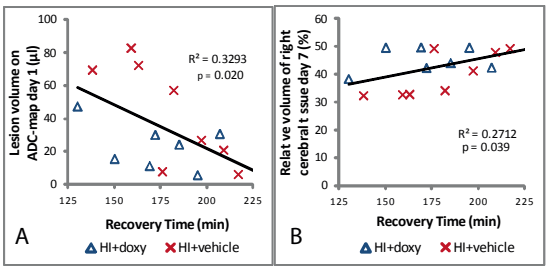

Figure 2 Correlations with recovery time.
Scatter plots show the correlations between recovery time (time between operation with severing of right common carotid artery and exposure to hypoxia) and measures of injury on day one **(A)** and day seven **(B)**. *Lines represent the fitted linear regression lines for all subjects. R^2 and p-value for each line are given.*

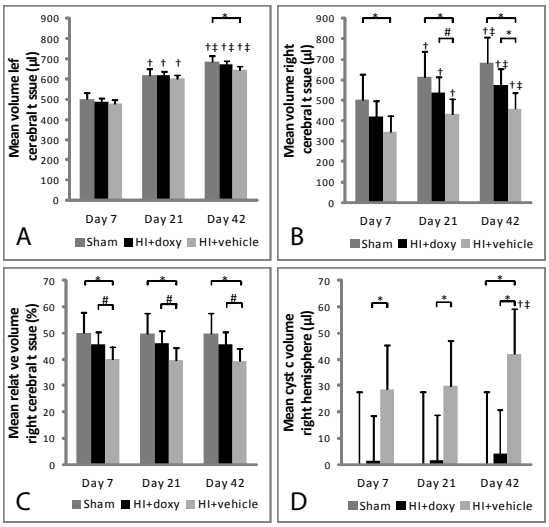

Figure 3 Development of cerebral tissue volumes and cysts on MRI.
Mean volumes of left (**A**) and right (**B**) cerebral tissue, relative volumes of right cerebral tissue (**C**) and cystic volumes (**D**) on days 7, 21 and 42 after HI in Sham, HI+doxy and HI+vehicle. *The bars show estimated marginal means for each group with error bars indicating 95% Confidence intervals. † $p < 0.05$ for day 21 or 42 vs. day 7; ‡ $p < 0.05$ for day 21 vs. 42; * $p < 0.05$ between groups; # $p < 0.05$ between HI+doxy and HI+vehicle in linear mixed model with recovery time included as covariate.*

and 42 (Table 1). The lesion volumes on ADC day one were also negatively correlated with FA values of white matter tracts on later time-points (Table 1).

Table 1 Correlations between lesion volume on ADC one day after HI and different outcome measures on day 7, 21 and 42: Total brain volume, volumes of left and right cerebral tissue, cystic volume, relative volume of right cerebral tissue, mean FA values in left and right white matter (WM) and in corpus callosum, volume of manganese-enhanced tissue on day 7, change in cyst volume from day 7 to 42 and injury score on histology day 42. Coefficients with R^2 from linear regression analyses are shown with statistical significance indicated by § p<0.005 and * p<0.001.

	Day 7			**Day 21**			**Day 42**		
Dependent variable	Constant	B	R^2	Constant	B	R^2	Constant	B	R^2
Total brain volume	986.332	-3.003	0.654*	1244.066	-0.402	0.708*	1342.614	-4.186	0.663*
Left cerebral tissue volume	493.292	-0.262	0.103	617.716	-0.217	0.037	669.469	-0.277	0.054
Right cerebral tissue volume	504.697	-3.587	0.855*	637.525	-4.661	0.889*	689.233	-5.145	0.870*
Cystic volume	-11.657	0.845	0.850*	-11.175	0.857	0.816*	-16.088	1.235	0.871*
Relative right cerebral volume	51.638	-0.265	0.950*	51.863	-0.274	0.958*	51.894	-0.286	0.951*
FA in left WM	0.440	0.000	0.014	0.554	0.000	0.184	0.578	-0.001	0.651§
FA in right WM	0.449	-0.001	0.596*	0.574	-0.002	0.751*	0.569	-0.002	0.711*
FA in CC	0.504	-0.001	0.175	0.607	-0.002	0.475§	0.649	-0.004	0.719*

Dependent variable	Constant	B	R^2
Volume of manganese-enhanced tissue day 7	-2.532	0.259	0.845*
Change in cyst volume from day 7 to 42	-4.695	0.408	0.910*
Injury score on histology day 42	-0.366	0.046	0.884*

Group differences in development of cerebral tissue and cyst volumes on MRI

Test for fixed effects within a linear mixed model showed larger cyst volumes among HI+vehicle than HI+doxy (p=0.013), with a tendency towards interaction between days after HI and experiment group (p=0.059) that was due to an increase in mean cyst volume from day 21 to 42 in the HI+vehicle group (Figure 3). There was an overall tendency towards HI+doxy having larger mean volume of right cerebral tissue (p=0.074) and larger relative volumes of right cerebral tissue (p=0.069) than HI+vehicle. After including recovery time in the mixed linear models these differences became significant (p=0.034 and p=0.044 respectively). The volume of the right cerebral tissue increased from day 7 to day 42 after HI. A significant interaction between days after HI and experiment group was seen (p=0.003), resulting in smaller mean volume of right cerebral tissue among HI+vehicle than HI+doxy on day 42 (Figure 3). While HI+vehicle had lower mean absolute and relative volume of the right cerebral tissue than sham on all time points, there were no differences between HI+doxy and sham at any time-point (Figure 3).

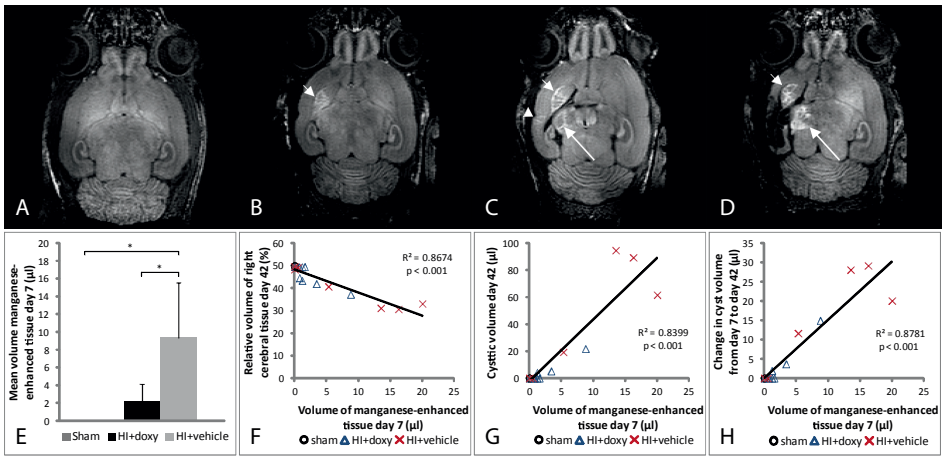

Figure 4 Manganese-enhancement on day seven after HI.
Images in upper row show the variation of manganese-enhancement on day seven after HI in pups with different severity of injury corresponding to that on histology day 42. ***A***: Sham with normal manganese-enhancement. ***B***: HI+doxy pup with mild injury showed increased manganese-enhancement primarily in putamen (short arrow). ***C***: HI+vehicle pup with moderate injury showed increased manganese-enhancement in putamen (short arrow), thalamus (long arrow) and cortex (arrow head). ***D***: HI+vehicle pup with severe injury showed more increased manganese-enhancement in putamen (short arrow), thalamus (long arrow) and cortex (not in image slice). Bar chart ***E*** shows the volume of tissue with increased manganese-enhancement in right hemisphere among Sham, HI+doxy, HI+vehicle on day seven. The volume was zero in all sham animals. *The bars show means for each group with error bars indicating 95% Confidence intervals. * p < 0.05 between groups.* Scatter plots F-H show the correlation between volume of manganese-enhanced tissue day seven and relative volume of right brain hemisphere day 42 (*F*), cystic volume on day 42 (*G*) and change in cyst volume from day 7 to 42 (*H*). *Lines represent the fitted linear regression lines. R^2 and p-value for each line are given.*

Manganese-enhancement on day seven after HI

Increased manganese-enhancement was seen on day seven after HI in the right cortex, putamen and thalamus in injured pups. HI+vehicle pups had more manganese-enhancement in the right cerebral tissue than HI+doxy pups and sham on day seven after HI (Figure 4). Larger volumes of manganese-enhanced tissue on day seven were correlated with smaller volumes of right cerebral brain tissue and larger cysts on days 21 and 42, and with a larger increase in cyst volume from day seven to day 42 (Figure 4).

Group differences in development of white matter on diffusion tensor imaging

Mean fractional anisotropy (FA) values of all groups increased from day seven to 21 in the left and right white matter areas (WM) and were higher on day 21 and 42 compared to day seven, but with no difference between days 21 and 42. Test for fixed effects within a linear mixed model showed an overall tendency towards HI+doxy having higher mean FA in the right WM than HI+vehicle (p=0.077) with a significant interaction between days after HI and group (p=0.030). There was no difference in FA on day seven, but increasing differences over time

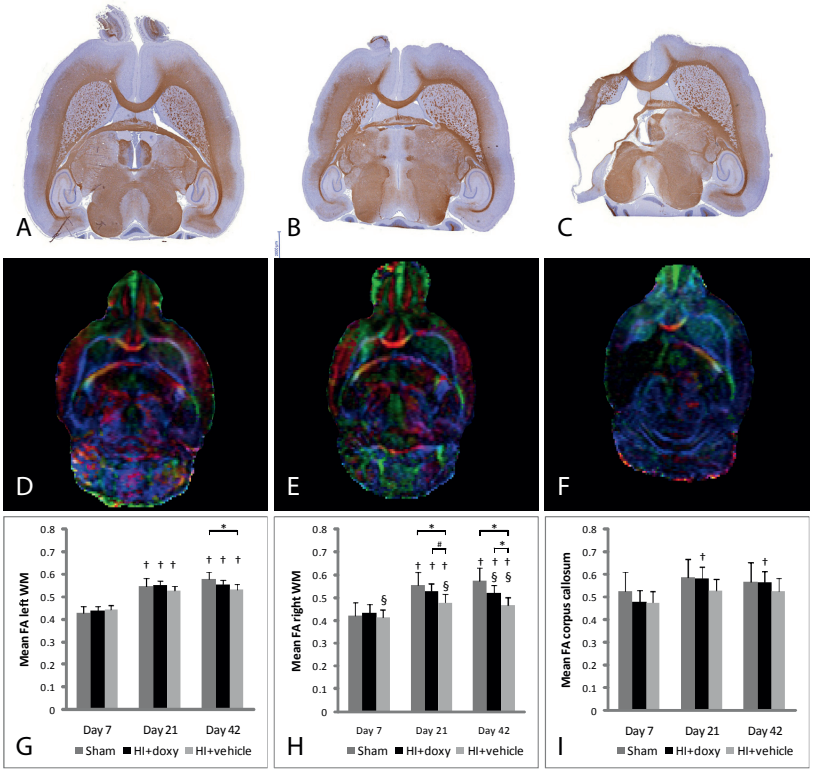

Figure 5 DTI and white matter immunohistochemistry.
Upper row*:** Images of histological slices stained for Myelin basic protein (MBP; brown) taken from the same pups as in middle row on day 42. ***Middle row: Images show directionally color-coded fractional anisotropy maps from day 42 after HI in pups with different severity of injury. **D**: Sham. **E**: HI+doxy pup with mild injury. **F**: HI+vehicle pup with severe injury. Notice the good correlation between MBP staining (A-C) and high fractional anisotropy (D-F) ***Lower row***: Bar charts show the mean fractional anisotropy (FA) in major white matter structures (WM) in the left (**G**) and right (**H**) hemispheres and corpus callosum (**I**) on days 7, 21 and 42 after HI in Sham, HI+doxy and HI+vehicle. *The bars show estimated marginal means for each group with error bars indicating 95% Confidence intervals. § $p < 0.05$ right vs. left hemisphere; † $p < 0.05$ day 7 vs. day 21 or 42; * $p < 0.05$ between groups; # $p < 0.05$ HI+doxy vs. HI+vehicle after controlling for recovery time.*

gave significantly higher FA values in right white matter areas among HI+doxy than HI+vehicle on day 42. The same tendency was also present on day 21 and became significant after including recovery time in the model (Figure 5). Mean radial diffusivity ($\lambda\perp$) decreased among all groups in left and right white matter areas with time after injury, but with less reduction among HI+vehicle giving higher $\lambda\perp$ among HI+vehicle than HI+doxy and sham on day 42. There was no difference between groups in FA and $\lambda\perp$ in left white matter and corpus callosum, and no significant differences in mean diffusivity or axial diffusivity were found between the two HI groups in any areas (Data can be seen in supplementary figure). Mean FA in the right white matter was lower than in the left among HI+vehicle pups on days seven, 21 and 42, and among

HI+doxy on day 42 (Figure 5). This was accompanied by higher $\lambda_{\perp}$ in the right WM than the left among HI+vehicle pups at all time points, but not among HI+doxy.

Immunohistochemistry on day 42

All four shams, four out of eight HI+doxy pups and three out of seven HI+vehicle pups had no detectable injury or cellular changes on histology or immunohistochemistry day 42. The same animals had normal relative volumes of right cerebral tissue at all time-points. Animals with detectable injury could be classified into mild, moderate and severe injury based on the histological score (Figure 6). Among animals with detectable injury, HI+doxy pups had less neuronal loss and tissue loss with lower histological scores than HI+vehicle pups ($p=0.021$), and HI+doxy pups had also less activated microglial cells (lower CD68 score, $p=0.042$). Lesion volume on ADC day one and the relative volume of right cerebral tissue on day seven correlated highly with the histological score (Table 1 and Figure 6). In animals with moderate and severe injury, the right WM hippocampal fimbria and external capsule was thinner and had less intense and more scattered MBP staining than in the left hemisphere (Figure 5).

Discussion

To our knowledge this is the first study using a longitudinal design to look at the effect of anti-inflammatory treatment on development of brain injury after neonatal hypoxia-ischemia, and also the first study that examines the long-term effects of doxycycline treatment in the neonatal rat. Our results indicate a moderate neuroprotective of doxycycline treatment, mainly seen at follow up as less cyst formation, sparing of cerebral tissue and less injury to major white matter tracts. Interestingly, the effects of treatment seemed to increase with time after the insult. Another major finding is the high degree of correlation between lesion size on early ADC-maps and other measures of injury at long-term follow-up. The finding that the recovery time between CCA operation and hypoxia plays a role in the ensuing size of the injury is also of importance and has to our knowledge not been reported before.

Strengths and weaknesses

The main weakness of the study is the large variation in lesion size among both treatment groups in combination with few animals. This has reduced the power of the study to show significant effects of treatment, and also limit the validity of the study. However, the longitudinal design with repeated high resolution MRI allowed us to follow both structural changes in cerebral tissue and changes in white matter microstructure over time after HI. This made it possible to account for individual variation when comparing treatment effects on injury development. It also allowed the investigation of an interaction between treatment and time after HI. The use of different methods and outcome measures that all point in the same direction also strengthens the study that together with the longitudinal design compensate for some of the limitations.

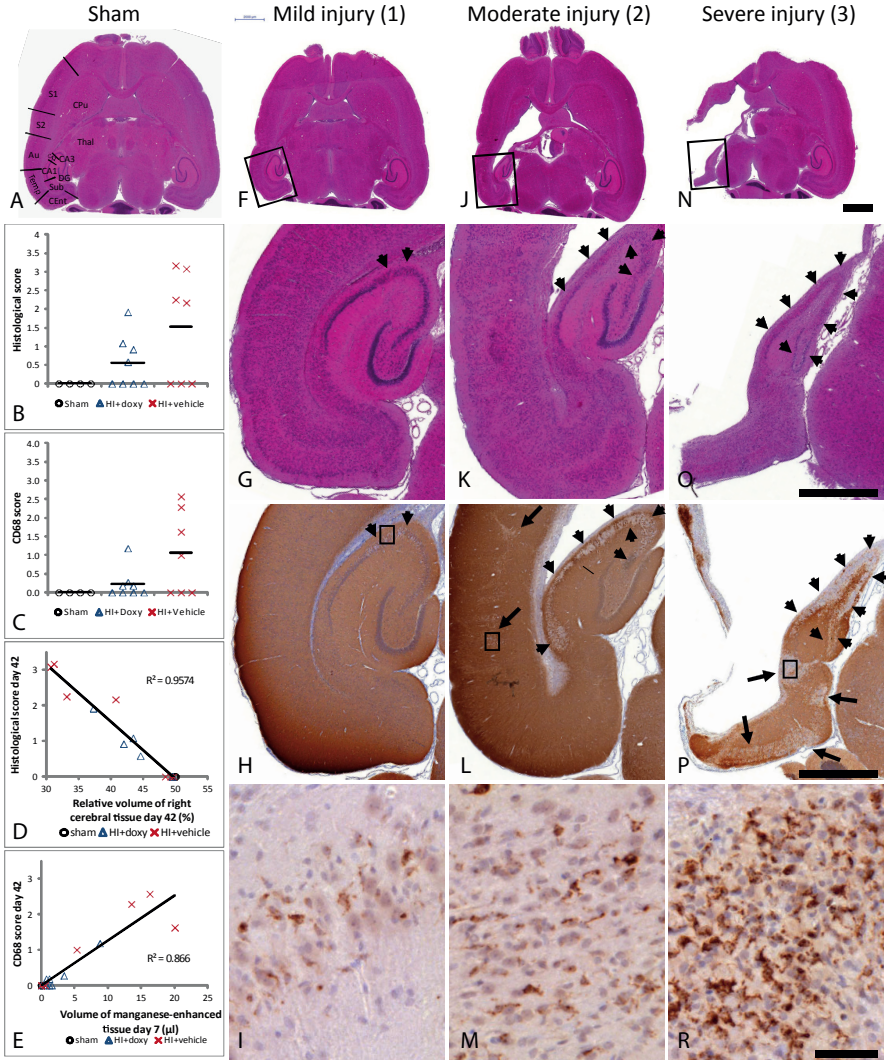

Figure 6 Histology and immunohistochemistry on day 42.
Extent of neuronal and tissue loss was scored from 0-4 in all areas shown in **A**. The average injury score for each pup is showed in graph **B.** Density of CD68 positive microglial cells was scored from 0-3 in the same areas and the average score for each pup is shown in graph **C** with symbols indicating group and bars indicating group means. Scatter plot **D** shows the correlation between relative volume of the right cerebral tissue on day seven and histological score on day 42. Scatter plot **E** shows the correlation between volume of manganese-enhanced tissue on day seven and CD-68 score on day 42. Lines represent the fitted linear regression lines. R^2 for each line is given. Examples of pups with histological scores of approximately 1 (mild injury), 2 (moderate injury) and 3 (severe injury) are shown in **F, J and N** (Scale bar = 2 mm). Tissue loss and cyst formation increased with severity of injury. The size of putamen and thalamus were slightly reduced in mild injury, moderately to severely reduced with dilatation of the lateral ventricle in moderate injury, and was almost non-existing with large cyst formation in severely injured pups. Higher magnification of the hippocampal structure and parts of cortex on HE stain (**G, K and O**) and on MAP-2 stain (**H, L and P**) show selective neuronal loss in the hippocampal structure (arrow heads), patchy neuronal loss (arrows) mainly in layer III of cortex (**L**), and thinning of cortex and tissue loss in the severely injured (**O-P**) (Scale bar = 1 mm). **I, M and R** show high magnification examples of CD68 staining (brown) from areas marked with square in H, L and M respectively (Scale bar = 50 µm).

Lesions on early ADC-maps

The reduction in ADC seen in ipsilateral cortex, hippocampus, thalamus and putamen after HI is in accordance with previous studies, and can be explained by cytotoxic oedema, reducing the extracellular space and inhibiting the free water diffusion (Gass *et al.*, 2001). Reduced ADC in these areas has also been correlated with high numbers of apoptotic cells (Lodygensky *et al.*, 2011). However, we also found increased ADC in the white matter of the external capsule, close to the hippocampus. A similar finding has been found to concur with pronounced oligodendroglial reactions and microglial activation without apparent cell death (Lodygensky *et al.*, 2011), and with modest apoptotic activity (Wendland *et al.*, 2008). One possible explanation to the increased ADC is vasogenic oedema related to these cellular reactions in the white matter (Olah *et al.*, 2001; Lodygensky *et al.*, 2011).

The estimated lesion volume on ADC day one was highly correlated with later measures of lesion size, which made it a good predictor of the final injury. A similar correlation was found by Wang *et al* (2006). They estimated the lesion volumes on ADC-maps 1-2 hours post-HI by using a threshold set to ≤80% of the ADC in the contralateral hemisphere. The estimated lesion volume on ADC-map was found to correlate with, but underestimate the final lesion volume on day 10 after HI. One problem with using such a threshold is that high pathological ADC values are not included. In our study we developed a method for estimating the lesion size that also took into account the tissue with pathological high ADC. This can explain the higher correlation and better estimation with our method than that used by Wang *et al* (2006), but the difference may also be related to the different time-points for ADC imaging.

Recovery time influences lesion size

Using 75 minutes of hypoxia, we have previously experienced consistently large injuries in this animal model (Wideroe *et al.*, 2009; Wideroe *et al.*, 2011). In this study, 60 minutes of hypoxia was chosen to achieve more moderate injuries. However, this also resulted in large variation in lesion size among both HI groups.

Much of this variation could be explained by the time interval between CCA operation and hypoxia, with shorter recovery time giving larger lesions. The time interval is important for recovery following anaesthesia and operation, allowing the pup to feed properly before hypoxia. Short recovery time may give less feeding with subsequent risk of depletion of glucose reservoirs during hypoxia, which is known to increase hypoxic-ischemic injury (Vannucci & Hagberg, 2004; Vannucci & Vannucci, 2005). In our study the recovery time was within the recommended time interval of 2-4 hours (Vannucci & Vannucci, 2005), however did still influence the severity of the injury. Studies of optimal recovery time in order to produce consistent injuries in newborn rats should be undertaken, and recovery time should be considered a possible confounder in future studies using this animal model.

Effect of doxycycline treatment increases with time after HI

Lower mean lesion volume on ADC on day one among HI+doxy versus HI+vehicle pups indicates early treatment effects. This is in accordance with effects of doxycycline and minocycline on neurotransmitters, pro-inflammatory cytokines and mRNA expression during the first 24 hours after HI that has previously been described (Fox *et al.*, 2005; Jantzie *et al.*, 2006; Kremlev *et al.*, 2007; Jantzie & Todd, 2010). However, our results show an increasing difference in injury between HI+doxy and HI+vehicle pups with increasing time from HI. This may indicate that a single injection of doxycycline has a long lasting effect that becomes more pronounced with time. Due to the slow elimination of doxycycline, circulating therapeutic levels can be expected for days after a single dose, with possible persistent inhibitory effects on microglia and macrophages. This is supported by previous reports that a single dose of doxycycline reduces apoptosis, promotes neuronal survival and reduces microglial activation also during the first week after HI (Jantzie *et al.*, 2005).

Reduced manganese-enhancement may reflect less inflammation in doxycycline treated pups

We have previously shown that manganese-enhancement in cerebral areas on day seven after HI reflects microglial activation and reactive astrocytosis (Wideroe *et al.*, 2009). Lower volumes of manganese-enhanced tissue among doxycycline treated pups may therefore reflect less inflammation due to doxycycline treatment, which has also been observed by others using histological methods (Jantzie *et al.*, 2005; Jantzie & Todd, 2010). Reduced microglial activity may also contribute to reduced cyst-formation, which was the main effect of doxycycline seen in our study. This is supported by the correlation between volumes of manganese-enhanced tissue on day seven and cystic volume on day 42 and change in cystic volume from day seven to day 42 that probably reflects the propensity of manganese-enhanced tissue to undergo liquefaction (Wideroe *et al.*, 2011).

The long-term effect of doxycycline seen in our study with sparing of grey matter, reduced cyst volumes and less activated microglial cells on day 42 after HI may indicate that the reduced microglial activity is permanent in the treated animals. The interaction between treatment group and time after HI further supports a long lasting effect of doxycycline. Higher doses or repeated injections could further potentiate the observed neuroprotective effects.

Effects on white matter development and maturation

The increase in FA values from day seven to days 21 and 42 was due to a significant reduction in radial diffusivity ($\lambda\perp$), with unchanged axial diffusivity. This was most prominent in white matter in the left hemisphere and corpus callosum. These changes can be related to maturation of white matter and increased myelination, as reported by others (Bockhorst *et al.*, 2008). Evidence of injury to the white matter areas in the right hemisphere was seen primarily among HI+vehicle pups as less increase in FA and less reduction of $\lambda\perp$ with days after HI than among sham and HI+doxy pups. This can be interpreted as delayed or arrested myelination of

the WM tracts (Song *et al.*, 2002; Song *et al.*, 2005), and is supported by the histology that showed thinning and reduced myelin basic protein staining in the right white matter tracts among animals with moderate and severe injury. These changes on DTI indicate a possible protective effect of doxycycline also on white matter injury, either directly or indirectly through reduced grey matter injury. These results are supported by other studies where minocycline has been shown to attenuate white matter injury in P3 and P4 rats, by reducing oligodendrocyte progenitor cell loss during the first week of life (Cai *et al.*, 2006; Carty *et al.*, 2008) and improving myelination after three weeks (Fan *et al.*, 2006).

Conclusions

A single dose of doxycycline given after a hypoxic-ischemic insult to the neonatal brain reduced cyst formation and attenuated injury to cerebral grey and white matter tissue. The treatment effects became more pronounced with time, suggesting that doxycycline also protects the growth of cerebral tissue and maturation of white matter tracts. Early MRI, including ADC-maps taken one day after HI, volumetric MRI and manganese-enhancement on day seven after hypoxia-ischemia were highly predictive for injury size and white matter diffusion changes at long-term follow up. This indicates that short-term treatment effects found in previous studies can be extrapolated to long-term outcomes. Combined, these results clearly suggest a potential for doxycycline treatment of hypoxic-ischemic brain injury in the neonate.

Acknowledgements

The authors would like to thank FUGE Molecular Imaging Center (Trondheim, Norway), statistician Øyvind Salvesen, Professor Sverre Torp, lab technicians Borgny Ytterhus, Toril Rolfsen and Paulo Girão (all at the Medical Faculty, NTNU). This study was financially supported by a grant from the Medical Faculty at the Norwegian University of Science and Technology.

References

Arvin, K.L., Han, B.H., Du, Y., Lin, S.Z., Paul, S.M. & Holtzman, D.M. (2002) Minocycline markedly protects the neonatal brain against hypoxic-ischemic injury. Ann Neurol, **52**, 54-61.

Behrens, T.E., Woolrich, M.W., Jenkinson, M., Johansen-Berg, H., Nunes, R.G., Clare, S., Matthews, P.M., Brady, J.M. & Smith, S.M. (2003) Characterization and propagation of uncertainty in diffusion-weighted MR imaging. Magn Reson Med, **50**, 1077-1088.

Bockhorst, K.H., Narayana, P.A., Liu, R., Ahobila-Vijjula, P., Ramu, J., Kamel, M., Wosik, J., Bockhorst, T., Hahn, K., Hasan, K.M. & Perez-Polo, J.R. (2008) Early postnatal development of rat brain: in vivo diffusion tensor imaging. J Neurosci Res, **86**, 1520-1528.

Buller, K.M., Carty, M.L., Reinebrant, H.E. & Wixey, J.A. (2009) Minocycline: a neuroprotective agent for hypoxic-ischemic brain injury in the neonate? J Neurosci Res, **87**, 599-608.

Cai, Z., Lin, S., Fan, L.W., Pang, Y. & Rhodes, P.G. (2006) Minocycline alleviates hypoxic-ischemic injury to developing oligodendrocytes in the neonatal rat brain. Neuroscience, **137**, 425-435.

Carty, M.L., Wixey, J.A., Colditz, P.B. & Buller, K.M. (2008) Post-insult minocycline treatment attenuates hypoxia-ischemia-induced neuroinflammation and white matter injury in the neonatal rat: a comparison of two different dose regimens. Int J Dev Neurosci, **26**, 477-485.

Clark, W.M., Calcagno, F.A., Gabler, W.L., Smith, J.R. & Coull, B.M. (1994) Reduction of central nervous system reperfusion injury in rabbits using doxycycline treatment. Stroke, **25**, 1411-1415; discussion 1416.

Fan, L.W., Lin, S., Pang, Y., Rhodes, P.G. & Cai, Z. (2006) Minocycline attenuates hypoxia-ischemia-induced neurological dysfunction and brain injury in the juvenile rat. Eur J Neurosci, **24**, 341-350.

Ferriero, D.M. (2004) Neonatal brain injury. N Engl J Med, **351**, 1985-1995.

Fox, C., Dingman, A., Derugin, N., Wendland, M.F., Manabat, C., Ji, S., Ferriero, D.M. & Vexler, Z.S. (2005) Minocycline confers early but transient protection in the immature brain following focal cerebral ischemia-reperfusion. J Cereb Blood Flow Metab, **25**, 1138-1149.

Gass, A., Niendorf, T. & Hirsch, J.G. (2001) Acute and chronic changes of the apparent diffusion coefficient in neurological disorders--biophysical mechanisms and possible underlying histopathology. J Neurol Sci, **186 Suppl 1**, S15-23.

Geddes, R., Vannucci, R.C. & Vannucci, S.J. (2001) Delayed cerebral atrophy following moderate hypoxia-ischemia in the immature rat. Dev Neurosci, **23**, 180-185.

Gonzalez, F.F. & Ferriero, D.M. (2009) Neuroprotection in the newborn infant. Clin Perinatol, **36**, 859-880, vii.

Jantzie, L.L., Cheung, P.Y. & Todd, K.G. (2005) Doxycycline reduces cleaved caspase-3 and microglial activation in an animal model of neonatal hypoxia-ischemia. J Cereb Blood Flow Metab, **25**, 314-324.

Jantzie, L.L., Rauw, G.A. & Todd, K.G. (2006) The effects of doxycycline administration on amino acid neurotransmitters in an animal model of neonatal hypoxia-ischemia. Neurochem Int, **49**, 717-728.

Jantzie, L.L. & Todd, K.G. (2010) Doxycycline inhibits proinflammatory cytokines but not acute cerebral cytogenesis after hypoxia-ischemia in neonatal rats. J Psychiatry Neurosci, **35**, 20-32.

Khwaja, O. & Volpe, J.J. (2008) Pathogenesis of cerebral white matter injury of prematurity. Arch Dis Child Fetal Neonatal Ed, **93**, F153-161.

Kremlev, S.G., Roberts, R.L. & Palmer, C. (2007) Minocycline modulates chemokine receptors but not interleukin-10 mRNA expression in hypoxic-ischemic neonatal rat brain. J Neurosci Res, **85**, 2450-2459.

Lodygensky, G.A., West, T., Moravec, M.D., Back, S.A., Dikranian, K., Holtzman, D.M. & Neil, J.J. (2011) Diffusion characteristics associated with neuronal injury and glial activation following hypoxia-ischemia in the immature brain. Magn Reson Med, **66**, 839-845.

Mcrae, A., Gilland, E., Bona, E. & Hagberg, H. (1995) Microglia Activation after Neonatal Hypoxic-Ischemia. Dev Brain Res, **84**, 245-252.

Mori, S. & Zhang, J. (2006) Principles of diffusion tensor imaging and its applications to basic neuroscience research. Neuron, **51**, 527-539.

Olah, L., Wecker, S. & Hoehn, M. (2001) Relation of apparent diffusion coefficient changes and metabolic disturbances after 1 hour of focal cerebral ischemia and at different reperfusion phases in rats. J Cereb Blood Flow Metab, **21**, 430-439.

Paxinos, G. & Watson, C. (1998) The rat brain in stereotaxic coordinates. Academic Press, San Diego.

Rice, J.E., 3rd, Vannucci, R.C. & Brierley, J.B. (1981) The influence of immaturity on hypoxic-ischemic brain damage in the rat. Ann Neurol, **9**, 131-141.

Smith, S.M., Jenkinson, M., Woolrich, M.W., Beckmann, C.F., Behrens, T.E., Johansen-Berg, H., Bannister, P.R., De Luca, M., Drobnjak, I., Flitney, D.E., Niazy, R.K., Saunders, J., Vickers, J., Zhang, Y., De Stefano, N., Brady, J.M. & Matthews, P.M. (2004) Advances in functional and structural MR image analysis and implementation as FSL. Neuroimage, **23 Suppl 1**, S208-219.

Song, S.K., Sun, S.W., Ramsbottom, M.J., Chang, C., Russell, J. & Cross, A.H. (2002) Dysmyelination revealed through MRI as increased radial (but unchanged axial) diffusion of water. Neuroimage, **17**, 1429-1436.

Song, S.K., Yoshino, J., Le, T.Q., Lin, S.J., Sun, S.W., Cross, A.H. & Armstrong, R.C. (2005) Demyelination increases radial diffusivity in corpus callosum of mouse brain. Neuroimage, **26**, 132-140.

Vannucci, R.C. & Vannucci, S.J. (2005) Perinatal hypoxic-ischemic brain damage: evolution of an animal model. Dev Neurosci, **27**, 81-86.

Vannucci, S.J. & Hagberg, H. (2004) Hypoxia-ischemia in the immature brain. J Exp Biol, **207**, 3149-3154.

Volpe, J.J. (2009) Brain injury in premature infants: a complex amalgam of destructive and developmental disturbances. Lancet Neurol, **8**, 110-124.

Wang, Y., Cheung, P.T., Shen, G.X., Wu, E.X., Cao, G., Bart, I., Wong, W.H. & Khong, P.L. (2006) Hypoxic-ischemic brain injury in the neonatal rat model: relationship between lesion size at early MR imaging and irreversible infarction. AJNR Am J Neuroradiol, **27**, 51-54.

Wendland, M.F., Faustino, J., West, T., Manabat, C., Holtzman, D.M. & Vexler, Z.S. (2008) Early diffusion-weighted MRI as a predictor of caspase-3 activation after hypoxic-ischemic insult in neonatal rodents. Stroke, **39**, 1862-1868.

Wideroe, M., Brekken, C., Kavelaars, A., Pedersen, T.B., Goa, P.E., Heijnen, C., Skranes, J. & Brubakk, A.M. (2011) Longitudinal Manganese-Enhanced Magnetic Resonance Imaging of Delayed Brain Damage after Hypoxic-Ischemic Injury in the Neonatal Rat. Neonatology, **100**, 363-372.

Wideroe, M., Olsen, O., Pedersen, T.B., Goa, P.E., Kavelaars, A., Heijnen, C., Skranes, J., Brubakk, A.M. & Brekken, C. (2009) Manganese-enhanced magnetic resonance imaging of hypoxic-ischemic brain injury in the neonatal rat. Neuroimage, **45**, 880-890.

Wixey, J.A., Reinebrant, H.E., Spencer, S.J. & Buller, K.M. (2011) Efficacy of post-insult minocycline administration to alter long-term hypoxia-ischemia-induced damage to the serotonergic system in the immature rat brain. Neuroscience, **182**, 184-192.

Woolrich, M.W., Jbabdi, S., Patenaude, B., Chappell, M., Makni, S., Behrens, T., Beckmann, C., Jenkinson, M. & Smith, S.M. (2009) Bayesian analysis of neuroimaging data in FSL. Neuroimage, **45**, S173-186.

Zhang, Y., Brady, M. & Smith, S. (2001) Segmentation of brain MR images through a hidden Markov random field model and the expectation-maximization algorithm. IEEE Trans Med Imaging, **20**, 45-57.

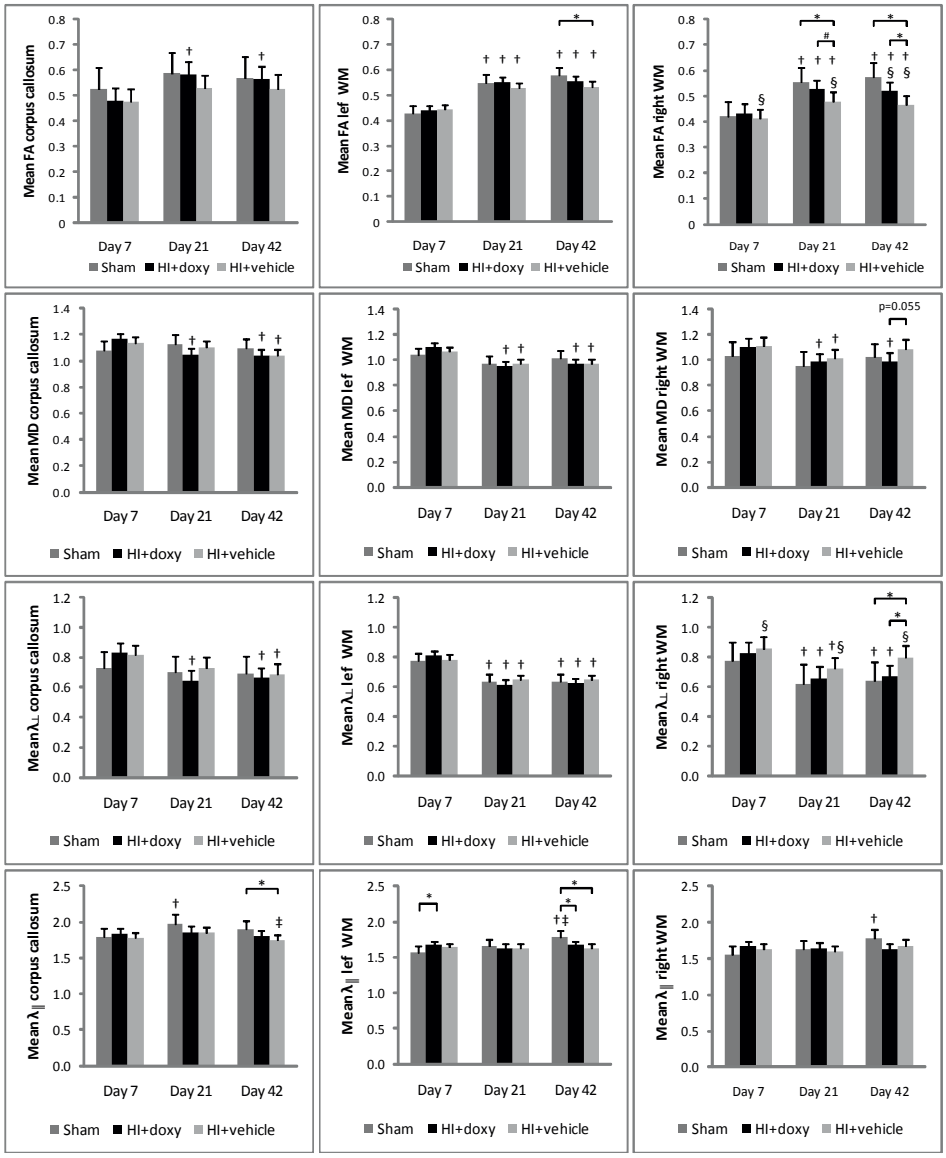

Supplementary figure - DTI data.

Fractional anisotropy (FA), mean diffusivity (MD), radial diffusivity ($\lambda_\perp$) and axial diffusivity ($\lambda_\parallel$) on days 7, 21 and 42 after hypoxia ischemia in corpus callosum (CC), major white matter structures (WM) in the left and right hemispheres of sham operated pups and pups treated with doxycycline (HI+doxy) and with saline (HI+vehicle). MD, $\lambda_\perp$ and $\lambda_\parallel$ are shown in units of 10^{-3} mm^2/s. *The bars show estimated marginal means for each group with error bars indicating 95% Confidence intervals. P values for difference between HI+doxy and HI+vehicle are displayed above the bars. § p < 0.05 right vs. left hemisphere; † p < 0.05 HI+vehicle vs. Sham; * p < 0.05 day 21 or 42 vs. day 7.*

Paper IV

Is not included due to copyright

Dissertations at the Faculty of Medicine, NTNU

1977

1. Knut Joachim Berg: EFFECT OF ACETYLSALICYLIC ACID ON RENAL FUNCTION
2. Karl Erik Viken and Arne Ødegaard: STUDIES ON HUMAN MONOCYTES CULTURED *IN VITRO*

1978

3. Karel Bjørn Cyvin: CONGENITAL DISLOCATION OF THE HIP JOINT.
4. Alf O. Brubakk: METHODS FOR STUDYING FLOW DYNAMICS IN THE LEFT VENTRICLE AND THE AORTA IN MAN.

1979

5. Geirmund Unsgaard: CYTOSTATIC AND IMMUNOREGULATORY ABILITIES OF HUMAN BLOOD MONOCYTES CULTURED IN VITRO

1980

6. Størker Jørstad: URAEMIC TOXINS
7. Arne Olav Jenssen: SOME RHEOLOGICAL, CHEMICAL AND STRUCTURAL PROPERTIES OF MUCOID SPUTUM FROM PATIENTS WITH CHRONIC OBSTRUCTIVE BRONCHITIS

1981

8. Jens Hammerstrøm: CYTOSTATIC AND CYTOLYTIC ACTIVITY OF HUMAN MONOCYTES AND EFFUSION MACROPHAGES AGAINST TUMOR CELLS *IN VITRO*

1983

9. Tore Syversen: EFFECTS OF METHYLMERCURY ON RAT BRAIN PROTEIN.
10. Torbjørn Iversen: SQUAMOUS CELL CARCINOMA OF THE VULVA.

1984

11. Tor-Erik Widerøe: ASPECTS OF CONTINUOUS AMBULATORY PERITONEAL DIALYSIS.
12. Anton Hole: ALTERATIONS OF MONOCYTE AND LYMPHOCYTE FUNCTIONS IN REALTION TO SURGERY UNDER EPIDURAL OR GENERAL ANAESTHESIA.
13. Terje Terjesen: FRACTURE HEALING AND STRESS-PROTECTION AFTER METAL PLATE FIXATION AND EXTERNAL FIXATION.
14. Carsten Saunte: CLUSTER HEADACHE SYNDROME.
15. Inggard Lereim: TRAFFIC ACCIDENTS AND THEIR CONSEQUENCES.
16. Bjørn Magne Eggen: STUDIES IN CYTOTOXICITY IN HUMAN ADHERENT MONONUCLEAR BLOOD CELLS.
17. Trond Haug: FACTORS REGULATING BEHAVIORAL EFFECTS OG DRUGS.

1985

18. Sven Erik Gisvold: RESUSCITATION AFTER COMPLETE GLOBAL BRAIN ISCHEMIA.
19. Terje Espevik: THE CYTOSKELETON OF HUMAN MONOCYTES.
20. Lars Bevanger: STUDIES OF THE Ibc (c) PROTEIN ANTIGENS OF GROUP B STREPTOCOCCI.
21. Ole-Jan Iversen: RETROVIRUS-LIKE PARTICLES IN THE PATHOGENESIS OF PSORIASIS.
22. Lasse Eriksen: EVALUATION AND TREATMENT OF ALCOHOL DEPENDENT BEHAVIOUR.
23. Per I. Lundmo: ANDROGEN METABOLISM IN THE PROSTATE.

1986

24. Dagfinn Berntzen: ANALYSIS AND MANAGEMENT OF EXPERIMENTAL AND CLINICAL PAIN.
25. Odd Arnold Kildahl-Andersen: PRODUCTION AND CHARACTERIZATION OF MONOCYTE-DERIVED CYTOTOXIN AND ITS ROLE IN MONOCYTE-MEDIATED CYTOTOXICITY.
26. Ola Dale: VOLATILE ANAESTHETICS.

1987

27. Per Martin Kleveland: STUDIES ON GASTRIN.
28. Audun N. Øksendal: THE CALCIUM PARADOX AND THE HEART.
29. Vilhjalmur R. Finsen: HIP FRACTURES

1988

30. Rigmor Austgulen: TUMOR NECROSIS FACTOR: A MONOCYTE-DERIVED REGULATOR OF CELLULAR GROWTH.
31. Tom-Harald Edna: HEAD INJURIES ADMITTED TO HOSPITAL.
32. Joseph D. Borsi: NEW ASPECTS OF THE CLINICAL PHARMACOKINETICS OF METHOTREXATE.
33. Olav F. M. Sellevold: GLUCOCORTICOIDS IN MYOCARDIAL PROTECTION.
34. Terje Skjærpe: NONINVASIVE QUANTITATION OF GLOBAL PARAMETERS ON LEFT VENTRICULAR FUNCTION: THE SYSTOLIC PULMONARY ARTERY PRESSURE AND CARDIAC OUTPUT.
35. Eyvind Rødahl: STUDIES OF IMMUNE COMPLEXES AND RETROVIRUS-LIKE ANTIGENS IN PATIENTS WITH ANKYLOSING SPONDYLITIS.
36. Ketil Thorstensen: STUDIES ON THE MECHANISMS OF CELLULAR UPTAKE OF IRON FROM TRANSFERRIN.
37. Anna Midelfart: STUDIES OF THE MECHANISMS OF ION AND FLUID TRANSPORT IN THE BOVINE CORNEA.
38. Eirik Helseth: GROWTH AND PLASMINOGEN ACTIVATOR ACTIVITY OF HUMAN GLIOMAS AND BRAIN METASTASES - WITH SPECIAL REFERENCE TO TRANSFORMING GROWTH FACTOR BETA AND THE EPIDERMAL GROWTH FACTOR RECEPTOR.
39. Petter C. Borchgrevink: MAGNESIUM AND THE ISCHEMIC HEART.
40. Kjell-Arne Rein: THE EFFECT OF EXTRACORPOREAL CIRCULATION ON SUBCUTANEOUS TRANSCAPILLARY FLUID BALANCE.
41. Arne Kristian Sandvik: RAT GASTRIC HISTAMINE.
42. Carl Bredo Dahl: ANIMAL MODELS IN PSYCHIATRY.

1989

43. Torbjørn A. Fredriksen: CERVICOGENIC HEADACHE.
44. Rolf A. Walstad: CEFTAZIDIME.
45. Rolf Salvesen: THE PUPIL IN CLUSTER HEADACHE.
46. Nils Petter Jørgensen: DRUG EXPOSURE IN EARLY PREGNANCY.
47. Johan C. Ræder: PREMEDICATION AND GENERAL ANAESTHESIA IN OUTPATIENT GYNECOLOGICAL SURGERY.
48. M. R. Shalaby: IMMUNOREGULATORY PROPERTIES OF TNF-α AND THE RELATED CYTOKINES.
49. Anders Waage: THE COMPLEX PATTERN OF CYTOKINES IN SEPTIC SHOCK.
50. Bjarne Christian Eriksen: ELECTROSTIMULATION OF THE PELVIC FLOOR IN FEMALE URINARY INCONTINENCE.
51. Tore B. Halvorsen: PROGNOSTIC FACTORS IN COLORECTAL CANCER.

1990

52. Asbjørn Nordby: CELLULAR TOXICITY OF ROENTGEN CONTRAST MEDIA.
53. Kåre E. Tvedt: X-RAY MICROANALYSIS OF BIOLOGICAL MATERIAL.
54. Tore C. Stiles: COGNITIVE VULNERABILITY FACTORS IN THE DEVELOPMENT AND MAINTENANCE OF DEPRESSION.
55. Eva Hofsli: TUMOR NECROSIS FACTOR AND MULTIDRUG RESISTANCE.
56. Helge S. Haarstad: TROPHIC EFFECTS OF CHOLECYSTOKININ AND SECRETIN ON THE RAT PANCREAS.
57. Lars Engebretsen: TREATMENT OF ACUTE ANTERIOR CRUCIATE LIGAMENT INJURIES.
58. Tarjei Rygnestad: DELIBERATE SELF-POISONING IN TRONDHEIM.
59. Arne Z. Henriksen: STUDIES ON CONSERVED ANTIGENIC DOMAINS ON MAJOR OUTER MEMBRANE PROTEINS FROM ENTEROBACTERIA.
60. Steinar Westin: UNEMPLOYMENT AND HEALTH: Medical and social consequences of a factory closure in a ten-year controlled follow-up study.
61. Ylva Sahlin: INJURY REGISTRATION, a tool for accident preventive work.
62. Helge Bjørnstad Pettersen: BIOSYNTHESIS OF COMPLEMENT BY HUMAN ALVEOLAR MACROPHAGES WITH SPECIAL REFERENCE TO SARCOIDOSIS.
63. Berit Schei: TRAPPED IN PAINFUL LOVE.
64. Lars J. Vatten: PROSPECTIVE STUDIES OF THE RISK OF BREAST CANCER IN A COHORT OF NORWEGIAN WOMAN.

1991

65. Kåre Bergh: APPLICATIONS OF ANTI-C5a SPECIFIC MONOCLONAL ANTIBODIES FOR THE ASSESSMENT OF COMPLEMENT ACTIVATION.
66. Svein Svenningsen: THE CLINICAL SIGNIFICANCE OF INCREASED FEMORAL ANTEVERSION.
67. Olbjørn Klepp: NONSEMINOMATOUS GERM CELL TESTIS CANCER: THERAPEUTIC OUTCOME AND PROGNOSTIC FACTORS.
68. Trond Sand: THE EFFECTS OF CLICK POLARITY ON BRAINSTEM AUDITORY EVOKED POTENTIALS AMPLITUDE, DISPERSION, AND LATENCY VARIABLES.
69. Kjetil B. Åsbakk: STUDIES OF A PROTEIN FROM PSORIATIC SCALE, PSO P27, WITH RESPECT TO ITS POTENTIAL ROLE IN IMMUNE REACTIONS IN PSORIASIS.
70. Arnulf Hestnes: STUDIES ON DOWN´S SYNDROME.
71. Randi Nygaard: LONG-TERM SURVIVAL IN CHILDHOOD LEUKEMIA.
72. Bjørn Hagen: THIO-TEPA.
73. Svein Anda: EVALUATION OF THE HIP JOINT BY COMPUTED TOMOGRAMPHY AND ULTRASONOGRAPHY.

1992

74. Martin Svartberg: AN INVESTIGATION OF PROCESS AND OUTCOME OF SHORT-TERM PSYCHODYNAMIC PSYCHOTHERAPY.
75. Stig Arild Slørdahl: AORTIC REGURGITATION.
76. Harold C Sexton: STUDIES RELATING TO THE TREATMENT OF SYMPTOMATIC NON-PSYCHOTIC PATIENTS.
77. Maurice B. Vincent: VASOACTIVE PEPTIDES IN THE OCULAR/FOREHEAD AREA.
78. Terje Johannessen: CONTROLLED TRIALS IN SINGLE SUBJECTS.
79. Turid Nilsen: PYROPHOSPHATE IN HEPATOCYTE IRON METABOLISM.
80. Olav Haraldseth: NMR SPECTROSCOPY OF CEREBRAL ISCHEMIA AND REPERFUSION IN RAT.
81. Eiliv Brenna: REGULATION OF FUNCTION AND GROWTH OF THE OXYNTIC MUCOSA.

1993

82. Gunnar Bovim: CERVICOGENIC HEADACHE.
83. Jarl Arne Kahn: ASSISTED PROCREATION.
84. Bjørn Naume: IMMUNOREGULATORY EFFECTS OF CYTOKINES ON NK CELLS.
85. Rune Wiseth: AORTIC VALVE REPLACEMENT.
86. Jie Ming Shen: BLOOD FLOW VELOCITY AND RESPIRATORY STUDIES.
87. Piotr Kruszewski: SUNCT SYNDROME WITH SPECIAL REFERENCE TO THE AUTONOMIC NERVOUS SYSTEM.
88. Mette Haase Moen: ENDOMETRIOSIS.
89. Anne Vik: VASCULAR GAS EMBOLISM DURING AIR INFUSION AND AFTER DECOMPRESSION IN PIGS.
90. Lars Jacob Stovner: THE CHIARI TYPE I MALFORMATION.
91. Kjell Å. Salvesen: ROUTINE ULTRASONOGRAPHY IN UTERO AND DEVELOPMENT IN CHILDHOOD.

1994

92. Nina-Beate Liabakk: DEVELOPMENT OF IMMUNOASSAYS FOR TNF AND ITS SOLUBLE RECEPTORS.
93. Sverre Helge Torp: *erb*B ONCOGENES IN HUMAN GLIOMAS AND MENINGIOMAS.
94. Olav M. Linaker: MENTAL RETARDATION AND PSYCHIATRY. Past and present.
95. Per Oscar Feet: INCREASED ANTIDEPRESSANT AND ANTIPANIC EFFECT IN COMBINED TREATMENT WITH DIXYRAZINE AND TRICYCLIC ANTIDEPRESSANTS.
96. Stein Olav Samstad: CROSS SECTIONAL FLOW VELOCITY PROFILES FROM TWO-DIMENSIONAL DOPPLER ULTRASOUND: Studies on early mitral blood flow.
97. Bjørn Backe: STUDIES IN ANTENATAL CARE.
98. Gerd Inger Ringdal: QUALITY OF LIFE IN CANCER PATIENTS.
99. Torvid Kiserud: THE DUCTUS VENOSUS IN THE HUMAN FETUS.
100. Hans E. Fjøsne: HORMONAL REGULATION OF PROSTATIC METABOLISM.
101. Eylert Brodtkorb: CLINICAL ASPECTS OF EPILEPSY IN THE MENTALLY RETARDED.
102. Roar Juul: PEPTIDERGIC MECHANISMS IN HUMAN SUBARACHNOID HEMORRHAGE.
103. Unni Syversen: CHROMOGRANIN A. Phsysiological and Clinical Role.

1995

104. Odd Gunnar Brakstad: THERMOSTABLE NUCLEASE AND THE *nuc* GENE IN THE DIAGNOSIS OF *Staphylococcus aureus* INFECTIONS.
105. Terje Engan: NUCLEAR MAGNETIC RESONANCE (NMR) SPECTROSCOPY OF PLASMA IN MALIGNANT DISEASE.
106. Kirsten Rasmussen: VIOLENCE IN THE MENTALLY DISORDERED.
107. Finn Egil Skjeldestad: INDUCED ABORTION: Timetrends and Determinants.
108. Roar Stenseth: THORACIC EPIDURAL ANALGESIA IN AORTOCORONARY BYPASS SURGERY.
109. Arild Faxvaag: STUDIES OF IMMUNE CELL FUNCTION *in mice infected with* MURINE RETROVIRUS.

1996

110. Svend Aakhus: NONINVASIVE COMPUTERIZED ASSESSMENT OF LEFT VENTRICULAR FUNCTION AND SYSTEMIC ARTERIAL PROPERTIES. Methodology and some clinical applications.
111. Klaus-Dieter Bolz: INTRAVASCULAR ULTRASONOGRAPHY.
112. Petter Aadahl: CARDIOVASCULAR EFFECTS OF THORACIC AORTIC CROSS-CLAMPING.
113. Sigurd Steinshamn: CYTOKINE MEDIATORS DURING GRANULOCYTOPENIC INFECTIONS.
114. Hans Stifoss-Hanssen: SEEKING MEANING OR HAPPINESS?
115. Anne Kvikstad: LIFE CHANGE EVENTS AND MARITAL STATUS IN RELATION TO RISK AND PROGNOSIS OF CANCER.
116. Torbjørn Grøntvedt: TREATMENT OF ACUTE AND CHRONIC ANTERIOR CRUCIATE LIGAMENT INJURIES. A clinical and biomechanical study.
117. Sigrid Hørven Wigers: CLINICAL STUDIES OF FIBROMYALGIA WITH FOCUS ON ETIOLOGY, TREATMENT AND OUTCOME.
118. Jan Schjøtt: MYOCARDIAL PROTECTION: Functional and Metabolic Characteristics of Two Endogenous Protective Principles.
119. Marit Martinussen: STUDIES OF INTESTINAL BLOOD FLOW AND ITS RELATION TO TRANSITIONAL CIRCULATORY ADAPATION IN NEWBORN INFANTS.
120. Tomm B. Müller: MAGNETIC RESONANCE IMAGING IN FOCAL CEREBRAL ISCHEMIA.
121. Rune Haaverstad: OEDEMA FORMATION OF THE LOWER EXTREMITIES.
122. Magne Børset: THE ROLE OF CYTOKINES IN MULTIPLE MYELOMA, WITH SPECIAL REFERENCE TO HEPATOCYTE GROWTH FACTOR.
123. Geir Smedslund: A THEORETICAL AND EMPIRICAL INVESTIGATION OF SMOKING, STRESS AND DISEASE: RESULTS FROM A POPULATION SURVEY.

1997

124. Torstein Vik: GROWTH, MORBIDITY, AND PSYCHOMOTOR DEVELOPMENT IN INFANTS WHO WERE GROWTH RETARDED *IN UTERO*.
125. Siri Forsmo: ASPECTS AND CONSEQUENCES OF OPPORTUNISTIC SCREENING FOR CERVICAL CANCER. Results based on data from three Norwegian counties.
126. Jon S. Skranes: CEREBRAL MRI AND NEURODEVELOPMENTAL OUTCOME IN VERY LOW BIRTH WEIGHT (VLBW) CHILDREN. A follow-up study of a geographically based year cohort of VLBW children at ages one and six years.
127. Knut Bjørnstad: COMPUTERIZED ECHOCARDIOGRAPHY FOR EVALUTION OF CORONARY ARTERY DISEASE.
128. Grethe Elisabeth Borchgrevink: DIAGNOSIS AND TREATMENT OF WHIPLASH/NECK SPRAIN INJURIES CAUSED BY CAR ACCIDENTS.
129. Tor Elsås: NEUROPEPTIDES AND NITRIC OXIDE SYNTHASE IN OCULAR AUTONOMIC AND SENSORY NERVES.
130. Rolf W. Gråwe: EPIDEMIOLOGICAL AND NEUROPSYCHOLOGICAL PERSPECTIVES ON SCHIZOPHRENIA.
131. Tonje Strømholm: CEREBRAL HAEMODYNAMICS DURING THORACIC AORTIC CROSSCLAMPING. An experimental study in pigs

1998

132. Martinus Bråten: STUDIES ON SOME PROBLEMS REALTED TO INTRAMEDULLARY NAILING OF FEMORAL FRACTURES.

133. Ståle Nordgård: PROLIFERATIVE ACTIVITY AND DNA CONTENT AS PROGNOSTIC INDICATORS IN ADENOID CYSTIC CARCINOMA OF THE HEAD AND NECK.
134. Egil Lien: SOLUBLE RECEPTORS FOR **TNF** AND **LPS**: RELEASE PATTERN AND POSSIBLE SIGNIFICANCE IN DISEASE.
135. Marit Bjørgaas: HYPOGLYCAEMIA IN CHILDREN WITH DIABETES MELLITUS
136. Frank Skorpen: GENETIC AND FUNCTIONAL ANALYSES OF DNA REPAIR IN HUMAN CELLS.
137. Juan A. Pareja: SUNCT SYNDROME. ON THE CLINICAL PICTURE. ITS DISTINCTION FROM OTHER, SIMILAR HEADACHES.
138. Anders Angelsen: NEUROENDOCRINE CELLS IN HUMAN PROSTATIC CARCINOMAS AND THE PROSTATIC COMPLEX OF RAT, GUINEA PIG, CAT AND DOG.
139. Fabio Antonaci: CHRONIC PAROXYSMAL HEMICRANIA AND HEMICRANIA CONTINUA: TWO DIFFERENT ENTITIES?
140. Sven M. Carlsen: ENDOCRINE AND METABOLIC EFFECTS OF METFORMIN WITH SPECIAL EMPHASIS ON CARDIOVASCULAR RISK FACTORES.

1999

141. Terje A. Murberg: DEPRESSIVE SYMPTOMS AND COPING AMONG PATIENTS WITH CONGESTIVE HEART FAILURE.
142. Harm-Gerd Karl Blaas: THE EMBRYONIC EXAMINATION. Ultrasound studies on the development of the human embryo.
143. Noèmi Becser Andersen:THE CEPHALIC SENSORY NERVES IN UNILATERAL HEADACHES. Anatomical background and neurophysiological evaluation.
144. Eli-Janne Fiskerstrand: LASER TREATMENT OF PORT WINE STAINS. A study of the efficacy and limitations of the pulsed dye laser. Clinical and morfological analyses aimed at improving the therapeutic outcome.
145. Bård Kulseng: A STUDY OF ALGINATE CAPSULE PROPERTIES AND CYTOKINES IN RELATION TO INSULIN DEPENDENT DIABETES MELLITUS.
146. Terje Haug: STRUCTURE AND REGULATION OF THE HUMAN UNG GENE ENCODING URACIL-DNA GLYCOSYLASE.
147. Heidi Brurok: MANGANESE AND THE HEART. A Magic Metal with Diagnostic and Therapeutic Possibilites.
148. Agnes Kathrine Lie: DIAGNOSIS AND PREVALENCE OF HUMAN PAPILLOMAVIRUS INFECTION IN CERVICAL INTRAEPITELIAL NEOPLASIA. Relationship to Cell Cycle Regulatory Proteins and HLA DQBI Genes.
149. Ronald Mårvik: PHARMACOLOGICAL, PHYSIOLOGICAL AND PATHOPHYSIOLOGICAL STUDIES ON ISOLATED STOMACS.
150. Ketil Jarl Holen: THE ROLE OF ULTRASONOGRAPHY IN THE DIAGNOSIS AND TREATMENT OF HIP DYSPLASIA IN NEWBORNS.
151. Irene Hetlevik: THE ROLE OF CLINICAL GUIDELINES IN CARDIOVASCULAR RISK INTERVENTION IN GENERAL PRACTICE.
152. Katarina Tunòn: ULTRASOUND AND PREDICTION OF GESTATIONAL AGE.
153. Johannes Soma: INTERACTION BETWEEN THE LEFT VENTRICLE AND THE SYSTEMIC ARTERIES.
154. Arild Aamodt: DEVELOPMENT AND PRE-CLINICAL EVALUATION OF A CUSTOM-MADE FEMORAL STEM.
155. Agnar Tegnander: DIAGNOSIS AND FOLLOW-UP OF CHILDREN WITH SUSPECTED OR KNOWN HIP DYSPLASIA.
156. Bent Indredavik: STROKE UNIT TREATMENT: SHORT AND LONG-TERM EFFECTS
157. Jolanta Vanagaite Vingen: PHOTOPHOBIA AND PHONOPHOBIA IN PRIMARY HEADACHES

2000

158. Ola Dalsegg Sæther: PATHOPHYSIOLOGY DURING PROXIMAL AORTIC CROSS-CLAMPING CLINICAL AND EXPERIMENTAL STUDIES
159. xxxxxxxxx (blind number)
160. Christina Vogt Isaksen: PRENATAL ULTRASOUND AND POSTMORTEM FINDINGS – A TEN YEAR CORRELATIVE STUDY OF FETUSES AND INFANTS WITH DEVELOPMENTAL ANOMALIES.
161. Holger Seidel: HIGH-DOSE METHOTREXATE THERAPY IN CHILDREN WITH ACUTE LYMPHOCYTIC LEUKEMIA: DOSE, CONCENTRATION, AND EFFECT CONSIDERATIONS.

162. Stein Hallan: IMPLEMENTATION OF MODERN MEDICAL DECISION ANALYSIS INTO CLINICAL DIAGNOSIS AND TREATMENT.
163. Malcolm Sue-Chu: INVASIVE AND NON-INVASIVE STUDIES IN CROSS-COUNTRY SKIERS WITH ASTHMA-LIKE SYMPTOMS.
164. Ole-Lars Brekke: EFFECTS OF ANTIOXIDANTS AND FATTY ACIDS ON TUMOR NECROSIS FACTOR-INDUCED CYTOTOXICITY.
165. Jan Lundbom: AORTOCORONARY BYPASS SURGERY: CLINICAL ASPECTS, COST CONSIDERATIONS AND WORKING ABILITY.
166. John-Anker Zwart: LUMBAR NERVE ROOT COMPRESSION, BIOCHEMICAL AND NEUROPHYSIOLOGICAL ASPECTS.
167. Geir Falck: HYPEROSMOLALITY AND THE HEART.
168. Eirik Skogvoll: CARDIAC ARREST Incidence, Intervention and Outcome.
169. Dalius Bansevicius: SHOULDER-NECK REGION IN CERTAIN HEADACHES AND CHRONIC PAIN SYNDROMES.
170. Bettina Kinge: REFRACTIVE ERRORS AND BIOMETRIC CHANGES AMONG UNIVERSITY STUDENTS IN NORWAY.
171. Gunnar Qvigstad: CONSEQUENCES OF HYPERGASTRINEMIA IN MAN
172. Hanne Ellekjær: EPIDEMIOLOGICAL STUDIES OF STROKE IN A NORWEGIAN POPULATION. INCIDENCE, RISK FACTORS AND PROGNOSIS
173. Hilde Grimstad: VIOLENCE AGAINST WOMEN AND PREGNANCY OUTCOME.
174. Astrid Hjelde: SURFACE TENSION AND COMPLEMENT ACTIVATION: Factors influencing bubble formation and bubble effects after decompression.
175. Kjell A. Kvistad: MR IN BREAST CANCER – A CLINICAL STUDY.
176. Ivar Rossvoll: ELECTIVE ORTHOPAEDIC SURGERY IN A DEFINED POPULATION. Studies on demand, waiting time for treatment and incapacity for work.
177. Carina Seidel: PROGNOSTIC VALUE AND BIOLOGICAL EFFECTS OF HEPATOCYTE GROWTH FACTOR AND SYNDECAN-1 IN MULTIPLE MYELOMA.

2001

178. Alexander Wahba: THE INFLUENCE OF CARDIOPULMONARY BYPASS ON PLATELET FUNCTION AND BLOOD COAGULATION – DETERMINANTS AND CLINICAL CONSEQUENSES
179. Marcus Schmitt-Egenolf: THE RELEVANCE OF THE MAJOR hISTOCOMPATIBILITY COMPLEX FOR THE GENETICS OF PSORIASIS
180. Odrun Arna Gederaas: BIOLOGICAL MECHANISMS INVOLVED IN 5-AMINOLEVULINIC ACID BASED PHOTODYNAMIC THERAPY
181. Pål Richard Romundstad: CANCER INCIDENCE AMONG NORWEGIAN ALUMINIUM WORKERS
182. Henrik Hjorth-Hansen: NOVEL CYTOKINES IN GROWTH CONTROL AND BONE DISEASE OF MULTIPLE MYELOMA
183. Gunnar Morken: SEASONAL VARIATION OF HUMAN MOOD AND BEHAVIOUR
184. Bjørn Olav Haugen: MEASUREMENT OF CARDIAC OUTPUT AND STUDIES OF VELOCITY PROFILES IN AORTIC AND MITRAL FLOW USING TWO- AND THREE-DIMENSIONAL COLOUR FLOW IMAGING
185. Geir Bråthen: THE CLASSIFICATION AND CLINICAL DIAGNOSIS OF ALCOHOL-RELATED SEIZURES
186. Knut Ivar Aasarød: RENAL INVOLVEMENT IN INFLAMMATORY RHEUMATIC DISEASE. A Study of Renal Disease in Wegener's Granulomatosis and in Primary Sjögren's Syndrome
187. Trude Helen Flo: RESEPTORS INVOLVED IN CELL ACTIVATION BY DEFINED URONIC ACID POLYMERS AND BACTERIAL COMPONENTS
188. Bodil Kavli: HUMAN URACIL-DNA GLYCOSYLASES FROM THE UNG GENE: STRUCTRUAL BASIS FOR SUBSTRATE SPECIFICITY AND REPAIR
189. Liv Thommesen: MOLECULAR MECHANISMS INVOLVED IN TNF- AND GASTRIN-MEDIATED GENE REGULATION
190. Turid Lingaas Holmen: SMOKING AND HEALTH IN ADOLESCENCE; THE NORD-TRØNDELAG HEALTH STUDY, 1995-97
191. Øyvind Hjertner: MULTIPLE MYELOMA: INTERACTIONS BETWEEN MALIGNANT PLASMA CELLS AND THE BONE MICROENVIRONMENT

192. Asbjørn Støylen: STRAIN RATE IMAGING OF THE LEFT VENTRICLE BY ULTRASOUND. FEASIBILITY, CLINICAL VALIDATION AND PHYSIOLOGICAL ASPECTS
193. Kristian Midthjell: DIABETES IN ADULTS IN NORD-TRØNDELAG. PUBLIC HEALTH ASPECTS OF DIABETES MELLITUS IN A LARGE, NON-SELECTED NORWEGIAN POPULATION.
194. Guanglin Cui: FUNCTIONAL ASPECTS OF THE ECL CELL IN RODENTS
195. Ulrik Wisløff: CARDIAC EFFECTS OF AEROBIC ENDURANCE TRAINING: HYPERTROPHY, CONTRACTILITY AND CALCUIM HANDLING IN NORMAL AND FAILING HEART
196. Øyvind Halaas: MECHANISMS OF IMMUNOMODULATION AND CELL-MEDIATED CYTOTOXICITY INDUCED BY BACTERIAL PRODUCTS
197. Tore Amundsen: PERFUSION MR IMAGING IN THE DIAGNOSIS OF PULMONARY EMBOLISM
198. Nanna Kurtze: THE SIGNIFICANCE OF ANXIETY AND DEPRESSION IN FATIQUE AND PATTERNS OF PAIN AMONG INDIVIDUALS DIAGNOSED WITH FIBROMYALGIA: RELATIONS WITH QUALITY OF LIFE, FUNCTIONAL DISABILITY, LIFESTYLE, EMPLOYMENT STATUS, CO-MORBIDITY AND GENDER
199. Tom Ivar Lund Nilsen: PROSPECTIVE STUDIES OF CANCER RISK IN NORD-TRØNDELAG: THE HUNT STUDY. Associations with anthropometric, socioeconomic, and lifestyle risk factors
200. Asta Kristine Håberg: A NEW APPROACH TO THE STUDY OF MIDDLE CEREBRAL ARTERY OCCLUSION IN THE RAT USING MAGNETIC RESONANCE TECHNIQUES

2002

201. Knut Jørgen Arntzen: PREGNANCY AND CYTOKINES
202. Henrik Døllner: INFLAMMATORY MEDIATORS IN PERINATAL INFECTIONS
203. Asta Bye: LOW FAT, LOW LACTOSE DIET USED AS PROPHYLACTIC TREATMENT OF ACUTE INTESTINAL REACTIONS DURING PELVIC RADIOTHERAPY. A PROSPECTIVE RANDOMISED STUDY.
204. Sylvester Moyo: STUDIES ON STREPTOCOCCUS AGALACTIAE (GROUP B STREPTOCOCCUS) SURFACE-ANCHORED MARKERS WITH EMPHASIS ON STRAINS AND HUMAN SERA FROM ZIMBABWE.
205. Knut Hagen: HEAD-HUNT: THE EPIDEMIOLOGY OF HEADACHE IN NORD-TRØNDELAG
206. Li Lixin: ON THE REGULATION AND ROLE OF UNCOUPLING PROTEIN-2 IN INSULIN PRODUCING ß-CELLS
207. Anne Hildur Henriksen: SYMPTOMS OF ALLERGY AND ASTHMA VERSUS MARKERS OF LOWER AIRWAY INFLAMMATION AMONG ADOLESCENTS
208. Egil Andreas Fors: NON-MALIGNANT PAIN IN RELATION TO PSYCHOLOGICAL AND ENVIRONTENTAL FACTORS. EXPERIENTAL AND CLINICAL STUDES OF PAIN WITH FOCUS ON FIBROMYALGIA
209. Pål Klepstad: MORPHINE FOR CANCER PAIN
210. Ingunn Bakke: MECHANISMS AND CONSEQUENCES OF PEROXISOME PROLIFERATOR-INDUCED HYPERFUNCTION OF THE RAT GASTRIN PRODUCING CELL
211. Ingrid Susann Gribbestad: MAGNETIC RESONANCE IMAGING AND SPECTROSCOPY OF BREAST CANCER
212. Rønnaug Astri Ødegård: PREECLAMPSIA – MATERNAL RISK FACTORS AND FETAL GROWTH
213. Johan Haux: STUDIES ON CYTOTOXICITY INDUCED BY HUMAN NATURAL KILLER CELLS AND DIGITOXIN
214. Turid Suzanne Berg-Nielsen: PARENTING PRACTICES AND MENTALLY DISORDERED ADOLESCENTS
215. Astrid Rydning: BLOOD FLOW AS A PROTECTIVE FACTOR FOR THE STOMACH MUCOSA. AN EXPERIMENTAL STUDY ON THE ROLE OF MAST CELLS AND SENSORY AFFERENT NEURONS

2003

216. Jan Pål Loennechen: HEART FAILURE AFTER MYOCARDIAL INFARCTION. Regional Differences, Myocyte Function, Gene Expression, and Response to Cariporide, Losartan, and Exercise Training.

217. Elisabeth Qvigstad: EFFECTS OF FATTY ACIDS AND OVER-STIMULATION ON INSULIN SECRETION IN MAN
218. Arne Åsberg: EPIDEMIOLOGICAL STUDIES IN HEREDITARY HEMOCHROMATOSIS: PREVALENCE, MORBIDITY AND BENEFIT OF SCREENING.
219. Johan Fredrik Skomsvoll: REPRODUCTIVE OUTCOME IN WOMEN WITH RHEUMATIC DISEASE. A population registry based study of the effects of inflammatory rheumatic disease and connective tissue disease on reproductive outcome in Norwegian women in 1967-1995.
220. Siv Mørkved: URINARY INCONTINENCE DURING PREGNANCY AND AFTER DELIVERY: EFFECT OF PELVIC FLOOR MUSCLE TRAINING IN PREVENTION AND TREATMENT
221. Marit S. Jordhøy: THE IMPACT OF COMPREHENSIVE PALLIATIVE CARE
222. Tom Christian Martinsen: HYPERGASTRINEMIA AND HYPOACIDITY IN RODENTS – CAUSES AND CONSEQUENCES
223. Solveig Tingulstad: CENTRALIZATION OF PRIMARY SURGERY FOR OVARAIN CANCER. FEASIBILITY AND IMPACT ON SURVIVAL
224. Haytham Eloqayli: METABOLIC CHANGES IN THE BRAIN CAUSED BY EPILEPTIC SEIZURES
225. Torunn Bruland: STUDIES OF EARLY RETROVIRUS-HOST INTERACTIONS – VIRAL DETERMINANTS FOR PATHOGENESIS AND THE INFLUENCE OF SEX ON THE SUSCEPTIBILITY TO FRIEND MURINE LEUKAEMIA VIRUS INFECTION
226. Torstein Hole: DOPPLER ECHOCARDIOGRAPHIC EVALUATION OF LEFT VENTRICULAR FUNCTION IN PATIENTS WITH ACUTE MYOCARDIAL INFARCTION
227. Vibeke Nossum: THE EFFECT OF VASCULAR BUBBLES ON ENDOTHELIAL FUNCTION
228. Sigurd Fasting: ROUTINE BASED RECORDING OF ADVERSE EVENTS DURING ANAESTHESIA – APPLICATION IN QUALITY IMPROVEMENT AND SAFETY
229. Solfrid Romundstad: EPIDEMIOLOGICAL STUDIES OF MICROALBUMINURIA. THE NORD-TRØNDELAG HEALTH STUDY 1995-97 (HUNT 2)
230. Geir Torheim: PROCESSING OF DYNAMIC DATA SETS IN MAGNETIC RESONANCE IMAGING
231. Catrine Ahlén: SKIN INFECTIONS IN OCCUPATIONAL SATURATION DIVERS IN THE NORTH SEA AND THE IMPACT OF THE ENVIRONMENT
232. Arnulf Langhammer: RESPIRATORY SYMPTOMS, LUNG FUNCTION AND BONE MINERAL DENSITY IN A COMPREHENSIVE POPULATION SURVEY. THE NORD-TRØNDELAG HEALTH STUDY 1995-97. THE BRONCHIAL OBSTRUCTION IN NORD-TRØNDELAG STUDY
233. Einar Kjelsås: EATING DISORDERS AND PHYSICAL ACTIVITY IN NON-CLINICAL SAMPLES
234. Arne Wibe: RECTAL CANCER TREATMENT IN NORWAY – STANDARDISATION OF SURGERY AND QUALITY ASSURANCE

2004

235. Eivind Witsø: BONE GRAFT AS AN ANTIBIOTIC CARRIER
236. Anne Mari Sund: DEVELOPMENT OF DEPRESSIVE SYMPTOMS IN EARLY ADOLESCENCE
237. Hallvard Lærum: EVALUATION OF ELECTRONIC MEDICAL RECORDS – A CLINICAL TASK PERSPECTIVE
238. Gustav Mikkelsen: ACCESSIBILITY OF INFORMATION IN ELECTRONIC PATIENT RECORDS; AN EVALUATION OF THE ROLE OF DATA QUALITY
239. Steinar Krokstad: SOCIOECONOMIC INEQUALITIES IN HEALTH AND DISABILITY. SOCIAL EPIDEMIOLOGY IN THE NORD-TRØNDELAG HEALTH STUDY (HUNT), NORWAY
240. Arne Kristian Myhre: NORMAL VARIATION IN ANOGENITAL ANATOMY AND MICROBIOLOGY IN NON-ABUSED PRESCHOOL CHILDREN
241. Ingunn Dybedal: NEGATIVE REGULATORS OF HEMATOPOIETEC STEM AND PROGENITOR CELLS
242. Beate Sitter: TISSUE CHARACTERIZATION BY HIGH RESOLUTION MAGIC ANGLE SPINNING MR SPECTROSCOPY
243. Per Arne Aas: MACROMOLECULAR MAINTENANCE IN HUMAN CELLS – REPAIR OF URACIL IN DNA AND METHYLATIONS IN DNA AND RNA

244. Anna Bofin: FINE NEEDLE ASPIRATION CYTOLOGY IN THE PRIMARY INVESTIGATION OF BREAST TUMOURS AND IN THE DETERMINATION OF TREATMENT STRATEGIES
245. Jim Aage Nøttestad: DEINSTITUTIONALIZATION AND MENTAL HEALTH CHANGES AMONG PEOPLE WITH MENTAL RETARDATION
246. Reidar Fossmark: GASTRIC CANCER IN JAPANESE COTTON RATS
247. Wibeke Nordhøy: MANGANESE AND THE HEART, INTRACELLULAR MR RELAXATION AND WATER EXCHANGE ACROSS THE CARDIAC CELL MEMBRANE

2005

248. Sturla Molden: QUANTITATIVE ANALYSES OF SINGLE UNITS RECORDED FROM THE HIPPOCAMPUS AND ENTORHINAL CORTEX OF BEHAVING RATS
249. Wenche Brenne Drøyvold: EPIDEMIOLOGICAL STUDIES ON WEIGHT CHANGE AND HEALTH IN A LARGE POPULATION. THE NORD-TRØNDELAG HEALTH STUDY (HUNT)
250. Ragnhild Støen: ENDOTHELIUM-DEPENDENT VASODILATION IN THE FEMORAL ARTERY OF DEVELOPING PIGLETS
251. Aslak Steinsbekk: HOMEOPATHY IN THE PREVENTION OF UPPER RESPIRATORY TRACT INFECTIONS IN CHILDREN
252. Hill-Aina Steffenach: MEMORY IN HIPPOCAMPAL AND CORTICO-HIPPOCAMPAL CIRCUITS
253. Eystein Stordal: ASPECTS OF THE EPIDEMIOLOGY OF DEPRESSIONS BASED ON SELF-RATING IN A LARGE GENERAL HEALTH STUDY (THE HUNT-2 STUDY)
254. Viggo Pettersen: FROM MUSCLES TO SINGING: THE ACTIVITY OF ACCESSORY BREATHING MUSCLES AND THORAX MOVEMENT IN CLASSICAL SINGING
255. Marianne Fyhn: SPATIAL MAPS IN THE HIPPOCAMPUS AND ENTORHINAL CORTEX
256. Robert Valderhaug: OBSESSIVE-COMPULSIVE DISORDER AMONG CHILDREN AND ADOLESCENTS: CHARACTERISTICS AND PSYCHOLOGICAL MANAGEMENT OF PATIENTS IN OUTPATIENT PSYCHIATRIC CLINICS
257. Erik Skaaheim Haug: INFRARENAL ABDOMINAL AORTIC ANEURYSMS – COMORBIDITY AND RESULTS FOLLOWING OPEN SURGERY
258. Daniel Kondziella: GLIAL-NEURONAL INTERACTIONS IN EXPERIMENTAL BRAIN DISORDERS
259. Vegard Heimly Brun: ROUTES TO SPATIAL MEMORY IN HIPPOCAMPAL PLACE CELLS
260. Kenneth McMillan: PHYSIOLOGICAL ASSESSMENT AND TRAINING OF ENDURANCE AND STRENGTH IN PROFESSIONAL YOUTH SOCCER PLAYERS
261. Marit Sæbø Indredavik: MENTAL HEALTH AND CEREBRAL MAGNETIC RESONANCE IMAGING IN ADOLESCENTS WITH LOW BIRTH WEIGHT
262. Ole Johan Kemi: ON THE CELLULAR BASIS OF AEROBIC FITNESS, INTENSITY-DEPENDENCE AND TIME-COURSE OF CARDIOMYOCYTE AND ENDOTHELIAL ADAPTATIONS TO EXERCISE TRAINING
263. Eszter Vanky: POLYCYSTIC OVARY SYNDROME – METFORMIN TREATMENT IN PREGNANCY
264. Hild Fjærtoft: EXTENDED STROKE UNIT SERVICE AND EARLY SUPPORTED DISCHARGE. SHORT AND LONG-TERM EFFECTS
265. Grete Dyb: POSTTRAUMATIC STRESS REACTIONS IN CHILDREN AND ADOLESCENTS
266. Vidar Fykse: SOMATOSTATIN AND THE STOMACH
267. Kirsti Berg: OXIDATIVE STRESS AND THE ISCHEMIC HEART: A STUDY IN PATIENTS UNDERGOING CORONARY REVASCULARIZATION
268. Björn Inge Gustafsson: THE SEROTONIN PRODUCING ENTEROCHROMAFFIN CELL, AND EFFECTS OF HYPERSEROTONINEMIA ON HEART AND BONE

2006

269. Torstein Baade Rø: EFFECTS OF BONE MORPHOGENETIC PROTEINS, HEPATOCYTE GROWTH FACTOR AND INTERLEUKIN-21 IN MULTIPLE MYELOMA
270. May-Britt Tessem: METABOLIC EFFECTS OF ULTRAVIOLET RADIATION ON THE ANTERIOR PART OF THE EYE
271. Anne-Sofie Helvik: COPING AND EVERYDAY LIFE IN A POPULATION OF ADULTS WITH HEARING IMPAIRMENT

272. Therese Standal: MULTIPLE MYELOMA: THE INTERPLAY BETWEEN MALIGNANT PLASMA CELLS AND THE BONE MARROW MICROENVIRONMENT
273. Ingvild Saltvedt: TREATMENT OF ACUTELY SICK, FRAIL ELDERLY PATIENTS IN A GERIATRIC EVALUATION AND MANAGEMENT UNIT – RESULTS FROM A PROSPECTIVE RANDOMISED TRIAL
274. Birger Henning Endreseth: STRATEGIES IN RECTAL CANCER TREATMENT – FOCUS ON EARLY RECTAL CANCER AND THE INFLUENCE OF AGE ON PROGNOSIS
275. Anne Mari Aukan Rokstad: ALGINATE CAPSULES AS BIOREACTORS FOR CELL THERAPY
276. Mansour Akbari: HUMAN BASE EXCISION REPAIR FOR PRESERVATION OF GENOMIC STABILITY
277. Stein Sundstrøm: IMPROVING TREATMENT IN PATIENTS WITH LUNG CANCER – RESULTS FROM TWO MULITCENTRE RANDOMISED STUDIES
278. Hilde Pleym: BLEEDING AFTER CORONARY ARTERY BYPASS SURGERY - STUDIES ON HEMOSTATIC MECHANISMS, PROPHYLACTIC DRUG TREATMENT AND EFFECTS OF AUTOTRANSFUSION
279. Line Merethe Oldervoll: PHYSICAL ACTIVITY AND EXERCISE INTERVENTIONS IN CANCER PATIENTS
280. Boye Welde: THE SIGNIFICANCE OF ENDURANCE TRAINING, RESISTANCE TRAINING AND MOTIVATIONAL STYLES IN ATHLETIC PERFORMANCE AMONG ELITE JUNIOR CROSS-COUNTRY SKIERS
281. Per Olav Vandvik: IRRITABLE BOWEL SYNDROME IN NORWAY, STUDIES OF PREVALENCE, DIAGNOSIS AND CHARACTERISTICS IN GENERAL PRACTICE AND IN THE POPULATION
282. Idar Kirkeby-Garstad: CLINICAL PHYSIOLOGY OF EARLY MOBILIZATION AFTER CARDIAC SURGERY
283. Linn Getz: SUSTAINABLE AND RESPONSIBLE PREVENTIVE MEDICINE. CONCEPTUALISING ETHICAL DILEMMAS ARISING FROM CLINICAL IMPLEMENTATION OF ADVANCING MEDICAL TECHNOLOGY
284. Eva Tegnander: DETECTION OF CONGENITAL HEART DEFECTS IN A NON-SELECTED POPULATION OF 42,381 FETUSES
285. Kristin Gabestad Nørsett: GENE EXPRESSION STUDIES IN GASTROINTESTINAL PATHOPHYSIOLOGY AND NEOPLASIA
286. Per Magnus Haram: GENETIC VS. AQUIRED FITNESS: METABOLIC, VASCULAR AND CARDIOMYOCYTE ADAPTATIONS
287. Agneta Johansson: GENERAL RISK FACTORS FOR GAMBLING PROBLEMS AND THE PREVALENCE OF PATHOLOGICAL GAMBLING IN NORWAY
288. Svein Artur Jensen: THE PREVALENCE OF SYMPTOMATIC ARTERIAL DISEASE OF THE LOWER LIMB
289. Charlotte Björk Ingul: QUANITIFICATION OF REGIONAL MYOCARDIAL FUNCTION BY STRAIN RATE AND STRAIN FOR EVALUATION OF CORONARY ARTERY DISEASE. AUTOMATED VERSUS MANUAL ANALYSIS DURING ACUTE MYOCARDIAL INFARCTION AND DOBUTAMINE STRESS ECHOCARDIOGRAPHY
290. Jakob Nakling: RESULTS AND CONSEQUENCES OF ROUTINE ULTRASOUND SCREENING IN PREGNANCY – A GEOGRAPHIC BASED POPULATION STUDY
291. Anne Engum: DEPRESSION AND ANXIETY – THEIR RELATIONS TO THYROID DYSFUNCTION AND DIABETES IN A LARGE EPIDEMIOLOGICAL STUDY
292. Ottar Bjerkeset: ANXIETY AND DEPRESSION IN THE GENERAL POPULATION: RISK FACTORS, INTERVENTION AND OUTCOME – THE NORD-TRØNDELAG HEALTH STUDY (HUNT)
293. Jon Olav Drogset: RESULTS AFTER SURGICAL TREATMENT OF ANTERIOR CRUCIATE LIGAMENT INJURIES – A CLINICAL STUDY
294. Lars Fosse: MECHANICAL BEHAVIOUR OF COMPACTED MORSELLISED BONE – AN EXPERIMENTAL IN VITRO STUDY
295. Gunilla Klensmeden Fosse: MENTAL HEALTH OF PSYCHIATRIC OUTPATIENTS BULLIED IN CHILDHOOD
296. Paul Jarle Mork: MUSCLE ACTIVITY IN WORK AND LEISURE AND ITS ASSOCIATION TO MUSCULOSKELETAL PAIN

297. Björn Stenström: LESSONS FROM RODENTS: I: MECHANISMS OF OBESITY SURGERY – ROLE OF STOMACH. II: CARCINOGENIC EFFECTS OF *HELICOBACTER PYLORI* AND SNUS IN THE STOMACH

2007

298. Haakon R. Skogseth: INVASIVE PROPERTIES OF CANCER – A TREATMENT TARGET ? IN VITRO STUDIES IN HUMAN PROSTATE CANCER CELL LINES
299. Janniche Hammer: GLUTAMATE METABOLISM AND CYCLING IN MESIAL TEMPORAL LOBE EPILEPSY
300. May Britt Drugli: YOUNG CHILDREN TREATED BECAUSE OF ODD/CD: CONDUCT PROBLEMS AND SOCIAL COMPETENCIES IN DAY-CARE AND SCHOOL SETTINGS
301. Arne Skjold: MAGNETIC RESONANCE KINETICS OF MANGANESE DIPYRIDOXYL DIPHOSPHATE (MnDPDP) IN HUMAN MYOCARDIUM. STUDIES IN HEALTHY VOLUNTEERS AND IN PATIENTS WITH RECENT MYOCARDIAL INFARCTION
302. Siri Malm: LEFT VENTRICULAR SYSTOLIC FUNCTION AND MYOCARDIAL PERFUSION ASSESSED BY CONTRAST ECHOCARDIOGRAPHY
303. Valentina Maria do Rosario Cabral Iversen: MENTAL HEALTH AND PSYCHOLOGICAL ADAPTATION OF CLINICAL AND NON-CLINICAL MIGRANT GROUPS
304. Lasse Løvstakken: SIGNAL PROCESSING IN DIAGNOSTIC ULTRASOUND: ALGORITHMS FOR REAL-TIME ESTIMATION AND VISUALIZATION OF BLOOD FLOW VELOCITY
305. Elisabeth Olstad: GLUTAMATE AND GABA: MAJOR PLAYERS IN NEURONAL METABOLISM
306. Lilian Leistad: THE ROLE OF CYTOKINES AND PHOSPHOLIPASE A_2S IN ARTICULAR CARTILAGE CHONDROCYTES IN RHEUMATOID ARTHRITIS AND OSTEOARTHRITIS
307. Arne Vaaler: EFFECTS OF PSYCHIATRIC INTENSIVE CARE UNIT IN AN ACUTE PSYCIATHRIC WARD
308. Mathias Toft: GENETIC STUDIES OF LRRK2 AND PINK1 IN PARKINSON'S DISEASE
309. Ingrid Løvold Mostad: IMPACT OF DIETARY FAT QUANTITY AND QUALITY IN TYPE 2 DIABETES WITH EMPHASIS ON MARINE N-3 FATTY ACIDS
310. Torill Eidhammer Sjøbakk: MR DETERMINED BRAIN METABOLIC PATTERN IN PATIENTS WITH BRAIN METASTASES AND ADOLESCENTS WITH LOW BIRTH WEIGHT
311. Vidar Beisvåg: PHYSIOLOGICAL GENOMICS OF HEART FAILURE: FROM TECHNOLOGY TO PHYSIOLOGY
312. Olav Magnus Søndenå Fredheim: HEALTH RELATED QUALITY OF LIFE ASSESSMENT AND ASPECTS OF THE CLINICAL PHARMACOLOGY OF METHADONE IN PATIENTS WITH CHRONIC NON-MALIGNANT PAIN
313. Anne Brantberg: FETAL AND PERINATAL IMPLICATIONS OF ANOMALIES IN THE GASTROINTESTINAL TRACT AND THE ABDOMINAL WALL
314. Erik Solligård: GUT LUMINAL MICRODIALYSIS
315. Elin Tollefsen: RESPIRATORY SYMPTOMS IN A COMPREHENSIVE POPULATION BASED STUDY AMONG ADOLESCENTS 13-19 YEARS. YOUNG-HUNT 1995-97 AND 2000-01; THE NORD-TRØNDELAG HEALTH STUDIES (HUNT)
316. Anne-Tove Brenne: GROWTH REGULATION OF MYELOMA CELLS
317. Heidi Knobel: FATIGUE IN CANCER TREATMENT – ASSESSMENT, COURSE AND ETIOLOGY
318. Torbjørn Dahl: CAROTID ARTERY STENOSIS. DIAGNOSTIC AND THERAPEUTIC ASPECTS
319. Inge-Andre Rasmussen jr.: FUNCTIONAL AND DIFFUSION TENSOR MAGNETIC RESONANCE IMAGING IN NEUROSURGICAL PATIENTS
320. Grete Helen Bratberg: PUBERTAL TIMING – ANTECEDENT TO RISK OR RESILIENCE ? EPIDEMIOLOGICAL STUDIES ON GROWTH, MATURATION AND HEALTH RISK BEHAVIOURS; THE YOUNG HUNT STUDY, NORD-TRØNDELAG, NORWAY
321. Sveinung Sørhaug: THE PULMONARY NEUROENDOCRINE SYSTEM. PHYSIOLOGICAL, PATHOLOGICAL AND TUMOURIGENIC ASPECTS
322. Olav Sande Eftedal: ULTRASONIC DETECTION OF DECOMPRESSION INDUCED VASCULAR MICROBUBBLES
323. Rune Bang Leistad: PAIN, AUTONOMIC ACTIVATION AND MUSCULAR ACTIVITY RELATED TO EXPERIMENTALLY-INDUCED COGNITIVE STRESS IN HEADACHE PATIENTS

324. Svein Brekke: TECHNIQUES FOR ENHANCEMENT OF TEMPORAL RESOLUTION IN THREE-DIMENSIONAL ECHOCARDIOGRAPHY
325. Kristian Bernhard Nilsen: AUTONOMIC ACTIVATION AND MUSCLE ACTIVITY IN RELATION TO MUSCULOSKELETAL PAIN
326. Anne Irene Hagen: HEREDITARY BREAST CANCER IN NORWAY. DETECTION AND PROGNOSIS OF BREAST CANCER IN FAMILIES WITH *BRCA1*GENE MUTATION
327. Ingebjørg S. Juel : INTESTINAL INJURY AND RECOVERY AFTER ISCHEMIA. AN EXPERIMENTAL STUDY ON RESTITUTION OF THE SURFACE EPITHELIUM, INTESTINAL PERMEABILITY, AND RELEASE OF BIOMARKERS FROM THE MUCOSA
328. Runa Heimstad: POST-TERM PREGNANCY
329. Jan Egil Afset: ROLE OF ENTEROPATHOGENIC *ESCHERICHIA COLI* IN CHILDHOOD DIARRHOEA IN NORWAY
330. Bent Håvard Hellum: *IN VITRO* INTERACTIONS BETWEEN MEDICINAL DRUGS AND HERBS ON CYTOCHROME P-450 METABOLISM AND P-GLYCOPROTEIN TRANSPORT
331. Morten André Høydal: CARDIAC DYSFUNCTION AND MAXIMAL OXYGEN UPTAKE MYOCARDIAL ADAPTATION TO ENDURANCE TRAINING

2008

332. Andreas Møllerløkken: REDUCTION OF VASCULAR BUBBLES: METHODS TO PREVENT THE ADVERSE EFFECTS OF DECOMPRESSION
333. Anne Hege Aamodt: COMORBIDITY OF HEADACHE AND MIGRAINE IN THE NORD-TRØNDELAG HEALTH STUDY 1995-97
334. Brage Høyem Amundsen: MYOCARDIAL FUNCTION QUANTIFIED BY SPECKLE TRACKING AND TISSUE DOPPLER ECHOCARDIOGRAPHY – VALIDATION AND APPLICATION IN EXERCISE TESTING AND TRAINING
335. Inger Anne Næss: INCIDENCE, MORTALITY AND RISK FACTORS OF FIRST VENOUS THROMBOSIS IN A GENERAL POPULATION. RESULTS FROM THE SECOND NORD-TRØNDELAG HEALTH STUDY (HUNT2)
336. Vegard Bugten: EFFECTS OF POSTOPERATIVE MEASURES AFTER FUNCTIONAL ENDOSCOPIC SINUS SURGERY
337. Morten Bruvold: MANGANESE AND WATER IN CARDIAC MAGNETIC RESONANCE IMAGING
338. Miroslav Fris: THE EFFECT OF SINGLE AND REPEATED ULTRAVIOLET RADIATION ON THE ANTERIOR SEGMENT OF THE RABBIT EYE
339. Svein Arne Aase: METHODS FOR IMPROVING QUALITY AND EFFICIENCY IN QUANTITATIVE ECHOCARDIOGRAPHY – ASPECTS OF USING HIGH FRAME RATE
340. Roger Almvik: ASSESSING THE RISK OF VIOLENCE: DEVELOPMENT AND VALIDATION OF THE BRØSET VIOLENCE CHECKLIST
341. Ottar Sundheim: STRUCTURE-FUNCTION ANALYSIS OF HUMAN ENZYMES INITIATING NUCLEOBASE REPAIR IN DNA AND RNA
342. Anne Mari Undheim: SHORT AND LONG-TERM OUTCOME OF EMOTIONAL AND BEHAVIOURAL PROBLEMS IN YOUNG ADOLESCENTS WITH AND WITHOUT READING DIFFICULTIES
343. Helge Garåsen: THE TRONDHEIM MODEL. IMPROVING THE PROFESSIONAL COMMUNICATION BETWEEN THE VARIOUS LEVELS OF HEALTH CARE SERVICES AND IMPLEMENTATION OF INTERMEDIATE CARE AT A COMMUNITY HOSPITAL COULD PROVIDE BETTER CARE FOR OLDER PATIENTS. SHORT AND LONG TERM EFFECTS
344. Olav A. Foss: "THE ROTATION RATIOS METHOD". A METHOD TO DESCRIBE ALTERED SPATIAL ORIENTATION IN SEQUENTIAL RADIOGRAPHS FROM ONE PELVIS
345. Bjørn Olav Åsvold: THYROID FUNCTION AND CARDIOVASCULAR HEALTH
346. Torun Margareta Melø: NEURONAL GLIAL INTERACTIONS IN EPILEPSY
347. Irina Poliakova Eide: FETAL GROWTH RESTRICTION AND PRE-ECLAMPSIA: SOME CHARACTERISTICS OF FETO-MATERNAL INTERACTIONS IN DECIDUA BASALIS
348. Torunn Askim: RECOVERY AFTER STROKE. ASSESSMENT AND TREATMENT; WITH FOCUS ON MOTOR FUNCTION
349. Ann Elisabeth Åsberg: NEUTROPHIL ACTIVATION IN A ROLLER PUMP MODEL OF CARDIOPULMONARY BYPASS. INFLUENCE ON BIOMATERIAL, PLATELETS AND COMPLEMENT

350. Lars Hagen: REGULATION OF DNA BASE EXCISION REPAIR BY PROTEIN INTERACTIONS AND POST TRANSLATIONAL MODIFICATIONS
351. Sigrun Beate Kjøtrød: POLYCYSTIC OVARY SYNDROME – METFORMIN TREATMENT IN ASSISTED REPRODUCTION
352. Steven Keita Nishiyama: PERSPECTIVES ON LIMB-VASCULAR HETEROGENEITY: IMPLICATIONS FOR HUMAN AGING, SEX, AND EXERCISE
353. Sven Peter Näsholm: ULTRASOUND BEAMS FOR ENHANCED IMAGE QUALITY
354. Jon Ståle Ritland: PRIMARY OPEN-ANGLE GLAUCOMA & EXFOLIATIVE GLAUCOMA. SURVIVAL, COMORBIDITY AND GENETICS
355. Sigrid Botne Sando: ALZHEIMER'S DISEASE IN CENTRAL NORWAY. GENETIC AND EDUCATIONAL ASPECTS
356. Parvinder Kaur: CELLULAR AND MOLECULAR MECHANISMS BEHIND METHYLMERCURY-INDUCED NEUROTOXICITY
357. Ismail Cüneyt Güzey: DOPAMINE AND SEROTONIN RECEPTOR AND TRANSPORTER GENE POLYMORPHISMS AND EXTRAPYRAMIDAL SYMPTOMS. STUDIES IN PARKINSON'S DISEASE AND IN PATIENTS TREATED WITH ANTIPSYCHOTIC OR ANTIDEPRESSANT DRUGS
358. Brit Dybdahl: EXTRA-CELLULAR INDUCIBLE HEAT-SHOCK PROTEIN 70 (Hsp70) – A ROLE IN THE INFLAMMATORY RESPONSE ?
359. Kristoffer Haugarvoll: IDENTIFYING GENETIC CAUSES OF PARKINSON'S DISEASE IN NORWAY
360. Nadra Nilsen: TOLL-LIKE RECEPTOR 2 –EXPRESSION, REGULATION AND SIGNALING
361. Johan Håkon Bjørngaard: PATIENT SATISFACTION WITH OUTPATIENT MENTAL HEALTH SERVICES – THE INFLUENCE OF ORGANIZATIONAL FACTORS.
362. Kjetil Høydal : EFFECTS OF HIGH INTENSITY AEROBIC TRAINING IN HEALTHY SUBJECTS AND CORONARY ARTERY DISEASE PATIENTS; THE IMPORTANCE OF INTENSITY,, DURATION AND FREQUENCY OF TRAINING.
363. Trine Karlsen: TRAINING IS MEDICINE: ENDURANCE AND STRENGTH TRAINING IN CORONARY ARTERY DISEASE AND HEALTH.
364. Marte Thuen: MANGANASE-ENHANCED AND DIFFUSION TENSOR MR IMAGING OF THE NORMAL, INJURED AND REGENERATING RAT VISUAL PATHWAY
365. Cathrine Broberg Vågbø: DIRECT REPAIR OF ALKYLATION DAMAGE IN DNA AND RNA BY 2-OXOGLUTARATE- AND IRON-DEPENDENT DIOXYGENASES
366. Arnt Erik Tjønna: AEROBIC EXERCISE AND CARDIOVASCULAR RISK FACTORS IN OVERWEIGHT AND OBESE ADOLESCENTS AND ADULTS
367. Marianne W. Furnes: FEEDING BEHAVIOR AND BODY WEIGHT DEVELOPMENT: LESSONS FROM RATS
368. Lene N. Johannessen: FUNGAL PRODUCTS AND INFLAMMATORY RESPONSES IN HUMAN MONOCYTES AND EPITHELIAL CELLS
369. Anja Bye: GENE EXPRESSION PROFILING OF *INHERITED* AND *ACQUIRED* MAXIMAL OXYGEN UPTAKE – RELATIONS TO THE METABOLIC SYNDROME.
370. Oluf Dimitri Røe: MALIGNANT MESOTHELIOMA: VIRUS, BIOMARKERS AND GENES. A TRANSLATIONAL APPROACH
371. Ane Cecilie Dale: DIABETES MELLITUS AND FATAL ISCHEMIC HEART DISEASE. ANALYSES FROM THE HUNT1 AND 2 STUDIES
372. Jacob Christian Hølen: PAIN ASSESSMENT IN PALLIATIVE CARE: VALIDATION OF METHODS FOR SELF-REPORT AND BEHAVIOURAL ASSESSMENT
373. Erming Tian: THE GENETIC IMPACTS IN THE ONCOGENESIS OF MULTIPLE MYELOMA
374. Ole Bosnes: KLINISK UTPRØVING AV NORSKE VERSJONER AV NOEN SENTRALE TESTER PÅ KOGNITIV FUNKSJON
375. Ola M. Rygh: 3D ULTRASOUND BASED NEURONAVIGATION IN NEUROSURGERY. A CLINICAL EVALUATION
376. Astrid Kamilla Stunes: ADIPOKINES, PEROXISOME PROFILERATOR ACTIVATED RECEPTOR (PPAR) AGONISTS AND SEROTONIN. COMMON REGULATORS OF BONE AND FAT METABOLISM
377. Silje Engdal: HERBAL REMEDIES USED BY NORWEGIAN CANCER PATIENTS AND THEIR ROLE IN HERB-DRUG INTERACTIONS
378. Kristin Offerdal: IMPROVED ULTRASOUND IMAGING OF THE FETUS AND ITS CONSEQUENCES FOR SEVERE AND LESS SEVERE ANOMALIES

379. Øivind Rognmo: HIGH-INTENSITY AEROBIC EXERCISE AND CARDIOVASCULAR HEALTH
380. Jo-Åsmund Lund: RADIOTHERAPY IN ANAL CARCINOMA AND PROSTATE CANCER

2009

381. Tore Grüner Bjåstad: HIGH FRAME RATE ULTRASOUND IMAGING USING PARALLEL BEAMFORMING
382. Erik Søndenaa: INTELLECTUAL DISABILITIES IN THE CRIMINAL JUSTICE SYSTEM
383. Berit Rostad: SOCIAL INEQUALITIES IN WOMEN'S HEALTH, HUNT 1984-86 AND 1995-97, THE NORD-TRØNDELAG HEALTH STUDY (HUNT)
384. Jonas Crosby: ULTRASOUND-BASED QUANTIFICATION OF MYOCARDIAL DEFORMATION AND ROTATION
385. Erling Tronvik: MIGRAINE, BLOOD PRESSURE AND THE RENIN-ANGIOTENSIN SYSTEM
386. Tom Christensen: BRINGING THE GP TO THE FOREFRONT OF EPR DEVELOPMENT
387. Håkon Bergseng: ASPECTS OF GROUP B STREPTOCOCCUS (GBS) DISEASE IN THE NEWBORN. EPIDEMIOLOGY, CHARACTERISATION OF INVASIVE STRAINS AND EVALUATION OF INTRAPARTUM SCREENING
388. Ronny Myhre: GENETIC STUDIES OF CANDIDATE TENE3S IN PARKINSON'S DISEASE
389. Torbjørn Moe Eggebø: ULTRASOUND AND LABOUR
390. Eivind Wang: TRAINING IS MEDICINE FOR PATIENTS WITH PERIPHERAL ARTERIAL DISEASE
391. Thea Kristin Våtsveen: GENETIC ABERRATIONS IN MYELOMA CELLS
392. Thomas Jozefiak: QUALITY OF LIFE AND MENTAL HEALTH IN CHILDREN AND ADOLESCENTS: CHILD AND PARENT PERSPECTIVES
393. Jens Erik Slagsvold: N-3 POLYUNSATURATED FATTY ACIDS IN HEALTH AND DISEASE – CLINICAL AND MOLECULAR ASPECTS
394. Kristine Misund: A STUDY OF THE TRANSCRIPTIONAL REPRESSOR ICER. REGULATORY NETWORKS IN GASTRIN-INDUCED GENE EXPRESSION
395. Franco M. Impellizzeri: HIGH-INTENSITY TRAINING IN FOOTBALL PLAYERS. EFFECTS ON PHYSICAL AND TECHNICAL PERFORMANCE
396. Kari Hanne Gjeilo: HEALTH-RELATED QUALITY OF LIFE AND CHRONIC PAIN IN PATIENTS UNDERGOING CARDIAC SURGERY
397. Øyvind Hauso: NEUROENDOCRINE ASPECTS OF PHYSIOLOGY AND DISEASE
398. Ingvild Bjellmo Johnsen: INTRACELLULAR SIGNALING MECHANISMS IN THE INNATE IMMUNE RESPONSE TO VIRAL INFECTIONS
399. Linda Tømmerdal Roten: GENETIC PREDISPOSITION FOR DEVELOPMENT OF PREEMCLAMPSIA – CANDIDATE GENE STUDIES IN THE HUNT (NORD-TRØNDELAG HEALTH STUDY) POPULATION
400. Trude Teoline Nausthaug Rakvåg: PHARMACOGENETICS OF MORPHINE IN CANCER PAIN
401. Hanne Lehn: MEMORY FUNCTIONS OF THE HUMAN MEDIAL TEMPORAL LOBE STUDIED WITH fMRI
402. Randi Utne Holt: ADHESION AND MIGRATION OF MYELOMA CELLS – IN VITRO STUDIES –
403. Trygve Solstad: NEURAL REPRESENTATIONS OF EUCLIDEAN SPACE
404. Unn-Merete Fagerli: MULTIPLE MYELOMA CELLS AND CYTOKINES FROM THE BONE MARROW ENVIRONMENT; ASPECTS OF GROWTH REGULATION AND MIGRATION
405. Sigrid Bjørnelv: EATING– AND WEIGHT PROBLEMS IN ADOLESCENTS, THE YOUNG HUNT-STUDY
406. Mari Hoff: CORTICAL HAND BONE LOSS IN RHEUMATOID ARTHRITIS. EVALUATING DIGITAL X-RAY RADIOGRAMMETRY AS OUTCOME MEASURE OF DISEASE ACTIVITY, RESPONSE VARIABLE TO TREATMENT AND PREDICTOR OF BONE DAMAGE
407. Siri Bjørgen: AEROBIC HIGH INTENSITY INTERVAL TRAINING IS AN EFFECTIVE TREATMENT FOR PATIENTS WITH CHRONIC OBSTRUCTIVE PULMONARY DISEASE
408. Susanne Lindqvist: VISION AND BRAIN IN ADOLESCENTS WITH LOW BIRTH WEIGHT
409. Torbjørn Hergum: 3D ULTRASOUND FOR QUANTITATIVE ECHOCARDIOGRAPHY

410. Jørgen Urnes: PATIENT EDUCATION IN GASTRO-OESOPHAGEAL REFLUX DISEASE. VALIDATION OF A DIGESTIVE SYMPTOMS AND IMPACT QUESTIONNAIRE AND A RANDOMISED CONTROLLED TRIAL OF PATIENT EDUCATION
411. Elvar Eyjolfsson: 13C NMRS OF ANIMAL MODELS OF SCHIZOPHRENIA
412. Marius Steiro Fimland: CHRONIC AND ACUTE NEURAL ADAPTATIONS TO STRENGTH TRAINING
413. Øyvind Støren: RUNNING AND CYCLING ECONOMY IN ATHLETES; DETERMINING FACTORS, TRAINING INTERVENTIONS AND TESTING
414. Håkon Hov: HEPATOCYTE GROWTH FACTOR AND ITS RECEPTOR C-MET. AUTOCRINE GROWTH AND SIGNALING IN MULTIPLE MYELOMA CELLS
415. Maria Radtke: ROLE OF AUTOIMMUNITY AND OVERSTIMULATION FOR BETA-CELL DEFICIENCY. EPIDEMIOLOGICAL AND THERAPEUTIC PERSPECTIVES
416. Liv Bente Romundstad: ASSISTED FERTILIZATION IN NORWAY: SAFETY OF THE REPRODUCTIVE TECHNOLOGY
417. Erik Magnus Berntsen: PREOPERATIV PLANNING AND FUNCTIONAL NEURONAVIGATION – WITH FUNCTIONAL MRI AND DIFFUSION TENSOR TRACTOGRAPHY IN PATIENTS WITH BRAIN LESIONS
418. Tonje Strømmen Steigedal: MOLECULAR MECHANISMS OF THE PROLIFERATIVE RESPONSE TO THE HORMONE GASTRIN
419. Vidar Rao: EXTRACORPOREAL PHOTOCHEMOTHERAPY IN PATIENTS WITH CUTANEOUS T CELL LYMPHOMA OR GRAFT-vs-HOST DISEASE
420. Torkild Visnes: DNA EXCISION REPAIR OF URACIL AND 5-FLUOROURACIL IN HUMAN CANCER CELL LINES

2010

421. John Munkhaugen: BLOOD PRESSURE, BODY WEIGHT, AND KIDNEY FUNCTION IN THE NEAR-NORMAL RANGE: NORMALITY, RISK FACTOR OR MORBIDITY ?
422. Ingrid Castberg: PHARMACOKINETICS, DRUG INTERACTIONS AND ADHERENCE TO TREATMENT WITH ANTIPSYCHOTICS: STUDIES IN A NATURALISTIC SETTING
423. Jian Xu: BLOOD-OXYGEN-LEVEL-DEPENDENT-FUNCTIONAL MAGNETIC RESONANCE IMAGING AND DIFFUSION TENSOR IMAGING IN TRAUMATIC BRAIN INJURY RESEARCH
424. Sigmund Simonsen: ACCEPTABLE RISK AND THE REQUIREMENT OF PROPORTIONALITY IN EUROPEAN BIOMEDICAL RESEARCH LAW. WHAT DOES THE REQUIREMENT THAT BIOMEDICAL RESEARCH SHALL NOT INVOLVE RISKS AND BURDENS DISPROPORTIONATE TO ITS POTENTIAL BENEFITS MEAN?
425. Astrid Woodhouse: MOTOR CONTROL IN WHIPLASH AND CHRONIC NON-TRAUMATIC NECK PAIN
426. Line Rørstad Jensen: EVALUATION OF TREATMENT EFFECTS IN CANCER BY MR IMAGING AND SPECTROSCOPY
427. Trine Moholdt: AEROBIC EXERCISE IN CORONARY HEART DISEASE
428. Øystein Olsen: ANALYSIS OF MANGANESE ENHANCED MRI OF THE NORMAL AND INJURED RAT CENTRAL NERVOUS SYSTEM
429. Bjørn H. Grønberg: PEMETREXED IN THE TREATMENT OF ADVANCED LUNG CANCER
430. Vigdis Schnell Husby: REHABILITATION OF PATIENTS UNDERGOING TOTAL HIP ARTHROPLASTY WITH FOCUS ON MUSCLE STRENGTH, WALKING AND AEROBIC ENDURANCE PERFORMANCE
431. Torbjørn Øien: CHALLENGES IN PRIMARY PREVENTION OF ALLERGY. THE PREVENTION OF ALLERGY AMONG CHILDREN IN TRONDHEIM (PACT) STUDY.
432. Kari Anne Indredavik Evensen: BORN TOO SOON OR TOO SMALL: MOTOR PROBLEMS IN ADOLESCENCE
433. Lars Adde: PREDICTION OF CEREBRAL PALSY IN YOUNG INFANTS. COMPUTER BASED ASSESSMENT OF GENERAL MOVEMENTS
434. Magnus Fasting: PRE- AND POSTNATAL RISK FACTORS FOR CHILDHOOD ADIPOSITY
435. Vivi Talstad Monsen: MECHANISMS OF ALKYLATION DAMAGE REPAIR BY HUMAN AlkB HOMOLOGUES
436. Toril Skandsen: MODERATE AND SEVERE TRAUMATIC BRAIN INJURY. MAGNETIC RESONANCE IMAGING FINDINGS, COGNITION AND RISK FACTORS FOR DISABILITY

437. Ingeborg Smidesang: ALLERGY RELATED DISORDERS AMONG 2-YEAR OLDS AND ADOLESCENTS IN MID-NORWAY – PREVALENCE, SEVERITY AND IMPACT. THE PACT STUDY 2005, THE YOUNG HUNT STUDY 1995-97
438. Vidar Halsteinli: MEASURING EFFICIENCY IN MENTAL HEALTH SERVICE DELIVERY: A STUDY OF OUTPATIENT UNITS IN NORWAY
439. Karen Lehrmann Ægidius: THE PREVALENCE OF HEADACHE AND MIGRAINE IN RELATION TO SEX HORMONE STATUS IN WOMEN. THE HUNT 2 STUDY
440. Madelene Ericsson: EXERCISE TRAINING IN GENETIC MODELS OF HEART FAILURE
441. Marianne Klokk: THE ASSOCIATION BETWEEN SELF-REPORTED ECZEMA AND COMMON MENTAL DISORDERS IN THE GENERAL POPULATION. THE HORDALAND HEALTH STUDY (HUSK)
442. Tomas Ottemo Stølen: IMPAIRED CALCIUM HANDLING IN ANIMAL AND HUMAN CARDIOMYOCYTES REDUCE CONTRACTILITY AND INCREASE ARRHYTHMIA POTENTIAL – EFFECTS OF AEROBIC EXERCISE TRAINING
443. Bjarne Hansen: ENHANCING TREATMENT OUTCOME IN COGNITIVE BEHAVIOURAL THERAPY FOR OBSESSIVE COMPULSIVE DISORDER: THE IMPORTANCE OF COGNITIVE FACTORS
444. Mona Løvlien: WHEN EVERY MINUTE COUNTS. FROM SYMPTOMS TO ADMISSION FOR ACUTE MYOCARDIAL INFARCTION WITH SPECIAL EMPHASIS ON GENDER DIFFERECES
445. Karin Margaretha Gilljam: DNA REPAIR PROTEIN COMPLEXES, FUNCTIONALITY AND SIGNIFICANCE FOR REPAIR EFFICIENCY AND CELL SURVIVAL
446. Anne Byriel Walls: NEURONAL GLIAL INTERACTIONS IN CEREBRAL ENERGY – AND AMINO ACID HOMEOSTASIS – IMPLICATIONS OF GLUTAMATE AND GABA
447. Cathrine Fallang Knetter: MECHANISMS OF TOLL-LIKE RECEPTOR 9 ACTIVATION
448. Marit Følsvik Svindseth: A STUDY OF HUMILIATION, NARCISSISM AND TREATMENT OUTCOME IN PATIENTS ADMITTED TO PSYCHIATRIC EMERGENCY UNITS
449. Karin Elvenes Bakkelund: GASTRIC NEUROENDOCRINE CELLS – ROLE IN GASTRIC NEOPLASIA IN MAN AND RODENTS
450. Kirsten Brun Kjelstrup: DORSOVENTRAL DIFFERENCES IN THE SPATIAL REPRESENTATION AREAS OF THE RAT BRAIN
451. Roar Johansen: MR EVALUATION OF BREAST CANCER PATIENTS WITH POOR PROGNOSIS
452. Rigmor Myran: POST TRAUMATIC NECK PAIN. EPIDEMIOLOGICAL, NEURORADIOLOGICAL AND CLINICAL ASPECTS
453. Krisztina Kunszt Johansen: GENEALOGICAL, CLINICAL AND BIOCHEMICAL STUDIES IN *LRRK2* – ASSOCIATED PARKINSON'S DISEASE
454. Pål Gjerden: THE USE OF ANTICHOLINERGIC ANTIPARKINSON AGENTS IN NORWAY. EPIDEMIOLOGY, TOXICOLOGY AND CLINICAL IMPLICATIONS
455. Else Marie Huuse: ASSESSMENT OF TUMOR MICROENVIRONMENT AND TREATMENT EFFECTS IN HUMAN BREAST CANCER XENOGRAFTS USING MR IMAGING AND SPECTROSCOPY
456. Khalid S. Ibrahim: INTRAOPERATIVE ULTRASOUND ASSESSMENT IN CORONARY ARTERY BYPASS SURGERY – WITH SPECIAL REFERENCE TO CORONARY ANASTOMOSES AND THE ASCENDING AORTA
457. Bjørn Øglænd: ANTHROPOMETRY, BLOOD PRESSURE AND REPRODUCTIVE DEVELOPMENT IN ADOLESCENCE OF OFFSPRING OF MOTHERS WHO HAD PREECLAMPSIA IN PREGNANCY
458. John Olav Roaldset: RISK ASSESSMENT OF VIOLENT, SUICIDAL AND SELF-INJURIOUS BEHAVIOUR IN ACUTE PSYCHIATRY – A BIO-PSYCHO-SOCIAL APPROACH
459. Håvard Dalen: ECHOCARDIOGRAPHIC INDICES OF CARDIAC FUNCTION – NORMAL VALUES AND ASSOCIATIONS WITH CARDIAC RISK FACTORS IN A POPULATION FREE FROM CARDIOVASCULAR DISEASE, HYPERTENSION AND DIABETES: THE HUNT 3 STUDY
460. Beate André: CHANGE CAN BE CHALLENGING. INTRODUCTION TO CHANGES AND IMPLEMENTATION OF COMPUTERIZED TECHNOLOGY IN HEALTH CARE
461. Latha Nrugham: ASSOCIATES AND PREDICTORS OF ATTEMPTED SUICIDE AMONG DEPRESSED ADOLESCENTS – A 6-YEAR PROSPECTIVE STUDY

462. Håvard Bersås Nordgaard: TRANSIT-TIME FLOWMETRY AND WALL SHEAR STRESS ANALYSIS OF CORONARY ARTERY BYPASS GRAFTS – A CLINICAL AND EXPERIMENTAL STUDY

Cotutelle with University of Ghent: Abigail Emily Swillens: A MULTIPHYSICS MODEL FOR IMPROVING THE ULTRASONIC ASSESSMENT OF LARGE ARTERIES

2011

463. Marte Helene Bjørk: DO BRAIN RHYTHMS CHANGE BEFORE THE MIGRAINE ATTACK? A LONGITUDINAL CONTROLLED EEG STUDY
464. Carl-Jørgen Arum: A STUDY OF UROTHELIAL CARCINOMA: GENE EXPRESSION PROFILING, TUMORIGENESIS AND THERAPIES IN ORTHOTOPIC ANIMAL MODELS
465. Ingunn Harstad: TUBERCULOSIS INFECTION AND DISEASE AMONG ASYLUM SEEKERS IN NORWAY. SCREENING AND FOLLOW-UP IN PUBLIC HEALTH CARE
466. Leif Åge Strand: EPIDEMIOLOGICAL STUDIES AMONG ROYAL NORWEGIAN NAVY SERVICEMEN. COHORT ESTABLISHMENT, CANCER INCIDENCE AND CAUSE-SPECIFIC MORTALITY
467. Katrine Høyer Holgersen: SURVIVORS IN THEIR THIRD DECADE AFTER THE NORTH SEA OIL RIG DISASTER OF 1980. LONG-TERM PERSPECTIVES ON MENTAL HEALTH
468. MarianneWallenius: PREGNANCY RELATED ASPECTS OF CHRONIC INFLAMMATORY ARTHRITIDES: DISEASE ONSET POSTPARTUM, PREGNANCY OUTCOMES AND FERTILITY. DATA FROM A NORWEGIAN PATIENT REGISTRY LINKED TO THE MEDICAL BIRTH REGISTRY OF NORWAY
469. Ole Vegard Solberg: 3D ULTRASOUND AND NAVIGATION – APPLICATIONS IN LAPAROSCOPIC SURGERY
470. Inga Ekeberg Schjerve: EXERCISE-INDUCED IMPROVEMENT OF MAXIMAL OXYGEN UPTAKE AND ENDOTHELIAL FUNCTION IN OBESE AND OVERWEIGHT INDIVIDUALS ARE DEPENDENT ON EXERCISE-INTENSITY
471. Eva Veslemøy Tyldum: CARDIOVASCULAR FUNCTION IN PREECLAMPSIA – WITH REFERENCE TO ENDOTHELIAL FUNCTION, LEFT VENTRICULAR FUNCTION AND PRE-PREGNANCY PHYSICAL ACTIVITY
472. Benjamin Garzón Jiménez de Cisneros: CLINICAL APPLICATIONS OF MULTIMODAL MAGNETIC RESONANCE IMAGING
473. Halvard Knut Nilsen: ASSESSING CODEINE TREATMENT TO PATIENTS WITH CHRONIC NON-MALIGNANT PAIN: NEUROPSYCHOLOGICAL FUNCTIONING, DRIVING ABILITY AND WEANING
474. Eiliv Brenner: GLUTAMATE RELATED METABOLISM IN ANIMAL MODELS OF SCHIZOPHRENIA
475. Egil Jonsbu: CHEST PAIN AND PALPITATIONS IN A CARDIAC SETTING; PSYCHOLOGICAL FACTORS, OUTCOME AND TREATMENT
476. Mona Høysæter Fenstad: GENETIC SUSCEPTIBILITY TO PREECLAMPSIA : STUDIES ON THE NORD-TRØNDELAG HEALTH STUDY (HUNT) COHORT, AN AUSTRALIAN/NEW ZEALAND FAMILY COHORT AND DECIDUA BASALIS TISSUE
477. Svein Erik Gaustad: CARDIOVASCULAR CHANGES IN DIVING: FROM HUMAN RESPONSE TO CELL FUNCTION
478. Karin Torvik: PAIN AND QUALITY OF LIFE IN PATIENTS LIVING IN NURSING HOMES
479. Arne Solberg: OUTCOME ASSESSMENTS IN NON-METASTATIC PROSTATE CANCER
480. Henrik Sahlin Pettersen: CYTOTOXICITY AND REPAIR OF URACIL AND 5-FLUOROURACIL IN DNA
481. Pui-Lam Wong: PHYSICAL AND PHYSIOLOGICAL CAPACITY OF SOCCER PLAYERS: EFFECTS OF STRENGTH AND CONDITIONING
482. Ole Solheim: ULTRASOUND GUIDED SURGERY IN PATIENTS WITH INTRACRANIAL TUMOURS
483. Sten Roar Snare: QUANTITATIVE CARDIAC ANALYSIS ALGORITHMS FOR POCKET-SIZED ULTRASOUND DEVICES
484. Marit Skyrud Bratlie: LARGE-SCALE ANALYSIS OF ORTHOLOGS AND PARALOGS IN VIRUSES AND PROKARYOTES
485. Anne Elisabeth F. Isern: BREAST RECONSTRUCTION AFTER MASTECTOMY – RISK OF RECURRENCE AFTER DELAYED LARGE FLAP RECONSTRUCTION – AESTHETIC OUTCOME, PATIENT SATISFACTION, QUALITY OF LIFE AND SURGICAL RESULTS;

HISTOPATHOLOGICAL FINDINGS AND FOLLOW-UP AFTER PROPHYLACTIC MASTECTOMY IN HEREDITARY BREAST CANCER

486. Guro L. Andersen: CEREBRAL PALSY IN NORWAY – SUBTYPES, SEVERITY AND RISK FACTORS
487. Frode Kolstad: CERVICAL DISC DISEASE – BIOMECHANICAL ASPECTS
488. Bente Nordtug: CARING BURDEN OF COHABITANTS LIVING WITH PARTNERS SUFFERING FROM CHRONIC OBSTRUCTIVE PULMONARY DISEASE OR DEMENTIA
489. Mariann Gjervik Heldahl: EVALUATION OF NEOADJUVANT CHEMOTHERAPY IN LOCALLY ADVANCED BREAST CANCER BASED ON MR METHODOLOGY
490. Lise Tevik Løvseth: THE SUBJECTIVE BURDEN OF CONFIDENTIALITY
491. Marie Hjelmseth Aune: INFLAMMATORY RESPONSES AGAINST GRAM NEGATIVE BACTERIA INDUCED BY TLR4 AND NLRP12
492. Tina Strømdal Wik: EXPERIMENTAL EVALUATION OF NEW CONCEPTS IN HIP ARTHROPLASTY
493. Solveig Sigurdardottir: CLINICAL ASPECTS OF CEREBRAL PALSY IN ICELAND. A POPULATION-BASED STUDY OF PRESCHOOL CHILDREN
494. Arne Reimers: CLINICAL PHARMACOKINETICS OF LAMOTRIGINE
495. Monica Wegling: KULTURMENNESKETS BYRDE OG SYKDOMMENS VELSIGNELSE. KAN MEDISINSK UTREDNING OG INTERVENSJON HA EN SELVSTENDIG FUNKSJON UAVHENGIG AV DET KURATIVE?
496. Silje Alvestad: ASTROCYTE-NEURON INTERACTIONS IN EXPERIMENTAL MESIAL TEMPORAL LOBE EPILEPSY – A STUDY OF UNDERLYING MECHANISMS AND POSSIBLE BIOMARKERS OF EPILEPTOGENESIS
497. Javaid Nauman: RESTING HEART RATE: A MATTER OF LIFE OR DEATH – PROSPECTIVE STUDIES OF RESTING HEART RATE AND CARDIOVASCULAR RISK (THE HUNT STUDY, NORWAY)
498. Thuy Nguyen: THE ROLE OF C-SRC TYROSINE KINASE IN ANTIVIRAL IMMUNE RESPONSES
499. Trine Naalsund Andreassen: PHARMACOKINETIC, PHARMACODYNAMIC AND PHARMACOGENETIC ASPECTS OF OXYCODONE TREATMENT IN CANCER PAIN
500. Eivor Alette Laugsand: SYMPTOMS IN PATIENTS RECEIVING OPIOIDS FOR CANCER PAIN – CLINICAL AND PHARMACOGENETIC ASPECTS
501. Dorthe Stensvold: PHYSICAL ACTIVITY, CARDIOVASCULAR HEALTH AND LONGEVITY IN PATIENTS WITH METABOLIC SYNDROME
502. Stian Thoresen Aspenes: PEAK OXYGEN UPTAKE AMONG HEALTHY ADULTS – CROSS-SECTIONAL DESCRIPTIONS AND PROSPECTIVE ANALYSES OF PEAK OXYGEN UPTAKE, PHYSICAL ACTIVITY AND CARDIOVASCULAR RISK FACTORS IN HEALTHY ADULTS (20-90 YEARS)
503. Reidar Alexander Vigen: PATHOBIOLOGY OF GASTRIC CARCINOIDS AND ADENOCARCINOMAS IN RODENT MODELS AND PATIENTS. STUDIES OF GASTROCYSTOPLASTY, GENDER-RELATED FACTORS, AND AUTOPHAGY
504. Halvard Høilund-Kaupang: MODELS AND METHODS FOR INVESTIGATION OF REVERBERATIONS IN NONLINEAR ULTRASOUND IMAGING
505. Audhild Løhre: WELLBEING AMONG SCHOOL CHILDREN IN GRADES 1-10: PROMOTING AND ADVERSE FACTORS
506. Torgrim Tandstad: VOX POPULI. POPULATION-BASED OUTCOME STUDIES IN TESTICULAR CANCER
507. Anna Brenne Grønskag: THE EPIDEMIOLOGY OF HIP FRACTURES AMONG ELDERLY WOMEN IN NORD-TRØNDELAG. HUNT 1995-97, THE NORD-TRØNDELAG HEALTH STUDY
508. Kari Ravndal Risnes: BIRTH SIZE AND ADULT MORTALITY: A SYSTEMATIC REVIEW AND A LONG-TERM FOLLOW-UP OF NEARLY 40 000 INDIVIDUALS BORN AT ST. OLAV UNIVERSITY HOSPITAL IN TRONDHEIM 1920-1960
509. Hans Jakob Bøe: LONG-TERM POSTTRAUMATIC STRESS AFTER DISASTER – A CONTROLLED STUDY OF SURVIVORS' HEALTH 27 YEARS AFTER THE CAPSIZED NORTH SEA OIL RIG
510. Cathrin Barbara Canto, Cotutelle with University of Amsterdam: LAYER SPECIFIC INTEGRATIVE PROPERTIES OF ENTORHINAL PRINCIPAL NEURONS
511. Ioanna Sandvig: THE ROLE OF OLFACTORY ENSHEATHING CELLS, MRI, AND BIOMATERIALS IN TRANSPLANT-MEDIATED CNS REPAIR

512. Karin Fahl Wader: HEPATOCYTE GROWTH FACTOR, C-MET AND SYNDECAN-1 IN MULTIPLE MYELOMA
513. Gerd Tranø: FAMILIAL COLORECTAL CANCER
514. Bjarte Bergstrøm: INNATE ANTIVIRAL IMMUNITY – MECHANISMS OF THE RIG-I-MEDIATED RESPONSE
515. Marie Søfteland Sandvei: INCIDENCE, MORTALITY, AND RISK FACTORS FOR ANEURYSMAL SUBARACHNOID HEMORRHAGE. PROSPECTIVE ANALYZES OF THE HUNT AND TROMSØ STUDIES
516. Mary-Elizabeth Bradley Eilertsen: CHILDREN AND ADOLESCENTS SURVIVING CANCER: PSYCHOSOCIAL HEALTH, QUALITY OF LIFE AND SOCIAL SUPPORT
517. Takaya Saito: COMPUTATIONAL ANALYSIS OF REGULATORY MECHANISM AND INTERACTIONS OF MICRORNAS

Godkjent for disputas, publisert post mortem: Eivind Jullumstrø: COLORECTAL CANCER AT LEVANGER HOSPITAL 1980-2004

518. Christian Gutvik: A PHYSIOLOGICAL APPROACH TO A NEW DECOMPRESSION ALGORITHM USING NONLINEAR MODEL PREDICTIVE CONTROL
519. Ola Storrø: MODIFICATION OF ADJUVANT RISK FACTOR BEHAVIOURS FOR ALLERGIC DISEASE AND ASSOCIATION BETWEEN EARLY GUT MICROBIOTA AND ATOPIC SENSITIZATION AND ECZEMA. EARLY LIFE EVENTS DEFINING THE FUTURE HEALTH OF OUR CHILDREN
520. Guro Fanneløb Giskeødegård: IDENTIFICATION AND CHARACTERIZATION OF PROGNOSTIC FACTORS IN BREAST CANCER USING MR METABOLOMICS
521. Gro Christine Christensen Løhaugen: BORN PRETERM WITH VERY LOW BIRTH WEIGHT – NEVER ENDING COGNITIVE CONSEQUENCES?
522. Sigrid Nakrem: MEASURING QUALITY OF CARE IN NURSING HOMES – WHAT MATTERS?
523. Brita Pukstad: CHARACTERIZATION OF INNATE INFLAMMATORY RESPONSES IN ACUTE AND CHRONIC WOUNDS

2012

524. Hans H. Wasmuth: ILEAL POUCHES
525. Inger Økland: BIASES IN SECOND-TRIMESTER ULTRASOUND DATING RELATED TO PREDICTION MODELS AND FETAL MEASUREMENTS
526. Bjørn Mørkedal: BLOOD PRESSURE, OBESITY, SERUM IRON AND LIPIDS AS RISK FACTORS OF ISCHAEMIC HEART DISEASE
527. Siver Andreas Moestue: MOLECULAR AND FUNCTIONAL CHARACTERIZATION OF BREAST CANCER THROUGH A COMBINATION OF MR IMAGING, TRANSCRIPTOMICS AND METABOLOMICS
528. Guro Aune: CLINICAL, PATHOLOGICAL, AND MOLECULAR CLASSIFICATION OF OVARIAN CARCINOMA
529. Ingrid Alsos Lian: MECHANISMS INVOLVED IN THE PATHOGENESIS OF PRE-ECLAMPSIA AND FETAL GROWTH RESTRICTION. TRANSCRIPTIONAL ANALYSES OF PLACENTAL AND DECIDUAL TISSUE
530. Karin Solvang-Garten: X-RAY REPAIR CROSS-COMPLEMENTING PROTEIN 1 – THE ROLE AS A SCAFFOLD PROTEIN IN BASE EXCISION REPAIR AND SINGLE STRAND BREAK REPAIR
531. Toril Holien: BONE MORPHOGENETIC PROTEINS AND MYC IN MULTIPLE MYELOMA
532. Rooyen Mavenyengwa: *STREPTOCOCCUS AGALACTIAE* IN PREGNANT WOMEN IN ZIMBABWE: EPIDEMIOLOGY AND SEROTYPE MARKER CHARACTERISTICS
533. Tormod Rimehaug: EMOTIONAL DISTRESS AND PARENTING AMONG COMMUNITY AND CLINIC PARENTS
534. Maria Dung Cao: MR METABOLIC CHARACTERIZATION OF LOCALLY ADVANCED BREAST CANCER – TREATMENT EFFECTS AND PROGNOSIS
535. Mirta Mittelstedt Leal de Sousa: PROTEOMICS ANALYSIS OF PROTEINS INVOLVED IN DNA BASE REPAIR AND CANCER THERAPY
536. Halfdan Petursson: THE VALIDITY AND RELEVANCE OF INTERNATIONAL CARDIOVASCULAR DISEASE PREVENTION GUIDELINES FOR GENERAL PRACTICE
537. Marit By Rise: LIFTING THE VEIL FROM USER PARTICIPATION IN CLINICAL WORK – WHAT IS IT AND DOES IT WORK?

538. Lene Thoresen: NUTRITION CARE IN CANCER PATIENTS. NUTRITION ASSESSMENT: DIAGNOSTIC CRITERIA AND THE ASSOCIATION TO SURVIVAL AND HEALTH-RELATED QUALITY OF LIFE IN PATIENTS WITH ADVANCED COLORECTAL CARCINOMA
539. Berit Doseth: PROCESSING OF GENOMIC URACIL IN MAN AND MOUSE
540. Gro Falkenér Bertheussen: PHYSICAL ACTIVITY AND HEALTH IN A GENERAL POPULATION AND IN CANCER SURVIVORS – METHODOLOGICAL, OBSERVATIONAL AND CLINICAL ASPECTS
541. Anne Kari Knudsen: CANCER PAIN CLASSIFICATION
542. Sjur Urdson Gjerald: A FAST ULTRASOUND SIMULATOR
543. Harald Edvard Mølmen Hansen: CARDIOVASCULAR EFFECTS OF HIGH INTENSITY AEROBIC INTERVAL TRAINING IN HYPERTENSITIVE PATIENTS, HEALTHY AGED AND YOUNG PERSONS
544. Sasha Gulati: SURGICAL RESECTION OF HIGH-GRADE GLIOMAS
545. John Chr. Fløvig: FREQUENCY AND EFFECT OF SUBSTANCES AND PSYCHOACTIVE MEDICATIONS THE WEEK BEFORE ADMISSION TO AN ACUTE PSYCHIATRIC DEPARTMENT
546. Kristin Moksnes Husby: OPTIMIZING OPIOID TREATMENT FOR CANCER PAIN – CLINICAL AND PHARMACOLOGICAL ASPECTS
547. Audun Hanssen-Bauer: X-RAY REPAIR CROSS-COMPLEMENTING PROTEIN 1 ASSOCIATED MULTIPROTEIN COMPLEXES IN BASE EXCISION REPAIR
548. Marit Saunes: ECZEMA IN CHILDREN AND ADOLESCENTS – EPIDEMIOLOGY, COURSE AND IMPACT. THE PREVENTION OF ALLERGY AMONG CHILDREN IN TRONDHEIM (PACT) STUDY, YOUNG-HUNT 1995-97
549. Guri Kaurstad: CARDIOMYOCYTE FUNCTION AND CALCIUM HANDLING IN ANIMAL MODELS OF INBORN AND ACQUIRED MAXIMAL OXYGEN UPTAKE
550. Kristian Svendsen: METHODOLOGICAL CHALLENGES IN PHARMACOEPIDEMIOLOGICAL STUDIES OF OPIOID CONSUMPTION
551. Signe Nilssen Stafne: EXERCISE DURING PREGNANCY
552. Marius Widerøe: MAGNETIC RESONANCE IMAGING OF HYPOXIC-ISCHEMIC BRAIN INJURY DEVELOPMENT IN THE NEWBORN RAT – MANGANESE AND DIFFUSION CONTRASTS